Durham E-Theses

Mineralogical mapping using airborne imaging spectrometry data

Mackin, Stephen

Mineralogical mapping using
airborne imaging spectrometry data.

A thesis presented for the degree of

Doctor of Philosophy

by

Stephen Mackin

University of Durham
Department of Geological Sciences
June 1989

i

DECLARATION.

The work contained in this thesis has not been submitted elsewhere for any other degree or qualification and that unless otherwise referenced it is the authors own work.

Dedicated to my

MUM

and

DAD

For their thoughts and love.

"No man is a failure who has friends"
Frank Capra film "ITS A WONDERFUL LIFE" (1947).

ABSTRACT

With the development of airborne, high spectral resolution imaging spectrometers, we now have a tool, that allows us to examine surface materials with enough spectral detail to identify them.

Identification is based on the analysis of position and shape of absorption features in the material spectra in the visible and infrared (0.4μm to 2.5μm). These absorption features are caused by the interaction of Electro-Magnetic Radiation (EMR) with the atoms and molecules of the surface material.

Airborne data were collected to evaluate these new high spectral resolution systems. The data quality was assessed prior to processing and analysis and several problems were noted for each data set (striping, geometric distortion, etc.). These problems required some preparation of the data.

After data preparation, data processing methods were evaluated, concentrating primarily on the log residuals and hull quotients methods. The processing steps convert the data to a form suitable for analysis. The data was analysed using the Spectral Analysis Manager (SPAM) package, developed by JPL.

Two Imaging spectrometers were evaluated. The AIS - 1 instrument was flown over an area in Queensland, Australia. Ground data and laboratory work confirmed the presence of anomalous areas detected by the instrument. The data quality was poor and only basic classification of the data was possible. Anomalies were classed as "GREEN VEGETATION", "DRY VEGETATION", "CLAY" or "CARBONATE" based on the position of the major absorptions observed.

The second instrument, the GER - II was flown over an area of Nevada, USA. Ground data and laboratory work confirmed the presence of the anomalies detected by the instrument. The data quality was somewhat better. Identification of sericite, dolomite and illite was possible. However, most of the area could still only be classed in the broad groupings listed above.

To conclude, the effectiveness of identification is limited to a large degree by the poor data quality. If the data quality can be improved, techniques can be applied to automatically locate and identify material spectra, from the airborne data alone.

ACKNOWLEDGEMENTS

TABLE OF CONTENTS.

CHAPTER 5. INTERPRETATION AND DISCUSSION OF THE RE-
SULTS, OBTAINED FROM THE AIS - 1 INSTRUMENT FLIGHT OVER
AN AREA OF NORTHERN QLD, AUSTRALIA.

CHAPTER 6.   INTERPRETATION AND DISCUSSION OF THE RESULTS, OBTAINED FROM THE GER - II INSTRUMENT FLIGHT OVER AN AREA OF NORTHERN NEVADA, USA.

CHAPTER 1

INTRODUCTION TO IMAGING SPECTROMETRY.

1.1 Introduction.

Since the advent of remote sensing, it has been known that the spectral response of different surficial materials varies with wavelength. Given a detailed enough spectrum it is possible to uniquely **identify** an individual mineral based on the analysis of general curve shape and specific localised absorption features present in this spectrum .

Recently with the development of passive, airborne, high spectral resolution imaging spectrometer systems, the necessary detail has been made available. With these systems it is possible to uniquely identify minerals based on their spectral response in the visible, near infrared and short wavelength infrared regions, 0.4μm to 2.5μm (Abrams and Goetz, 1985).

This project was devised specifically to test the potential of these new imaging spectrometers, in mapping the often subtle differences in mineralogy observed on the ground. To fully evaluate their use involves the consideration of approaches for,

(1) Data handling. The broad band Landsat series of satellites. collected data in a maximum of six bands in the visible, near-infrared and short wavelength infrared wavelength regions (0.4μm to 2.5μm), whereas the new high spectral resolution data sets described in this thesis contain up to 128 bands for the same wavelength range.

(2) Data processing. Primary processing techniques for the broad band Landsat data sets, involved processing band combinations to improve the **discrimination** of materials in a scene. Processing of high spectral resolution data involves the extraction of spectral features to **identify** surface materials from the data alone, requiring new processing techniques.

(3) Data analysis and display. The broad band Landsat data sets, could be displayed as a series of three band colour composites on a monitor. The

variations in colour were attributed to variations in spectral response of different surface materials. Ground follow up was then necessary to identify the materials discriminated. The analysis techniques for high spectral resolution data are based on the principle of identifying the surface materials by generating spectral plots that can be matched against library spectra of known surface materials.

(4) Interpretation. The primary role of interpretation for the broad band Landsat data sets is to equate the ground data collected to the multi-colour composite image and try to discriminate the different materials present on the basis of this colour variation. For high spectral resolution work, the data can be interpreted directly to determine the identity of surface materials.

The application of these new data sets to geological problems is considered in some depth, specifically for the tasks of geological mapping and mineral exploration. It is obvious that the increased ability to directly identify surface components could be extremely useful in the field of mineral exploration, where the variation in the mineralogy of an alteration zone at the surface could be of use in locating economic mineralisation. The uses and limitations of these new data sets are discussed later in this thesis.

The primary aims of the project are listed below,

(1) Develop algorithms to handle the data. This includes reformatting the data for use by the processing and analysis packages and determination of the wavelength regions of interest for analysis and interpretation.

(2) Identify problems associated with the data (noise, striping, etc.) and develop suitable algorithms to reduce these problems, prior to processing.

(3) Implement available processing techniques for high spectral resolution data, evaluate these methods and develop further where possible.

(4) Implement available analysis and display methods for high spectral resolution data, evaluate these methods and develop further where possible.

(5) Develop analysis and interpretation methods more suitable for extracting information from these high spectral resolution data sets.

(6) Evaluate the geological content of these new data sets and determine which geological applications could effectively use such data.

In this thesis the following division of the wavelength regions discussed will be used.

0.4μm - 1.0μm Visible/Near InfraRed (VNIR).

1.0μm - 2.5μm Short Wavelength InfraRed (SWIR).

2.5μm and above Mid InfraRed (MIR).

The discussion will be confined primarily to the wavelengths in the 0.4μm to 2.5μm range, the regions covered by the imaging spectrometers currently in use.

1.2 Principles of imaging spectrometry.

A brief description of our natural source of Electro-Magnetic Radiation (EMR), the sun, and its interaction with the atmosphere prior to reaching the earths surface is given. This is followed by the physics of interaction of EMR and matter, the basic mechanism that gives rise to the spectral absorption features we observe in the image data.

1.2.1 The Sun and atmosphere.

The sun emits radiation over a large continuous range of wavelengths and can be considered to be spectrally equivalent to a blackbody at a temperature of 5900 Kelvins(Chahine et al., 1983)(figure 1.1). In figure 1.1 we can see an idealised blackbody curve for 5900 Kelvins(solid line) and the same curve after interaction with, and absorption at specific wavelengths by, atmospheric gases. The peak irradiance of the sun is seen at approximately 0.49μm (in the visible) decreasing at longer wavelengths towards 3.0μm. At wavelengths shorter than the peak irradiance, the transmission of radiation is severly reduced by the absorption due to ozone in the upper atmosphere. Thus the limits of our observation of the earth's surface are set by atmospheric absorptions in the ultra-violet (<0.3μm) and mid infrared (>2.5μm), the decrease in solar irradiance and corresponding increase in the emittance of the earth's surface.

1.2.2 Physics of interaction.

There are two levels at which we can view the interaction of EMR with the surface. At one level we can discern how photons interact with matter producing energy transitions of various types, by absorbing the incoming ra-
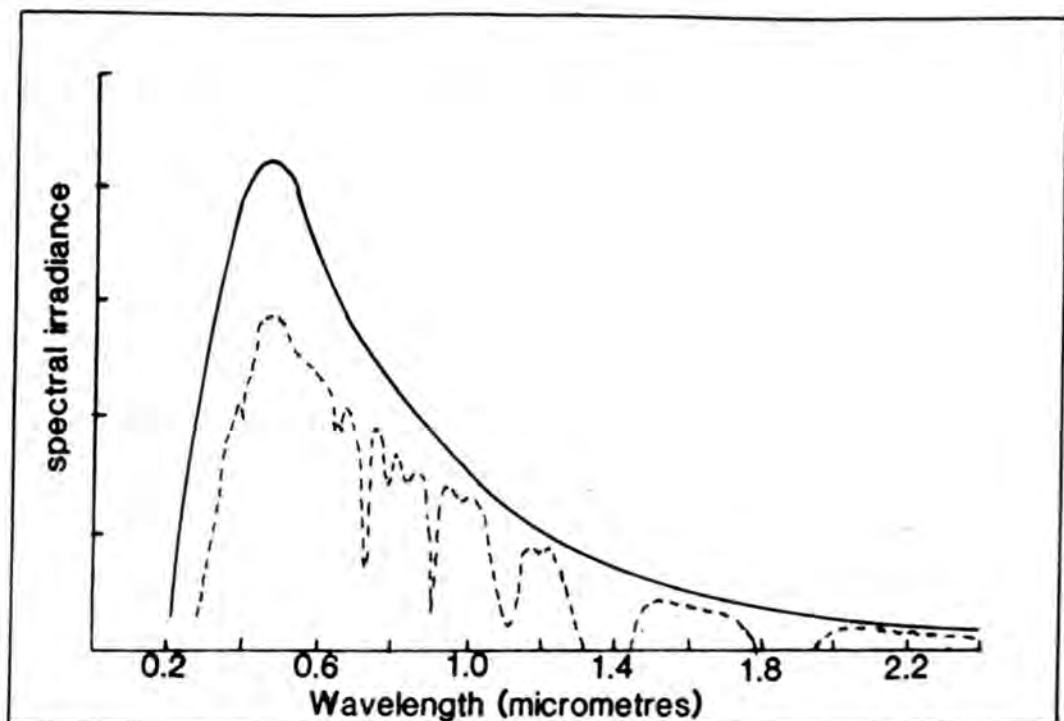
Figure 1.1   Spectral curve of a blackbody representing the Sun, with a
surface temperature of 5900 degrees Kelvin is shown (solid line). The
corresponding curve after absorption of the radiation by atmospheric
gases is shown by the dotted line. After Hunt, 1980.
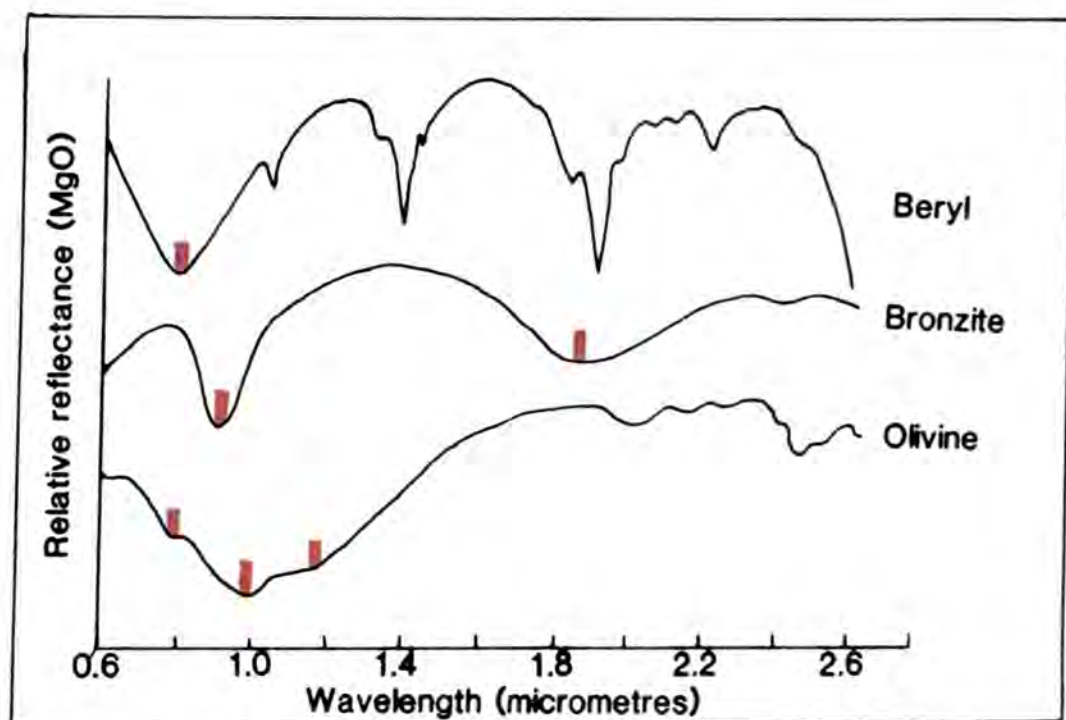
Figure 1.2   Spectra showing the absorptions (marked in red), due to
crystal field effects in the ferrous ion (Fe^{2+}). After Hunt, 1980 .

diation (Hunt, 1980). At the second level we can see the macroscopic effects of surface scattering and create elaborate models of both vegetated and particulate surfaces to explain some of the effects evident in our data. (Milton and Wardley, 1987; Hapke, 1981).

Absorption features observed in spectra obtained from laboratory or field instruments are due to energy transitions at the atomic or molecular level. The absorbed energy is used to carry out the transition and increase the potential energy of the system. The total energy of a system can be defined (for our purposes) by the sum of three different sources of energy directly related to rotational, vibrational and electronic transitions.

Rotational transitions - confined to gases, the transitions are seen in the mid and far infrared and microwave wavelength regions ($>2.5\mu$m). These transitions require very little energy.

Vibrational transitions - related to the movement of atoms about a fixed position (involving bending and stretching of bonds). They are observed only in the mid and far infrared ($>2.5\mu$m) and require more energy than rotational transitions. In gases the vibrational transitions are accompanied by rotational transitions which require much less energy.

Electronic transitions - require the re-configuration of the electron orbitals about atoms. This requires much more energy, therefore these transitions are confined to the higher energy regions of the spectrum, the visible (0.4μm - 0.78μm), ultra-violet ($<0.4\mu$m) and X-ray ($<0.4\mu$m) wavelength regions.

Apart from certain electronic transitions that appear in the VNIR and SWIR wavelength regions, it is obvious that all other transitions (rotational and vibrational) appear outside the working range of the current imaging spectrometers, in the mid and far infrared ($>2.5\mu$m). However, absorption features due to vibrational transitions are evident in the 0.4μm - 2.5μm wavelength region, these are not due to the direct fundamental frequency of transition but to some multiple or combination tone requiring several quanta of energy (Campbell and Dwek, 1984). To explain briefly, quantum mechanics can be used to prove that discrete vibrational energy levels are possible, defined by a series of selection rules. These rules apply to molecules

that vibrate in a manner approaching simple harmonic motion, producing the fundamental frequency of allowed transitions. However, the selection rules break down if the molecular vibrations are anharmonic, which can occur in the presence of other atoms or molecules. These anharmonic vibrations require much more energy (several quanta) to produce a transition. These are the overtones of higher energy that we see in the SWIR. These higher frequency (and hence shorter wavelength) overtones and combination tones allow the identifcation of a wide range of minerals, as will be discussed later in this chapter.

The macroscopic effects of EMR interacting with surface materials, are often very complex. Effects such as non-linear mixing as plant canopies develop (Heute et al., 1985) and variable absorption depths due to particle size variation and the presence of organic matter cause problems (Hapke, 1981; Crowley, 1986). Elaborate models of both vegetation cover (Milton and Wardley, 1987) and particulate surfaces (Hapke, 1981) have been developed, but at present, no attempt has been made to include these complex models in the identification process.

1.3 Geological applications.

The spectrum of any surface material consists of diagnostic absorption features and curve shape. The absorption features are representative of the vibrational overtones and combination tones due to the absorbed EMR. Vibrational bending - stretching overtones and combination tones and electronic transitions produce the characteristic absorptions in the 0.4μm - 2.5μm wavelength region and allow us to identify a wide range of minerals.

1.3.1 Electronic transitions.

Hunt (1980) outlines four basic processes that produce electronic transitions,

(1) Crystal field effects.

(2) Conduction band transitions.

(3) Charge transfer band transitions.

(4) Colour centres.

Crystal field effects. These effects account for most of the electronic

transitions observed in the visible and near infrared. The transitions do not occur in the common mineral forming elements (silicon, oxygen and aluminium), but in ions (e.g. Fe^{2+}, Cu^{2+}) that form a minor component of the mineral structure. The ions have incomplete d-electron orbitals. When part of a mineral structure the orbitals are split by interactions with the atoms of the structure and assume new energy levels in which the transitions take place.

The absorptions produced by the transitions vary in position and depth due to the variation in the host mineral structure, the valence state of the ions in which the transitions take place (e.g. Fe^{2+}, Fe^{3+}) and the type of bonding between the ions and the mineral structure. An example of the variation in depth and position for the ferrous ion (Fe^{2+}) is shown in figure 1.2.

Conduction band transitions. In some lattices the discrete energy levels of the electron shells merge into energy bands called conduction bands. Only high energy electrons exist in a conduction band and wander through the lattice structure rather than being attached to a specific atom. The edge of the conduction band is marked by a steep decrease in the reflected energy (a strong absorption). The position of the decrease is dependent on the conductivity of the material. Poorly conductive materials require high energy photons to displace an electron into the conduction band, so the decrease is at very short wavelengths (shorter than 0.4μm in the ultra-violet region). More conductive materials (e.g. sulphides) require lower energy photons to displace an electron into the conduction band and so the decrease is at longer wavelengths (longer than 0.4μm in the VNIR). Examples are shown for several sulphides in figure 1.3.

Charge transfer bands. Similar to conduction bands, except that the liberated electron migrates only as far as the neighbouring ion and does not enter a conduction band, thus remaining partly localised. Absorptions due to charge transfer bands are generally intense. The $Fe - O$ transfer band being one of the most commonly observed features of terrestrial minerals shows a steep decrease in reflectance in the visible part of the spectrum, figure 1.4.

Colour centres. Some minerals show variable absorption in the visible and therefore are coloured. The absorptions are due to defects in the crystal lattice structure. An example of this is the variable colour of the mineral
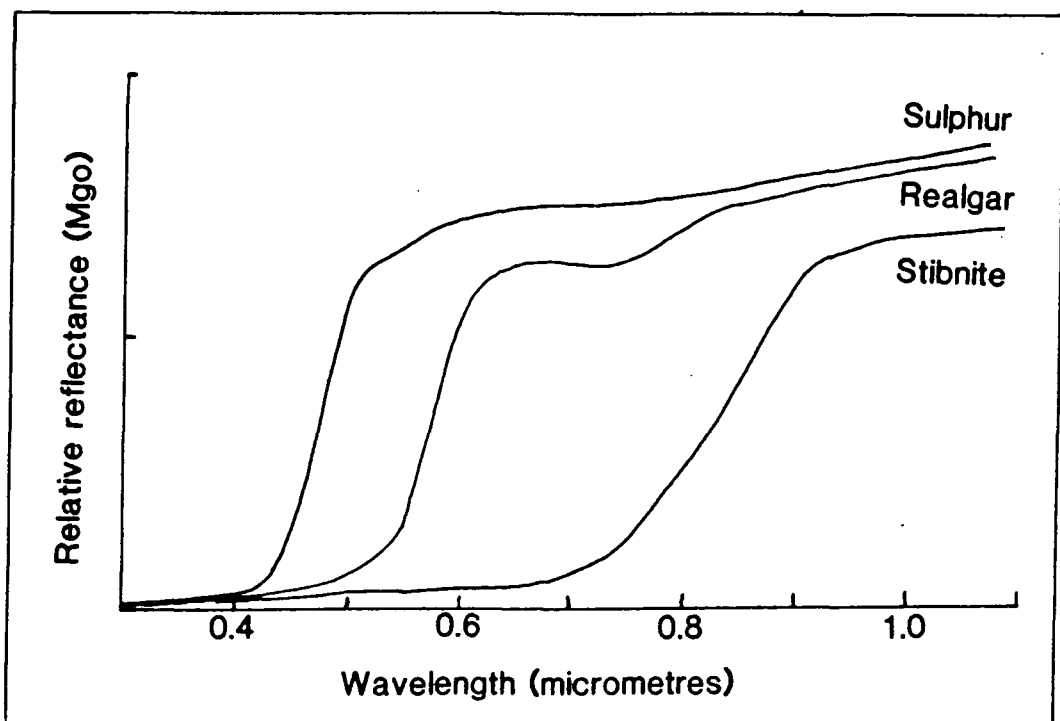
Figure 1.3   Spectra of sulphides showing the drop in intensity of reflected radiation in the visible wavelengths, due to conduction band absorptions. After Hunt, 1980 .
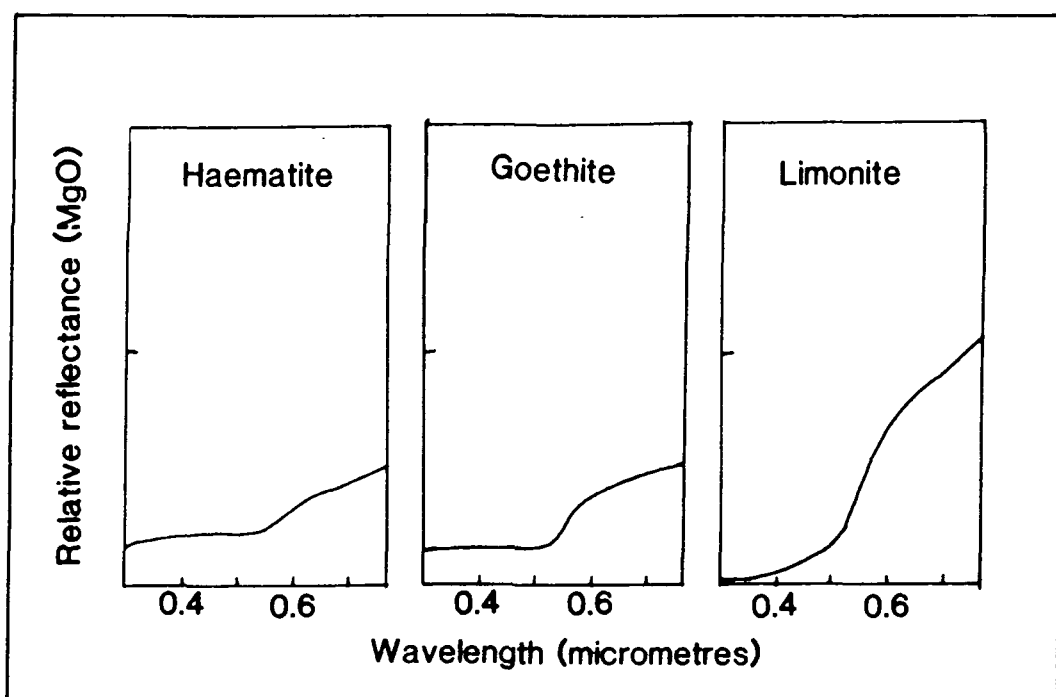
Figure 1.4 $Fe - O$ absorptions due to charge transfer are seen at visible wavelengths for some iron minerals. After Hunt, 1980 .

fluorite.

1.3.2 Vibrational transitions.

Vibrational transitions were discussed earlier in this chapter. Study of the rock forming minerals has shown that relatively few active groups $(OH^-, CO_3^{2-}, SO_4^{2-})$ are responsible for the mineral absorption features found in the 0.4μm - 2.5μm wavelength region. These groups, along with the Al^{3+} and Mg^{2+} ions, produce overtones and combination tones that explain the majority of the observed absorption features in the 0.4μm - 2.5μm wavelength region.

The hydroxyl ion (OH^-) is perhaps the most important of the active groups responsible for absorption features in the SWIR. The hydroxyl group is present in many rock forming minerals and also wherever water is present. Water may be present in the form of molecular water in the clay montmorillonite (for example) or localised in the mineral structure. In either case it produces the ubiquitous water absorption features centred at 1.4μm and 1.9μm. The broadness of these absorption features gives some indication of the ordering of the water in the mineral structure, highly ordered water leading to sharp narrow features in the spectra, disordered water leading to a broadening of these features.

When bonded with Al^{3+} or Mg^{2+}, combination tones of the fundamental stretching vibration of the OH group with bending vibrations of the $Al - OH$ and $Mg - OH$ bonds produces the diagnostic mineral absorption features observed at 2.2μm and 2.3μm of muscovite $(KAl_2(OH)_2(AlSi_3O_{10})$ and talc $(Mg_3(OH)_2(Si_2O_5)_2)$ (figure 1.5).

Other groups such as CO_3^{2-} (carbonate) and SO_4^{2-} (sulphate) produce similar diagnostic absorption features (Hunt et al., 1971). The position of the features depends on the mineral structure in which the carbonate or sulphate group is located and on the cations (Ca^{2+}, Mg^{2+}) to which they are bonded. Carbonate (CO_3^{2-}) minerals for example, show features related to bending and stretching vibrations of the planar CO_3^{2-} ion. The features are located in the SWIR at 1.9μm, 2.0μm, 2.16μm and 2.35μm. Figure 1.6 shows a typical Calcite $(Ca\ CO_3)$ spectrum and that for Dolomite $(Ca\ Mg\ (CO_3)_2)$, the only noticeable difference between them being the slight change in the position of the maximum absorption at 2.33μm for dolomite and 2.35μm for
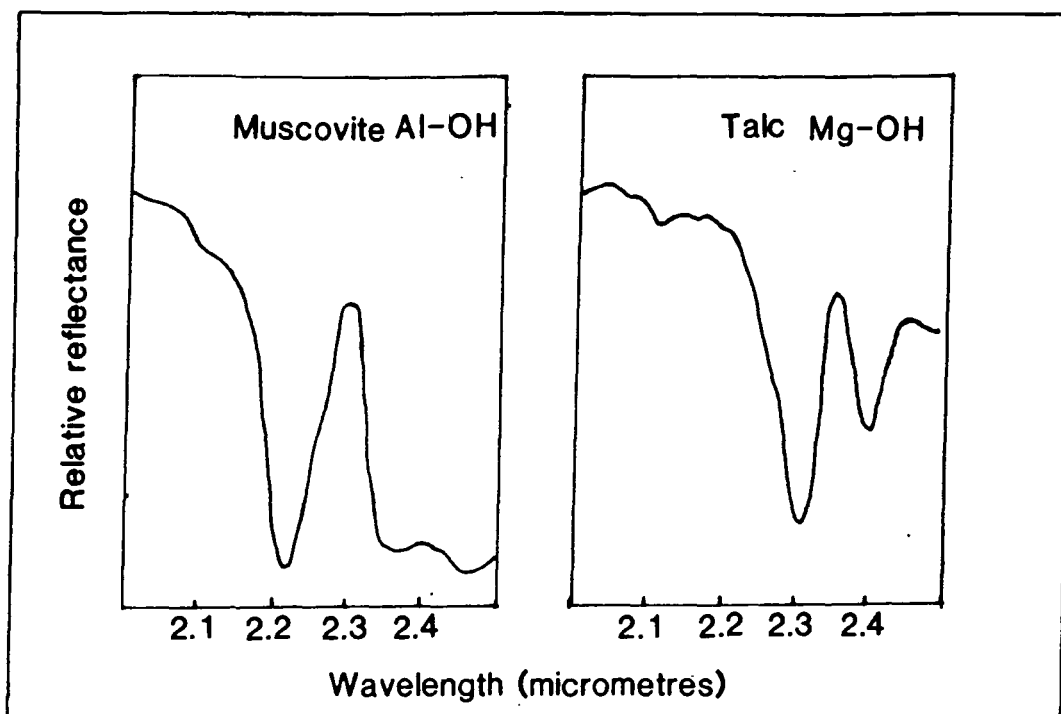
Figure 1.5   The spectra of the $Al - OH$ mineral muscovite and the $Mg -$ OH mineral talc have prominent absorption features in the SWIR, which can be clearly seperated based on the analysis of absorption position and shape.
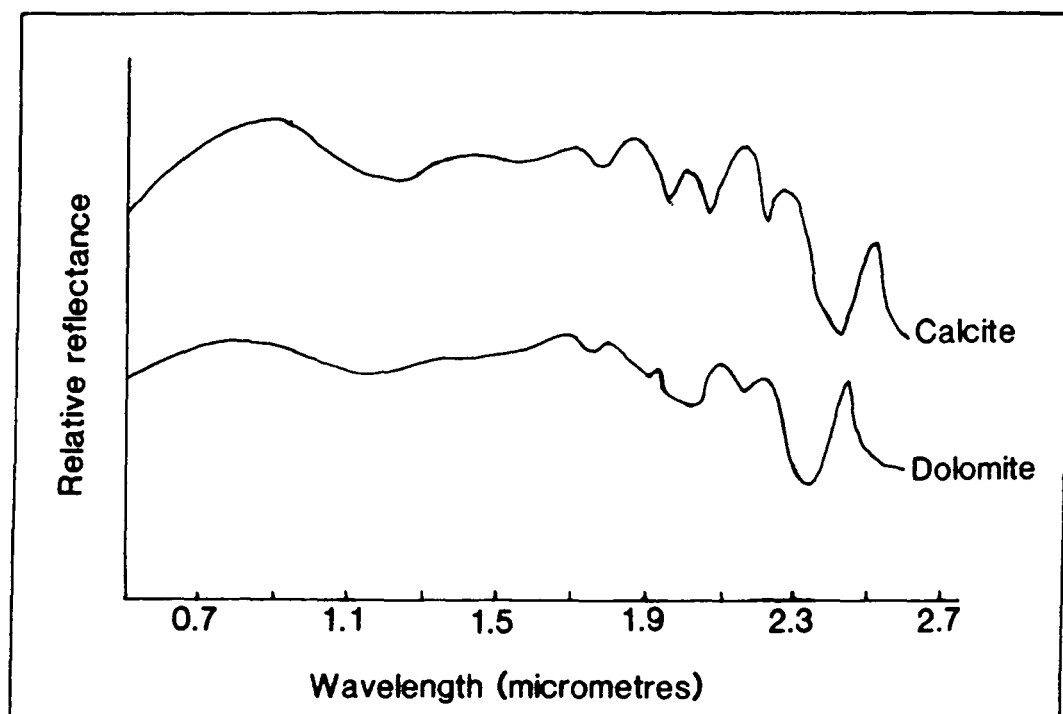
Figure 1.6   The carbonate spectra of calcite and dolomite are shown. The wavelength shift in the 2.32μm to 2.35μm wavelength region is due to the presence of the Mg^{2+} ion in the structure of the dolomite.

calcite, due to the variation in structure resulting from the introduction of the magnesium ion (Mg^{2+}) to form dolomite (Gaffey, 1985).

1.4 Mechanics and instrumentation.

Figure 1.7 shows the basic structure of an imaging spectrometer instrument. The operation of the instrument is summarised below and the variations in design of two airborne imaging spectrometers are described. The basic elements of an imaging spectrometer are,

(1) The optics assembly, usually containing the scanning assembly (if the device is a scanning device) and the blocking filters to allow the passage of a selected wavelength range of the solar radiation.

(2) A transmissive or reflective diffraction grating(s) to disperse the incoming radiation spectrally across a chosen wavelength range.

(3) A detector array on which the dispersed wavelengths of light are focused.

(4) Electronics to record and store the data acquired from the detector array.

The operation of the instrument is quite simple. Solar radiation reflected from a pixel area on the ground is focused by the optics assembly and a selected **broad** wavelength range is passed through a transmissive (or reflective) diffraction grating. The grating disperses the radiation spectrally on to the detector array. Each detector collects a signal for a particular **narrow** wavelength range of the dispersed radiation (As little as 10nm across). The electronics record the signal strength and store the data in digital form.

Major differences in design of the detector array occur and are related to whether the system is a scanning whiskbroom system or a non-scanning pushbroom system. Figure 1.7 shows a scanning system such as the Geophysical Environmental Research (GER) imaging instrument, while figure 1.8 shows the non-scanning Airborne Imaging Spectrometer (AIS). Each system has its advantages and disadvantages, which are listed in Table 1. Further details of these two quite different instruments are given later in the thesis.

1.5 Problems of imaging spectrometry.

LINE ARRAY

Spatial dimension

Wavelength
dispersion

Diffraction grating

Scan mirror

Swath width
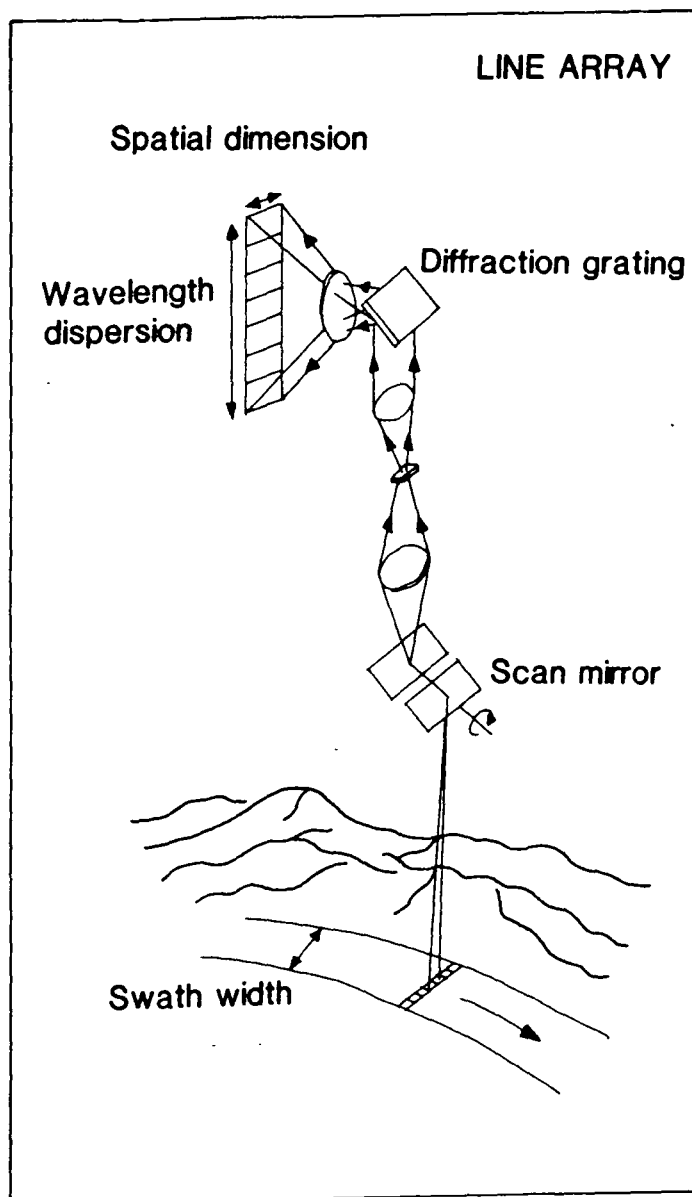
Figure 1.7 An outline of a **line array** imaging spectrometer. This design is used in the GER - II scanner.
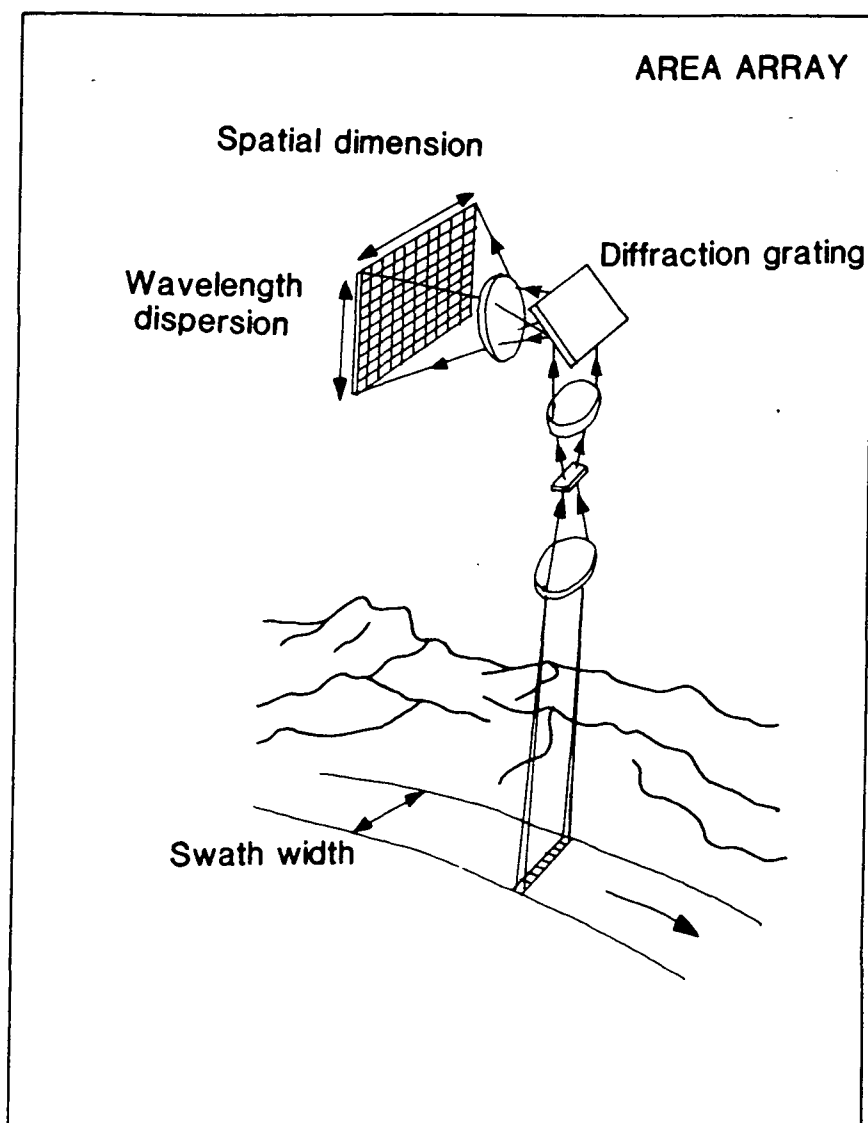
Figure 1.8   An outline of a **area array** imaging spectrometer. This design is used in the AIS - 1 instrument. After CSIRO, 1985..

Table 1.

COMPARISON OF AIS - 1 IMAGING SYSTEM AND GER - II SCANNING SYSTEM

INSTRUMENT	ADVANTAGES	DISADVANTAGES
AIS - 1 AREA ARRAY • 32 pixel swath • 128 bands • 1.2 µm - 2.4 µm • non scanning • contiguous	1. Area array allows long integration time for each pixel, so higher signal to noise in theory. 2. Full, contiguous spectral curves can be produced for direct comparison with established spectral libraries of minerals. 3. Same atmospheric path length for each pixel. Atmospheric correction should be easier.	1. Area array has narrow swath width at low altitudes. So easy to miss target areas. 2. Small swath makes it difficult to identify ground position. 3. Having to image same region of ground while the diffraction grating is cycled through four positions (to get the whole spectra) reduces integration time and lowers the signal to noise ratios.
GER - II LINE ARRAY • 512/1024 pixel swath • 63 bands • 0.4 µm - 2.4 µm • scanner • non contiguous	1. A scanner with line arrays provides a much wider swath which is of more use in an exploration environment. 2. Covers the visible wavelengths containing useful information on the presence of iron minerals and vegetation cover. 3. Variable scan speed can allow variable flight speed to increase signal to noise data.	1. Variable size of ground pixel from edges of scan to centre of scan produces bad geometric distortion. 2. Each of the three spectrometers used to generate spectra have different spectral sampling intervals. So that the whole spectra can NOT be directly compared to a library of mineral spectra. 3. Variable atmospheric effects for each pixel as the path length through the atmosphere varies as it is a scanner. This makes it difficult to compensate for the atmospheric effects. 4. Line arrays with a scanner have short integration times for the signal. So lower signal to noise ratios (in theory).

In previous sections, the interactions of EMR with the atmosphere and ground surface were mentioned. The principles of interaction seem quite simple, however problems do occur due to atmospheric absorptions, instrumental peculiarities and macroscopic surface effects (variable particle size etc.). These problem areas and their possible effects on the data are discussed in this section.

1.5.1 Atmospheric effects.

One of the more obvious complicating factors is the atmosphere, which separates the target from the light source (the Sun) and the target from the recording detectors (either airborne or spaceborne). The effects seen are due to absorption and scattering within the atmosphere.

Absorption takes place primarily by rotational, vibrational and electronic transitions within bonds of the atmospheric gases. The three primary absorbers are ozone, carbon dioxide and water vapour. The ozone absorptions are confined to wavelengths shorter than 0.4μm, which is outside our wavelength region of interest, 0.4μm - 2.5μm. However, major absorption features due to atmospheric water and carbon dioxide are clearly visible in the wavelength region 0.4μm - 2.5μm (Chahine et al., 1983), (figure 1.9). Absorptions not only reduce the amount of energy reaching the surface, but also can occur in regions where characteristic mineral spectral features are found, producing confusing masking effects (Kruse and Clark, 1986). In figure 1.10, the upper plot is a reflectance spectra of sericite, the lower plot (dotted) is the reflectance spectra, with the addition of atmospheric absorptions, showing the loss of the characteristic mineral spectral feature at 1.4μm.

Scattering can be caused by several atmospheric components. At shorter wavelengths, 0.4μm to 0.6μm, the molecular gases O_2 and N_2 are of a size to produce extensive Rayleigh scattering. The amount of scattering is wavelength dependent, being inversely proportional to the fourth power of the wavelength of light. Particulates of a size much greater than the atmospheric gases can also scatter light. The particulates produce strong forward scattering of light, with effects noticeable in the visible and near infrared wavelength regions up to 1.0μm (Chahine et al., 1983). This type of scattering is less wavelength dependent and is called Mie scattering. A combination of scattering effects in the visible and near infrared
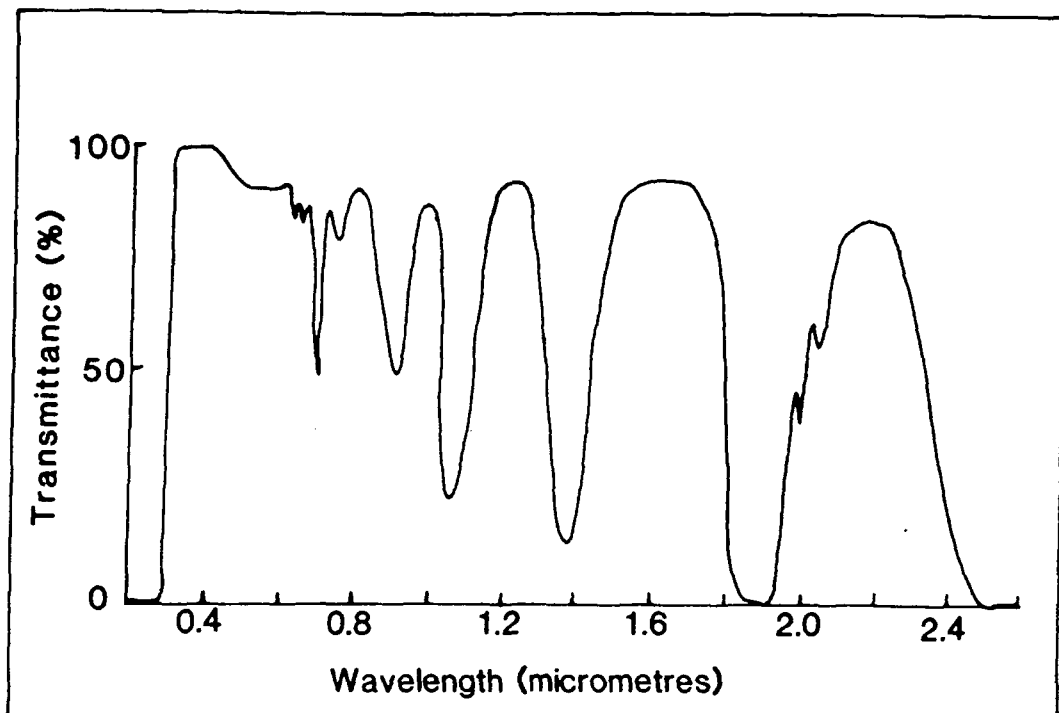
Figure 1.9   Atmospheric absorptions reduce the transmittance of solar radiation in the $0.4\mu m$ to $2.5\mu m$ wavelength region. The deep absorptions at $1.4\mu m$ and $1.9\mu m$ are due to atmospheric water, while the small features near $2.0\mu m$ are due to atmospheric carbon dioxide.
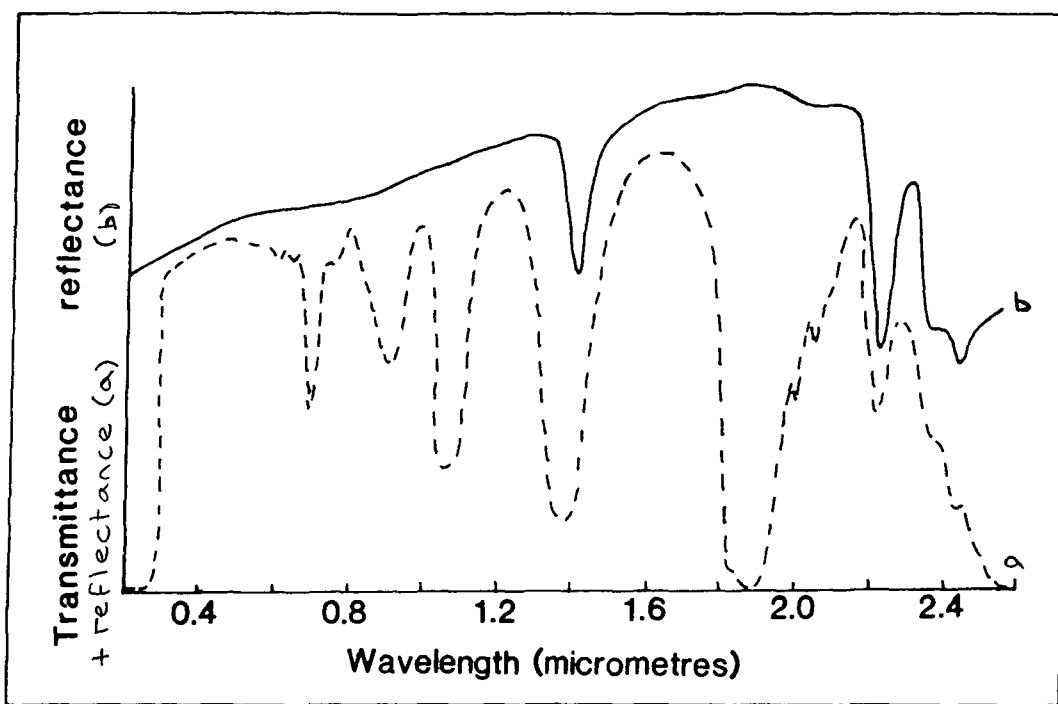
Figure 1.10   The sericite spectrum is masked by atmospheric absorptions. Note the loss of the strong, narrow absorption at $1.4\mu m$, due to the masking by atmospheric water in the composite curve (a).

coupled with variations in sun-sensor geometry can produce unusually strong variations in scene brightness across a scene, which can affect identification of surface components (Abrams, 1985).

Modelling of the atmosphere is possible for a variety of sun-sensor geometries. However, these models do not deal with variations in surface topography and surface composition that will affect the accuracy of their predicted atmosphere. This is an important area for further research, as our ability to extract smaller and smaller features for identification purposes will require a more accurate representation of masking atmospheric effects.

1.5.2 Instrument operation.

Each sensor has its own peculiarities of operation. These peculiarities express themselves in a deterioration of data quality. Effects such as striping due to poor calibration or variable detector cooling, data spikes due to electronics noise and other effects are often noticed by users of the data when it is first made available. Purpose written algorithms are necessary to correct for, or reduce the effects of these data quality problems.

1.5.3 Macroscopic ground surface effects.

The ground surface itself can be a source of problems in imaging spectrometry as mentioned earlier in this chapter. Hunt (1980) noted that the proportions of opaque and transparent crystalline minerals had a distinct effect on the depth of absorption features. For example the presence of opaque iron minerals tend to reduce the observed absorption depths of other minerals present, such as clay minerals. Hunt also noted that the grain size of the surface minerals also affects the depths of absorption features, as does the orientation of minerals in certain cases.

However, at a practical level, to determine these effects, requires a detailed knowledge of the mineralogy and grain size for every pixel. This of course defeats the purpose of collecting the data in the first place.

By making certain assumptions it is possible to model some of these effects (Hapke, 1981). In certain circumstances where a quantitative estimate of the proportions of minerals in a pixel is required (e.g. mixed pixels), modelling offers a partial solution. However, for the purposes of mineral exploration determination of the identity of ground surface materials is much more im-

portant, than any quantitative estimate of the mineral proportions.

1.6 Summary.

The current imaging spectrometers cover the spectral range $0.4\mu m$ to $2.5\mu m$ which falls within a window between atmospheric absorptions, decreasing solar irradiance and increasing earth emittance. The impinging EMR produces electronic and vibrational transitions in surface materials that allows the unique identification of the surface materials present in some cases. Models of macroscopic surface effects are currently being developed, to help in the identification process.

Two types of imaging instrument are described, a line array instrument (GER - II scanner) and an area array instrument (AIS - 1). Each instrument has advantages and disadvantages in its use, depending on the application.

Problems exist in using high spectral resolution data, especially in areas concerned with atmospheric effects, instrumental peculiarities and macroscopic surface effects.

1.7 Conclusions.

(1) It has been proven (Abrams and Goetz, 1985) that high spectral resolution data can be used to uniquely identify surface materials.

(2) Although the data in its basic processed form is suitable for analysis and identification, the accuracy of identification could be improved by modelling the ground macroscopic effects where possible.

(3) Work on modelling the atmosphere would improve identification accuracy, especially when the surface material to be studied has spectral features of use for identification, in areas of atmospheric absorption (Kruse and Clark, 1986).

CHAPTER 2

IMAGING SPECTROMETERS.

2.1 Introduction.

In chapter one, the basic mechanics, instrumentation and operation of imaging spectrometers were discussed. Two very different instruments were referenced, the Airborne Imaging Spectrometer (AIS) and the Geophysical Environmental Research (GER) imaging spectrometer.

The Airborne Imaging Spectrometer was the first of a series of experimental imaging spectrometer instruments developed by the Jet Propulsion Laboratory (JPL) in California and provided a basis for the development of later instruments. Data from this instrument, collected during the US-Australia Joint Scanner Project in 1985, were used to establish the basic techniques for data preparation and processing, described later in this thesis.

The GER instrument is of quite different design to the AIS instrument and can be considered to be a second generation instrument. The spectral range and swath width of the instrument are much greater. The data from this instrument was initially used to determine the effectiveness of the techniques established for the AIS - 1 instrument and secondly to determine how the variations in the operating parameters such as spectral width of each band affected the identification of surface components.

Many other imaging spectrometer instruments are now in use, however, the discussion below is confined to the two instruments for which data is available.

2.2 AIS - 1 instrumentation.

Details of the instrument design and operation have been published (Jet Propulsion Laboratory, 1985). The AIS - 1 instrument consists of four major elements, the optics, diffraction grating, detector array and electronics.

2.2.1 Optics.

The optical layout is shown in figure 2.1. Incoming radiation passes through an entrance window which contains a coloured glass filter. This filter transmits 80% of the radiation in the wavelength region 1.2μm to 2.4μm and acts as a blocking filter for wavelengths shorter than 1.2μm, preventing second order diffraction effects associated with leakage of these shorter wavelengths into the system.

The radiation is reflected by the gold coated mirrors of the fore-optics (M1 and M2) and focused on a small slit (4.23mm x 0.142mm), which forms the entrance to the spectrometer.

2.2.2 Diffraction grating.

The radiation passing through the slit is reflected from the spectrometer primary mirror (M3) which is also gold coated, onto the diffraction grating. The grating is a reflective diffraction grating which disperses the radiation onto the mirror (M4). This mirror focuses the dispersed radiation on the 32 x 32 element area array of detectors.

Thirty two cross track pixels are imaged simultaneously (figure 2.2), the radiation is dispersed by the diffraction grating to give thirty two separate wavelength bands, covering the 1.2μm to 1.5μm wavelength region. To obtain the full 128 bands covering the whole wavelength range from 1.2μm to 2.4μm, it is necessary to move the diffraction grating through four positions 0.42 degrees apart, while imaging the same thirty two cross track pixels (for details, see Table 2, nominal operating parameters).

2.2.3 Detector array.

The radiation from the diffraction grating is focused by a gold coated mirror (M4) onto the detector array. The radiation passes through a coloured glass filter that cuts off stray radiation from longer wavelengths outside the operating range. The detector array is a 32 x 32 element Mercury Cadmium Telluride ($HgCdTe$) area array.

2.2.4 Electronics.

The electronics sub-system is shown schematically in figure 2.3. Commands to control the AIS can be entered from a control panel. The electronics control the detectors and provide control for the grating drive and tape recorder. Data from the 32 x 32 area array is transferred onto two parallel

13
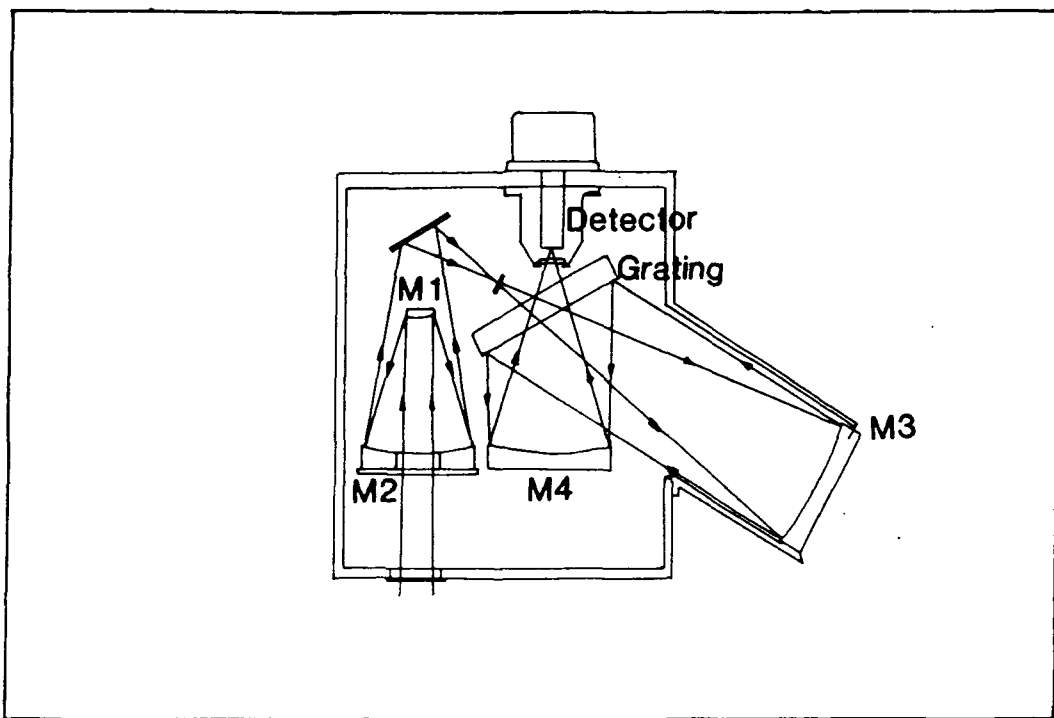
Figure 2.1   AIS - 1 optical layout. Note that the diffraction grating is a
reflective grating. After Jet Propulsion Laboratory, 1985.
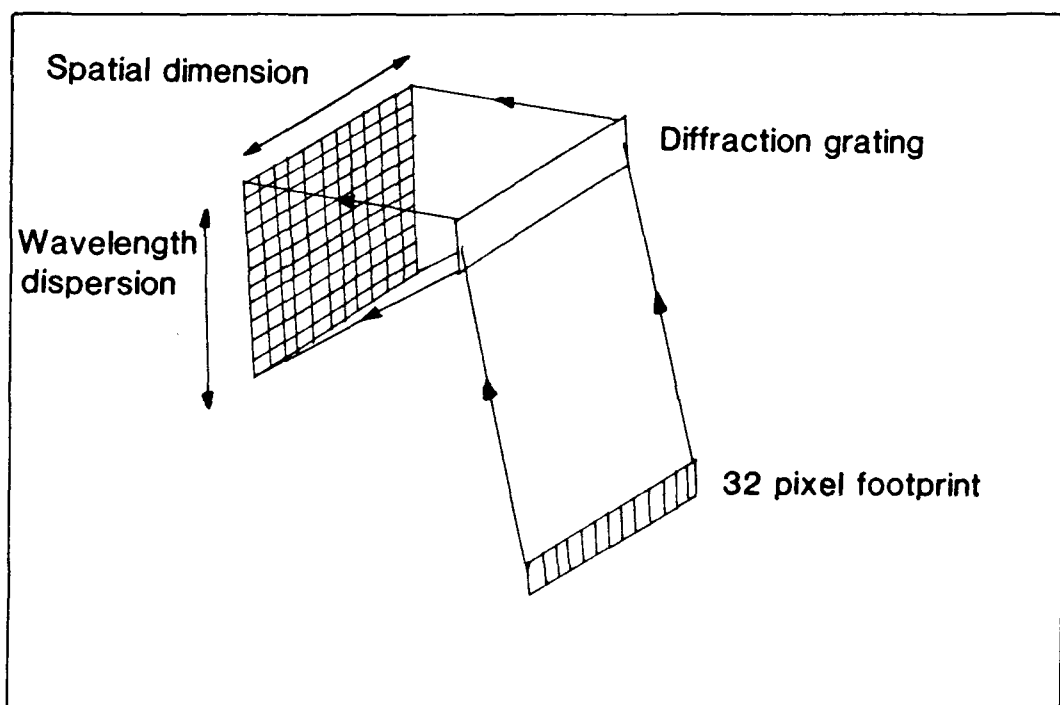
Figure 2.2   AIS - 1 area array of detectors. The 32 pixel wide footprint
is imaged and the radiation diffracted onto the area array.

AIS - 1 FLIGHT PARAMETERS	
1FOV	1.9 m RAD
FOV	3.7 degrees
61FOV at 6 km	12 m
Swath at 6 km	400 m
Spectral coverage	9.3 nm per band
Number of bands	128
Grating positions	
GPOS 0	0.9 - 1.2 μm
GPOS 1	1.2 - 1.5 μm
GPOS 2	1.5 - 1.8 μm
GPOS 3	1.8 - 2.1 μm
GPOS 4	2.1 - 2.4 μm

Table 2.

Figure 2.3   AIS - 1 electronics functional block diagram. Note that the data from the focal plane array is sent along two parallel signal chains. This proved to be the source of a data quality problem, outlined in the text. After Jet Propulsion Laboratory, 1985.
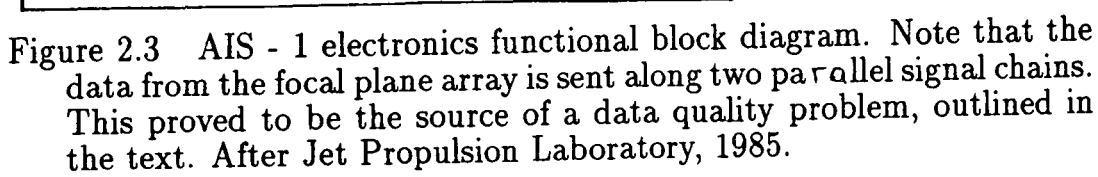
signal chains, half the array output going to each signal chain. This splitting of the output is the source of one of the noise problems observed in the AIS data, producing data spikes in bands 16, 32, 48, 64, 80, 96, 112 and 128, at each half array boundary. The spikes may be due to using calibration files that produce discontinuities at the array and half array boundaries, as suggested by Conel et al. (1986). The data from the two signal chains is multiplexed to an 8 bit analog to digital converter and recorded on tape.

2.3   Instrument calibration and data pre-processing.

The instrument calibration consists of a spectral alignment of the detector array and a detector response equalisation procedure, necessary to correct for the varying response of each detector in the 32 x 32 array (Tucker and Vane, 1986).

The spectral alignment consists of illuminating the detector array via the diffraction grating, with a specified wavelength of light from a monochromator, previously calibrated using a mercury vapour lamp. The array is moved until a chosen detector in a line of 32 detectors is illuminated centrally. The wavelengths at the beginning and end of this line of detectors are then determined to define the wavelength end points of the detector array. The accuracy of the alignment varies due to the difficulty of centrally locating the illumination on the chosen detector and due to the viewing geometry of the laboratory calibration set up (Tucker and Vane, 1986). A check on the accuracy of alignment can be made by observing known spectral features in the data, such as the atmospheric CO_2 absorptions at 2.00μm and 2.06μm(Lyon, 1986). If they are shifted a corresponding shift to the start and end wavelengths of the detector array should be made.

The detector response equalisation procedure corrects for the variation in detector response within the area array to a constant standard illumination. A calibrated light cannon provides a uniform source of irradiance which illuminates the detector array. Variations in the detector response as the light cannon is switched through ten different radiance levels are used to construct light transfer curves. Multipliers are generated, based on these curves, to correct for the non-linear response of the detectors (Conel et al., 1986).

After data collection the data is pre-processed at Jet Propulsion Laboratory (JPL). The eight recorded data bits are first of all placed back in their positions relative to the original twelve bit word (Jet Propulsion Laboratory, 1985) and stored in a sixteen bit (integer x 2) computer format.

The pre-processing operations are then performed using real numbers to maintain precision, these operations are

(1) Corrections are made for dark current variations recorded during the flight.

(2) "DEAD" elements producing zero signal values (figure 2.4), have their values replaced by simple linear interpolation across the "DEAD" elements. This doubles the sampling interval and reduces identification accuracy as the true data is not available for the interpolated element. Figure 2.5 shows the "DEAD" elements in the area array, and demonstrates the high number of "DEAD" elements in column 32.

(3) Despiking of the data to remove the effects of electronics noise is made using a nearest neighbour despiking algorithm.

(4) Variations in detector response are removed using the ground calibration light curve multipliers.

(5) The effects of the solar irradiance curve are removed from the data using the curve of a 5900   Kelvins blackbody.

The output from these operations are mapped back into a sixteen bit (integer x 2) computer format for distribution. The operations performed on the data tend to extend the data range from the original twelve bits to thirteen bits. The data is then sent to the investigator in its final format shown in figure 2.6.

2.4 Problems of operation.

The AIS - 1 instrument was flown extensively in both the United States and Australia during the time period December 1982 until April 1986. Several data quality problems were evident on examination of the collected data (Huntington et al., 1986). The major observed problems are listed below, they are,

(1) Vertical striping.
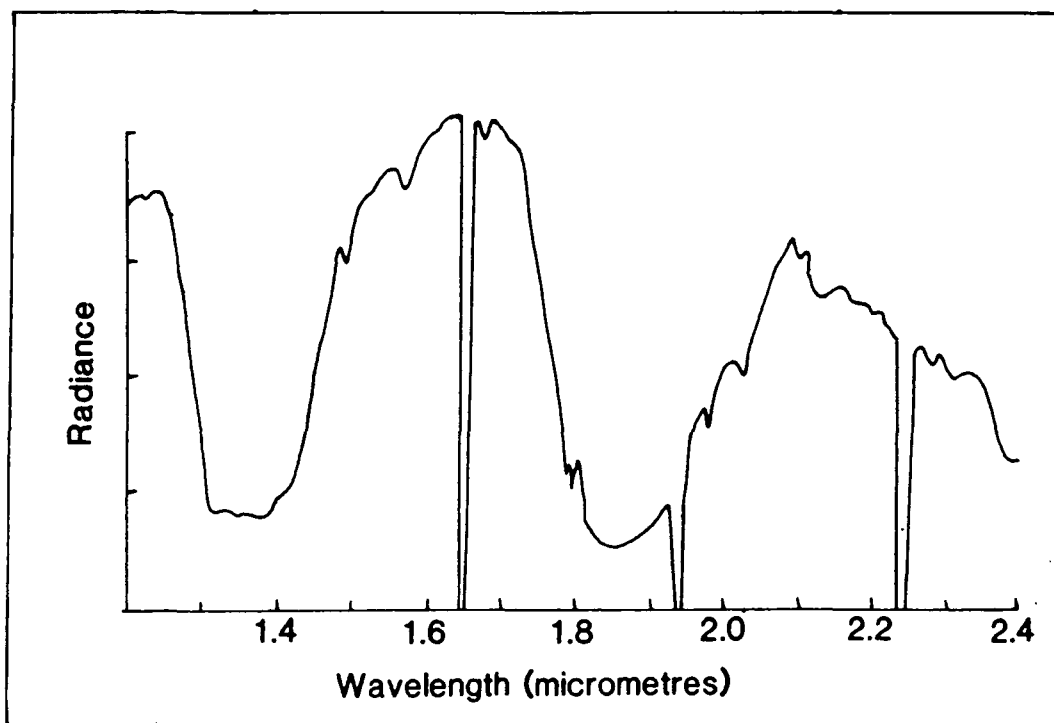
Figure 2.4   Non-functioning detector elements are present in the area array. They produce spectral "holes" that are removed by interpolating across the "holes". This reduces the spectral sampling interval in the area of the "hole".
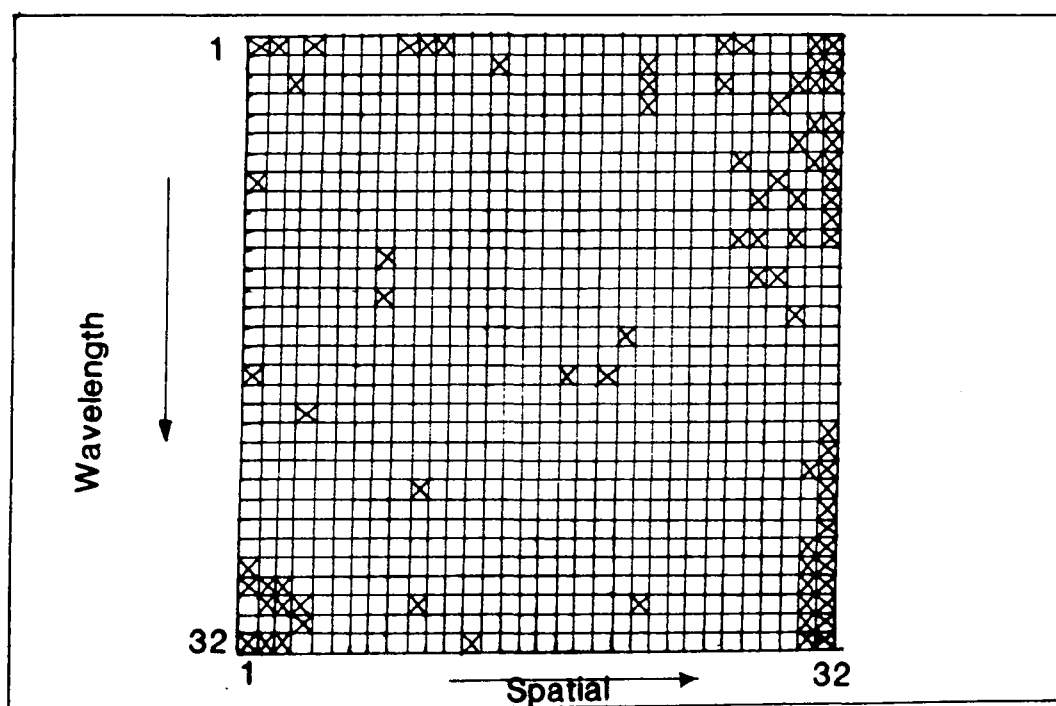
Figure 2.5   Laboratory calibration of the AIS detector array, revealed the presence of many non-functioning detector elements (marked by an "X" above), especially in column 32 of the array. After Jet Propulsion Laboratory, 1985.
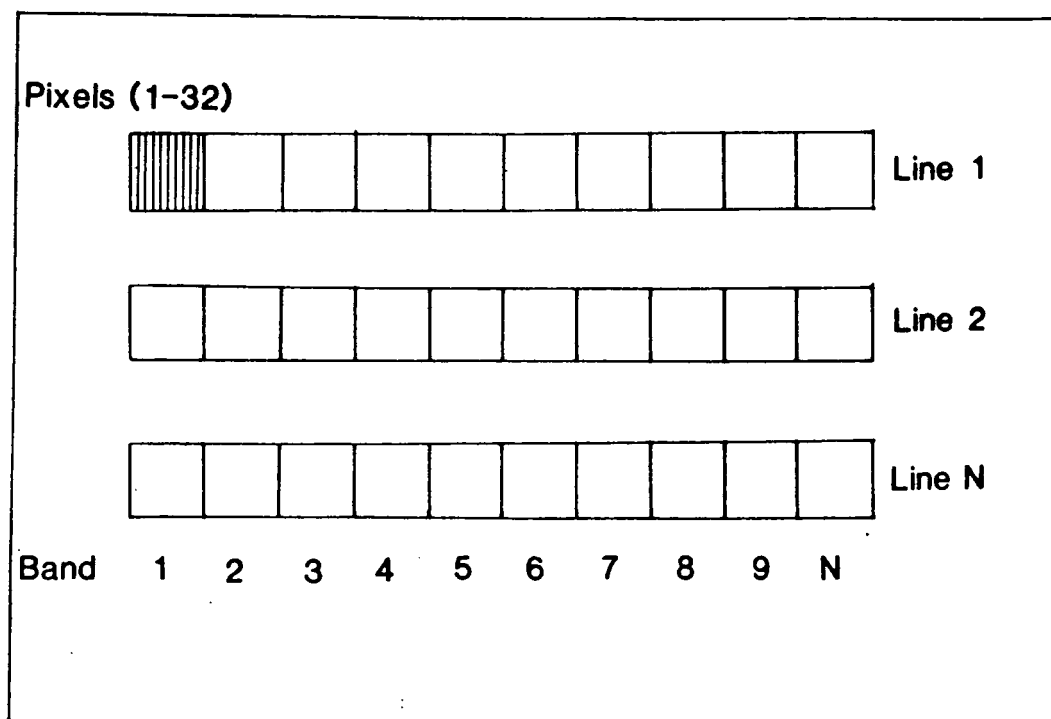
Figure 2.6   The AIS - 1 data format. It consists of one line of data per tape block. Each line contains all 128 bands for that line of 32 pixels on the ground.
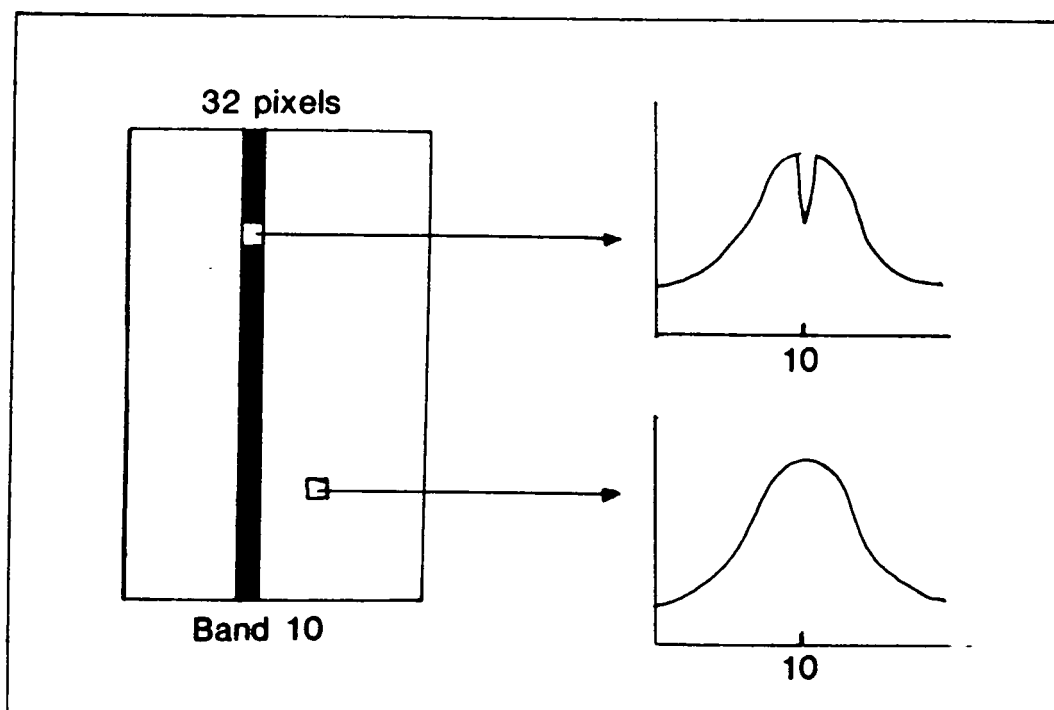
Figure 2.7   A darker column in band 10, produces a corresponding drop in the spectral response for a pixel from that darker column. The same material from a pixel in a lighter column does not show this decrease in response in band 10.

(2) Horizontal striping.

(3) Second order overlap.

(4) Data spikes.

(5) Random noise and geometric distortion.

2.4.1 Vertical striping.

This striping (plate 2.1) is due to inadequate detector response equalisation. The cause seems to be due to a change in response of individual detectors performance after the laboratory calibration file was constructed (Vane, 1986). Huntington et al. noted that a time varying response can be observed in some data along the flight line, which suggests a lack of detector stability.

The lack of suitable detector response equalisation can produce a variation in spectral curve shape of the same mineral, taken from two separate columns of different brightness, in the same band. In figure 2.7 we can see this effect. Two pixels of the **same** material, taken from two separate columns, will have different spectral responses in band 10, due to the vertical striping.

2.4.2 Horizontal striping.

The cause of this striping (plate 2.1) was traced to an inadequately secured detector array, which vibrated around the focal plane of the spectrometer during the flights. The effects of this vibration are discussed by Vane and Goetz (1988). The vibration tends to reduce the spectral and spatial resolution of the system and produces line by line wavelength shifts. Figures 2.8 and 2.9 show the effects of the vibration.

The offsets also affect the results of any spatial averaging techniques made over several lines, if the pixels making up the average spectra consist of those with features centred on 2.2μm and those with features centred on 2.18μm the average spectrum will be broader and centred on 2.19μm.

2.4.3 Second order overlap.

Second order overlap is discussed in some depth by Conel et al. (1986) and Cocks and Green (1986). The effect occurs by the spectral mixing of light of two different wavelengths, due to the way light is diffracted by the diffraction grating, this is related to the efficiency of the diffraction grating and its construction parameters. Light of a chosen wavelength is diffracted
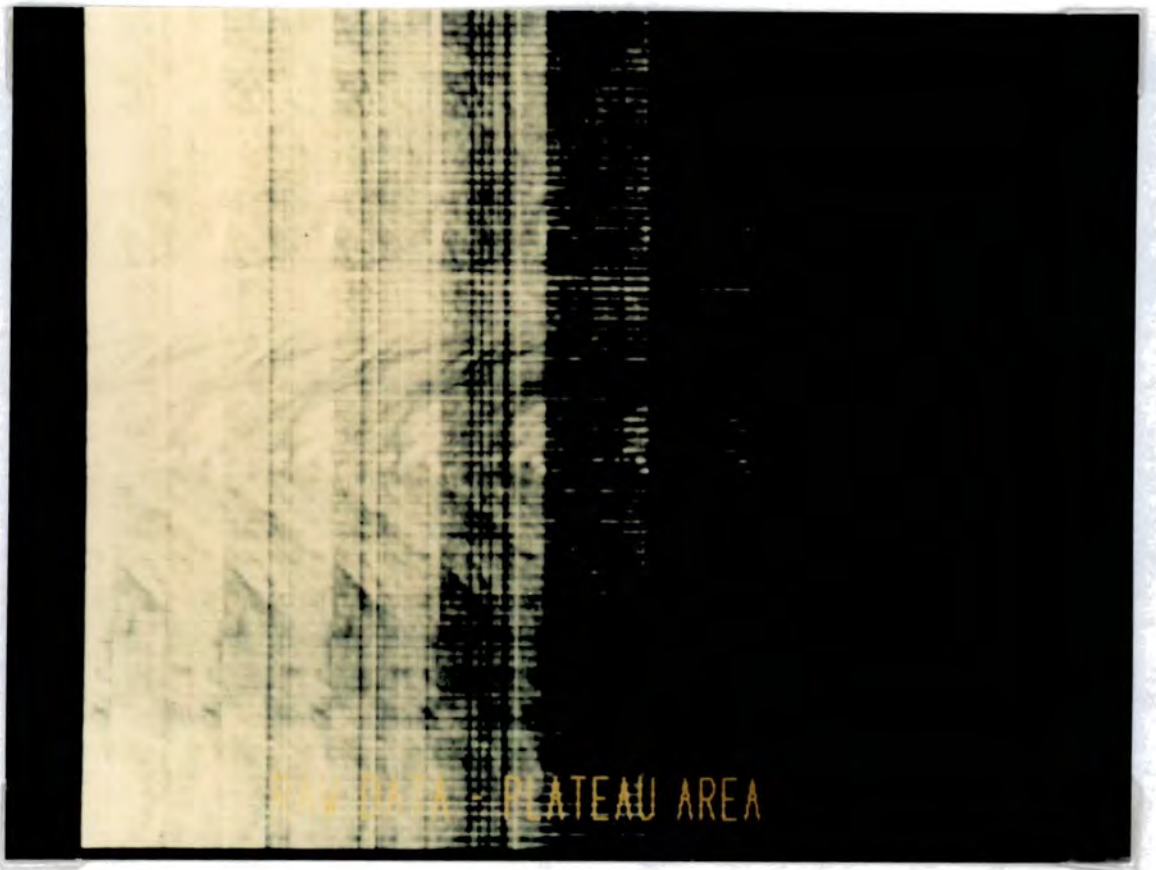
Plate 2.1 Vertical and horizontal striping is clearly visible in the AIS -
1 data, **after** the calibration steps have taken place.
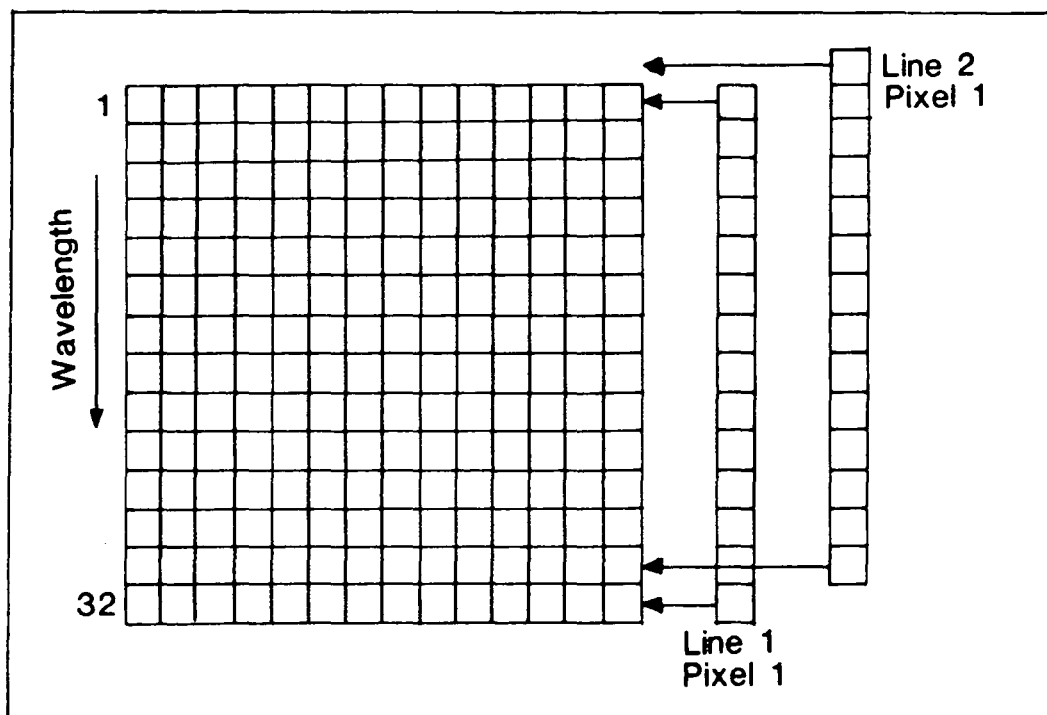
Figure 2.8 The vibrating detector array can move within the focal plane of the instrument, so that the diffracted radiation for a particular wavelength does not always impinge on the same detector. Producing wavelength shifts in the output data.
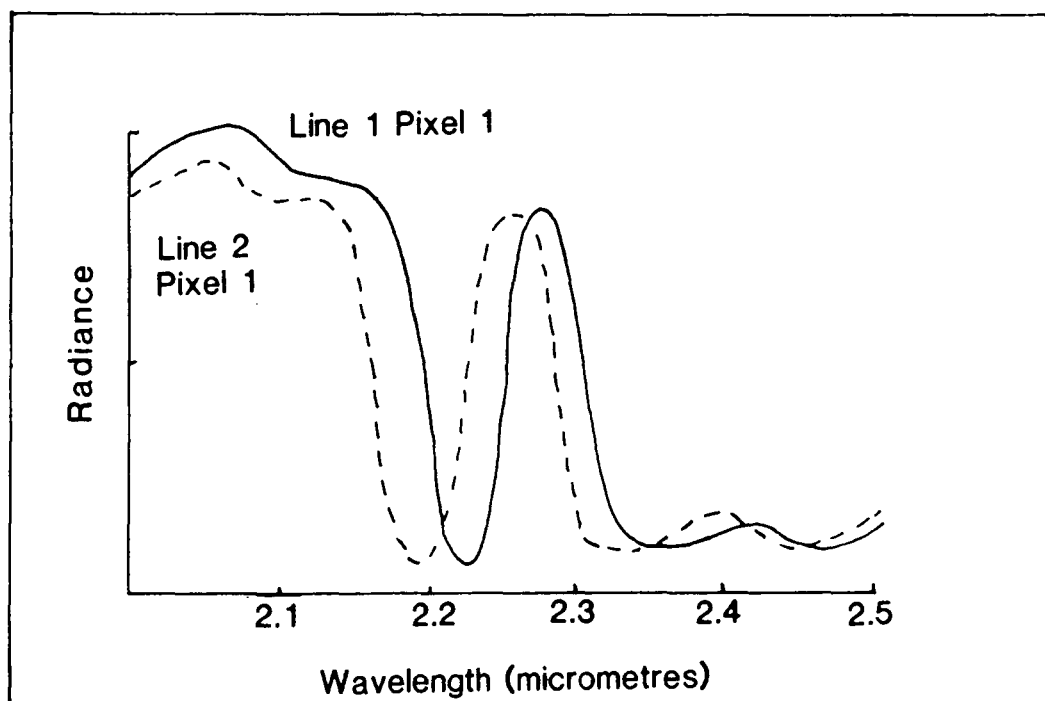
Figure 2.9 The effects of the detector array movement and corresponding wavelength shifts are shown for the mineral sericite. The diagnostic absorptions are shifted 20nm, preventing accurate identification based on absorption position.

The second order effect can be explained by reference to the following. When a wave front passes through a diffraction grating, constructive interference takes place when the path length of the diffracted light through the grating

$$p = n \lambda$$

Where n = an integer
     λ = a wavelength of light

The angle of diffraction

$$\text{Sin } \Theta_n = \frac{n \lambda}{s}$$

Where s = diffraction grating spacing

As n is increased, the angle of diffraction is also increased, the primary diffraction angle is called the first order diffraction, the larger diffraction angles are related to the higher orders, second, third etc.

So when we have two wavelengths of light where

$$\lambda_1 = 2\lambda_2$$

Then

$$\text{Sin}\Theta_1 = \frac{1 \lambda_1}{s} = \frac{2 \lambda_2}{s}$$

Therfore, the second order radiation for the shorter wavelength λ_2 will be diffracted at the same angle as the first order radiation from the longer wavelength λ_1.

through a known angle by a particular diffraction grating set up. However, light with a wavelength exactly half of the chosen wavelength will also have a component diffracted through the same angle. This overlap of the chosen wavelength and that component with a wavelength half the chosen value is called second order overlap (figure 2.10). See facing page.

In the case of the AIS - 1 instrument the design specified a wavelength range from 1.2μm to 2.4μm, with a blocking filter placed in the optics train to prevent the leakage of shorter wavelength radiation (shorter than 1.2μm) which could create second order overlap. However, in late 1983 the AIS - 1 instrument was adapted to measure wavelengths down to 0.9μm , for botanical studies. The blocking filter was changed to prevent leakage of wavelengths shorter than 0.8μm to cover the extended wavelength range. Laboratory tests suggested a minor second order overlap problem was present in the 1.6μm to 2.4μm wavelength region, with an additive secondary component of a few percent. Later data collection and laboratory rechecking of the instrument proved that the initial calculations of the size of the secondary component were incorrect and that the additive component could be of the order of several tens of percent (Vane, 1986). This contamination is evident in all data collected after 1983, which includes the data used in this study.

The effects of order overlap were modelled by Cocks and Green (1986) for a green vegetated surface (figure 2.11a) and for the mineral kaolinite (figure 2.11b. plate 2.2 shows some actual spectra obtained during the US-Australia joint scanner campaign for the AIS - 1 instrument. Plate 2.2 is compared with the modelled spectra of figures 2.11a and 2.11b, some of the additional effects of second order overlap are clearly visible. Firstly, the increase in slope of the peak between 1.6μm and 1.8μm. Secondly, there is a small bump on the left hand edge of the water absorption centred at 1.9μm. This infilling of the water absorption feature is shown clearly in the theoretical modelled data of figures 2.11a and 2.11b and practically in the AIS - 1 data shown in plate 2.2.

The effects of the order overlap problem are variable. They are dependent on the brightness of the materials in the 0.8μm to 1.2μm wavelength region. Bright materials in this region produce a much larger second order additive component than dark materials. The additive component will infill features in
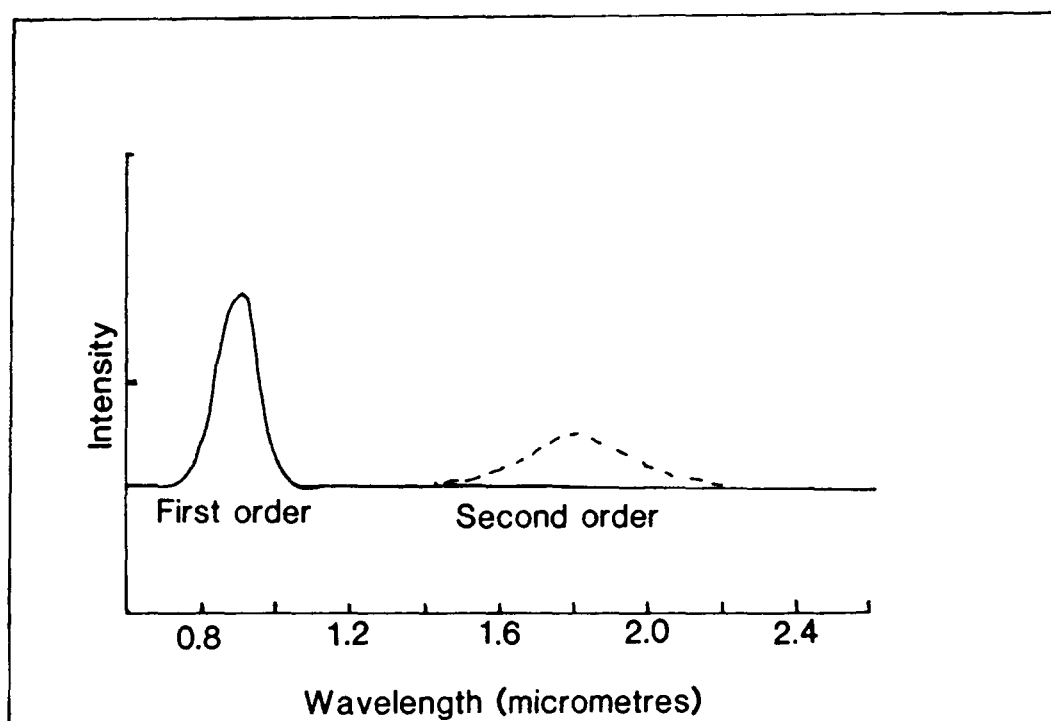
Figure 2.10   The placing of a blocking filter at $0.8\mu m$ in the AIS - 1 instrument, produced second order radiation effects that reduce data quality. After Vane, 1986.
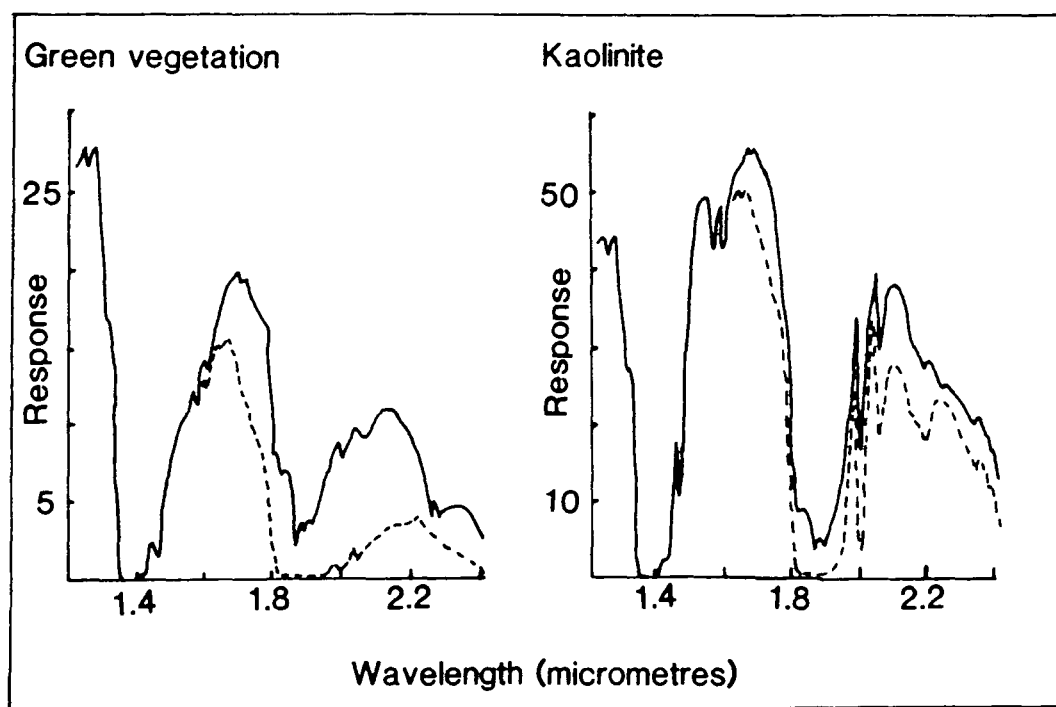
Figure 2.11   The spectral response of a green vegetated surface and the mineral kaolinite are shown, with second order overlap effects (solid line) and without second order effects (dotted line). The curves shown are based on modelling carried out by CSIRO. After Cocks and Green, 1986.
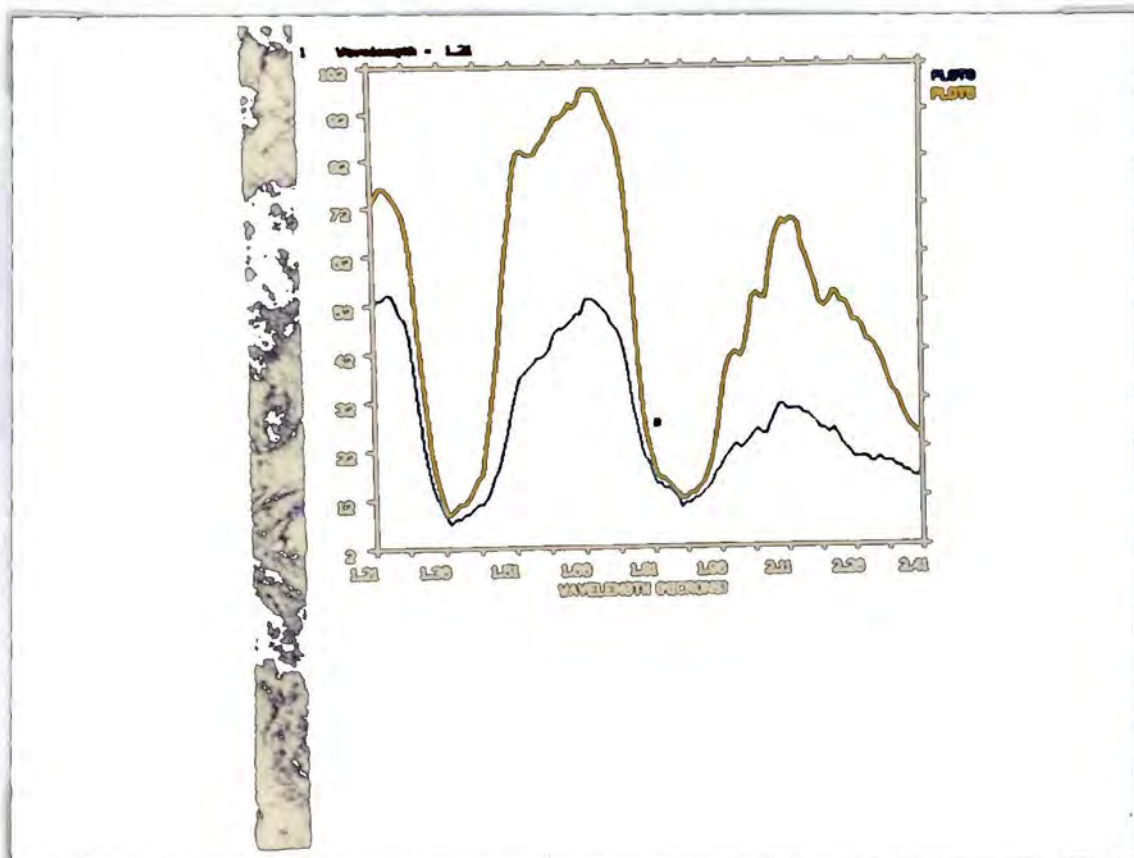
Plate 2.2 Two AIS - 1 spectra, showing the effects of second order overlap. Note the small "bump" on the left hand side of the water absorption feature at 1.85μm, below the red cursor.
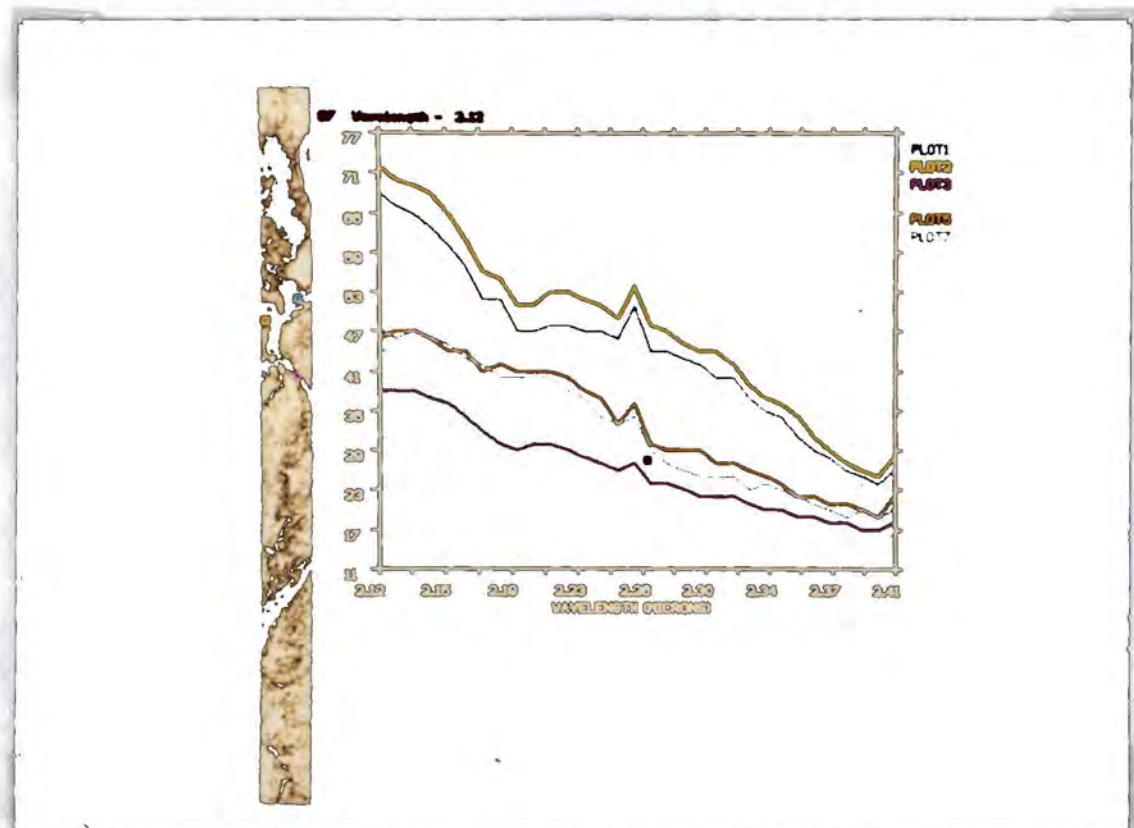
Plate 2.3 Data spikes, located at each array and half array boundary. They may be related to electronics noise, or to discontinuities in the calibration files of the detectors (Conel et al., 1986).

the 1.6μm to 2.4μm wavelength region. Spectral absorptions in the 0.8μm to 1.2μm region will also be represented, albeit on a smaller scale, in the 1.6μm to 2.4μm region, reducing identification accuracy.

Without additional information on the brightness of the surface materials in the 0.8μm to 1.2μm wavelength region, no correction is possible to remove these additive second order effects.

2.4.4 Data spikes.

These data spikes were observed in the data set (plate 2.3) collected during the US - Australia joint scanner project in October 1985. The spikes were not removed by the nearest neighbour despiking algorithm used by JPL as a pre-processing step due to their presence in every pixel. The data spikes occur in particular bands (16, 32, 48, 64, 80, 96, 112, 128). These bands are located at the 16th and 32nd detector in the area array in the spectral (wavelength) direction. The data from the detector array is read off in two halves and sent through two separate signal chains. The spikes may be related to discontinuities caused by poor calibration of the instrument across half array and array boundaries (Conel et al., 1986). The effect is such that the data from these bands cannot be reconstructed, therefore simple spectral interpolation across the spikes was used to remove them.

2.4.5 Random noise and geometric distortion.

Two other data quality problems were noted while studying the data set. Firstly the low signal to noise ratios of the data set. Noise peaks were very noticeable in the data, producing confusing effects when trying to identify the mineral spectra. Secondly the geometric distortion of the data caused by the plane banking and veering during the flight, which led to great difficulty in identifying position in the imagery and reduced the spectral quality of the recorded data.

2.5 GER - II instrumentation.

The instrument data parameters are shown in table 3. Those given are for a nominal flying height of 6060m.

The instrument design is shown in figure 2.12 and is described in detail by Collins and Chang (1988). This instrument differs from the AIS - 1 imaging

```
+--------------------------------------------------------------+
|                 GER - II  FLIGHT PARAMETERS                  |
+--------------------------------------------------------------+
|                                                              |
|  IFOV (Variable)            2.5 mRAD (0.14°)                 |
|                             3.3 mRAD (0.19°)                 |
|                             4.6 mRAD (0.26°)                 |
|                                                              |
|                                                              |
|  GIFOV at 6 km              15m                               |
|     (Variable)                                               |
|                             20m                              |
|                             27m                              |
|                                                              |
|  Spectrometer 1                                              |
|     -  Number of bands                 24                    |
|     -  Spectral coverage per band     25.4nm                 |
|     -  Total spectral coverage     0.49-1.083μm              |
|                                                              |
|  Spectrometer 2                                              |
|     -  Number of bands                  7                    |
|     -  Spectral coverage per band     120nm                  |
|     -  Total spectral coverage     1.08-1.80μm               |
|                                                              |
|  Spectrometer 3                                              |
|     -  Number of bands                 32                    |
|     -  Spectral coverage per band     16.5nm                 |
|     -  Total spectral coverage     1.98-2.49μm               |
|                                                              |
+--------------------------------------------------------------+
```

Table 3.
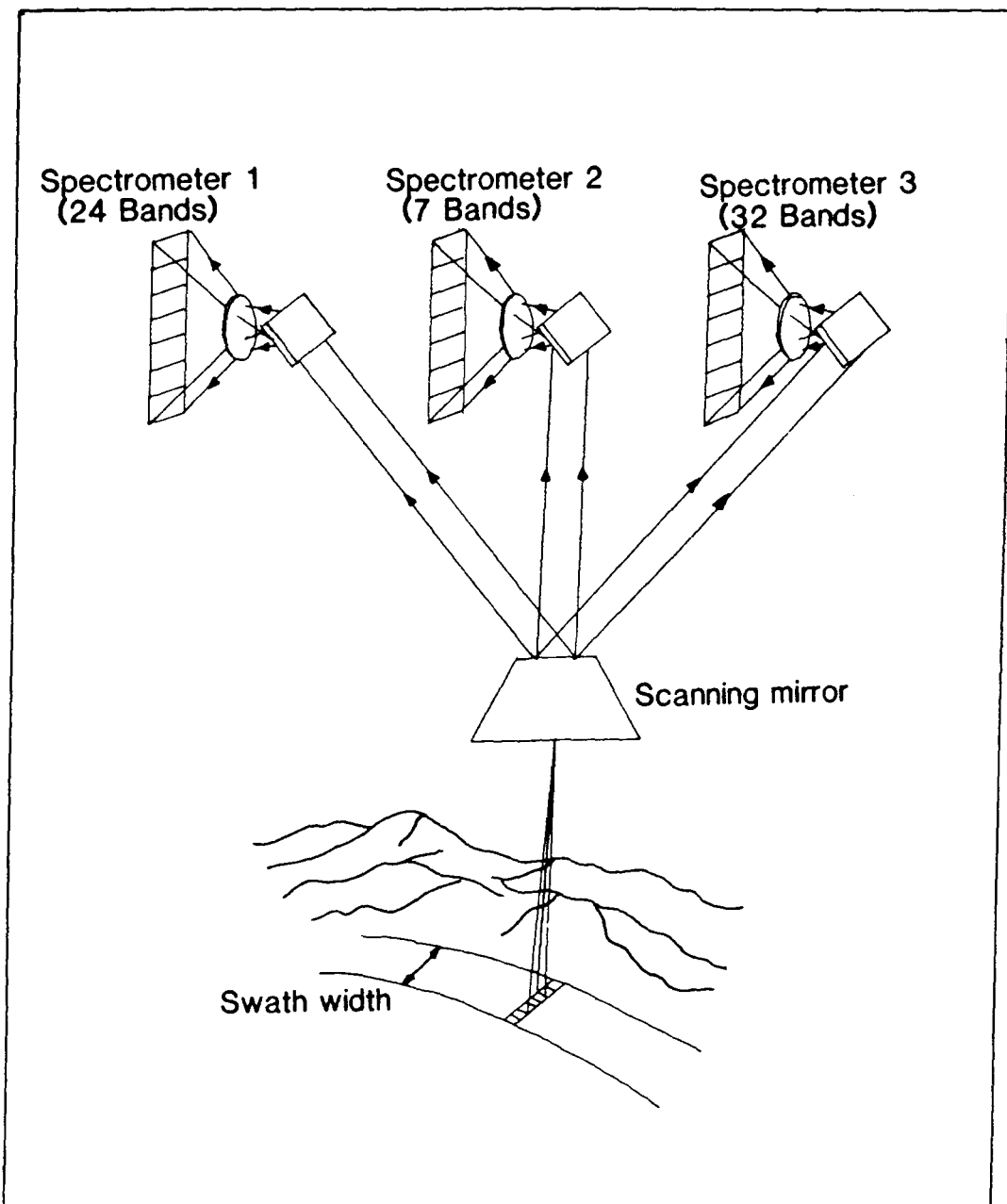
Figure 2.12   An outline schematic of the GER - II scanner. Radiation from a single pixel on the ground is split and sent to all three spectrometers. The radiation is dispersed by the diffraction gratings onto three seperate line arrays of detectors, one for each spectrometer.

spectrometer in that it is a scanning instrument, sending its output to three separate spectrometers with three separate line arrays of detectors.

A schematic diagram showing the geometry of the scan is seen in figure 2.13. The total scan angle is 90 degrees (plus or minus 45 degrees off nadir). The instantaneous field of view (IFOV) of the instrument depends on the aperture size, which can be one of three settings.

A single pixel is imaged at a time the radiation passes through the optics of the instrument onto a rotating cube with silvered mirrors on each face. The incoming radiation is split and sent to three separate diffraction gratings (figure 2.14) which disperse the radiation onto the line arrays of detectors.

The design of each diffraction grating is slightly different, leading to different output bandwidths for each wavelength region. The result is a non-contiguous data set with different bandwidths for each spectrometer, unlike the AIS - 1 instrument which provides contiguous data with a constant bandwidth across all recorded wavelengths.

2.6   Instrument calibration and data pre-processing.

Prior to distributing the acquired data, Geophysical Environmental Research (GER) calibrate and pre-process the data. A brief outline of the steps involved is given below,

(1) The data is translated from the aircraft system to a suitable computer format.

(2) The horizontal striping effects of the scanner are removed, by reference to the zero signal (DARK current) measured for each scan line.

(3) The instrument counts are converted to radiance using a calibration standard, traceable to the Bureau of standards radiance source.

(4) The system gyro information for each pixel (stored in band 64) is used to correct each pixel for aircraft roll movements.

(5) An electronic time constant correction is made to remove signal lag which sharpens the image.

(6) The interleaved data is separated into 63 separate images prior to distribution to the users.
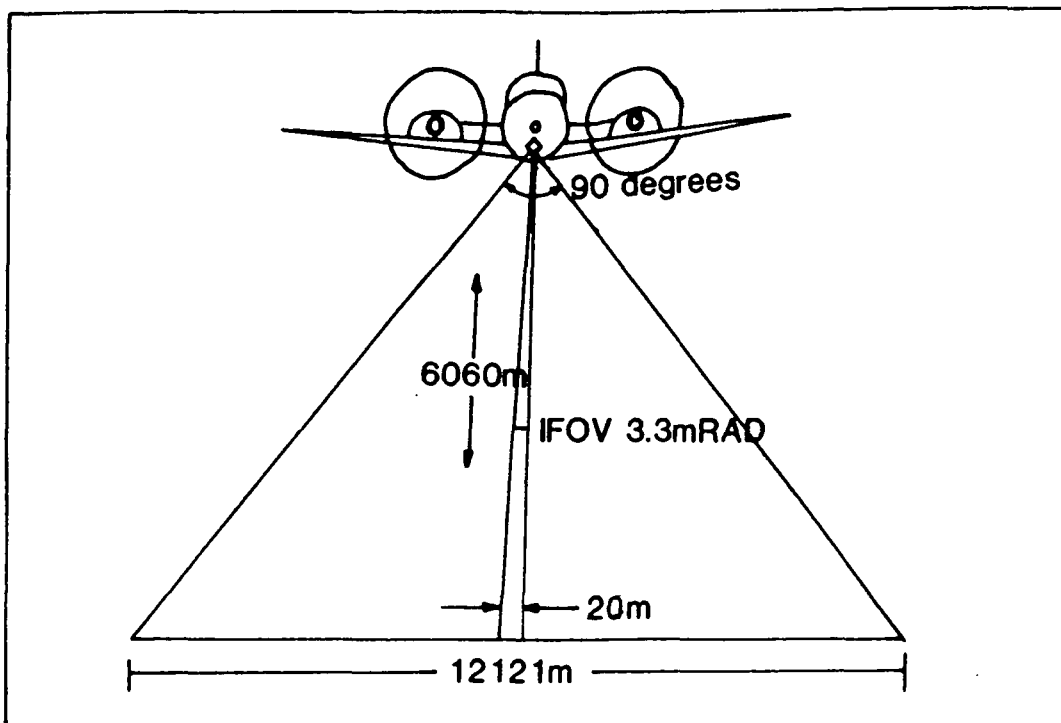
Figure 2.13   The geometry of the scan of the GER - II instrument is shown for a field of view of 3.3mRAD.
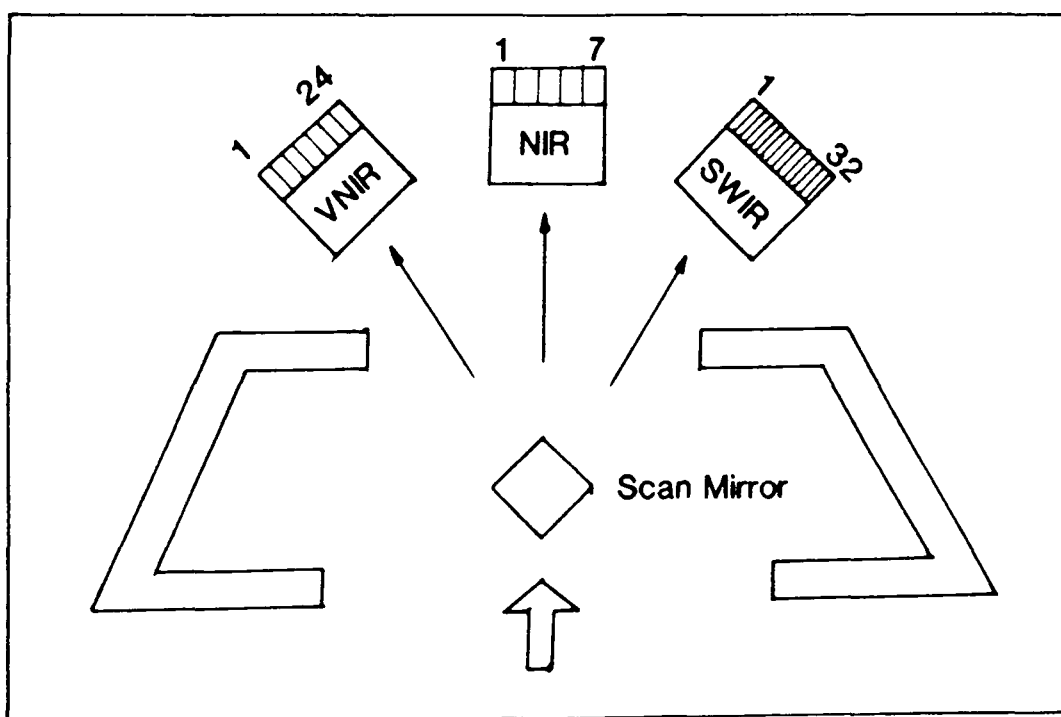
Figure 2.14   The incoming radiation is split and sent to three different spectrometers, which disperse the radiation on to the three line arrays of detectors.

2.7 Problems of operation.

The GER - II scanner has been flown in the United States and Australia. It was noted that even after calibration and pre-processing there were still data quality problems. These include,

(1) Cross-track shading.

(2) Horizontal striping.

(3) Geometric distortion.

(4) Random noise.

(5) Second order overlap.

2.7.1 Cross-track shading.

Cross-track shading was observed in the visible bands of the GER - II scanner data (plate 2.4). The effect may be due to a combination of atmospheric and macroscopic surface effects. The atmospheric effects of Mie scattering combined with anisotropic particulate scattering, related to variations in the sun - sensor geometry during scanning (Abrams, 1985), could produce these strong visual shading effects. The effects are shown in figure 2.15. A pixel taken from the brighter edge will be brighter in the visible bands, where the effect is very strong and relatively unchanged in the infrared bands. A pixel taken from the darker edge will be darker in the visible bands and again unchanged in the infrared bands. Thus if the same material is present on either side of the image the spectral response of a pixel taken from these areas will not be directly comparable due to this cross-track shading effect.

2.7.2 Horizontal striping.

In theory after data calibration, no horizontal striping should be evident. Referencing to each scan line dark current, calibration step 2, should eliminate differences between scan lines. However striping is very evident in the data. The residual striping is believed to be due to the switching off and on of the detector cooling system (W.Collins, pers. comm.). The switching takes place at irregular intervals and its effects are therefore difficult to remove. The overall effect is not only to produce line to line variations in intensity, but also large variations in intensity in a single scan line.

The switching on and off of the cooling system of the detectors should affect all the detectors in the array and therefore not affect the overall curve
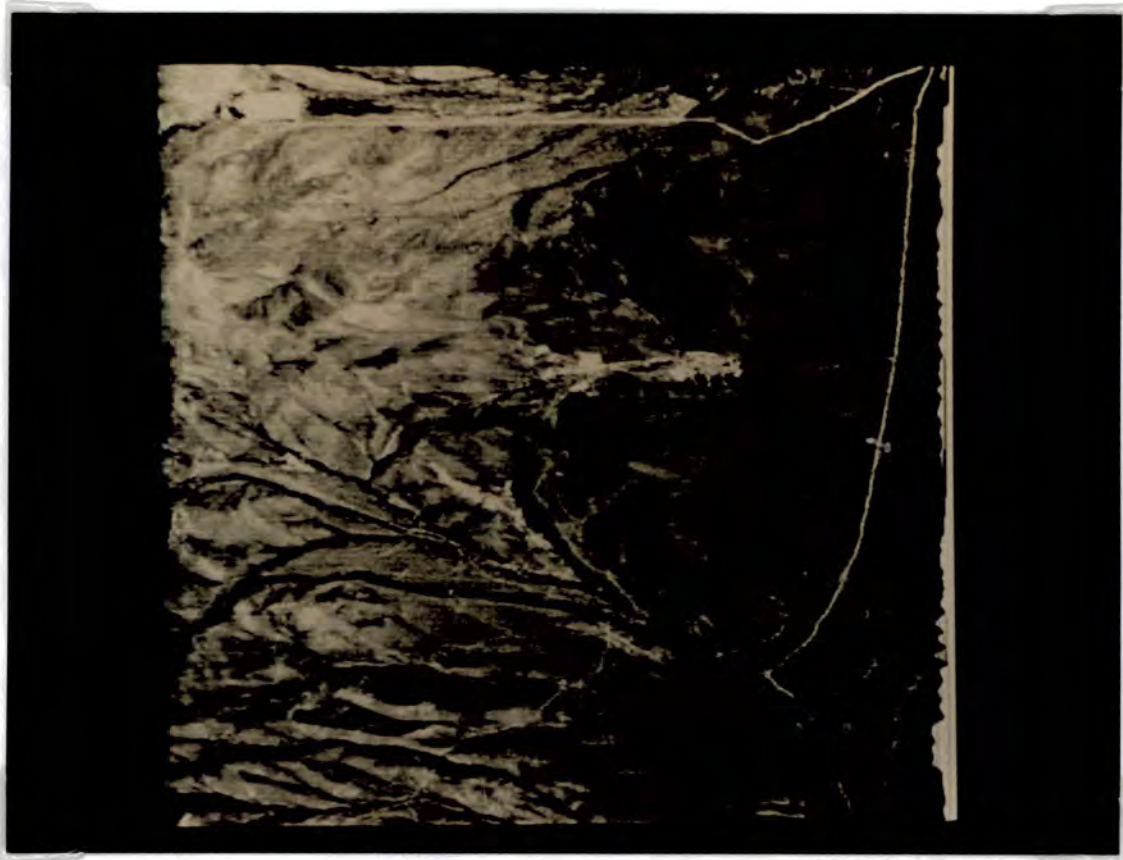
Plate 2.4   Cross track shading. Appears in the visible and near infrared
bands of the GER - II scanner data. It is due to a combination of
atmospheric and macroscopic surface effects for particular sun-sensor
geometries.
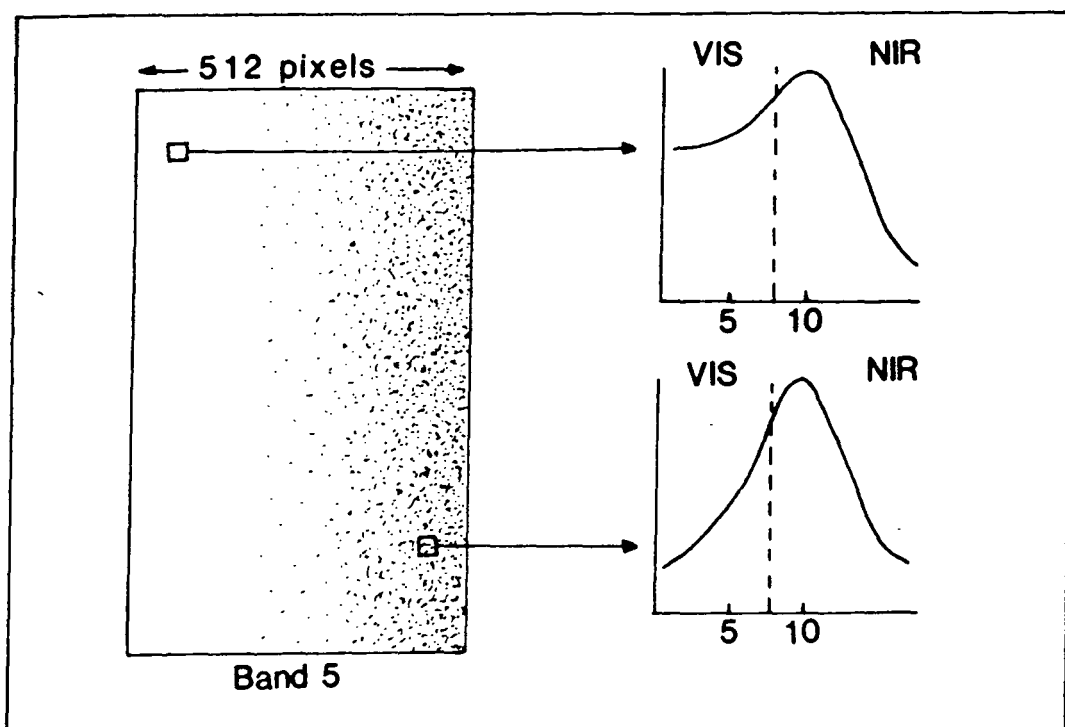
Figure 2.15   The effects of cross-track shading are very noticeable in the visible bands. The same material sampled from each side of the image, will have very different spectral responses in the visible wavelengths.
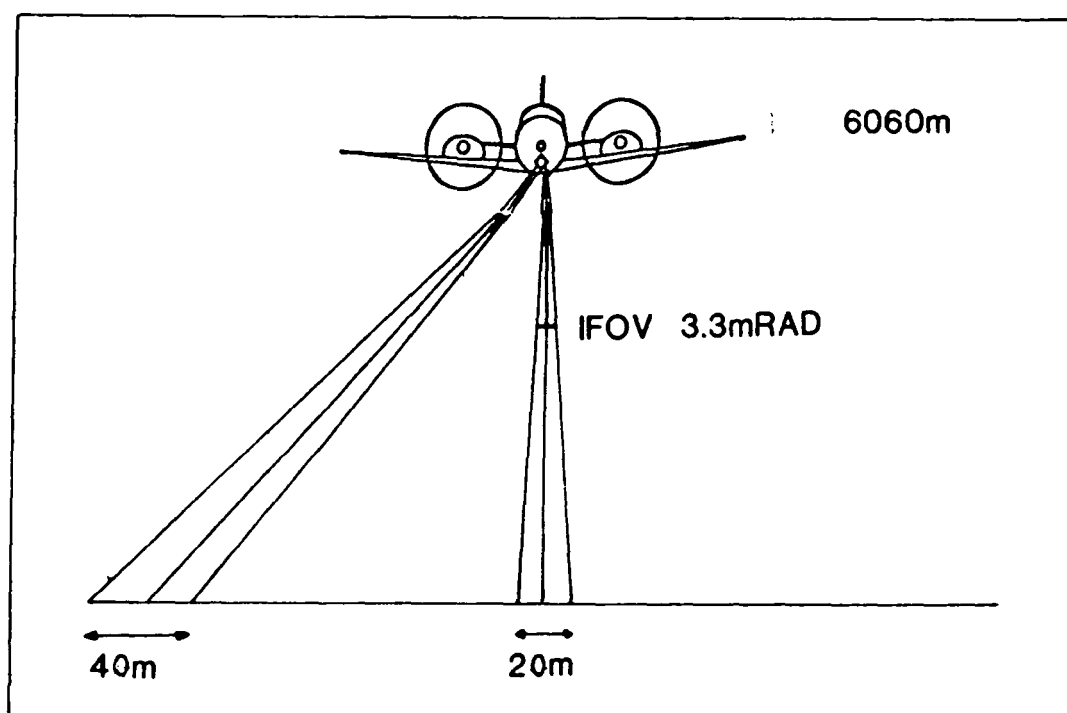
Figure 2.16   The geometry of the scan varies due to scan angle. The area scanned to form a pixel at the edge of the image is much larger than the area scanned directly below the aircraft. On displaying the data as square pixels, we see a compression of the image as we approach the edges.

shape, just its intensity. This has as yet to be confirmed.

2.7.3 Geometric distortion.

One of the major problems of dealing with the wide swath of the GER - II scanner, is the distortion introduced by the scanning process. In figure 2.16 we can see a view of a scan. Although the Instantaneous Field Of View (IFOV) set by the aperture size of the optical system is the same throughout the scan, the area of ground viewed will increase as the scan angle increases. The Ground Instantaneous Field Of View (GIFOV) for an IFOV of 3.3mRAD a flying height of 6060m will vary from 20 metres square at nadir, to 40 metres by 20 at the maximum extent of the scan (45 degrees from nadir). The data from these two very different sizes of ground area are of course recorded as just single data values. On displaying the data as square pixels on an image processing system, only those pixels at nadir will be truly representative of the original geometry on the ground. Those towards the edge of the scene will suffer extreme compression geometrically, to fit the square pixel of the image processing system.

A second effect of the scanning is shown in figure 2.17, where we have the presence of variable topographic relief. Without the hill being present in figure 2.17, the area scanned would be area B. However, due to the presence of the hill the actual area scanned is area A$'$. If we now make a correction purely for the geometric effects of scan angle, area A$'$ will be projected to be at point B, thus distorting the image.

2.7.4 Random noise.

Noise spikes are evident in the data which reduce the identification accuracy of the spectra. In the visible and near infrared wavelength regions, the data quality is very good, with stated signal to noise ratios of up to 5000 to 1 (Collins and Chang, 1988). In the SWIR wavelength region, the stated signal to noise ratios are between 100 to 1 and 500 to 1. However, some bands have very high noise values (Band 59 for example), where the signal to noise ratio is very low. These very noisy bands severely reduce identification accuracy in this important wavelength region, which covers absorption features of carbonates and $Mg - OH$ minerals. At this time, no reason has been established for the low signal to noise characteristics of the last eight bands of
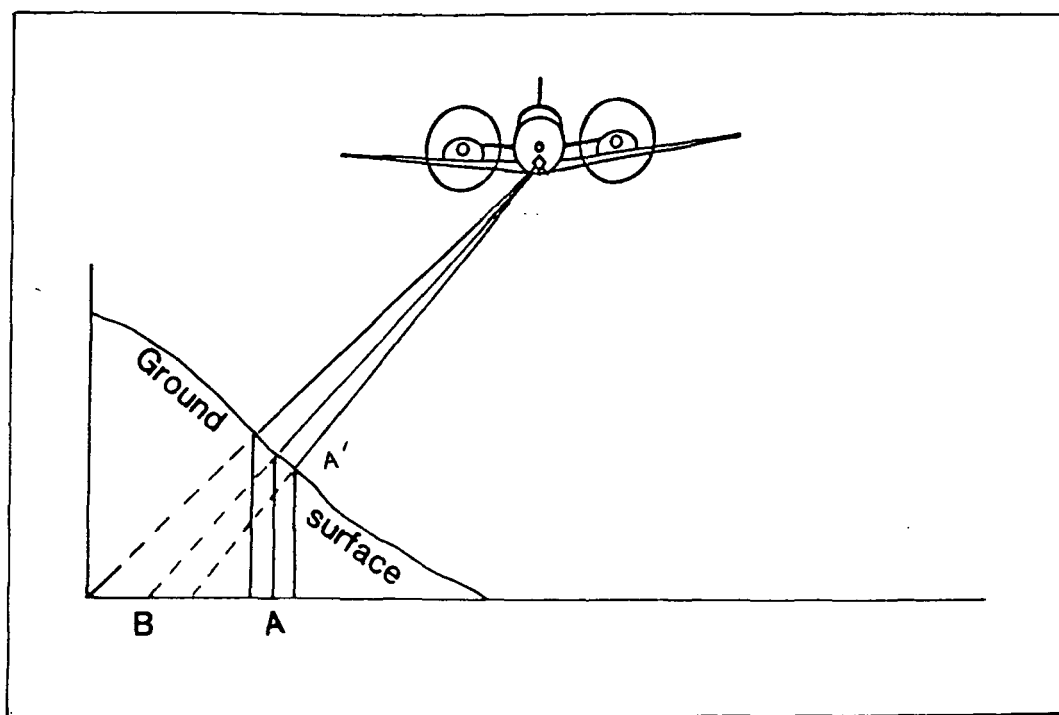
Figure 2.17   The true location of a pixel imaged on a hill side is at point
A, but relative to a flat surface it would be projected to point B. Any
geometric correction for scan angle variation will project the pixel at
point A′ to point B, creating a geometric distortion.

the SWIR data, although it can probably be attributed to the low sensitivity of the detectors at these wavelengths and the lower signal as the amount of solar irradiance decreases in this wavelength region.

2.7.5 Second order overlap.

The GER - II spectrometer number 1 covers the wavelength range 0.449μm to 1.083μm in the data set. In theory second order overlap effects such as those discussed for the AIS - 1 instrument should be present in the data. The effect should be seen from a point twice the starting wavelength of 0.449μm , which is 0.898μm, to the end wavelength of the spectrometer at 1.083μm, a total of about seven bands. Only the first four bands (0.449μm to 0.541μm) will contribute to this second order overlap. Fortunately for our purposes we can ignore these effects, due to the very low signal values of the first four bands of the GER - II data set, which contribute a negligible amount of second order radiation to the longer wavelength regions.

2.8 Summary.

The AIS - 1 is an early area array instrument. Problems due to detector vibration (producing horizontal striping), poor calibration (producing vertical striping), second order overlap and random noise were clearly identified. The GER - II scanner is a line array instrument. Problems were also observed in the GER - II data set, including detector cooling (producing horizontal striping), random noise and geometric distortion.

2.9 Conclusions.

(1) Calibration of the detectors should be improved to prevent problems such as the vertical striping in the AIS - 1 data set.

(2) The effects of the calibration and pre-processing steps should be made clear to all investigators. For example by interpolating across "DEAD" detectors we are doubling the sampling interval and possibly losing data of interest, such as absorption features that would be found at wavelengths covered by the "DEAD" detectors.

(3) A major effort should be made to improve the signal to noise ratios of the instruments as random noise has a direct bearing on identification accuracy.

(4) Algorithms to reduce the effect of geometric distortion are necessary, to accurately identify ground position when checking anomalies. This applies especially to the GER - II data sets, where geometric distortion is an accepted consequence of using this scanning device.

CHAPTER 3

DATA PREPARATION.

3.1 Introduction.

Early attempts to analyse the AIS -1 data and classify the scene materials proved difficult. The effects of the striping and background noise prevented accurate matching of extracted spectra. Simple techniques were developed to reduce, or if possible remove, the striping effects and reduce the background noise component. These techniques, developed for the AIS - 1 data, were later adapted for use with the GER - II imaging spectrometer to reduce striping, shading and noise problems observed in this data set.

Each instrument is considered separately below, with details of the techniques used to reduce the problems observed in the data. A consideration of the assumptions used when applying the techniques and the problems caused by applying the techniques are also included.

3.2 AIS - 1 data problems.

Data problems encountered with the AIS - 1 were described in Chapter 2, they included,

(1) Vertical striping and data spikes.

(2) Horizontal striping.

(3) Second order overlap.

(4) Random noise.

(5) Geometric distortion.

The fourth and fifth items on the list above are discussed only briefly. More detail on these two items is given under the relevant sections covering the GER - II scanner later in this chapter.

3.2.1 Vertical striping and data spikes.

An early look at the AIS - 1 data set confirmed the presence of many of the problems mentioned in the literature, in particular,

(1) Vertical striping due to poor calibration of the instrument (Huntington et al., 1986).

(2) The data range of the pixel values of some columns in some bands were very small. Values for this range were 4% to 5% of the data range of normal column values.

(3) Data spikes due to electronics noise ⌐or calibration effects⌐were evident at regular intervals (Bands 16, 32, 48, etc.).

To reduce these effects a despiking and destriping algorithm was developed. The algorithm processes the data in several distinct steps. In the first step all the column averages in each band are checked to determine which columns have a compressed data range, as mentioned in (2) above. These columns are flagged as "BAD" columns. The "BAD" columns are then replaced by spectral averaging across neighbouring bands on a pixel by pixel basis. In the first and last band the removal of "BAD" columns is achieved by spatial averaging across adjoining columns, again on a pixel by pixel basis.

In the second step the data spikes are removed. In this case the bands containing the data spikes are replaced by averaging spectrally across adjoining bands. The last band in the data set band 128 was replaced by extrapolated values from bands 126 and 127.

The last step is based on the work of Huntington et al. (1986). To remove the vertical striping, Huntington et al. used a simple algorithm that equalised the column mean of every column in a band, to the mean value of the central column in that band. In this case, each pixel value in a column is rescaled, so that the new mean value of the column equals that of the central column. The danger of using a single column to rescale the rest of the columns in a band was mentioned by Huntington et al., as the central column may itself have an extreme mean value producing unusual results. A modified version was produced which calculates the average of all the column means in a band and then equalises all column means in that band to this average mean value. This avoids the problem of using the central column mean as mentioned above.

The effects of applying the destriping algorithm to the data are shown in plate 3.1 (compare to plate 2.1). Visually the technique proved very effective in reducing the striping. However, residual vertical striping can still be observed in the data set and in some cases, can be seen to vary down the
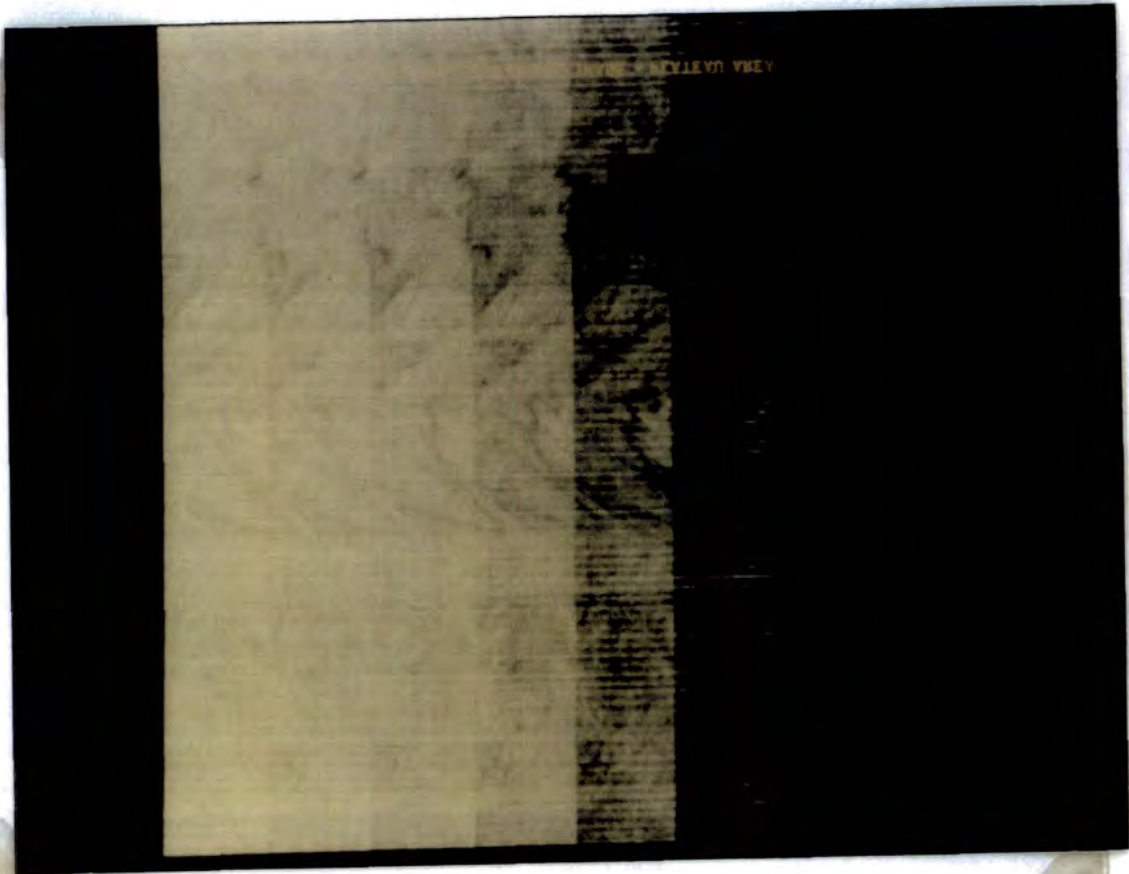
Plate 3.1   AIS - 1 data after vertical destriping (compare to Plate 2.1). Some residual vertical striping is still evident and may be related to variations in detector response during the flight (Huntington et al., 1986).
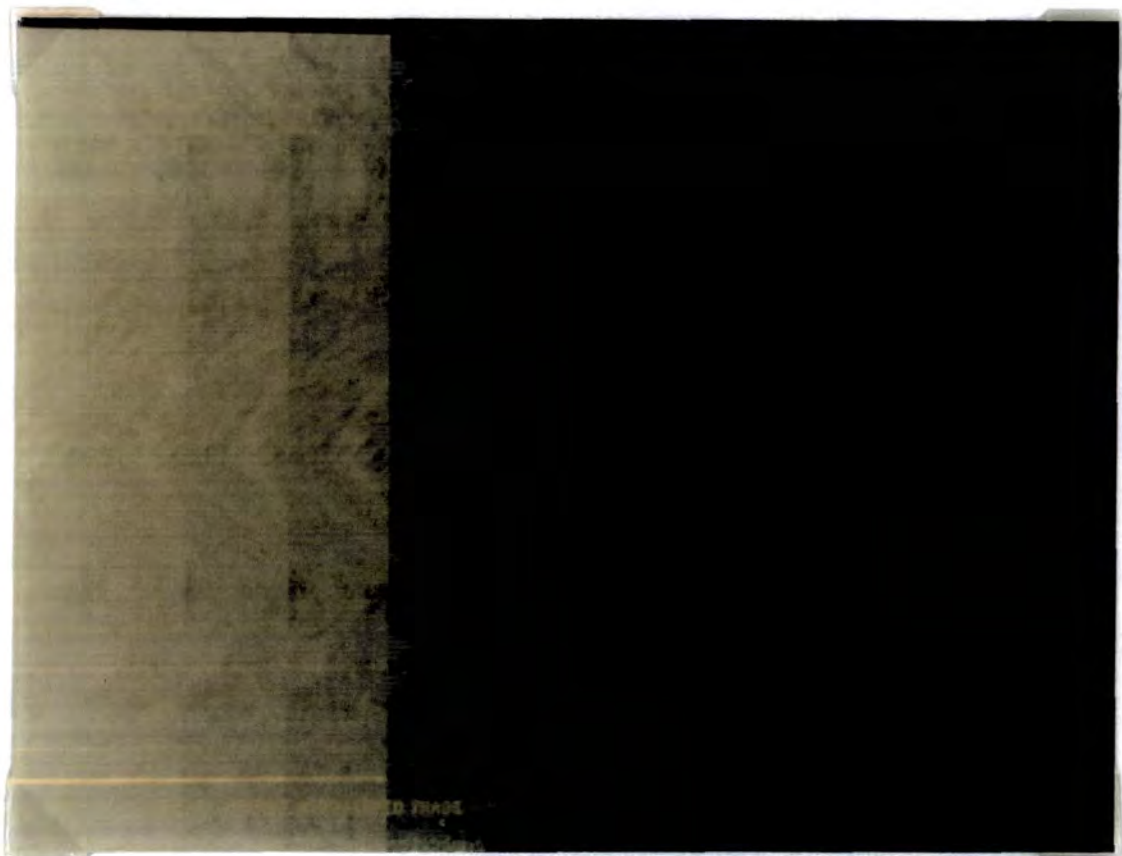
Plate 3.2   AIS - 1 data after horizontal destriping (compare to Plate 3.1). Residual horizontal striping has been reduced, but is still clearly evident.

flight line (Huntington et al., 1986). This may be due to a varying detector response during the flight and can not be corrected using this simple column equalisation technique.

Assumptions when using this algorithm. That the components making up the scene (trees, grass, clays etc.) are uniformly distributed in each column. That is the proportions of each of the different materials of differing brightness are the same in each column. If this is not the case, for example if a river runs along the length of a single column and has a brightness lower than the average scene material for that band, its brightness would be raised due to the column equalisation procedure. This would affect the spectral curve shape of the river for that band.

Problems of using this algorithm. In using this algorithm interpolation across the data spikes in particular bands takes place. These bands are therefore of no use in our data analysis, as the data they contain is fabricated from the adjoining bands. This should be noted when using this algorithm.

If the components making up the scene are not uniformly distributed in each column, then use of this algorithm will alter the spectral curve shapes of the materials making up the scene.

3.2.2   Horizontal striping.

The striping is clearly visible in the data. An algorithm was developed based on that mentioned by Huntington et al. (1986). In effect, a five row moving window is taken and the mean value of each of the five rows is calculated. These means are then totalled and divided by five to obtain the average mean value for the window. The mean of the central row of the five line moving window is then equalised to this average mean value. The window is then moved down one row and the values recalulated. This operation is performed on each band in turn.

The reason for using only five rows in the window calculation, is to reduce the effect of the varying brightness of ground surface components that may cover large areas of the narrow (32 pixel, 355m wide) flight line. In figure 3.1, if the flight line covers only two materials of differing brightness for that band and all rows are used in the equalisation step, the algorithm will set both materials to the same mean value and destroy the spectral variation in that band. However, if we use a five row moving window, the small row to row

WHOLE SCENE DESTRIPING

32 Pixels

Mean value 200

Mean value 100

Mean value 150

Before destriping

After destriping
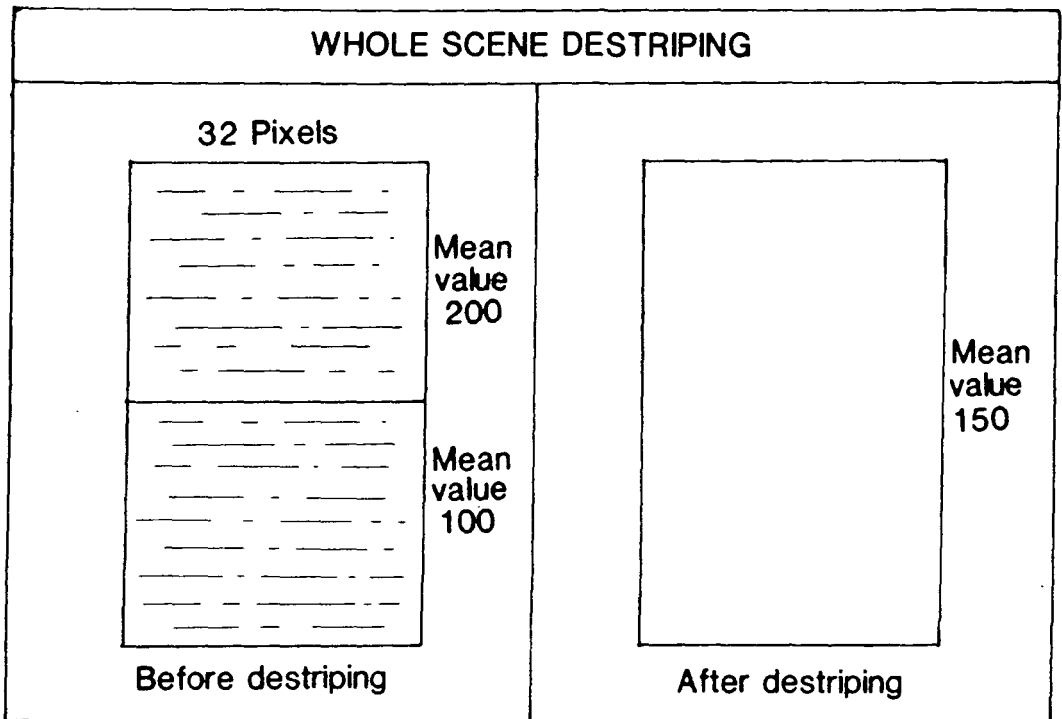
Figure 3.1   A single band containing two materials with different albedos. On destriping, the mean albedo of the two materials will be averaged to the same value, if we use all the lines of the data set to do the destriping correction.

5 LINE MOVING WINDOW DESTRIPING

32 Pixels

Mean value 200

Mean value 100

Mean value 200

BOUNDARY

Mean value 100

Before destriping

After destriping
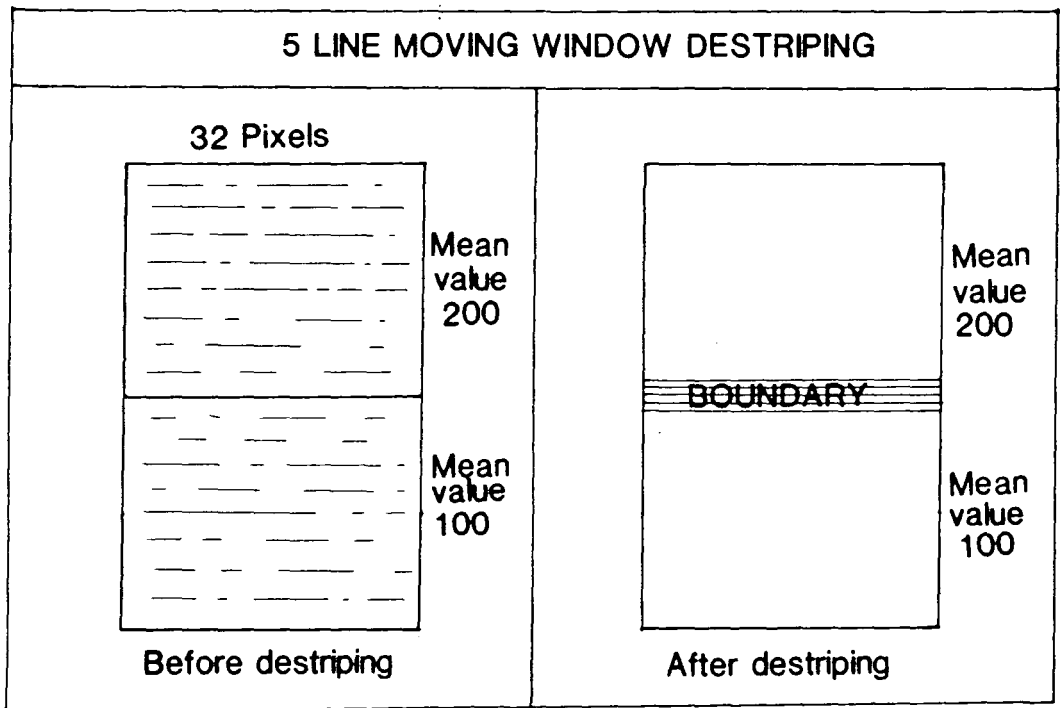
Figure 3.2   A single band containing two materials with different albedos. If we destripe using a five line (row) moving window, the horizontal striping is reduced and the line (row) values will only be badly affected at the boundary of the two materials.

variations are reduced (figure 3.2) and only the area of the flight line forming the boundary between the two materials is badly affected by the algorithm.

In chapter 2, the horizontal striping was attributed to an inadequately secured vibrating detector array. The vibration produced line(row) to line(row) wavelength shifts (figures 2.8 and 2.9, Chapter 2). In figure 3.3 we can see the spectral response across one grating position of 32 bands, for two separate lines both containing the same surface material. For any given band the two lines will have different values due to the vibration induced shift, any absorption features are affected by this shift, the central wavelength value for the absorptions being different for each line (figure 3.3). The algorithm will tend to average out the line to line variations, producing an average curve (figure 3.3, dotted line). This reduces the horizontal striping (plate 3.2, compare this to plate 3.1), but also produces wavelength shifts, as can be seen by the new wavelength value of the average curve.

Assumptions when using this algorithm. The only assumption is that used when discussing column equalisation to remove vertical striping. That is, that the varying brightness materials that make up each row are found in equal proportions in each row.

Problems of using this algorithm. It has already been demonstrated that at a boundary between two materials of different brightness there are unsatisfactory averaging effects. Given the narrow swath width of the flight line (about 355m) which will often intersect areas of varying brightness, care should be taken in interpreting spectra near these boundaries.

3.2.3 Second order overlap.

The additive effect of second order overlap is especially troublesome when a pixel has a high albedo in the 0.8μm to 1.2μm wavelength region relative to the 1.6μm to 2.4μm region, as in the case of green vegetation. However, with rocks the effect is reduced due to the somewhat lower relative differences between the two wavelength regions.

Additive contamination does exist, as discussed in Chapter 2. Unfortunately, since the information necessary to provide a suitable correction to the data is not available, no correction has been made. However, analysis of the data suggests that the major absorption features can still be successfully extracted from the data, with only the smaller features being affected by the
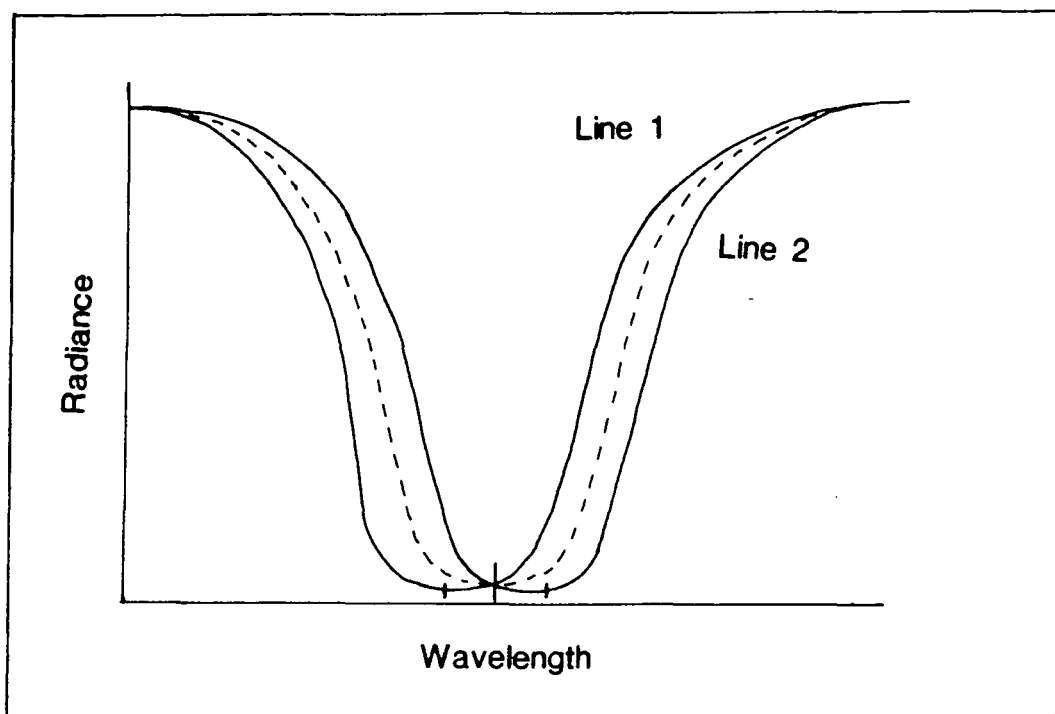
Figure 3.3　The vibrating detector array produces shifts in spectral features of the same material from different lines (rows). The horizontal striping correction will average away line to line variations (dotted line).
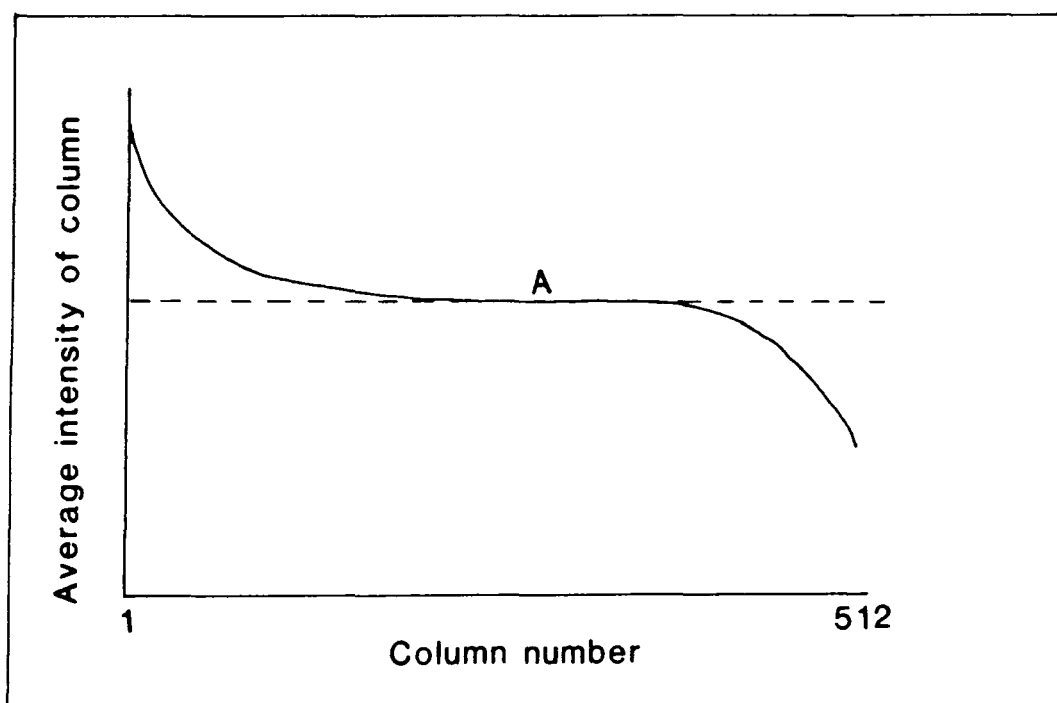
Figure 3.4　The extreme column means in the image showing the cross track shading, are set to the value of the average column mean for the affected band (Point A). Producing a flat distribution of column means across the image (dotted line).

additional second order contamination.

3.2.4 Random noise.

The effect of random noise is to reduce the identification accuracy of the matching algorithms. Details of the effects of noise and possible solutions for dealing with these effects, are given in more detail under the relevant section for the GER - II scanner later in this chapter.

3.2.5 Geometric distortion.

Given the AIS - 1 instrument configuration, we would not expect major geometric distortions to be evident in the data, although minor distortions such as roll distortions are to be expected. However, the AIS - 1 data does have several major geometric distortions, which are due to the pilot making major course corrections during data acquisition, in an attempt to fly over the assigned target areas this is one of the problems of having such a narrow swath width. The treatment of these distortions is described in detail under the relevant section for the GER - II scanner later in this chapter.

3.3 GER - II data problems.

Data problems encountered with the GER - II scanner were described in Chapter 2, they include,

(1) Cross track shading.

(2) Horizontal striping.

(3) Random noise.

(4) Second order overlap.

(5) Geometric distortion.

3.3.1 Cross track shading.

The effect is very noticeable in the visible bands of the first spectrometer, due perhaps to a combination of atmospheric scattering and macroscopic ground effects (Abrams, 1985). To reduce the effect, all column means are normalised to the average column mean for each band. The algorithm is a modified version of that used to remove the vertical striping in AIS - 1 data. Diagrammatically the extreme column means on each side of the image are set to the value of the average column mean (the scene mean) for the band (A in figure 3.4).

Assumptions when using this algorithm. As with AIS - 1 data, we assume that the composition of the surface in each column is the same, with equal proportions of varying albedo materials in each column.

Problems of using this algorithm. As with AIS - 1 data, if the assumption above is not followed and a large homogenous area of material is present over several (but not all) columns, then the spectral relationships of the materials will be altered by applying this algorithm.

3.3.2 Horizontal striping.

As stated previously, the irregular horizontal striping was produced by the switching on and off of the cooling system to the detectors. The switching is irregular producing differences in pixel brightness between rows and within rows. No simple algorithm can remove the effects entirely.

However, it is possible to reduce the difference in brightness between rows. A modified version of the algorithm used to destripe the AIS - 1 data has been used. This modified algorithm uses all rows of a band to calculate an average row mean value (scene mean), unlike the AIS - 1 algorithm which used a five row moving window averaging process. Each row mean is then equalised to this average row mean value (scene mean) This is very effective at removing row to row variations, but in the case where the cooling switching takes place in mid-row it is ineffective. Therefore there is residual striping evident in the data. There is a basic assumption here, that because the row length is much greater (512 pixels rather than 32), there is a greater likelihood that the rows contain equal proportions of scene components. This is only an assumption, further work is necessary to evaluate the effectiveness of these simple algorithms.

Assumptions when using this algorithm. As with the cross track shading correction, the assumption is made that the composition of the surface in each row is the same as all other rows, with equal proportions of varying albedo materials in each row.

Another assumption is that the striping is a row to row variation and is not variable along a single row.

Problems of using this algorithm. If a large homogenous area is present, covering several, but not all rows, then the spectral relationships of the materials in the band will be altered by applying this algorithm.

The striping is variable along single rows in some cases, and although the

striping can not be removed row to row variations can still be reduced.

3.3.3 Random noise.

Noise is clearly evident in both AIS - 1 and GER - II data sets and has detrimental effects on both feature extraction during processing and feature identification during analysis of spectra.

The effects are variable and depend on the generated signal (light targets will have higher signal to noise ratios than dark targets) and the signal to noise characteristics of the differing detectors covering various wavelength regions.

Random noise is a major problem during processing, where small features in the spectra are highlighted, including the small variations due to noise. During analysis the highlighted noise affects the accuracy of the matching algorithms, when trying to match to library reference spectra. Currently, the presence of noise prevents the use of an accurate automated system of surface material identification.

Their are two approaches to reducing this random noise element, thus allowing more accurate spectral matching. These are,

(1) A hardware improvement in detector technology, to increase the signal to noise ratios of the detectors.

(2) Averaging, whether spectrally or spatially to recover the underlying signal and reduce the noise.

In the first area, researchers are already designing, building and testing new sensors. This is really the only way to increase the effectiveness of analysis, by reducing the noise at source. In the second area, the use of spectral filtering algorithms can reduce the larger noise spikes that produce problems with the matching algorithms. Data preparation of both the AIS - 1 and GER - II data involved the use of a spectral filter to reduce this random noise element in the data. The filter used was a Shepard five point weighted moving average (Davis, 1986). However, unless the surface material has a very strong signal then even after spectral filtering of the data, we still find that single pixel plots of the spectra are difficult to interpret. To reduce the effects of this single pixel variation, an average of several pixels can be used at the analysis stage. This averaging reduces the effective spatial resolution of the data and increases the mixing problem. However, a considerable improvement

in the identification accuracy is possible using these average spectra.

3.3.4 Second order overlap.

Unlike the AIS - 1 instrument, data is available to make a complete correction for any second order overlap effects in the first spectrometer covering the visible and near infrared. With knowledge of the grating efficiencies in the first and second order and a knowledge of the radiance values in the wavelength region likely to cause the effect (in our case the first four bands), the effects of additive second order radiation can be removed.

However, the data values of the first four bands are so low that no useful information has been extracted from them. Therefore no correction was made, as the extra additive second order component will be a minor part of the high signal values of the last seven bands.

3.3.5 Geometric distortion.

After correcting for the various data quality problems, there is one more major problem to overcome before the imagery can be used as a base map of anomalous areas of alteration. This is the problem of geometric distortion.

Distortion due to the inherent variation in ground pixel size when using a scanner was described in Chapter 2, figure 2.16 and that due to variation in topography in Chapter 2, figure 2.17. It is possible to generate an algorithm to remove the distortion due to varying scan angle which is a problem in simple geometry. However, the distortion due to topography is highly variable and beyond simple correction.

Rather than develop an algorithm to correct for scan angle distortion, a commercial image processing algorithm was used to warp the image to UTM map co-ordinates.

This algorithm warps the imagery based on a set of Ground Control Points (GCP's) provided by the user. The process involves finding identifiable points on the image and attaching them to the same identifiable points digitised from a topographic map of the area of study. After collecting the points, the software will warp the image so that the points chosen in the image line up with the same points chosen on the topographic map. The accuracy of the warping is dependent on the accurate location of GCP's. Any inaccuracy in warping will prevent location of small targets, unless,

(a) The targets are clearly defined in the imagery against the background. That is they have clear precise boundaries.

(b) The targets on the ground are visually very distinct, for example the target may be a different colour, an unusual shape, or located near an identifiable ground feature.

3.4 Summary.

Destriping algorithms have been developed to reduce horizontal and vertical striping effects in the AIS - 1 and GER - II data sets. These algorithms are simple column and row equalisation procedures. When using these algorithms the basic assumption is made that each column and each row are covered by the same proportions of each surface material making up the scene. This may not be the case.

Second order overlap is definitely present in the AIS - 1 data. However, no suitable correction is possible, although the problem has been noted it has not been corrected. In the GER - II data, second order overlap effects may exist for the last seven bands of the first spectrometer. Fortunately the second order radiation is a very minor part of the signal due to the low signal values of the contaminating wavelength region.

Spectral filtering to reduce the effects of random noise has been tested, using a Shepard five point, weighted, moving average filter (Davis, 1986) and has proved successful in smoothing the data and increasing the identification accuracy at the analysis stage.

Finally, standard image processing techniques to correct for geometric distortion has been used successfully to improve positioning accuracy on the ground, when checking anomalous areas.

3.5 Conclusions.

(1) Destriping algorithms using row and column equalisation are simple methods to improve data quality for identification purposes at the analysis stage.

(2) No suitable correction for second order overlap effects in AIS - 1 data is possible.

(3) Spectral filtering of data to reduce random noise does improve identification accuracy. However, more detailed work on the effects of different spectral filters should be considered. This is a very important area for future research.

(4) Geometric distortion effects can be reduced using commercial image processing software (GCP's). However, if the geometric distortion is not fully corrected, difficulties in identifying small ground targets can be encontered. Location of targets was often dependent on having clear definable boundaries, or being located near an identifiable surface feature. Further work is needed to reduce the effects of geometric distortion and improve ground location accuracy.

CHAPTER 4

DATA PROCESSING AND DATA ANALYSIS.

4.1 Introduction.

The purpose of the data processing stage is to convert the data into a form suitable for analysis. The question we must ask, is, what is the most suitable form for analysis ?

In this chapter the processing methods available are discussed. Two methods in particular are discussed in detail, describing their operation and the problems of their use. Finally, an outline of the available analysis methods is given, detailing the strengths and weaknesses of the current techniques.

4.2 Data processing philosophy.

Prior to the development of airborne, high spectral resolution, imaging spectrometers, the only available high spectral resolution data was provided by field and laboratory spectroradiometers. To provide standardisation of spectra obtained from a variety of different instruments, obtained in a variety of different operating conditions, all spectra obtained were compared with a standard reference material. Ground surface radiance values obtained from a laboratory or field instrument, are ratioed against radiance values obtained under the same conditions from a standard reference panel, usually barium sulphate. The standard reference panel can be traced back, in theory, to a national / international standard to give a measure of the true reflectance of the material.

When using a laboratory or field instrument, the ground surface radiance and the standard reference panel radiance are simultaneously recorded on dual beam instruments, or recorded sequentially on single beam instruments. By comparing with standard reference panels we can produce identical reflectance spectra from different instruments.

The ratioing process that produces the reflectance spectra removes the

effects that are common in the radiance values of the ground surface target and the standard reference panel. For a field instrument using the sun as a light source, these effects are,

(1) The effects of atmospheric absorptions, masking spectral features.

(2) The effects of the drop off in intensity of the solar irradiance reaching the earth (See Chapter 1).

(3) Instrumental effects. Each instrument may have design peculiarities, that produce "steps" in the data. For example, when switching from one spectrometer grating to another for a different wavelength range of the instrument. These steps will be present in the target data and in the standard panel data and are removed by the ratioing operation.

Comparison with a standard reference panel has allowed the development of libraries of reflectance spectra, that can be matched with any spectra produced by a worker using the same standard.

With the introduction of airborne, high spectral resolution, imaging spectrometers, the basic philosophy of converting instrument radiance values to reflectance spectra has been extended. The primary aim of most workers has been to develop methods to convert the airborne radiance values to reflectance spectra, thus allowing direct comparison with established libraries of reflectance spectra for identification purposes.

4.3 Methods available.

A review of the available literature suggested several possible methods of converting the airborne data to reflectance spectra, or in some cases spectra approximating reflectance spectra (pseudo-reflectance spectra). The methods examined are listed below,

(1) Flat field correction. (Roberts et al., 1986).

(2) Empirical line method. (Conel et al., 1987).

(3) Log residuals. (Green and Craig, 1985).

(4) Internal Average Relative Reflectance (IARR). (Kruse et al., 1985).

(5) Hull quotients. (Green and Craig, 1985; Clark et al., 1987).

Each method is described briefly in the following section.

4.3.1   Flat field correction.

Using this method we assume that some chosen pixels in the scene are spectrally flat across all wavelengths of interest. The average spectral curve of the chosen pixels is then divided into every pixel in the whole image. This division removes the effects common to all pixels mentioned above, atmospheric absorptions, solar irradiance drop off and instrumental effects. The chosen pixels form the equivalent of a standard reference panel against which the data is ratioed. The resulting output spectra should be a flat straight line over the pixels chosen as the standard spectrally flat area and reflectance spectra for all other pixels. In practice a truly spectrally flat material is unlikely to exist in the image and so we have to find an area that approximates most closely to that ideal. To find such an area requires extensive ground knowledge and since, even then it is not truly spectrally flat the division can produce odd processing artifacts in the output spectra. Given this, the best that can be achieved by using this method are pseudo-reflectance spectra that approximate reflectance spectra.

4.3.2 Empirical line method.

This method has been described in some detail by Roberts et al. (1986) and Conel et al. (1987). The method requires several large homogenous areas occupying at least several pixels in the image, that are different spectrally. Ground measurements of each different homogenous target are taken using a field spectroradiometer referenced to a standard reference panel.

Each homogenous target will now have two measurements,

(1) An average spectral response derived from several measurements of a field instrument referenced to a standard reference panel (reflectance spectra).

(2) An average spectral response of several pixels from the collected airborne data. (Radiance values).

Assuming that the response of both airborne and ground instruments are linear from low brightness to high brightness targets for all wavelengths, then for a chosen band with several targets of differing brightness we can determine a straight line relationship between the airborne system and the ground measurements (figure 4.1). This relationship can then be determined for each band of the airborne instrument.

These calibration charts for each band, can then be used to equate the air-
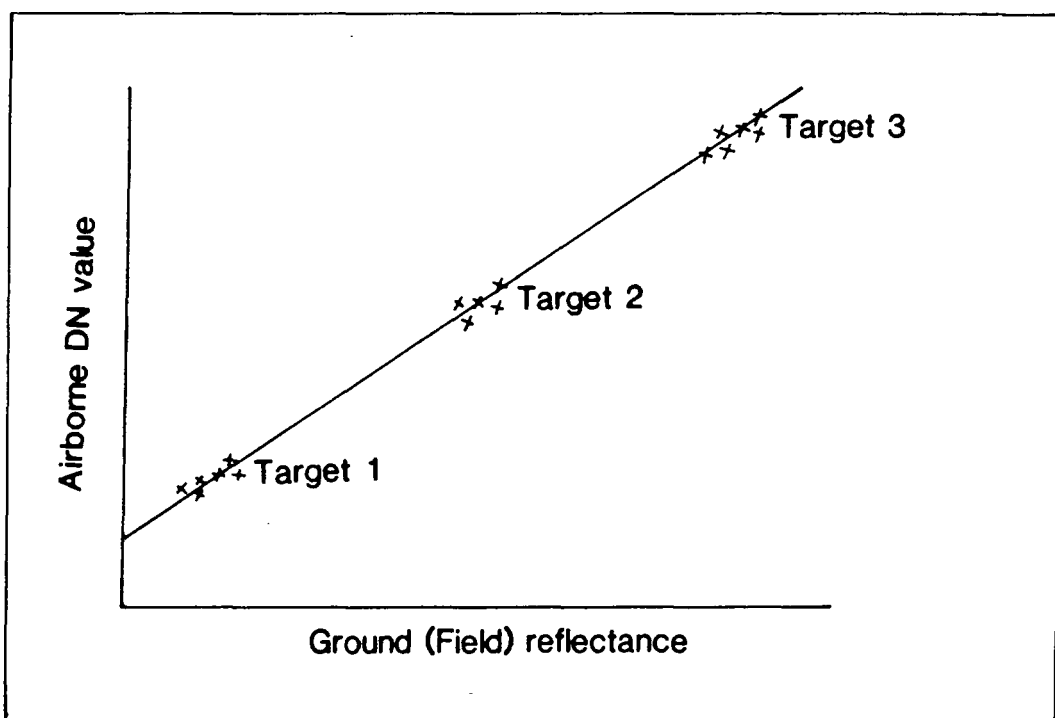
Figure 4.1   A linear relationship between ground reflectance data and airborne spectral data can be constructed, using a series of identifiable targets. The relationship is constructed for each band in turn, the airborne data can then be converted to ground reflectance by using these empirical charts.
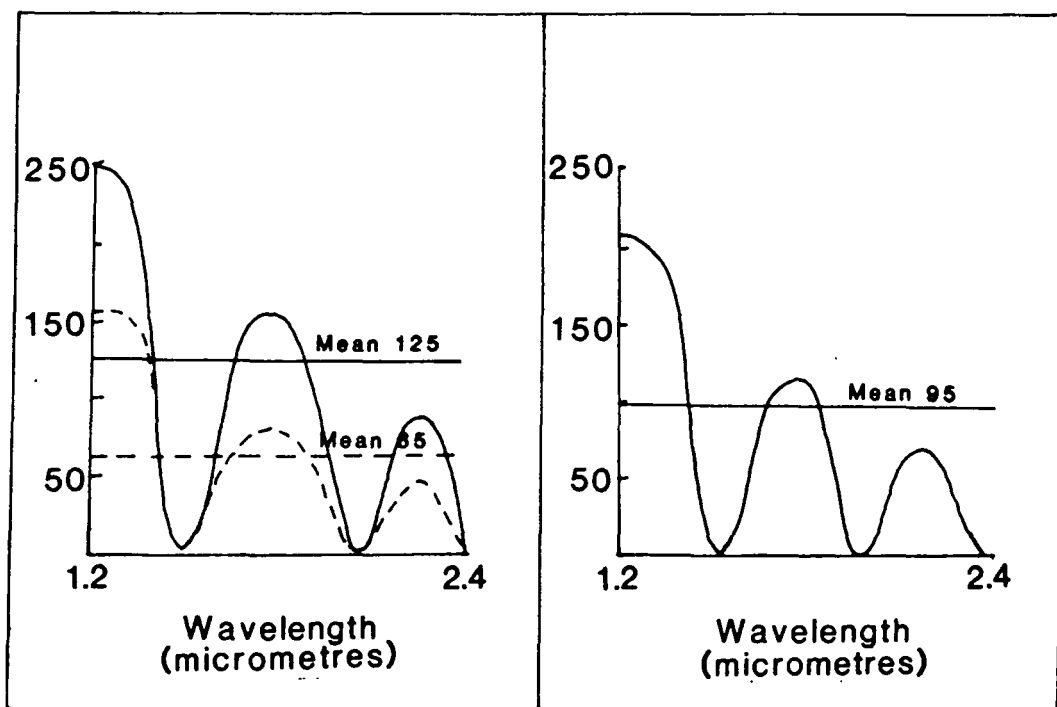
Figure 4.2   The topographic shading correction is the first step of log residuals. Each curves mean value is equalised to a common value, so that a material in both shadow (Mean of 65) and sunlight (Mean of 125) will be equalised to the same value (Mean of 95), eliminating the differences due to shadowing.

borne response of a material in each band to its equivalent ground reflectance.

This technique requires detailed ground spectral sampling using a field spectroradiometer and requires that suitable homogenous ground targets are available for such a study (which in some areas is unlikely). The output will be in the form of reflectance curves that are directly comparable to those available in libraries of reflectance spectra.

4.3.3 Log residuals.

This technique, described by Green and Craig (1985) has an advantage over the two mentioned above in that **no ground data** are necessary for its operation.

The effects of topographic shadowing in the image are first removed, by setting the mean intensity (across all bands) for each pixel, to that of the mean intensity (across all bands) for the scene (figure 4.2).

An average spectral curve from either a sub-scene of the data or the whole scene is then derived. This average curve will contain all those effects common to each pixel, atmospheric absorptions, solar irradiance drop off and instrumental effects and will be a composite of the spectral response of the various materials in the scene (or sub-scene). This average curve is subtracted from each pixel in turn, subtraction rather than division is used because of the use of log values. This has a similar effect to the division by the spectrally flat curve in the flat field method.

The residual curves produced contain many artifacts related to the use of an average curve that is not spectrally flat, the output of the processing being dependent on the proportions of the materials that make up the average curve. Therefore, we can only produce pseudo-reflectance curves that broadly approximate those available in libraries of reflectance spectra. This will of course lead to a loss of accuracy when trying to match the output spectra to the library reflectance spectra.

4.3.4 Internal Average Relative Reflectance (IARR).

This is a non-logarithmic method similar to log residuals developed by Kruse et al. (1985). Whereas log residuals is a single algorithm consisting of two basic operations, this method clearly separates each operation as a separate algorithm. The first algorithm removes the effects of topographic

shadowing by equalising the mean/of each pixel spectral curve to the mean *intensity*

intensity (across all bands) of the scene (figure 4.2). The second algorithm derives the average curve which is then divided into each pixel curve in turn. The result is equivalent to log residuals, producing the same artifacts of processing and spectra that only approximate reflectance spectra.

4.3.5 Hull quotients.

This technique is described by Clark et al. (1987) and is unlike all methods previously discussed. The basic operation involves fitting a 'hull" to the upper surface of each pixels spectral curve (figure 4.3). The operation has been likened to the stretching of a rubber band over the upper surface of the spectra. The effect is to remove the overall curve shape leaving a flat topped spectrum containing the absorption features. This technique does not remove the effects of atmospheric absorptions, the decrease in solar irradiance, or instrumental effects. The technique has two main advantages in that **no ground data** are necessary for use and that spectral artifacts of processing can not be produced, as the operation is performed on a pixel by pixel basis.

4.4 Choice of methods for processing.

The choice of processing method for both the AIS - 1 data and the GER - II data was limited by one condition, that **no ground data** were available for either area of study. With this restraint the FLAT FIELD and EMPIRICAL LINE methods were eliminated from consideration. This leaves the following techniques,

Log residuals.

Internal Average Relative Reflectance (IARR).

Hull quotients.

The first two methods (log residuals and IARR) are equivalent and produce very similar results, while the hull quotients method is a very different processing philosophy. Both methods are discussed in detail below.

4.5 Log residuals / IARR.

As was briefly mentioned, these are mathematical methods based solely on
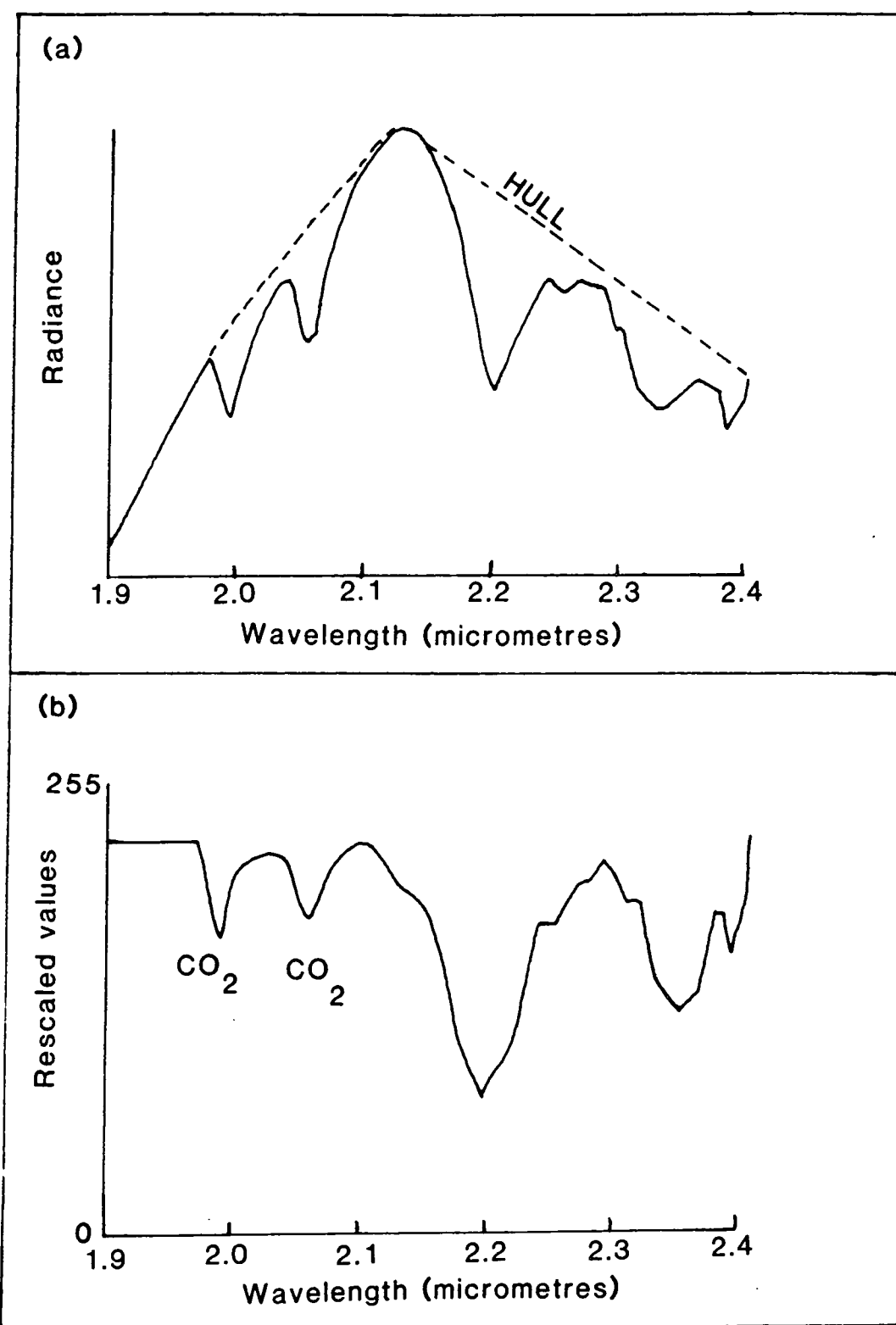
Figure 4.3   (a) The radiance spectra of sericite has a hull stretched over its upper surface (dotted line). The output (b) shows the removal of the spectral curve shape and the seperation of the curve elements into identifiable features. Note that atmospheric absorption features are still present (CO_2).

information extracted from the scene, with no use of ground data. The mathematical description of this technique is given by Green and Craig (1985). I shall confine my explanation to a visual and diagrammatical description. The methods can be viewed as two step processes, the steps are,

(1) Removal of the effects of topographic shadowing.

(2) Production of an average spectral curve from the data which is divided into each pixel spectral curve in the scene to produce the residual pseudo - reflectance curves.

In later discussion of these techniques, reference will only be made to the IARR method, although the discussion applies equally to the log residual method. The first step of the IARR method is essential and can best be explained by reference to figures 4.4 and 4.5 and table 4.

Figure 4.4 represents an image consisting of two materials separated by a diagonal boundary. The left hand side of the image is in shadow, the right hand side in bright sunlight. Four spectral curves are shown to the right of the image.

Curve A - is material 1 in bright sunlight.

Curve B - is material 1 in shadow.

Curve C - is material 2 in bright sunlight.

Curve D - is material 2 in shadow.

Each curve is for a three band image, the values against each point on the curves are the brightness values at these points. The fractional number next to each curve is the fractional amount of the image covered by each spectral curve.

If we do not perform this first step of IARR to remove the topographic shadowing and instead only perform the second step, the curve averaging step, we produce a set of output curves with values listed in table 4a. As we can see from the data, the effects are to reduce the absorption in band 2 (relative to bands 1 and 3) for curves C and D and increase the peak value in band 2 for curves A and B.

Now if we use the same original dataset and perform the normalisation step to remove the topographic shadowing, we create a new data set (figure 4.5). Here we have only two spectral curves,
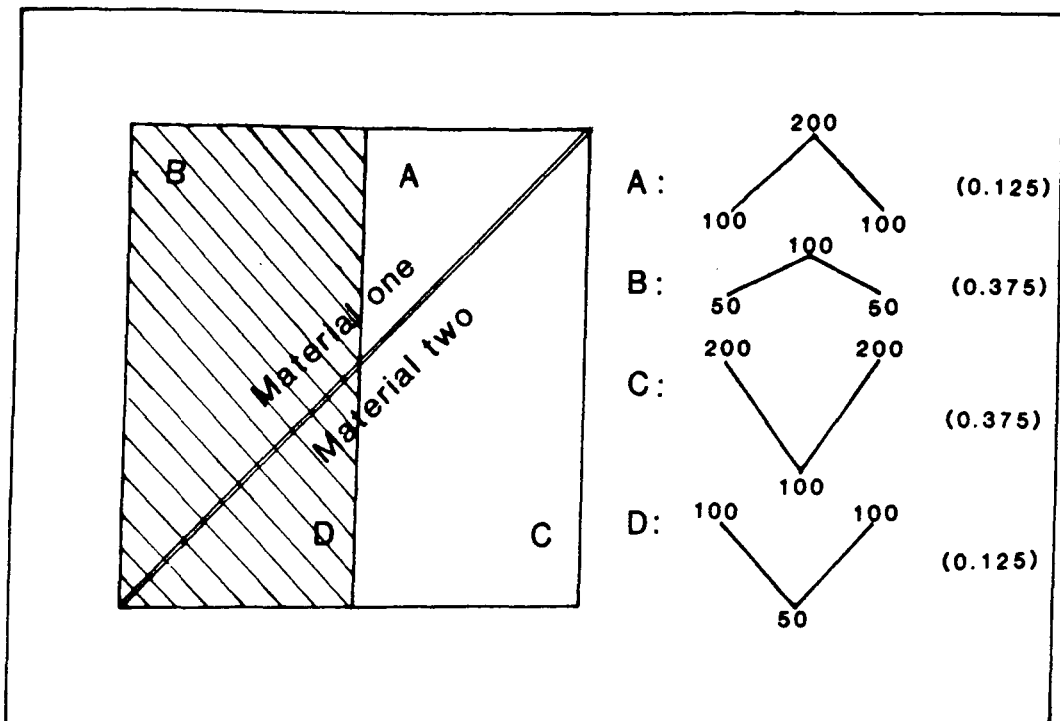
Figure 4.4 The image consists of two materials which are partly in shadow and partly in bright sunlight. To the right are the four spectral curves (A to D) that represent the two materials.
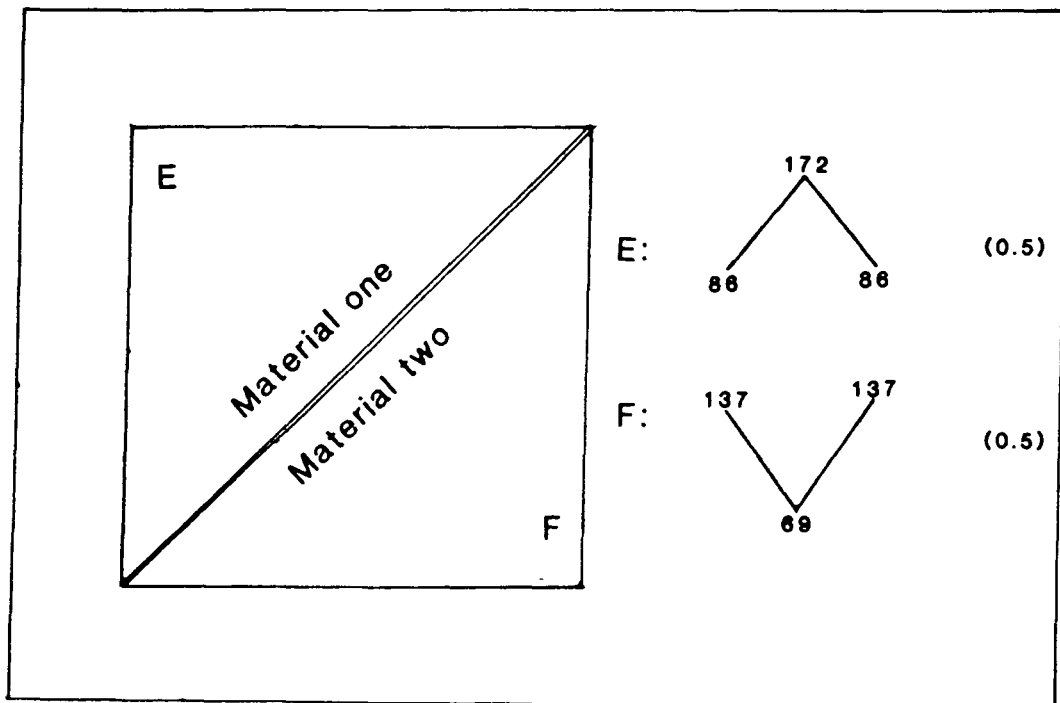
Figure 4.5 This is the same image as above, after the topographic shading effects have been removed. To the right are the two spectral curves of the materials represented in the image.

4A	BAND 1	BAND 2	BAND 3
Average (All curves)	118.75	106.25	118.75
Residuals			
A	0.842105	1.882352	0.842105
B	0.421052	0.941176	0.421052
C	1.684210	0.941176	1.684210
D	0.842105	0.470588	0.842105
Rescaled			
A	100 (100)	200 (224)	100 (100)
B	50 (50)	100 (112)	50 (50)
C	200 (200)	100 (112)	200 (200)
D	100 (100)	50 (56)	100 (100)

4B	BAND 1	BAND 2	BAND 3
Average (All curves)	111.71	120.31	111.71
Residuals			
E	0.769223	1.428559	0.769223
F	1.230776	0.571440	1.230776
Rescaled			
E	86 (86)	172 (160)	86 (86)
F	137 (137)	69 (64)	137 (137)

Table 4.

The upper part of the table (4A), contains the data after log residuals processing, without the application of the topographic shadowing correction. The lower part of the table (4B), contains the same data after log residuals processing, with the application of the topographic shadowing correction. The figures in brackets are the rescaled (new) values.

Curve E - is material 1.

Curve F - is material 2.

If we now perform the second step of IARR, the curve averaging step, on this data set, we produce the set of values given in table 4b. The general effect of rescaling is now reversed, increasing the depth of the absorption in band 2 (relative to bands 1 and 3) for curve F and reducing the peak value in band 2 for curve E.

It is apparent that if no correction is made for topographic shadowing, that the effects of IARR are not consistent. It is therefore important to carry out this first step.

The second step, the curve averaging step, is fairly straight forward and involves finding the average spectral curve of all the pixels in the scene and then dividing each pixel spectral curve by this average spectral curve, this produces the residual pseudo-reflectance output curves.

An example is shown in figure 4.6a. Here we see spectral curves of AIS - 1 data, for green vegetation (thicker line) and a bare rock surface. The two curves are obviously different, but also show the common features resulting from deep atmospheric water absorptions at 1.4μm and 1.9μm. After the topographic shadowing correction, we produce the output curves in figure 4.6b and an average curve in red, this assumes a 50 - 50 mixture of our two components. On dividing this average spectral curve into our 50 - 50 mixture we produce the output curves shown in figure 4.6c.

The technique has proved to be very useful in the production of pseudo-reflectance curves that approximate the true reflectance curves of spectral libraries. However, extensive study of this processing method when used on AIS - 1, GER - II and satellite Thematic Mapper (TM) data has shown that there are several problems in the use of this technique of which the user should be aware.

4.6 Log residuals / IARR - The problems.

The observed problems can be separated into three groups, those related to a failure to satisfy the basic assumptions of the method, those caused by the topographic shadowing correction and those caused by the curve averaging
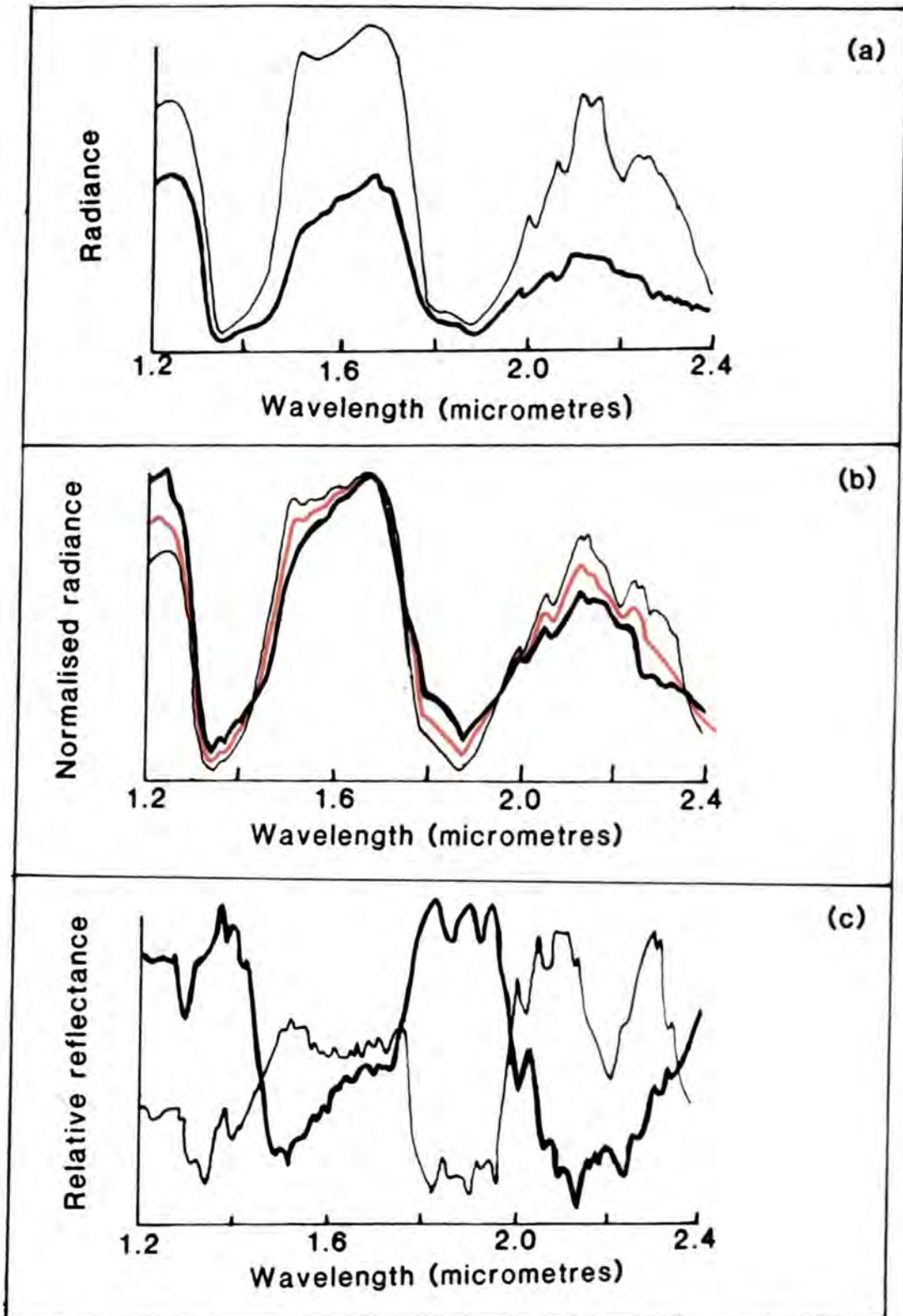
Figure 4.6   (a) Two spectral curves of AIS - 1 data for green vegetation
(thicker line) and a bare rock surface. (b) After the topographic shad-
ing correction, the output curves and an average curve (in red) for a
50 - 50 mixture. (c) The same curves after the curve averaging step
of log residuals.

step.

4.6.1 Failure of basic assumptions.

Mention has been made several times that the method removes the effects common in all pixels, one of the more important being atmospheric absorptions. For IARR to work successfully, two basic assumptions have to be satisfied.

(1) That the atmosphere is homogenous along the length of the flight line, over all surfaces.

(2) That there is no variation in topography or flying height when the data is collected.

Both assumptions are questionable. Firstly, we have to establish that microclimates related to a body of water, for example, do not exist. If they do, then the atmospheric water content near to them may vary and therefore the depths of the atmospheric absorptions.

The second assumption is even more questionable when we consider a real world exploration environment, where topographic variation may be very great. The depth of atmosphere between sensor and ground will vary greatly in this case as will the depths of the corresponding atmospheric absorption features.

The consequences resulting from the failure of these assumptions will be variable. Generally the effects are relatively minor as the major areas affected (the atmospheric water absorption bands) are of no real use in our data analysis.

4.6.2 Topographic shadowing correction - problems.

There are three problem effects produced by this first step of IARR processing. Firstly, the effects due to the presence of a dark material. Figure 4.7a shows the spectral curves of a synthetic data set consisting of two materials. The first material is spectrally flat apart from one absorption, while the second material is of darker and slopes down to lower values at longer wavelengths. The application of the topographic shadowing correction produces the curves shown in figure 4.7b. This results in greatly elevated data values at shorter wavelengths for the darker material, although it is still darker at longer wavelengths. Thus the normalisation step, although preserving the
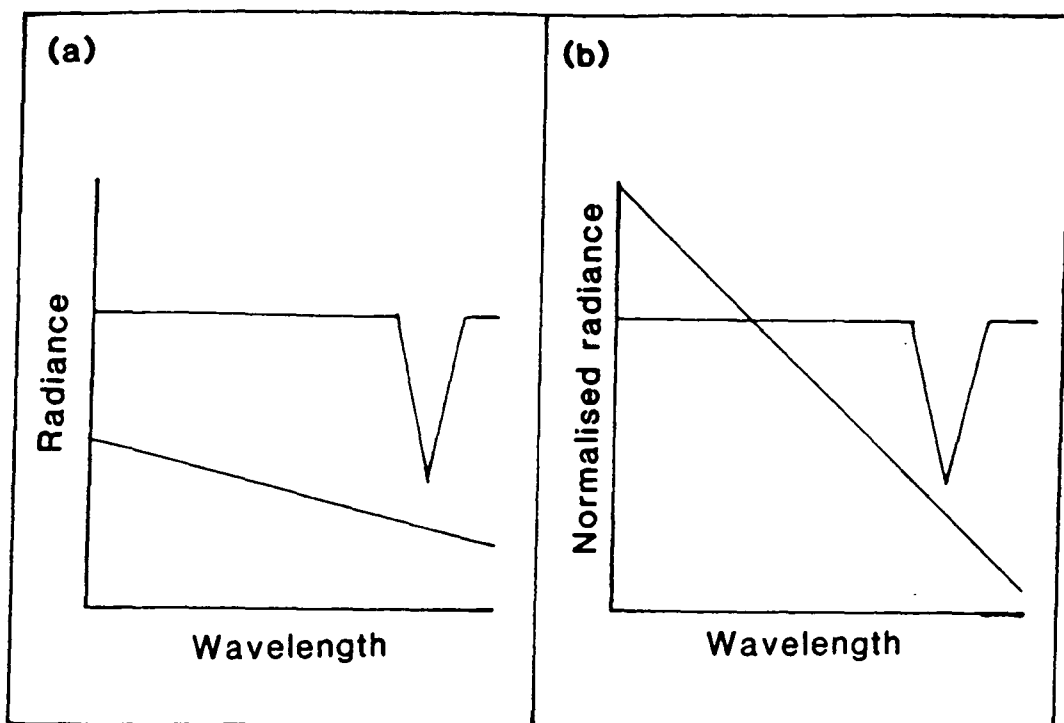
Figure 4.7   (a) The low albedo material (sloping line), has significantly increased values at shorter wavelengths (b) after the topographic shading correction. The spectral relationships within each material are the same, but the relationships between materials are changed.
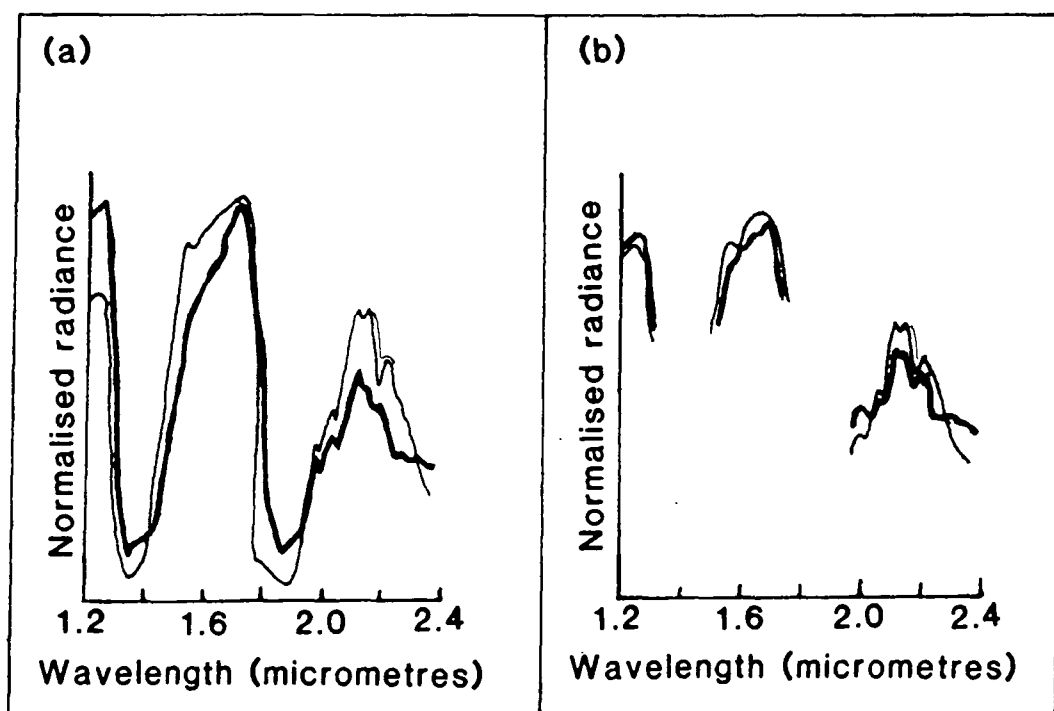
Figure 4.8   In (a) the effect of the topographic shadowing correction on the spectral curves of a bare rock surface and green vegetation (thicker line) are shown for the whole data set. The corresponding output (b) excluding the water absorption features, will highlight the clay absorptions (marked in red on both diagrams).

spectral relationships between bands of the same material, does not preserve relationships between different materials.

A real example of this problem is illustrated in figure 4.6a. These two spectral curves are taken from AIS - 1 data from an Australian flight. The brighter curve is that for a bare rock surface, the darker material is green vegetation (thicker line). Application of the normalisation step produces the spectral curves shown in figure 4.6b. The vegetation curve has been increased in brightness significantly at shorter wavelengths (the 1.2μm wavelength region) and is now much brighter than the rock surface. Note also the slight increase in brightness in the atmospheric water absorption bands (1.4μm and 1.9μm) of the vegetation curve.

On performing the second step of the IARR technique the output curves approximate those shown in figure 4.6c. Note two things,

(1) The areas of absorption in the 2.2μm region related to clays on the rock surface are actually visibly brighter in the residual data than the vegetation areas, so that visual observation of the band covering the 2.2μm region does not show the presence of the rock absorption, as vegetation will be darker.

(2) The areas of water absorption are bright in the vegetation curve (as they are brighter after the topographic shadowing correction). The areas of bare rock surface are darker in the regions of atmospheric water absorption.

The loss of spectral features in the 2.2μm wavelength region when visually examining a single band and the corresponding relationship of bright atmospheric water absorption bands with dark vegetated areas in the 2.2μm wavelength region, was noted by Huntington et al.(1986) and is due to the effect of the topographic shadowing correction on these two very different materials.

A correction to visually enhance the absorptions due to the bare rock surface is possible. Huntington et al. (1986) suggested that excluding the atmospheric water absorption bands from the AIS data and processing each section of data separately using log residuals was a solution. This is an improvement, in that the deep clay absorptions centred on 2.2μm do become visible, however, vegetation is still visually very dark.

The reason this method works to some degree, is that the relationships between the two spectral curves are altered, the topographic shading correction being made to each separate section of the data. In figure 4.8 we can compare the effect of the topographic shading correction on the complete data (figure 4.8a) with that for the segmented data (figure 4.8b). The final outputs are very different, although the vegetation is still visually very dark in this important wavelength region.

An alternative approach was developed, purely to highlight visually the absorptions in the 2.2μm wavelength region, so that areas of interest such as possible mineral alteration zones could be located on a single band image with ease. The first step in this process known as Ratio Group Normalising (RGN) * is exactly the same as IARR, the topographic shading correction. In figure 4.8a, the differences between the green vegetation curve and the bare rock surface curve after the correction are very apparent. The green vegetation curve is very bright in the 1.2μm wavelength region and very dark in the 2.1μm wavelength region relative to the bare rock surface. Since the problem of the visual masking of the rock surface clay absorption in the 2.2μm was related to the gross differences in curve shape between the two materials, a method was selected that separated the materials and processed each material separately.

The separation was achieved by using the simple ratio of a band at 1.2μm to a band at 2.1μm, where vegetation and rock have there greatest separation. The range that the ratio values could take was divided into 10 increments. The pixels were then assigned to an appropriate increment and an average curve, the second step of IARR, created for each incremental group. Each incremental group curve was then divided into each pixel in its incremental group producing the residuals.

The average curves created for each group will match the data more closely, but will still enhance small spectral features that are not common to the average curve. The result is that areas of bare rock surface that contain extra absorptions related to clay alteration will be strongly highlighted.

The output spectral curves from this method will be different from those produced by the IARR method, as several average curves are used producing a more variable and scene dependent response. As a method designed to visually

43

* A detailed description and examples of use of this method are given in Mackin et. al. (1987).

highlight absorptions in a band image, it proved to be far more effective than IARR processing.

The second problem of the topographic shadowing correction is related to minor variations in curve shape. Figure 4.9a shows two spectral curves from another synthetic data set, one red, one blue. The two curves are almost identical except for one extra absorption at longer wavelengths in the blue curve. In terms of proportions, the red curve forms 90% of the scene, the blue curve the remaining 10%. The extra absorption will have the effect of changing the mean value of the blue spectral curve relative to that without the extra absorption (red). On carrying out the topographic shadowing correction, this small difference produces an offset of the two spectral curves seen in figure 4.9b. The effects of small differences in curve shape are highlighted by the second step of the IARR processing, the curve averaging step and this case is no exception. In figure 4.9c we can see the residual blue curve. Not only do we see the strong feature related to the extra absorption in the blue curve, but also two artifacts, "bumps" related to the separation of the two curves during the topographic shadowing correction. With real data, these artifacts of processing would reduce the identification accuracy when matching the output spectra against library reflectance spectra which do not contain such artifacts.

The third, and final problem is due to the effects of additive atmospheric scattering in the visible wavelengths. After processing GER - II data over an area of Nevada, USA, using log residuals, a TM (Thematic mapper, Landsat 4) scene of the same area was processed in the same manner, to establish which features could be extracted from this broad band sensor. During analysis the data revealed this third problem of the topographic shadowing correction. The correction is a rescaling of spectral curves based on each spectral curves mean value. When two curves are identical in shape but with different amounts of shadowing, that is different intensities, carrying out the correction should produce two curves that are identical in both shape and intensity. The reason this works is that the shadowing reduces the signal in a manner that can be restored by multiplying each pixel band value by a constant, equal to the bright pixel curve mean value divided by the dark pixel curve mean value and is a multiplicative correction. Use of this correction assumes that there are
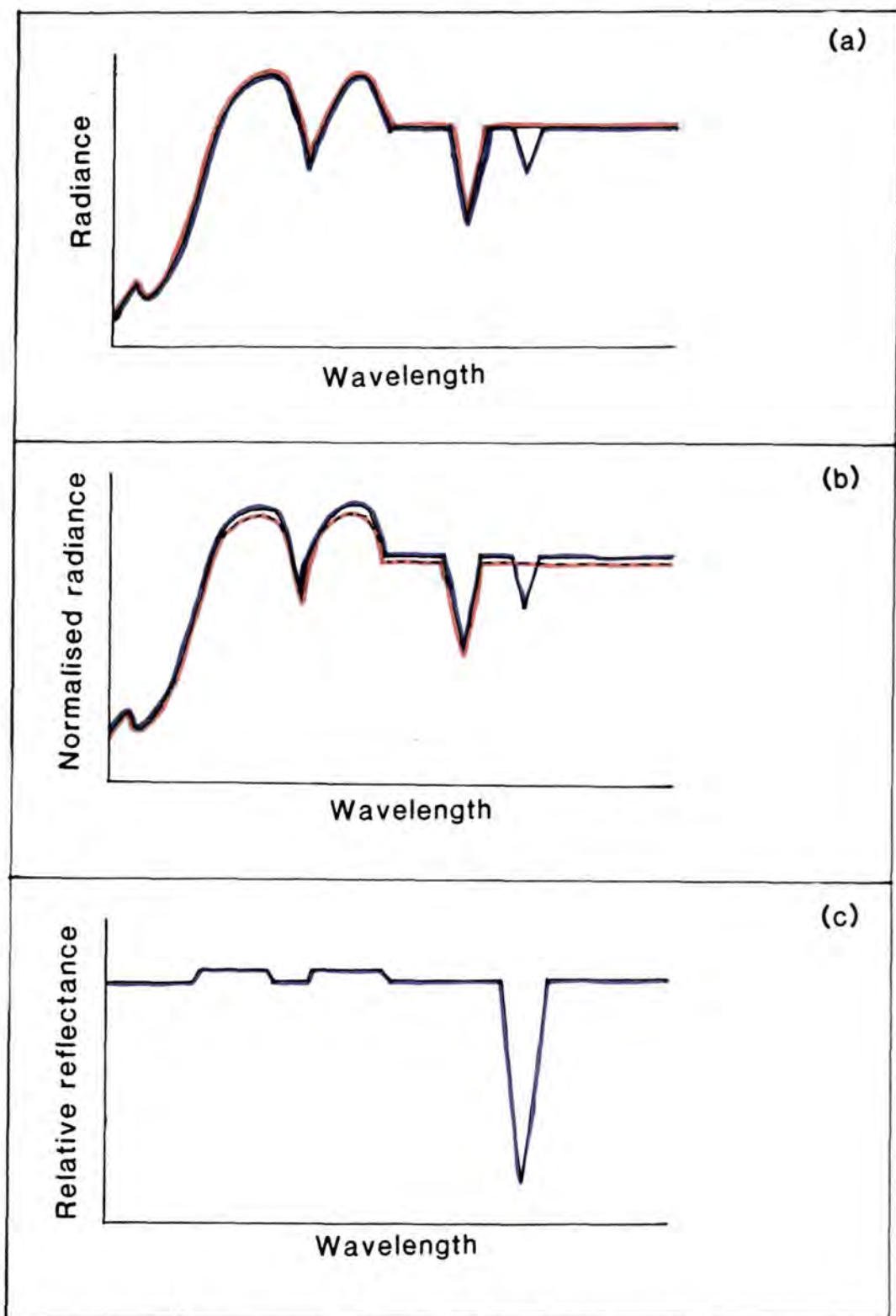
Figure 4.9 (a) Two spectral curves (red and blue) with the same curve shape and intensity, with one curve (blue) having an extra absorption. (b) The extra absorption decreases the average pixel value of the curve, which is highlighted by the topographic shading correction, seperating the two curves. (c) The log residual (blue) curve shows the enhanced extra absorption, but also two artifacts of processing.

no additive factors in the data.

Analysis of a TM scene after processing with IARR showed that residual topographic shadowing effects were very noticeable in Band 1, one of the visible bands. The shadowing proved to be a negative image of the original data, in that the shadowed areas of the original image were now the brightest parts of the processed image. Minor shadowing effects were also visible in Band 7 of the processed data, covering the 2.2μm wavelength region. In this case however, the shadowing was not the negative form.

The reason for these unusual effects is illustrated in figure 4.10 . Here we have two identical spectral curves extending from the visible to the SWIR one in shadow (mean of 10.5) and one in bright sunlight (mean of 20.5). The curves are essentially the same, except in the visible / NIR.
In this wavelength region there is a significant contribution to the spectral curve from light scattered by atmospheric particulates. This light has never reached the ground and will be a common value added to each spectral curve, in this model a value equal to one unit. Its intensity is not dependent on the amount of reflected radiation from the surface, as it is purely due to atmospheric scattering of light into the sensor. On rescaling, this additive scattering component will produce higher values in the visible (band 1 of TM) for shaded areas (thicker line) and lower values in the 2.2μm wavelength region (band 7 of TM), thus producing the observed effects (figure 4.10b). A correction for the additive effects of the atmosphere **prior** to using log residuals processing is necessary to avoid this problem. The CSIRO research group in Australia performs such a correction prior to any processing of its data (Dr. T. Munday, pers. comm.).

4.6.3 Curve averaging - problems.

There are three problem effects produced by this second step of IARR processing. The first of these is due to varying proportions of scene components. One obvious feature of the curve averaging step is that each material making up the average spectral curve will do so in proportion, so that if one scene component is very common it will dominate the spectral response. The data in figure 4.9a is used as an input to IARR processing. The output shown in figure 4.11 shows the residual curve (blue) for varying proportions of this material (10%, 50% and 90%) in the original data. This is shown in figure
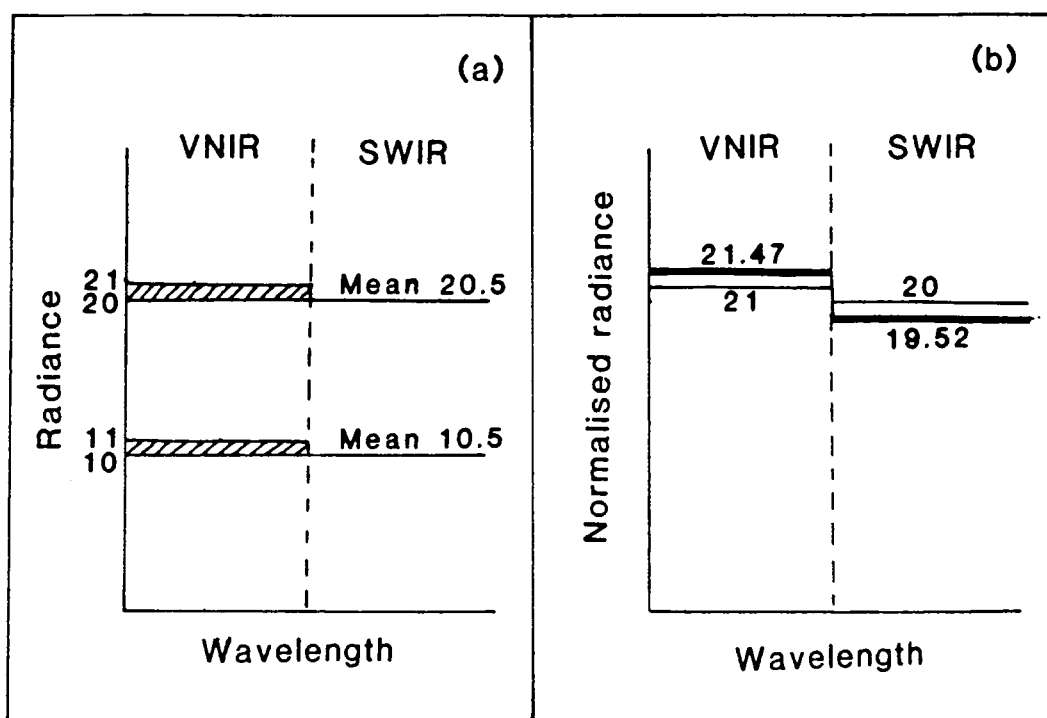
Figure 4.10   (a) Additive atmospheric scattering adds one unit to the spectra of a material in shadow (mean of 10.5) and in sunlight (mean of 20.5). (b) The added term affects the topographic shading correction, making the shadowed curve (thicker line) brighter in the VNIR and darker in the SWIR.
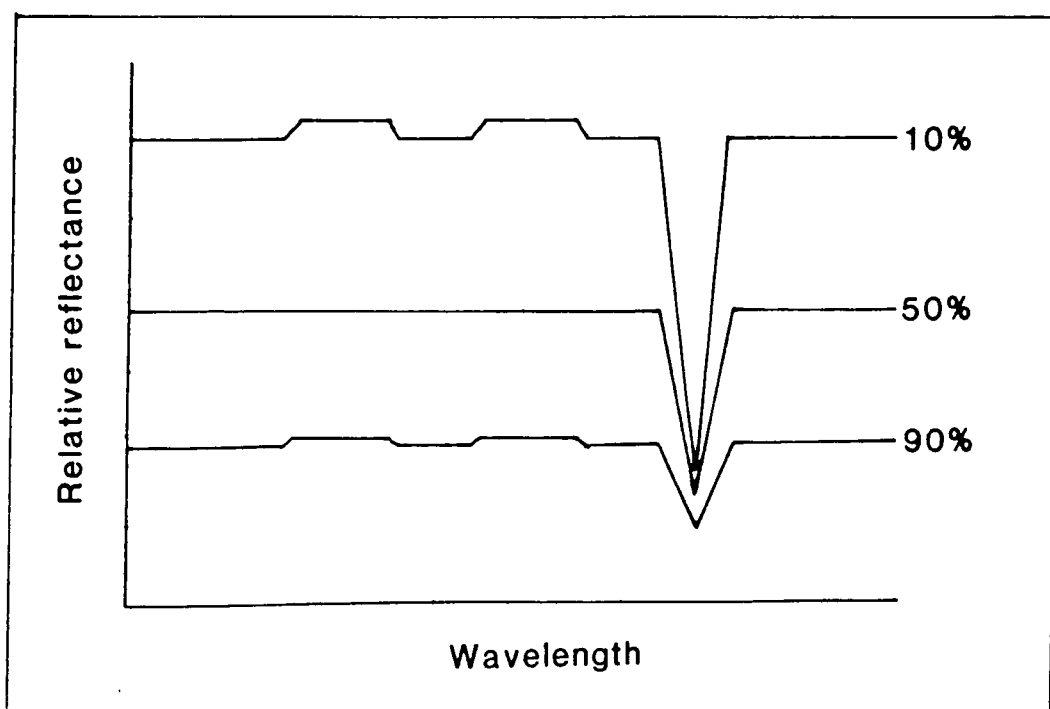
Figure 4.11   Varying the percentage of a scene component in the scene average will affect the output curves. The curves shown are the log residuals output of the data from figure , for percentages of 10%, 50% and 90% of the material with the extra absorption.

4.11. In the first curve, the material with the extra absorption (the blue curve) forms 10% of the scene, in the second curve it forms 50% and in third curve it forms 90%. The effect of varying the proportions is to vary the size of the extra absorption and also vary the size of the artifacts created by the processing. From this we can deduce, that it is impossible to directly estimate the proportion of a material in a pixel based on the depth of its absorption features, as the depth of absorption is related to the proportion of the material in the whole scene.

Another consequence of a single material covering a large area of a scene, for example covering 90% of the scene, is that the absorptions due to that material may be so severely reduced in depth, that they will be indistinguishable from the background noise and thus we have a loss of data.

A second problem effect is the generation of pseudo-absorption features during the curve averaging step (Kruse et al., 1985). An example using real data from the AIS - 1 instrument is shown in figure 4.12. Figure 4.12a shows three spectral curves for three different materials covering the wavelength range 2.12μm to 2.41μm. The red curve is that for a bare rock surface, the blue curve for dry vegetation and the green curve for green vegetation. A mixture was derived using equal proportions of each material to create an average curve (black).

The residual output curve for dry vegetation (blue) is shown in figure 4.12b after performing the curve averaging step using the average curve from figure 4.12a. As we can see the dry vegetation curve has been badly distorted and produces an absorption resembling calcite. The effects are dependent on both the spectral curve shape of the components and their proportions. This is a major effect which is entirely scene dependent. Without knowledge of the scene components it is therefore possible to produce spurious absorptions that resemble true mineral absorption features.

The final problem effect is due to random noise in IARR data, the effect is fairly obvious. When we produce our average curve, the effects of noise are suppressed due to the averaging process. When the average curve is divided back into each pixel, even if the pixel curve is close in shape to the average curve, the minor variations due to noise will be highlighted. In figure 4.13 the noise is highlighted and can cause problems when matching with the relatively

46
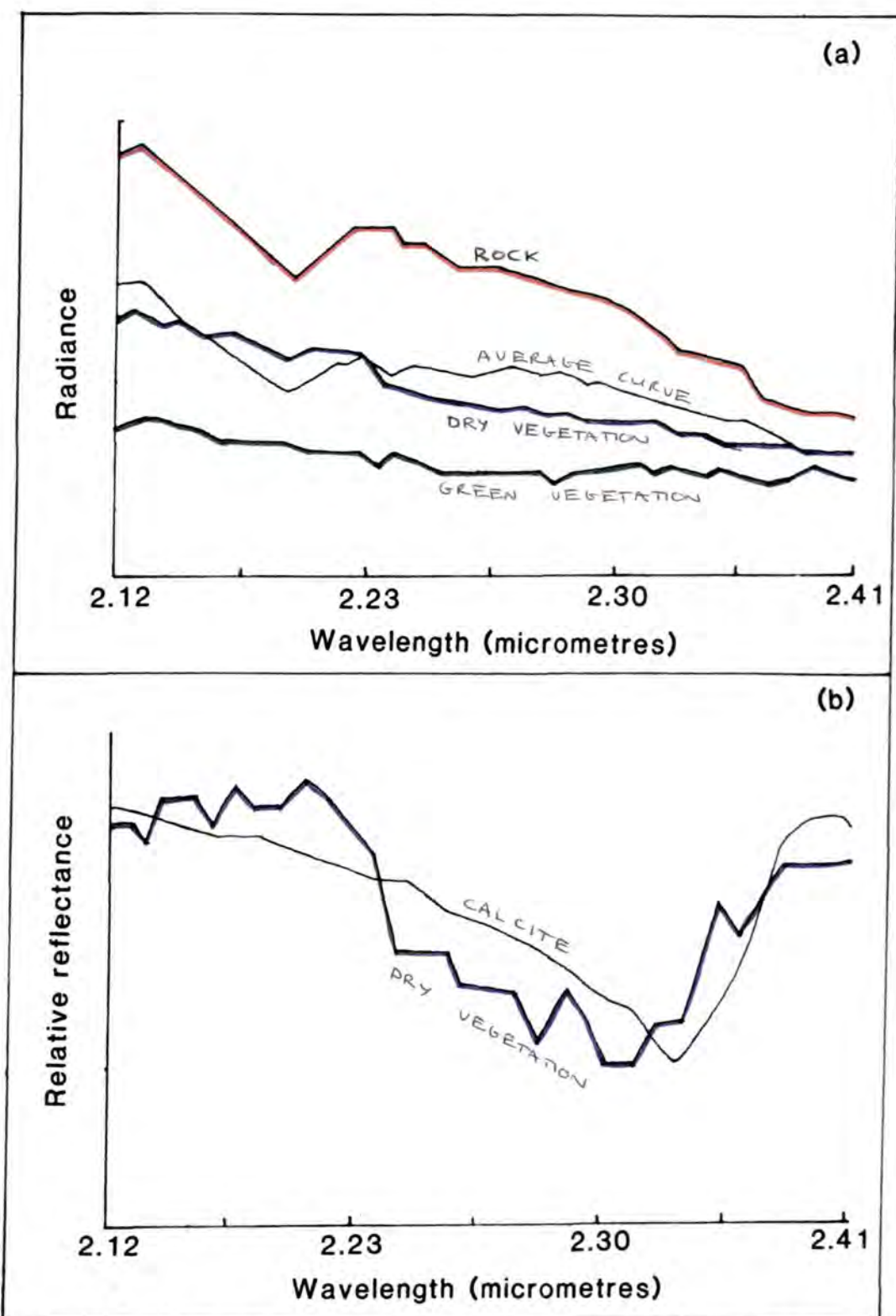
Figure 4.12 (a) The spectral curves of three materials are shown, with their average curve (black). (b) After performing the second step of log residuals, the curve averaging step (using the black curve). The dry vegetation residual curve is compared with a reflectance spectrum of calcite.
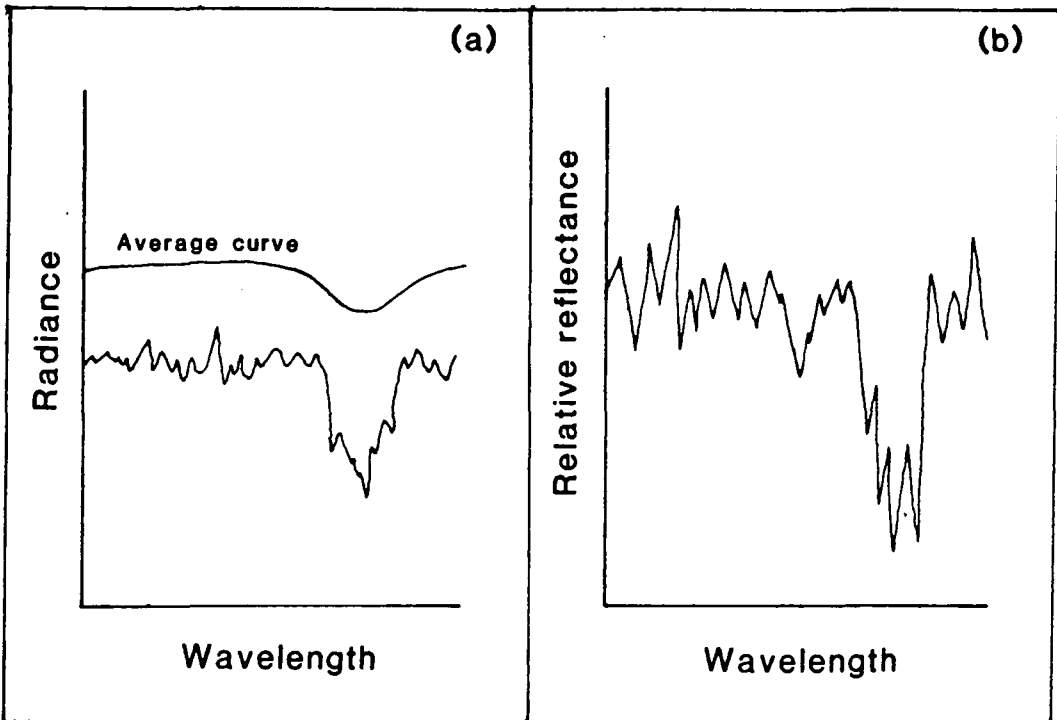
Figure 4.13   (a) The average curve of several pixels contains little noise, although an individual pixel may be quite noisy. (b) The division of the average curve into each pixel and the consequent rescaling highlights the noise element.
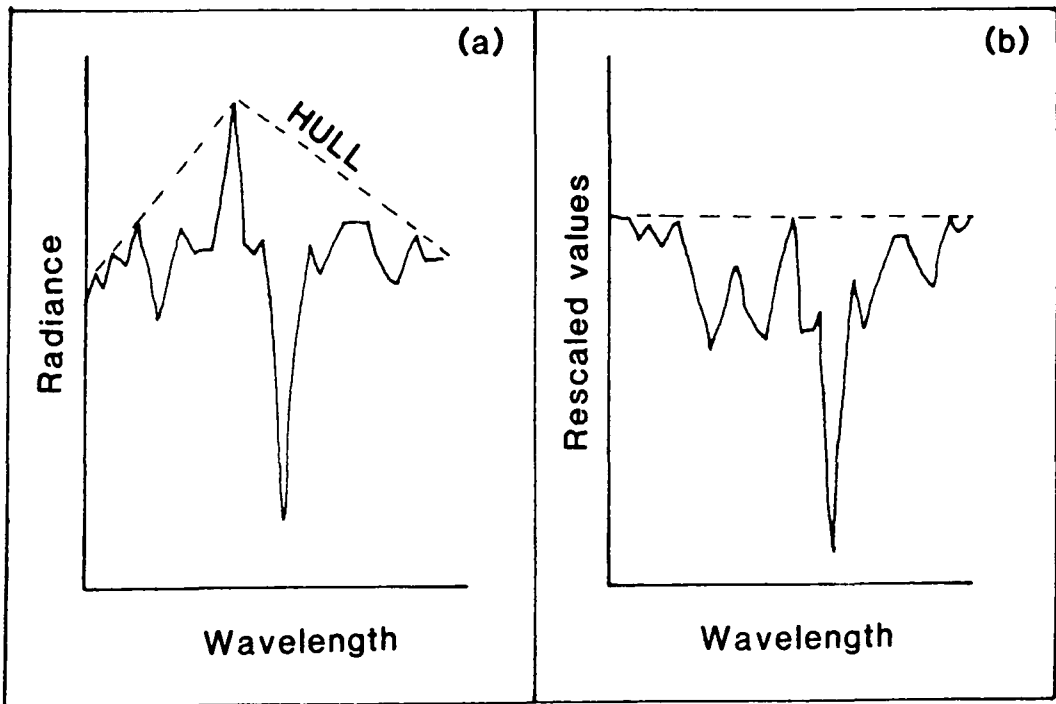
Figure 4.14   (a) The original noisy data and its fitted hull (dotted line). (b) The output showing the distorted features due to the presence of noise.

noise free reference spectra found in spectral libraries.

4.7 Hull quotients.

Earlier, we briefly discussed the basic method of producing a hull quotient output. This method is an entirely different processing philosophy to that of log residuals / IARR. Whereas log residuals / IARR is a mathematical averaging process, producing reflectance like spectra, hull quotients processes on a pixel by pixel basis and its output can not be compared with library reflectance spectra. The output of hull quotients is **not** dependent on the scene components or their proportions in a scene. However, variations in the atmosphere will affect the output to some degree.

The advantages of hull quotients are,

(1) There is no need for topographic shadowing correction as the intensities are not important. The positions of the absorptions, there relative depths and the feature shapes are important.

(2) The output is **not** dependent on the components making up the scene or the proportions of these components.

(3) Artifacts can not be created as no averaging is taking place.

4.8 Hull quotients - The problems.

As was the case with log residuals / IARR, there are several problem areas that need to be considered when using this processing technique. The problem areas are,

(1) Problems associated with variability in the data (Atmospheric and random noise).

(2) Problems associated with the spectral curve shape of surface materials.

(3) Problems at the analysis stage due to the lack of a suitable hull quotients reference spectral library for matching purposes.

The first problem area is related to the variability of the data itself. There are in fact two problems, atmospheric variability and random noise.

Although the hull quotients output is not affected by varying the scene components, or their proportions, atmospheric variations between scenes and

within a single scene will affect the form of the output. For example, if two separate flights were flown over the same area when the atmospheric conditions were different, the output curves from hull quotients processing would be different. We would see variations in the depths of atmospheric absorptions and the effects of atmospheric scattering, producing a different set of absolute values for the same pixel in the two different scenes. How detrimental these effects are for mineral exploration is questionable and needs further study. However, given that most spectral features of interest are away from wavelength regions where scattering is important and given that the areas of major atmospheric absorption contain little data of use to us, due to the low signal to noise ratios, then effects due to atmospheric variability may not be such a great problem.

The other and far more important effects regarding variability in the data itself, are the effects of random noise. As we discussed previously these effects are detrimental to processing using log residuals / IARR and reduce identification accuracy at the analysis stage. In figure 4.14 we can see what happens when we try to use hull quotients on noisy data. The noise spikes are picked out as spectral "highs" and the output spectrum is affected by the noise, reducing the identification accuracy. To use this technique effectively we need, ideally, noise free data. As sensor technolgy improves and by using effective spectral filtering techniques, it may be possible to produce output spectra that can be clearly and unequivocally identified. Even using the relatively noisy instruments currently available, it is possible to extract and identify mineral spectra in some cases. Figure 4.15 shows the output from hull quotients processing for the mineral sericite from GER - II airborne data and the corresponding log residuals spectrum, in both spectra the major absorptions are clearly identified.

The second problem area related to the spectral curve shape of the raw data. The hull quotients technique can be considered to be a rubber band stretched over the upper surface of the spectra, producing flat topped spectra containing identifiable features. However, if the spectral curve is concave rather than convex, the output spectra will not be matched effectively. This will badly affect any automated feature identification system that relies on isolating spectral features. An example is given in figure 4.16, the original

48
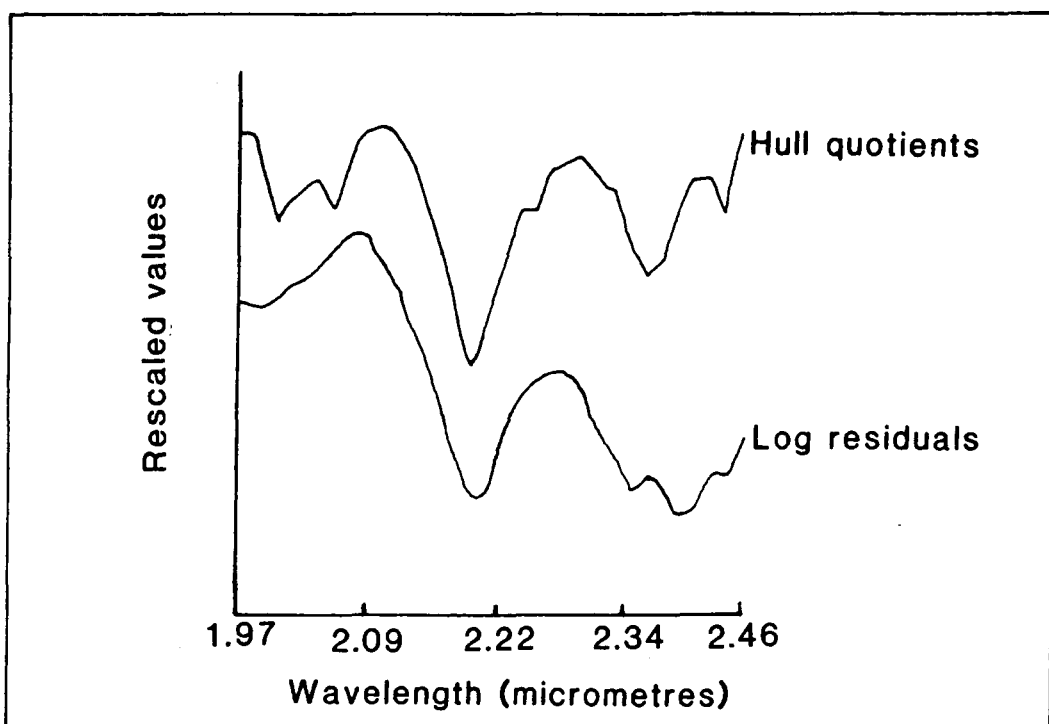
Figure 4.15   The upper plot is the hull quotients output over an area
rich in sericite. That below is the log residuals output of the same
area. The major absorptions are clearly visible in both spectra, with
the added atmospheric CO_2 absorptions in the hull quotients spectra
around 2.00μm.
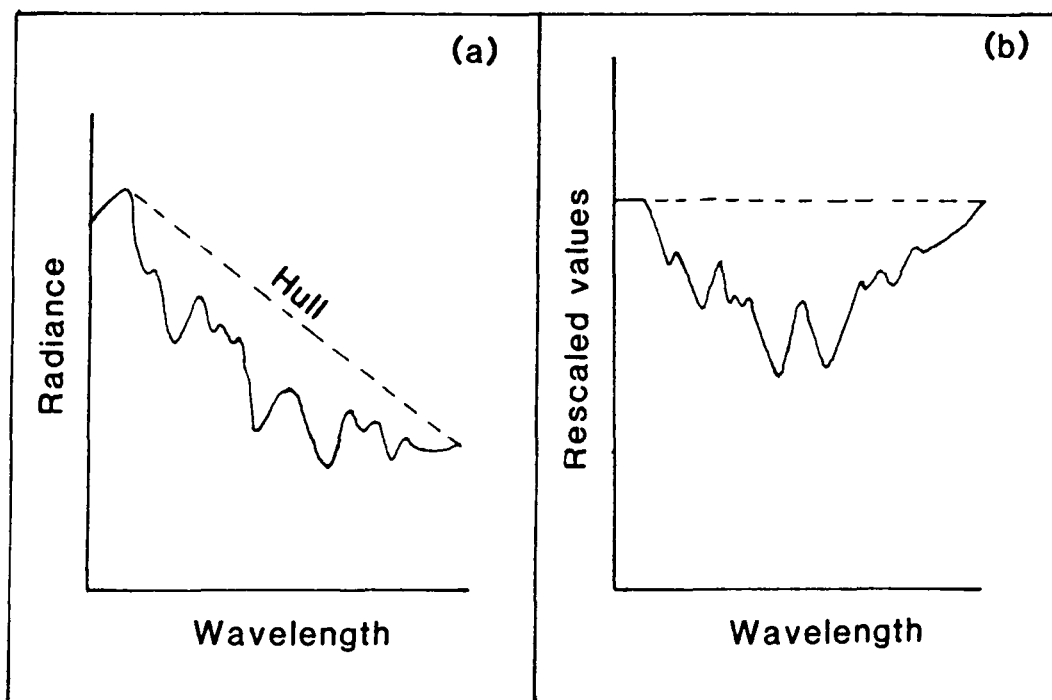
Figure 4.16   (a) Fitting the hull to a concave curve shape. (b) The output
does not contain isolated features that can easily be identified.

data and the corresponding hull quotients output spectrum are shown. As we can see, the shape precludes easy separation of individual features from the background. This problem may also apply to hull quotients, when used on a data set covering the 0.4μm to 2.5μm wavelength region, that contains the solar irradiance curve. Further work needs to be done to fully evaluate this problem. Work is proceeding in developing a form of hull quotients that can be applied to concave spectral curves (Clark et al., 1987). At the present time the techniques to use hull quotients and feature matching are still under development.

The third problem area is the lack of a suitable hull quotients spectral matching library for **airborne data**. This is only a problem at present, but will be rectified by the development in the near future of such a library. Clark et al. 1987, have used a hull quotients library for identifying minerals from **laboratory** reflectance spectra. It is only a matter of time before such libraries are generally available for **airborne data**.

The use of the hull quotients technique is at an early stage. Several problems are evident in its use. Its major advantage however, is the extraction of features which are independent of the overall scene composition and component proportions.

This technique may offer the most reliable output to be analysed by an automated feature identification system. However, if the problems of scene noise, variable atmosphere and unusual curve shape, can not be solved, the use of this method will be severly limited.

4.9   Analytical methods.

Most current image processing and analysis software has been developed to process low spectral resolution data such as TM (Thematic Mapper, Landsat 4) or MSS (Multi-Spectral Scanner, Early Landsat sattelites). The data sets have a maximum of six bands of data, covering the VNIR and SWIR wavelength regions.

With such a low number of bands we can not identify surface materials, as small absorptions of interest form only a small part of the total signal in a single broad band. In this case we can only carry out relatively simple

operations on the very limited number of bands to help discriminate between different surface materials.

Most standard techniques have been developed to enhance this ability to discriminate between materials. The output normally consists of a three band colour composite of the three bands that allow the greatest discrimination. However, without suitable ground reference data to identify the separated components, the information is of little use.

When we use high spectral resolution data, we have many more bands, for example AIS - 1 data sets have 128 bands, with this amount of spectral detail we can identify ground surface materials. However, using standard analysis techniques we can not practically use all this extra data, so data compression involving an actual loss of data is necessary. The data compression takes the form of a statistical reduction of the data, selecting those bands that account for most of the variance in the scene and displaying them as a three band colour composite (Feldman, 1987). The output is scene dependent and can only be used for discrimination. This defeats the purpose of collecting the extra information.

Due to the lack of suitable analysis techniques, the Jet Propulsion Laboratory (JPL) in California has developed the SPectral Analysis Manager (SPAM) to analyse high spectral resolution data sets, without the loss of information inherent in the broad band analysis techniques. The SPAM package is described in detail below.

4.10 SPectral Analysis Manager (SPAM).

Detailed descriptions of SPAM are available (Mazer et al., 1988) and thus the description given here is confined to an overview of the package, its most useful features and its limitations.

The SPAM package written in "C" was originally developed for use on a Rastertech Model 1/25 image processor, using a Sun workstation as a host computer. One of the original aims of this research project was to implement this software package on a VAX host computer, driving an IIS Model 75 image processor. This involved the conversion of the device interface code to call IIS system 600 software subroutines, to carry out the screen handling and data

MAIN

SESSION STARTING AND SAVING	GENERAL IMAGE PROCESSING	SPECTRAL-PROCESSING ROUTINES	SPECTRAL LIBRARY ACCESS	SEGMENTATION AND MIXTURE ANALYSIS	MISC SUPPORT COMMANDS
GET HARDCOPY KEEP (LIBCODE) PHOTO SNAPSHOT	FILTER FUNC DISP HIST RATIO STRETCH	CURVEGEN PLOT SCAN STORESPEC WAVELENG	DELETE DIGIPLOT DIRECTORY LIBPLOT SAVEPLOT	CLUSTER FIND IDENTIFY MERGE MIXTURE SEGDISP	ERASE HELP NORM RETURN

PARAMETER PROCESSING	SUBROUTINE LIBRARIES	VIRTUAL DEVICE AND OS ROUTINES
PAR TOKEN	HISTSUBS LIBRSUBS PLOTSUBS SEGSUBS SPAMSUBS SUBS	VDI VOS

Figure 4.17 The structural organisation of the original implementation of the SPAM package.

loading. The entire code was then compiled as a set of subroutines called through an IIS main routine. This routine was installed in what is called a user device executive (USERDE), which is basically a user environment that sets up a display device of an image processor (in this case the Model 75) in such a way, that the IIS system 600 software subroutines can operate the device. The outline of SPAM given below relates to this version.

Figure 4.17 shows the structural organisation of the SPAM package. Use of the package has shown it to be a very effective display package for spectral data.

Its major strengths are,

(1) The ability to PLOT spectra of individual pixels.

(2) The availability of a library of reflectance spectra of various surface materials and the ability to plot such library spectral curves.

(3) The ability to STORE spectra extracted from an image in a user spectral library and to retrieve and plot such spectra at a later date.

(4) A HARDCOPY function to get hardcopy output of displayed spectral plots.

(5) The WAVELENGTH function, using cursor control to get an accurate value of the wavelength at a chosen point from the spectral plot.

(6) The ZOOM function to zoom image and graphics to determine plot positions effectively on the image. It was found that small areas of interest could not be located and plotted using the cursor. This function was designed to enlarge an area 2, 4 or 8 times and find the X and Y co-ordinates of the pixel(s) to be plotted.

Other SPAM routines have a more limited use, these include,

(1) The MIXTURE algorithm, which fits up to six spectral curves chosen from the library or image to all the pixels in the scene (using a least squares fit). Output mixture maps are produced that represent the proportions of each of the six chosen minerals in each pixel based on the closeness of fit. The algorithm will match each pixel to the six spectra you provide. However, it will not identify the pixels on the ground, only match each pixel with your six chosen spectra. A bad choice of the six spectral curves will not be picked up by the algorithm, giving erroneous and misleading

results.

(2) The CURVEGEN routine allows a user to draw any spectral curve shape on the screen, under cursor control. The curve drawn can then be stored in the user library.

(3) The FUNC routine allows the user to mathematically manipulate spectral curves, for example adding percentages of different spectral curves to produce mixtures.

The major weaknesses of the SPAM package are,

(1) The lack of suitable spectral matching techniques, to match data extracted from the image with known reflectance library spectra. There are matching algorithms in the package such as FIND, however, they are noise sensitive and not specifically directed at the more important spectral regions such as the 2.2μm wavelength region.

(2) The CLUSTER and MIXTURE algorithms are heavily biased to determining the major scene components and again are noise sensitive. Minor components of the scene, that may be important in an exploration context are overlooked using these methods.

(3) The package will currently only deal with data sets that have an even spacing between bands with no gaps. This is of limited use when using data such as the GER - II data with its variable bandwidth.

(4) The interactive use of the system is very limited when dealing with large data sets. This leads to long delays when using MIXTURE (40 minutes) and CLUSTER (20 minutes) on a 512 x 512 x 32 data set.

To conclude, the SPAM package is a very effective display and plotting package. However, its spectral matching and classification algorithms are of limited use and are not effective in finding minor scene components.

4.11 Discussion.

Two very different processing methods have been discussed, the log residuals/ IARR processing method and the hull quotients method. The former produces an output which can be matched to library reflectance spectra and represents and extension of established methods, into an area where no ground data is available to extract reflectance values.

52

The latter method does not reduce the data to reflectance output spectra. Instead, the overall curve shape is removed and the spectral features that are the mineral absorptions are isolated. This method may provide the basis for an automated feature identification system.

It is clear that the current spectral matching and classification routines of available analysis packages (such as SPAM) are not very effective. The matching algorithms tend to be slow, badly affected by noise and biased towards the identification of the more abundant components in a scene. The hull quotients method is seen as a way to extract identifiable features that can be analysed in isolation from the rest of the mineral spectrum. The use of this processing technique to perform such a task is discussed in detail later in this thesis.

4.12 Summary.

Several processing methods were considered, but only three satisfied the major constraint that no ground data be required. These three methods are log residuals, IARR and hull quotients. The first two methods are equivalent and are based on the reduction of the data to reflectance like spectra for direct comparison to reflectance spectra from libraries. The hull quotients method is a totally different processing philosophy, which is based on the reduction of the data to a set of identifiable features, that may be analysed by an automated feature identification system.

In the area of analysis, data compression methods are more suited to the analysis of Landsat data sets (TM and MSS). Packages are being developed to analyse high spectral resolution data in a more suitable way. The SPAM package is an example of such a package. SPAM has many useful features such as its ability to plot spectral data and use a reflectance spectral library. However the major problem with SPAM lies in the area of matching spectral curves derived from the image with the reference spectral library. No suitable classification and matching algorithms are available, especially for minor scene components.

4.13 Conclusions.

(1) The collection of suitable ground data is time consuming, sometimes impossible, if there are no suitable ground targets and is impractical for grass roots exploration.

(2) Without ground data it is impossible to achieve true reflectance output spectra from airborne data.

(3) The use of log residuals / IARR methods (which require no ground data), to reduce the data to pseudo-reflectance has proved to be an effective technique in certain circumstances allowing direct comparisons between the output spectra and relectance spectral libraries.

(4) The log residuals / IARR methods can produce pseudo-absorptions and spectral artifacts that can be confusing at the identification stage.

(5) The log residuals / IARR methods are scene dependent, the outputs are variable based on the spectral curve shapes and proportions of the materials that make up the scene.

(6) The hull quotients method provides an alternative processing philosophy that produces output spectra that are not affected by the overall composition of the scene, or the proportions of the materials making up the scene. This technique also requires no ground data to operate.

(7) The hull quotients spectra do contain variable atmospheric effects. Further work is necessary to determine whether these effects are important and whether they can be removed by atmospheric modelling.

(8) The decrease in the solar irradiance curve towards $3.0 \mu m$ may be a problem when using hull quotients, preventing the extraction of individual features for use in the identification process.

(9) Presently no suitable spectral library exists for matching hull quotients output curves **from airborne data**.

(10) Visual and discriminatory methods of analysis such as those used to analyse TM and MSS data are impractical for high spectral resolution data sets.

(11) Methods of data compression prevent identification of surface materials, only allowing discrimination between surface materials this needs excessive ground data and is scene dependent.

(12) The SPAM package is an early attempt to use high spectral resolution data effectively. The ability to plot and display spectra and the use of a reflectance spectral library have proved to be very useful.

(13) The limitations of the spectral matching techniques of the SPAM package are clear. More suitable techniques need to be developed, that will also identify the minor components in a scene.

(14) Some form of selection criteria must form part of an identification system of material spectra. Otherwise, the important interactive element of the use of such a package will be lost.

(15) The RGN technique (Mackin et al., 1987) is a hybrid form of the log residuals / IARR techniques and is much more effective at **visually** highlighting absorption features in the data than log residuals / IARR.

CHAPTER 5

INTERPRETATION AND DISCUSSION OF THE RESULTS, OBTAINED FROM THE AIS - 1 INSTRUMENT FLIGHT OVER AN AREA OF NORTHERN QLD., AUSTRALIA.

5.1 Introduction.

High spectral resolution data was collected during the US - Australia joint scanner project, using the AIS - 1 imaging spectrometer. The AIS - 1 data was collected on the 26th October 1985, the parameters of the flight are listed in Table 5.

The flight was over an area 60 km south-east of Charters Towers in Northern Queensland, Australia, figure 5.1. The aims of the study were,

(1) To test the mineralogical mapping capabilities of the experimental AIS - 1 system.

(2) To assess its performance in an area of variable vegetation density and deep weathering profiles.

5.2 Climate, topography and vegetation.

The climate of the area is tropical, with warm, dry winters and hot, wet summers, July to October being the driest period.

The topographic relief is variable, and highly dependent on the underlying geology. The Ravenswood Granodiorite Complex underlies most of the area and tends to give rise to undulating dissected country with a dendritic drainage pattern. A major volcanic unit, the Mount Windsor Volcanics forms a more prominent range of hills (Seventy Mile Range), which rises 100m to 250m above the surrounding Ravenswood Granodiorite Complex. Large areas of flat tablelands are found, especially in the south-western part of the area covered by the flight lines. These areas consist of laterite, produced during an earlier period of extensive tropical weathering, the tablelands are partly dissected, forming mesas and buttes of various sizes (Wyatt et al., 1971).

```
┌─────────────────────────────────────────────┐
│              AIS - 1   PLATEAU TEST SITE      │
│                                               │
│                  QUEENSLAND, AUSTRALIA        │
├─────────────────────────────────────────────┤
│                                               │
│   LOCATION    -   60km south-east of Charters │
│                                               │
│                   Towers, Queensland.         │
│                                               │
│   DATE OF FLIGHT  -   October 26th 1985.      │
│                                               │
│   ATMOSPHERIC CONDITIONS  _   Good.           │
│                                               │
│   ALTITUDE   -    6120m   A.S.L.              │
│                   5870m   above ground        │
│                                               │
├─────────────────────────────────────────────┤
│                                               │
│                                               │
│   APERTURE     -     1.9 M RAD   (0.11°)      │
│                                               │
│   GIFOV        -     11.1m                    │
│                                               │
│   SWATH WIDTH  -   355m                       │
│                                               │
│   LINE LENGTHS -   Flight Line 1  -  18.5 km  │
│                                               │
│                    Flight Line 2  -  28.0 km  │
│                                               │
└─────────────────────────────────────────────┘
```

Table 5.
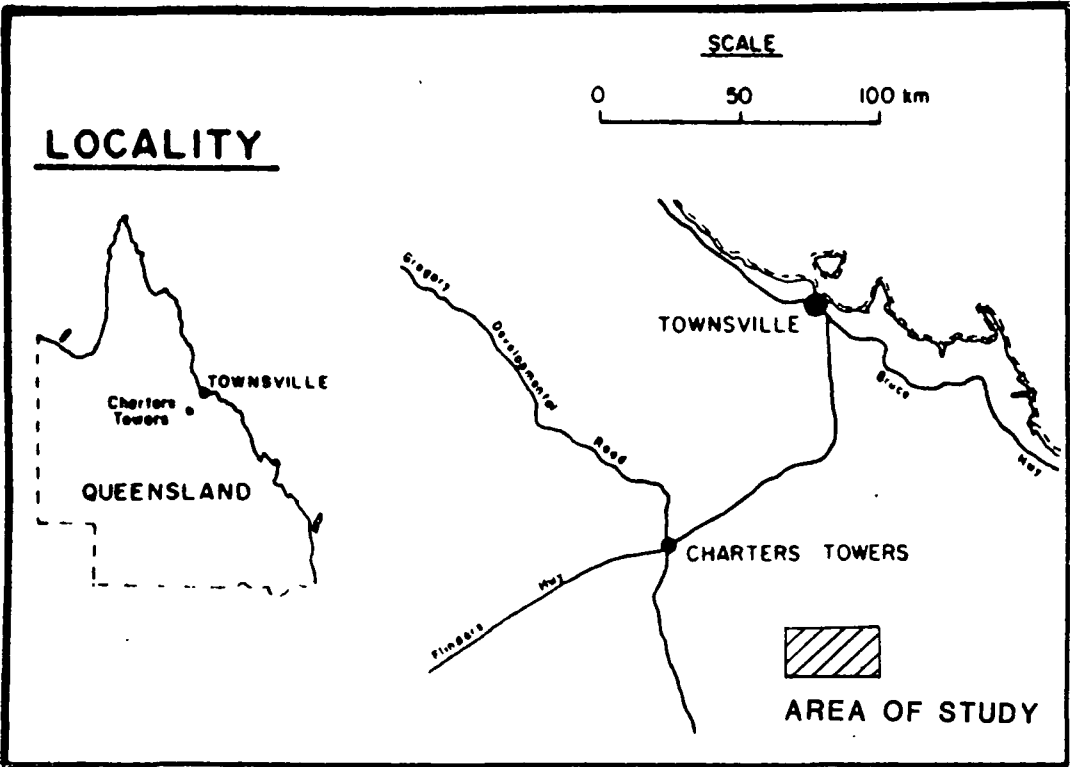
Figure 5.1   Locality map, showing the area of study in Queensland, Australia.

The vegetation distribution is uneven and is partly dependent on the underlying geology. The Ravenswood Granodiorite Complex is dotted with areas of eucalypt woodland and savannah cover, the eucalypt species being broadly related to the underlying rock type. For example the broad leaved iron bark eucalypt favours the acid volcanics and intrusions of granitic composition, while the andesites of the south-west have a fairly open eucalypt cover but a dense grass understorey.

5.3   General geology.

The area is located over the boundary between two major structural elements the Lolworth - Ravenswood block and the Drummond basin. A geological map (figure 5.2) shows the major geologic units in the area, and the positions of the two lines flown over the area.

A brief geological history of the area is given below, based on the work of Wyatt et al., (1971).

CAMBRO-ORDOVICIAN. The earliest sediments and volcanic rocks were formed during this period. Of particular interest are the Cape River Beds now comprising metamorphosed sediments and the lenses of acid and intermediate volcanic rocks known as the Mount Windsor Volcanics, which form the backbone of the Seventy Mile Range.

MID-ORDOVICIAN and UPPER SILURIAN - LOWER DEVONIAN. The early Cambro-Ordovician sediments and volcanic rocks suffered the variable effects of dynamic and thermal metamorphism, which accompanied the intrusion of the Ravenswood Granodiorite Complex, now underlying most of the area of study. The complex is a huge batholith emplaced in several stages, an early granodioritic phase and a later granitic phase have been recognised. The granitic phase tends to form plutons that occur towards the edge of the batholith. Most of the gold mined during the last century occurred either in the Ravenswood Granodiorite or in the overlying Cape River Beds in the form of tabular lodes. All this early activity was confined to the northern structural element, the Lolworth-Ravenswood block, which became a major structural high and erosional feature at the end of the Lower Devonian.

UPPER DEVONIAN - LOWER CARBONIFEROUS. The Lolworth-
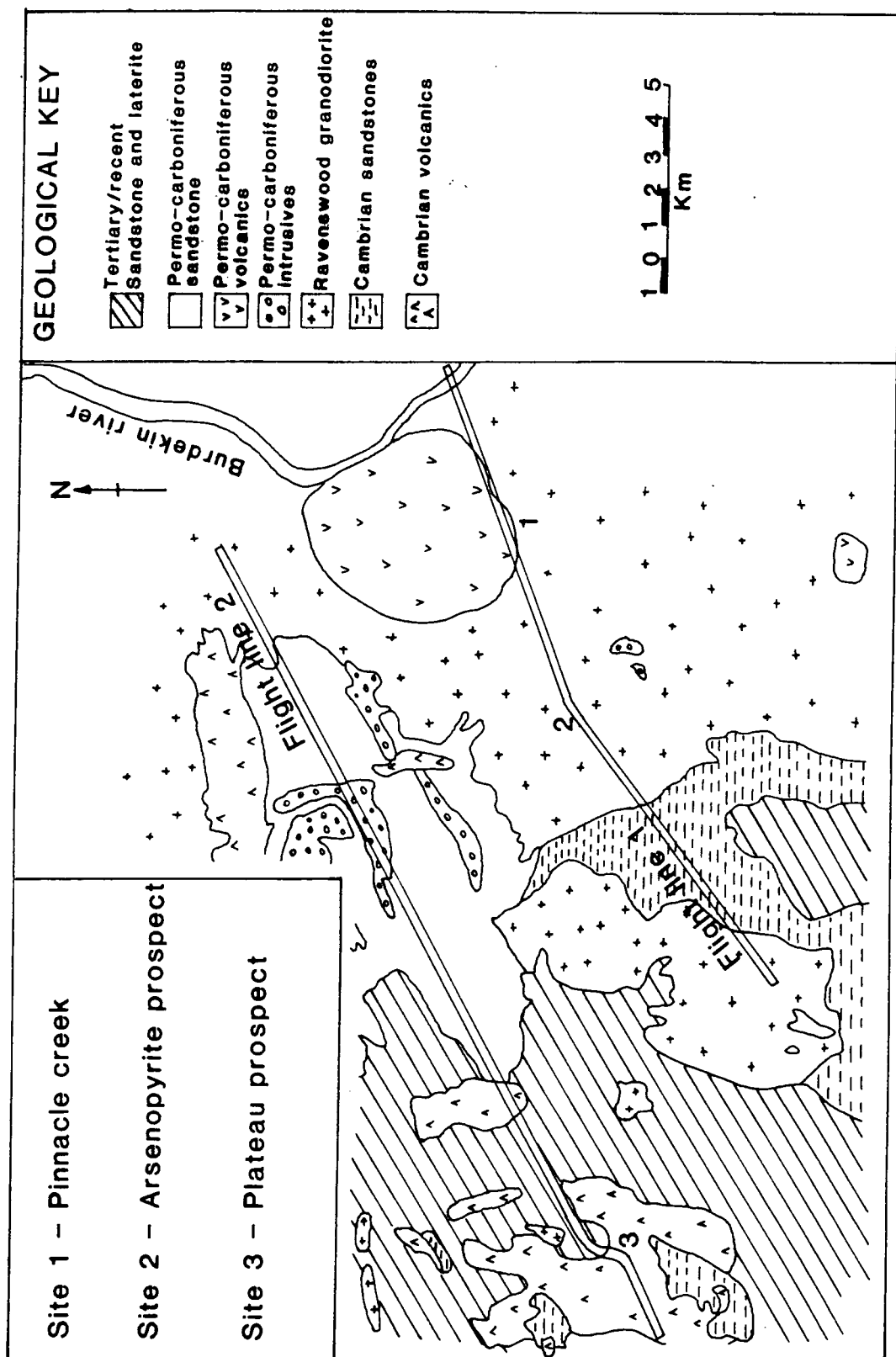
Figure 5.2 Geological and location map of the area of study. Site numbers are described in the text.

Ravenswood block was a source of sediments to the other main structural element, the Drummond Basin to the south. The sediments consist of abundant lithic and feldspathic sandstones with some conglomerate and volcanic members. The sediments were deposited in fluvial and lacustrine environments and form a sequence 4000m thick. These sediments were folded during the middle Carboniferous.

UPPER CARBONIFEROUS. Both structural elements were fractured during this period and acid magma erupted as lavas and pyroclastics. High level plugs, granite stocks and complexes were also emplaced during this period.

TERTIARY. Deposition of argillaceous and feldspathic sandstones in fluvial and lacustrine environments took place in the early Tertiary, followed by a period of extensive lateritisation. A horizontal blanket deposit of argillaceous sandstone and siltstone, the Campaspe beds, disconformably overlies the lateritised surface. Recent dissection of the surface has left only isolated remnants of the lateritised surface, these are strongly in evidence in the south west of the area of study.

5.4   Mineralisation and alteration.

The mineralisation and alteration of the country rocks, are confined to two quite separate episodes. The first in the upper Devonian (395 million years ago) is known as the Ravenswood II epoch.

During this period of mineralisation, mesothermal veins were emplaced in NNW and ENE trending fractures, within the granodiorite. Mineralisation was primarily base metals with a little gold. The fractures tend to be narrow and contain sulphide rich gossans with little silicification.

Alteration of the country rocks is generally of quite low grade, propylitic, with the sericitisation of feldspars and breakdown of biotite and amphibole to give chorite, epidote and a little calcite. In the lode/shear systems, chlorite, calcite, quartz and sericite are the most abundant alteration minerals.

The second period of mineralisation was during the Permo-Carboniferous, with the emplacement of high level rhyolite and granite plugs and stocks. Epithermal gold rich systems are known to accompany such high level intrusions. The alteration mineralogy is very distinct, consisting of alunite, jarosite, py-

rophyllite and kaolinite. No evidence for this alteration suite has been seen in the AIS - 1 data.

5.5   AIS - 1 Data processing and analysis.

Prior to the first visit to the field area, the AIS - 1 data set was prepared, processed and partly analysed.

The processing methods chosen were the log residuals / IARR method, which requires no ground data and the Ratio Group Normalising method.

The output needed for the field studies, were simple map images, that highlighted anomalous areas for detailed ground follow up. The log residuals / IARR output could not be used as a visual guide, due to the confusing masking effects of green vegetation (See Chapter 4). However, the modified Ratio Group Normalising (RGN) technique could be used on the same prepared data to produce the necessary output images.

Figure 5.3 is a diagram showing the data preparation and processing steps. Two anomaly maps were produced from the output of the RGN technique. One map is centred on the main clay absorption area of 2.2μm, the other on the main carbonate absorption area around 2.35μm. These anomaly maps were checked against aerial photographs of the area, to help determine ground position more accurately.

The prepared data from the two flight lines indicated three sites, which showed highly anomalous features. Ground data was collected from these sites during a single field season, the site locations are marked in figure 5.2. After the field season, the AIS - 1 data was processed using the normal log residuals / IARR method. Spectra were extracted from the log residuals / IARR output from specific locations at the three sites checked in the field. The log residuals / IARR method was used, as there were a lower number of spectral artifacts than when using the RGN method. The output spectra from log residuals / IARR should be closer in shape to library reflectance spectra than that from RGN processing.

Analysis was carried out using the SPAM package, for spectral plotting of the data and plotting of library reflectance spectra. Due to the poor data quality of the instrument (even after spectral filtering), spectral plots were

```
┌─────────────────────────┐
│    Tape to disk copy    │
└─────────────────────────┘
│
┌──────────────────────────────────────────┐
│ Rescale data to byte for display device  │
└──────────────────────────────────────────┘
│
┌ ─ ─ ─ ─ ─ ─ ─ ─ ─ ─ ─ ─ ─ ─ ─ ─ ─ ─ ─ ┐
│           DATA PREPARATION              │
├ ─ ─ ─ ─ ─ ─ ─ ─ ─ ─ ─ ─ ─ ─ ─ ─ ─ ─ ─ ┤
│   Vertical destriping  -  Testvert.for  │
│                                         │
│   Horizontal destriping - Cleanhoriz.for│
│                                         │
│   Spectral noise filter  -  Filter.for  │
└ ─ ─ ─ ─ ─ ─ ─ ─ ─ ─ ─ ─ ─ ─ ─ ─ ─ ─ ─ ┘

┌ ─ ─ ─ ─ ─ ─ ─ ─ ─ ─ ─ ─ ─ ─ ─ ─ ─ ─ ─ ┐
│           DATA PROCESSING               │
├ ─ ─ ─ ─ ─ ─ ─ ─ ─ ─ ─ ─ ─ ─ ─ ─ ─ ─ ─ ┤
│ Log residuals    IARR - Step 1    RGN - Step 1 │
│ Logr.for         Norm.for         Norm.for     │
│                                                │
│                  IARR - Step 2    RGN - Step 2 │
│                  Aver.for         Model.for    │
└ ─ ─ ─ ─ ─ ─ ─ ─ ─ ─ ─ ─ ─ ─ ─ ─ ─ ─ ─ ┘

┌ ─ ─ ─ ─ ─ ─ ─ ─ ─ ─ ─ ─ ─ ─ ─ ─ ─ ─ ─ ┐
│              ANALYSIS                    │
├ ─ ─ ─ ─ ─ ─ ─ ─ ─ ─ ─ ─ ─ ─ ─ ─ ─ ─ ─ ┤
│   SPAM──────────────── Images of bands  │
│   Spectral curves      at 2.2um and 2.35um │
└ ─ ─ ─ ─ ─ ─ ─ ─ ─ ─ ─ ─ ─ ─ ─ ─ ─ ─ ─ ┘
```
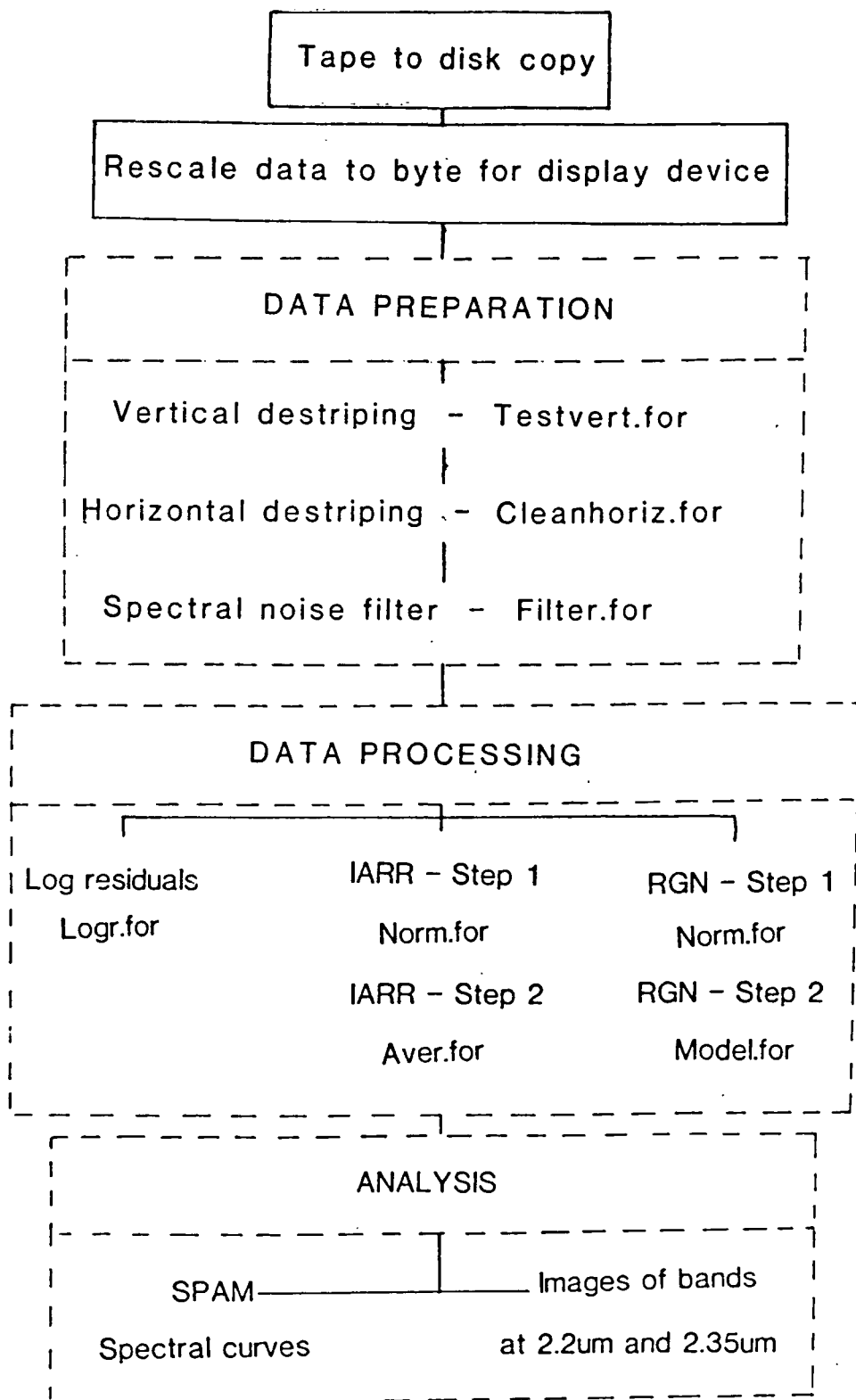
Figure 5.3 Outline of the data preparation, processing and analysis steps.

obtained from an average of several pixels, usually nine. This tended to enhance the signal, but increased the problem of spectral mixing of several components over the larger area.

5.6 Expected spectral responses.

The collected data from the three sites along with laboratory studies of returned samples, confirmed the presence of several minerals, that have identifiable absorption features in the 1.2μm to 2.4μm wavelength range (the AIS - 1 data range). The major surface materials identified with spectral features in this data range are,

(1) Green vegetation.

(2) Dry vegetation.

(3) Sericite [Muscovite].

(4) Illite.

(5) Kaolinite.

(6) Chlorite.

(7) Calcite.

(8) Epidote.

Figure 5.4 shows the spectral response, covering the wavelength range 0.4μm to 2.4μm for the materials listed above. Green vegetation is not included, as only the two major water absorption features at 1.4μm and 1.9μm are present within the spectral coverage of the AIS - 1.

The two anomaly maps produced by RGN processing, could isolate anomalies related to sericite, kaolinite, and illite (2.2μm) and epidote, calcite and chlorite (2.35μm) as indicated in figure 5.4.

Certain features of the material spectra are diagnostic, these features are listed below for the materials identified.

GREEN VEGETATION (1).

Has very few features in its reflectance spectrum. Usually, just the two major absorptions due to cellular water, at 1.4μm and 1.9μm (Elvidge, 1988).

DRY VEGETATION (2).

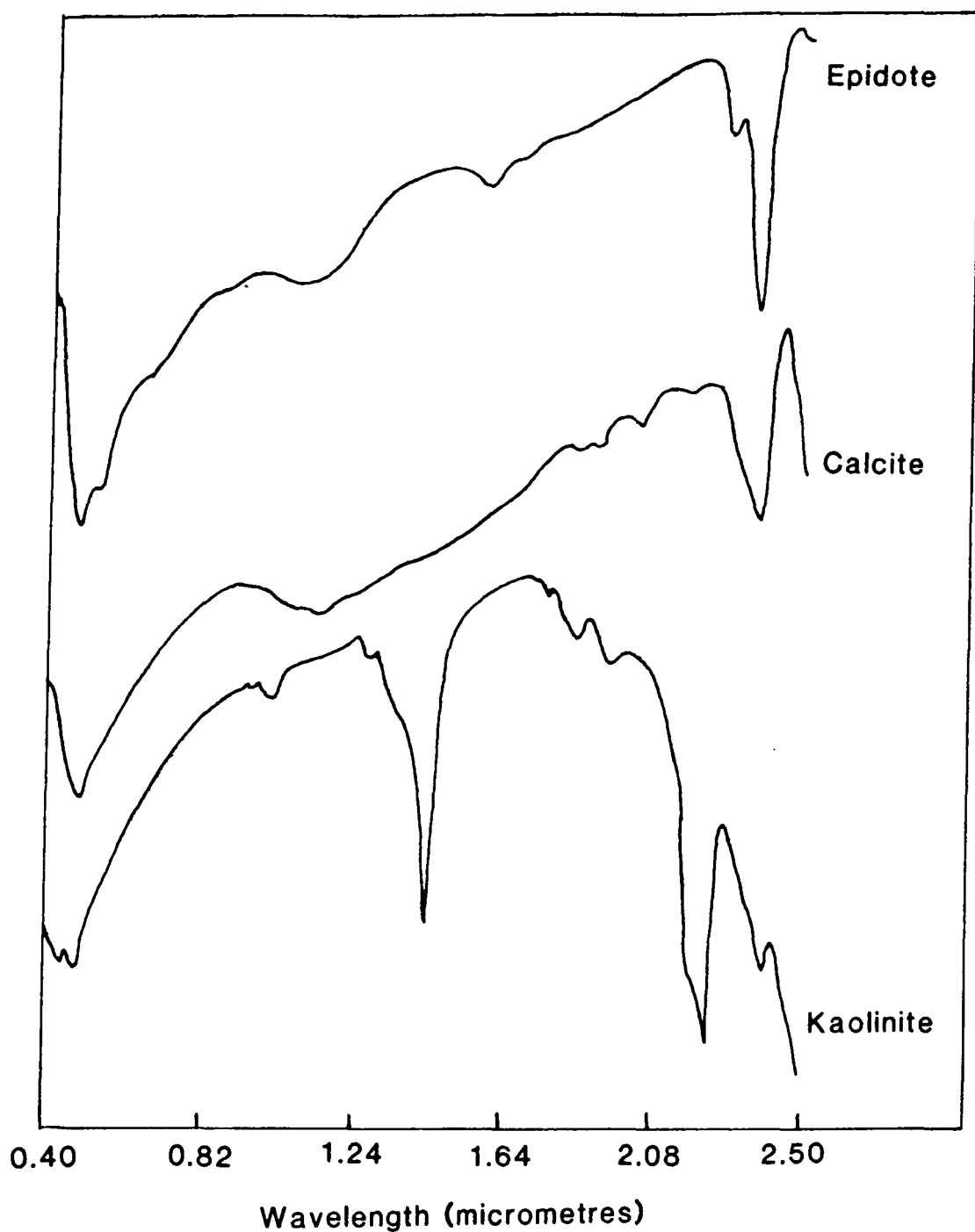Has many distinctive absorption features due to cellulose and other plant

Figure 5.4 Laboratory reflectance spectra collected using an IRIS Mk IV spectroradiometer, referenced to a barium sulphate reference panel. The materials shown, commonly occur at the sites of interest.

Dry vegetation

Sericite

Illite

Chlorite

0.40   0.82   1.24   1.64   2.08   2.50

Wavelength (micrometres)
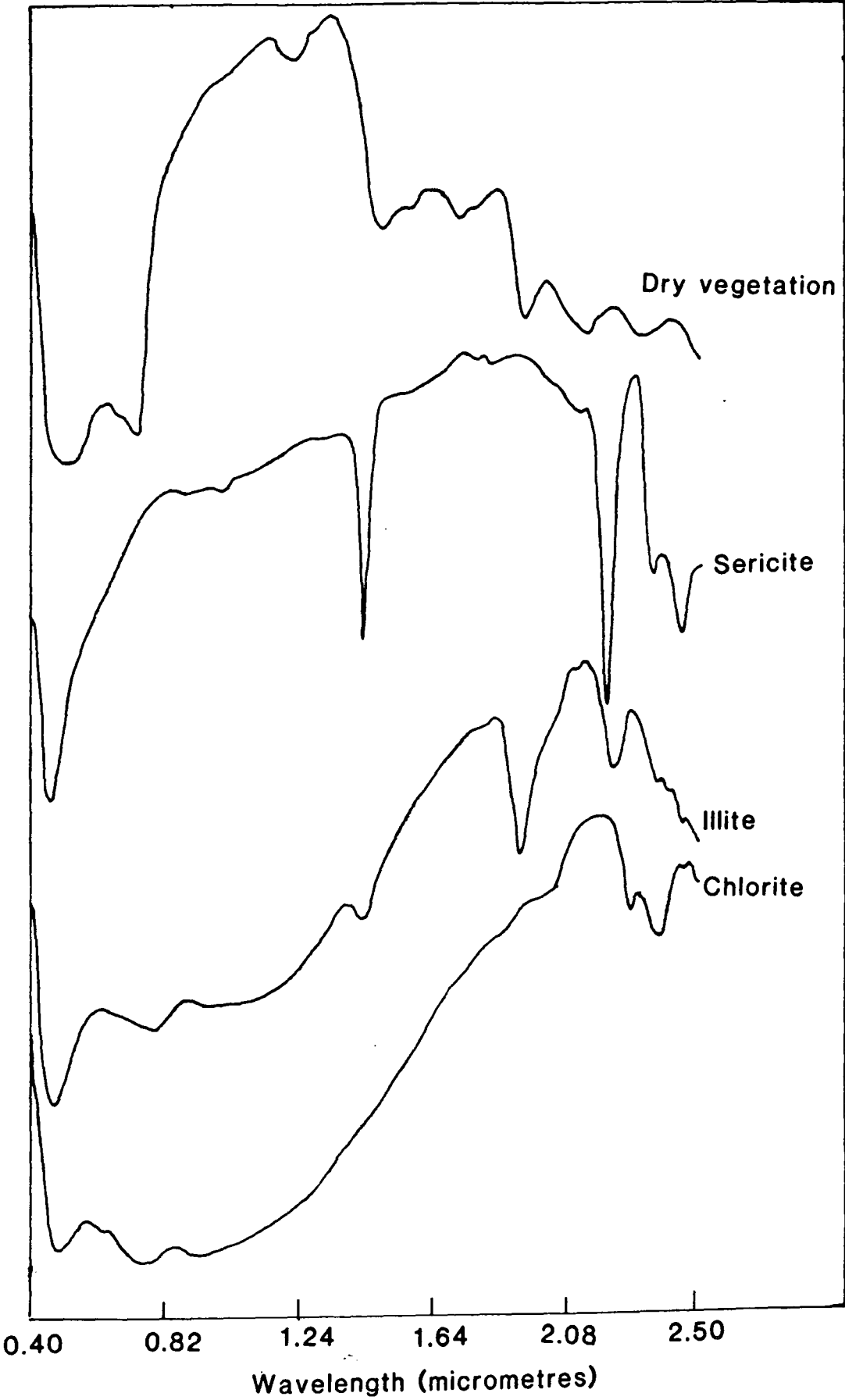
materials. The reflectance spectrum has a distinct absorption at 2.1μm and a steep drop off in reflectance between 2.27μm and 2.32μm (Elvidge, 1988).

SERICITE (3).

Has distinct absorptions due to $Al - OH$ bending - stretching vibrations of the mineral bonds. The diagnostic features are a deep, narrow absorption centred at 2.2μm, with a steep drop off in reflectance to 2.32μm(Hunt et al., 1970). Outside this wavelength region, the 1.4μm water absorption band will tend to be deep and narrow, related to the presence of the OH ion. Generally, the 1.4μm feature will be obscured in airborne data, by atmospheric water absorptions.

ILLITE (4).

Has similar absorptions to sericite as its structure is very similar. Its main features are related to $Al - OH$ bending - stretching vibrations. The main differences from sericite are its main absorption, which is broader and at a slightly longer wavelength (2.21μm), a less pronounced drop off in reflectance to 2.32μm and the broader and less well pronounced 1.4μm water absorption feature, with a deep, broad water absorption feature at 1.9μm. The features at 1.4μm and 1.9μm will tend to be obscured in airborne data, by the masking effect of the deep atmospheric water absorptions of the atmosphere.

KAOLINITE (5).

Another clay, of different structure to sericite and illite. The differences in structure produce slightly different diagnostic absorptions. The main absorption at 2.2μm still exists, but is much broader, extending down to 2.16μm, where the spectral curve flattens, producing a distinct shoulder in the spectral response. The decrease to longer wavelengths is much more gradual and is less deep (Hunt et al., 1970).

CHLORITE (6).

Not a single mineral, but a series of magnesium aluminosilicates. The major absorption features are centred around 2.32μm. The shape of the spectral curve in this region is more indicative than the major absorption position (Hunt et al., 1970).

CALCITE (7).

The major diagnostic features are related to the bending - stretching vibra-

tions of the $C - O$ bonds in the carbonate ion. The major feature is centred at 2.35μm and is distinctly asymmetrical (figure 5.4). Smaller features are seen at 2.00μm and 2.06μm, but these are generally obscured in airborne data by the carbon dioxide absorptions of the atmosphere (Gaffey, 1985).

EPIDOTE (8).

This mineral is a calcium aluminosilicate, its most obvious spectral features are its deep symmetric absorption centred around 2.34μm to 2.35μm, with a minor absorption centred at 2.25μm.

Finally, note that some common surface minerals have no diagnostic absorption features in the 1.2μm to 2.4μm wavelength region. These include quartz and feldspar (Hunt et al., 1970).

5.7   Site locations.

The two flight lines run in a north-east to south-west direction. The three anomalous sites shown are marked 1, 2 and 3 on the map, figure 5.2.

These sites are,

Site 1 - Pinnacle Creek.

Site 2 - Arsenopyrite prospect.

Site 3 - plateau prospect.

5.8   Site 1 - Pinnacle Creek.

The area lies at the north-eastern end of the flight lines and is marked 1 on figure 5.2.

5.8.1   Topography and vegetation.

The area is centred on a bend in the main watercourse, Pinnacle creek. The topography rises gently to the south within the bend of the creek and steeply to the north. The topographic range is of the order of a hundred metres. The vegetation is primarily scattered eucalypt with a little scattered green and dry grass. The vegetation density increases along the banks of the major creeks in the area, although the canopy is still incomplete. The species of eucalypt varies in the area in response to the underlying geology, the more acid volcanic rocks supporting a thin cover of broad leaved iron bark, while
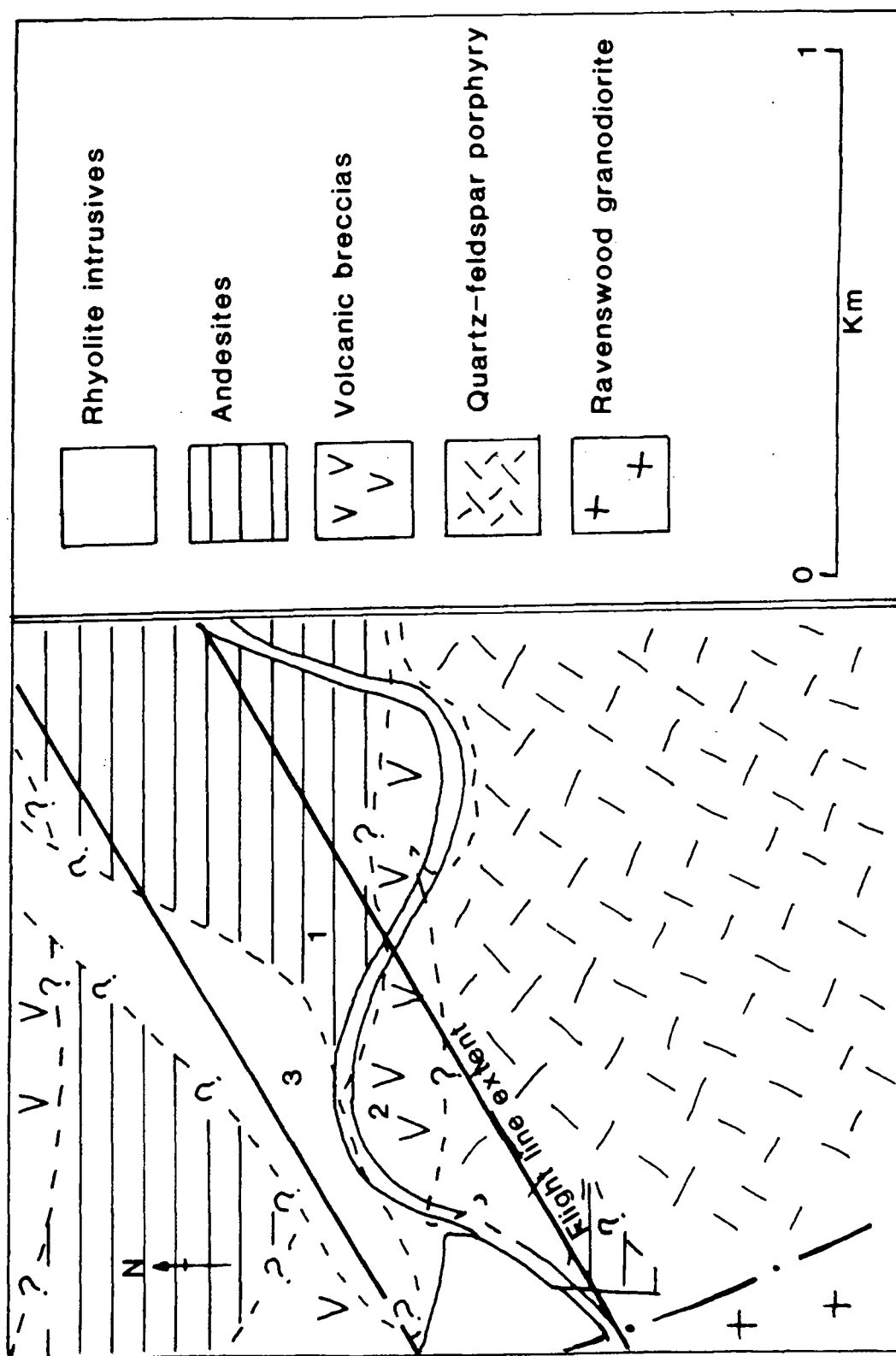
Figure 5.5   Geological map of the Pinnacle creek area.   The location numbers are referred to in the text. After Lorroway, 1976.

the less acid members support a thicker cover of a narrow leaved species.

5.8.2 General geology.

The area was mapped on a detailed scale by Lorraway (1976). The geological map of this area, figure 5.5, is based largely on his work. There are six main units in the area,

(1) Ravenswood granodiorite (Ordovician - Devonian).

(2) Volcanic breccias (mid-upper Carboniferous).

(3) Quartz-feldspar porphyry (mid-upper Carboniferous).

(4) Andesite lavas (mid-upper Carboniferous).

(5) Intrusive rhyolite (mid-upper Carboniferous).

The relationships between the six units are shown in figure 5.6 and the geological history follows. The intrusion of the Ravenswood Granodiorite Complex took place in Ordovician - Devonian time and was followed by a period of extensive weathering in the area, producing an unconformable boundary between the granodiorite and the much younger, mid-upper Carboniferous, volcanic breccias. These two units were intruded by a quartz-feldspar porphyry in the area south of Pinnacle creek, figure 5.6. The volcanic breccias sandwich two separate andesitic units, the andesite lavas of the South and the fresher andesite lavas. The whole sequence is cut by intrusive rhyolite dykes. All the units in the area have suffered low grade regional metamorphism related to the thickness of the former, overlying volcanic pile which has subsequently been eroded away.

Of these six units, three are represented in the flight line covering this area. The geological map, figure 5.5, also shows the boundaries of the flight line and a series of locations, numbered 1 to 3, that are described in detail below.

LOCATION 1. Is an area of scattered eucalypt with thin, patchy, dry grass (Number 1, figure 5.5, plate 5.1). The rocks are andesites, with an exterior colour varying from blue-grey to green to mauve. On fresher surfaces they are fine grained and grey, with pink and white phenocrysts of feldspar. Some anhedral quartz is visible. Some of the fresher samples are rich in epidote, while the more weathered green and mauve rocks (plate 5.2) are rich in calcite and chlorite, with extensive calcite veining visible at some locations

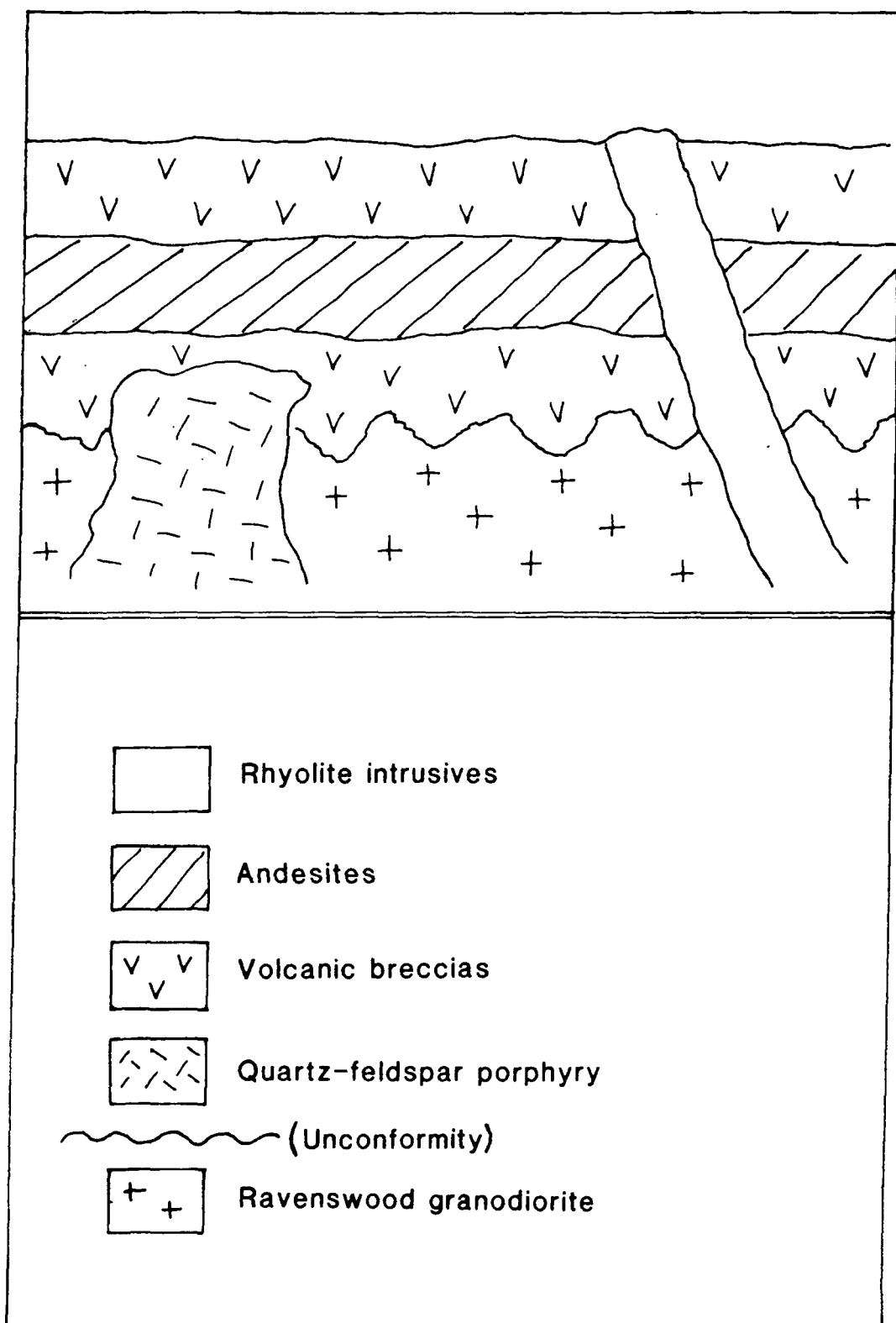Figure 5.6   A geological schematic section of the Pinnacle creek area.

Plate 5.1   Location 1 at Pinnacle creek (Site 1). Scattered eucalypt are present. Outcrop of the andesites is limited, most samples form float on the soil surface.
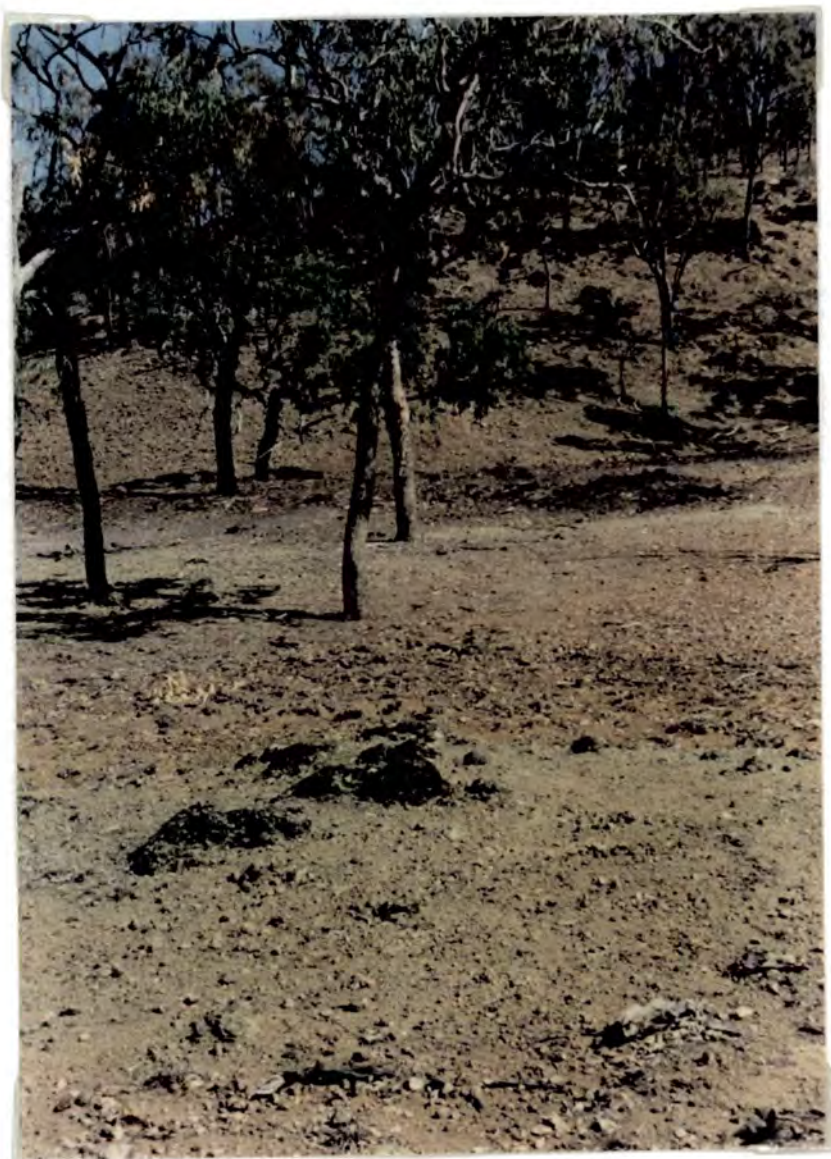
Plate 5.2   Location 1 at Pinnacle creek (Site 1). The weathered andesites
are clearly seen in the foreground and middle distance. Note the lack
of a grass understorey.

(plate 5.3).

Thin section studies of the fresher material revealed that feldspar was altering to zeolites and calcite. The matrix contains much calcite, possibly as a later addition, with quartz and chlorite in places. Some of the veining observed in hand specimen proved to be rich in epidote.

X-Ray Diffraction (XRD) analyses of the soils showed a mineralogical variation from mixtures of quartz, feldspar, illite and epidote to quartz, feldspar, sericite and chlorite on moving from areas underlain by the fresher material to the green and mauve weathered andesites.

The laboratory spectra shown in figure 5.7 for rocks and soils, displayed strong epidote absorption features, centred at 2.35μm. These are from the area previously identified in thin section and XRD studies to be rich in epidote. The more weathered area of green and mauve coloured rocks, however, had soils whose spectrum showed only a small clay feature, centred at 2.2μm, with a decrease in reflectance towards 2.35μm. This decrease may be due to the presence of epidote, chlorite or calcite, as calcite was observed to be a major constituent of late veining.

The airborne spectra are quite noisy. However in figure 5.8 we can see spectra from the AIS - 1 data collected over the andesite lavas of the south. The spectra show broad, deep absorption features between 2.23μm and 2.37μm. The features are too poorly defined to be clearly identifiable as a single mineral and may be due to a combination of minerals with absorptions in this wavelength region, such as chlorite, calcite and epidote.

LOCATION 2. Is located on the volcanic breccias (plate 5.4), that form the low lying area in the bend of Pinnacle creek (number 2, figure 5.5). Outcrop is very sparse, with scattered surface rocks and a thin vegetation cover. The rocks are generally cream coloured and heavily pitted, sometimes green, with a porphyritic andesitic matrix. The clasts comprise fragments of andesite and biotite rich granite. The breccias are highly porous and permeable and have suffered intense alteration by both physical and chemical weathering. The primary textures are not normally visible due to the extensive masses of epidote, quartz, chlorite, sericite and opaques (Lorraway, 1976).

Thin section studies of the rocks sampled in this area revealed a large variation in composition, due to the inhomogenous composition of the original

Plate 5.3   Location 1 at Pinnacle creek (Site 1). The weathered green
and mauve andesites show extensive calcite veining.

Plate 5.4   Location 2 at Pinnacle creek (Site 1). This area is underlain
by the volcanic breccias. They are heavily weathered, little outcrop
is evident.   Note the very thin vegetation cover and the extensive
scattered rock debris.
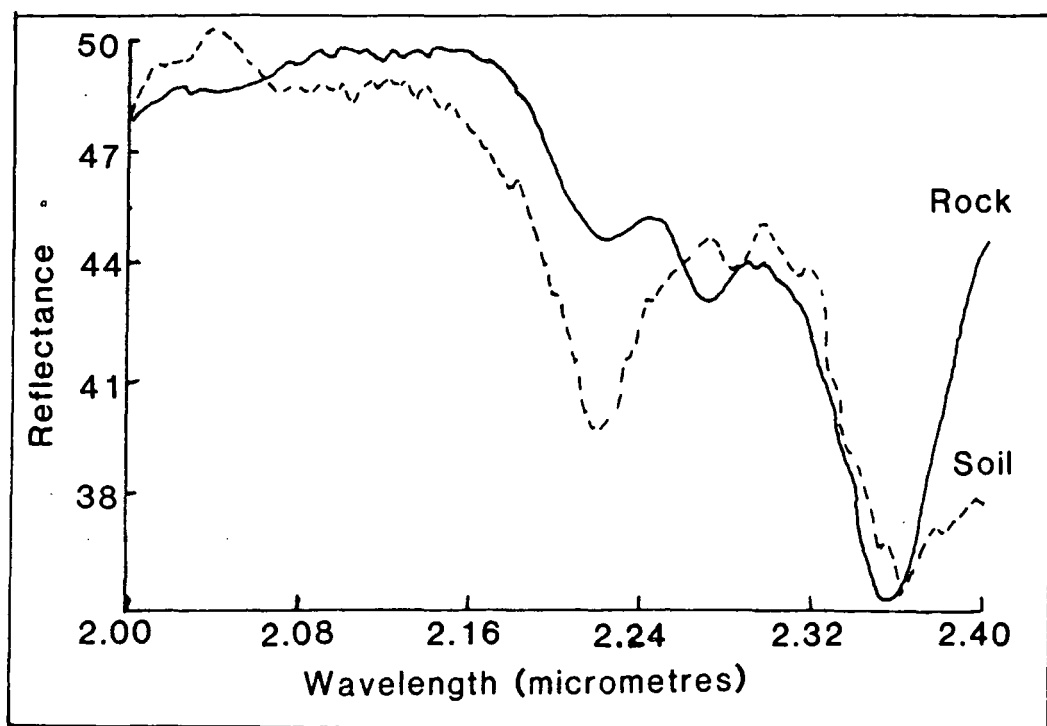
Figure 5.7   Laboratory spectra from Pinnacle creek, location 1. The
deep epidote absorptions are clearly visible in the rock spectra. The
soil spectra shows a small clay feature and a drop off in reflectance to
2.35μm that may be related to epidote or calcite.

Figure 5.8   The airborne spectra   from Pinnacle creek, location 1. The
broad absorption centred near 2.33μm may be related to the presence
of calcite, chlorite and epidote. Two 3×3 pixel areas are
plotted above.

breccia. Some samples consist almost entirely of epidote and quartz, often heavily fragmented, while others proved to be almost entirely composed of sericite and quartz with a little iron staining. In most cases high proportions of both quartz and sericite were evident.

XRD analyses of the soils in this area pointed to very high proportions of quartz and sericite, with a little feldspar.

Laboratory spectra of rocks and soils collected in this area are shown in figure 5.9. There is a very large sericite feature centred at approximately 2.2μm, which is clearly due to the sericite present in both the rock and the soil matrix.

The AIS - 1 spectrum shows similar, but broader, features containing much less detail, figure 5.10. This spectrum is useful in identifying the presence of a strong clay feature, the feature strongly resembles the laboratory spectra of sericite.

LOCATION 3. Lies on the rhyolite intrusives (number 3, figure 5.5. plate 5.5). Vegetation cover comprises primarily broad leaved iron bark (a species of eucalypt), with no understorey. The rocks are pink in colour and porphyritic, ranging in composition from rhyolite to dacite. The phenocrysts are plagioclase, minor biotite and hornblende which is present in small amounts. The plagioclase is altered to sericite and calcite, the biotite to sericite, calcite and chlorite, with some epidote and the hornblende to opaques. The matrix of the rock consists of aligned plagioclase feldspars and is pervasively altered to abundant calcite, chlorite, sericite and quartz, with minor opaques (Lorraway, 1976).

Thin section studies showed the presence of an interlocking mosaic of small quartz grains with some scattered muscovite. Calcite and zeolites are seen to replace feldspar. The matrix contains large quantities of calcite. No XRD analyses were performed on the soils in this area.

The laboratory spectra of rock and soil samples, seen in figure 5.11, show the presence of a strong clay feature at 2.2μm, which resembles a mixture of kaolinite and sericite in the soils, but is more clearly sericite in the rock samples. Strangely, although there is much evidence to support the presence of calcite including previous studies of Lorraway (1976) and thin section studies, there is no evidence for its presence in the laboratory spectra of samples taken
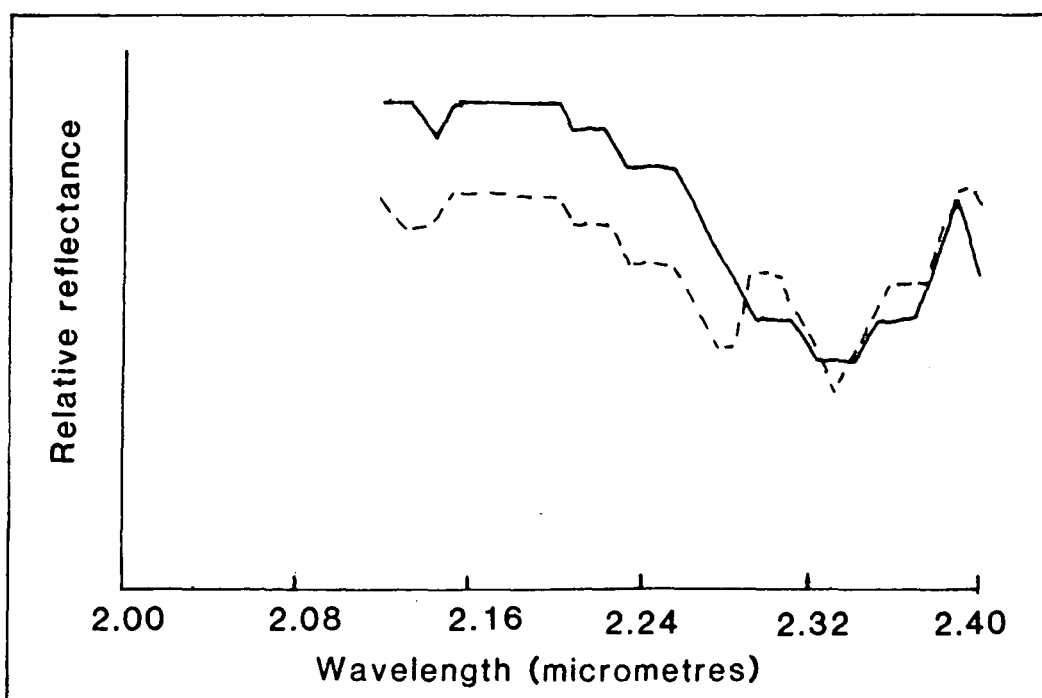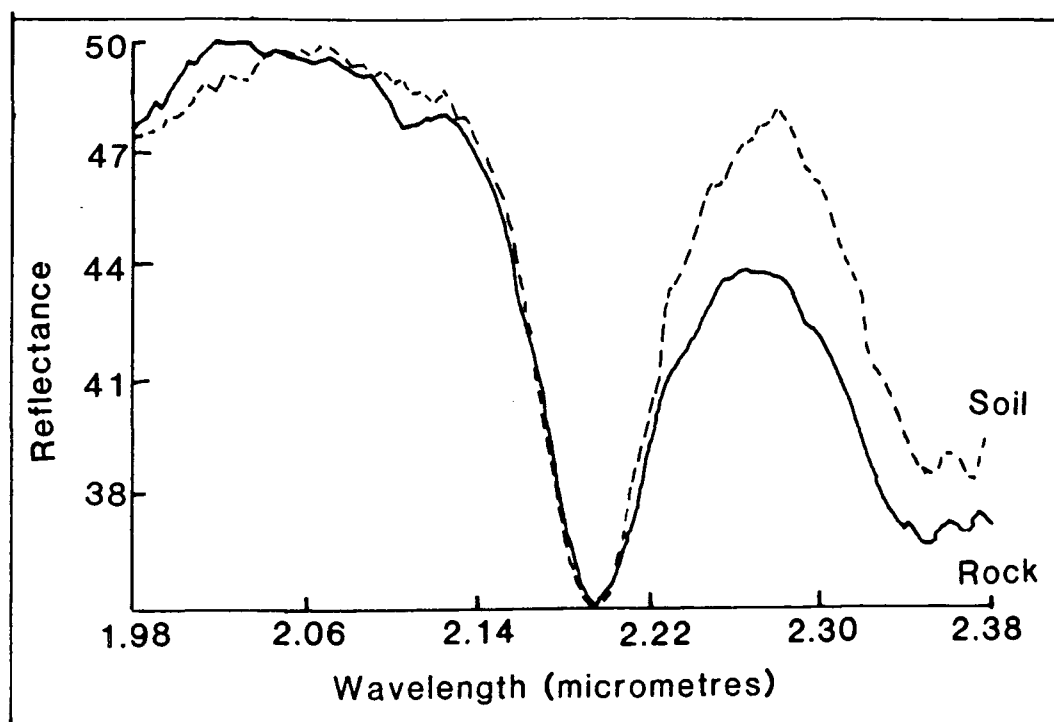
Figure 5.9   Laboratory spectra from Pinnacle creek, location 2. A strong
absorption centred at 2.2μm is due to sericite in both rock and soil.
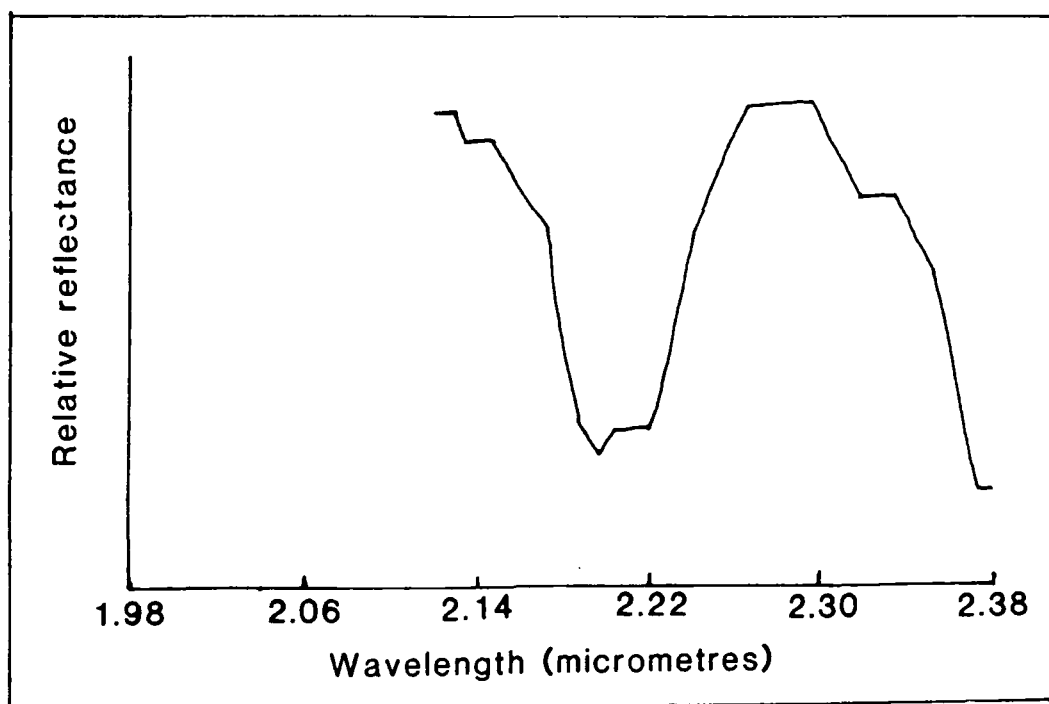
Figure 5.10   The airborne spectrum from Pinnacle creek, location 2. A
strong feature is present, centred at 2.2μm, suggesting clay. The curve
shape is too poorly defined to identify the clay species. Although
it clearly resembles the ground laboratory data.

Plate 5.5   Location 3 at Pinnacle creek (Site 1). An area of rhyolite intrusives. The vegetation consists of broad leaved iron bark (a species of eucalypt), with no understorey, on a creamy-white rock surface.
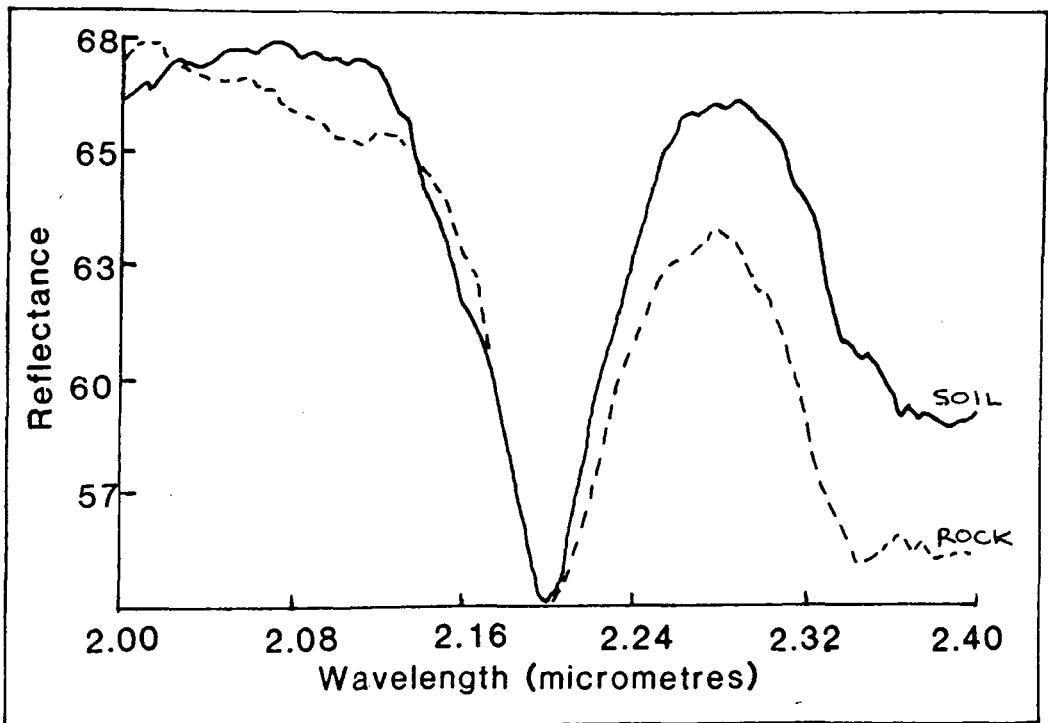
Figure 5.11   Laboratory spectra from Pinnacle creek, location 3. A strong 2.2μm absorption is present in both rock and soil, the curve shape approximates that of sericite.
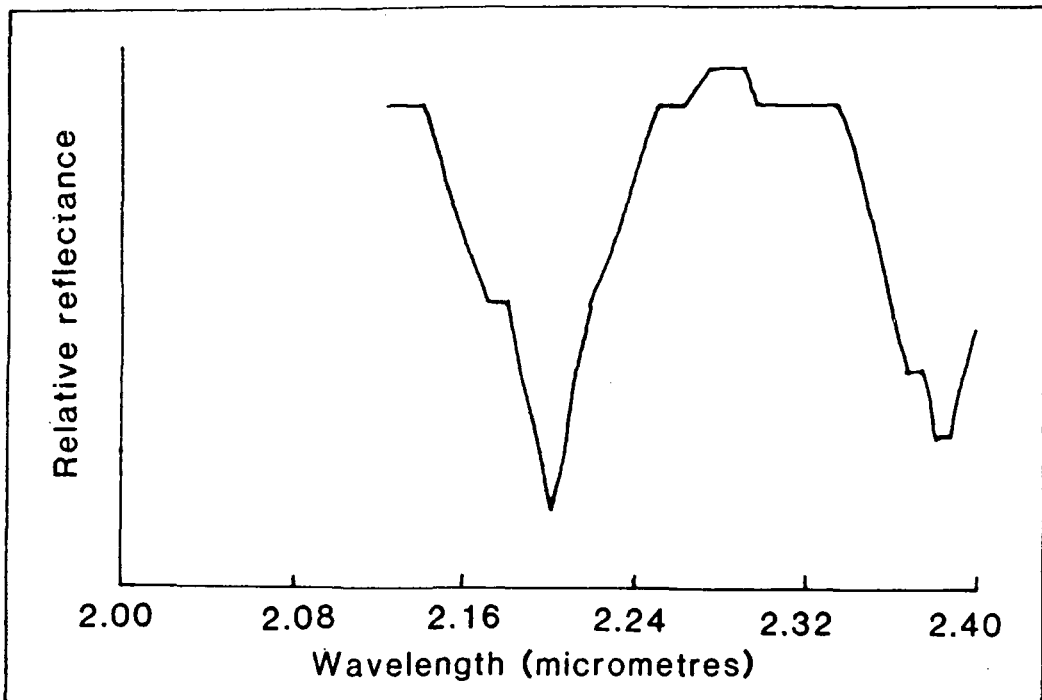
Figure 5.12   An airborne spectrum from Pinnacle creek, location 3. A strong feature of a clay mineral is evident at 2.2μm. The curve is poorly defined for identification of the mineral species, although curve shape and major absorption position are strongly suggestive of the mineral sericite and are very similar to the soil curve in Fig. 5.11.
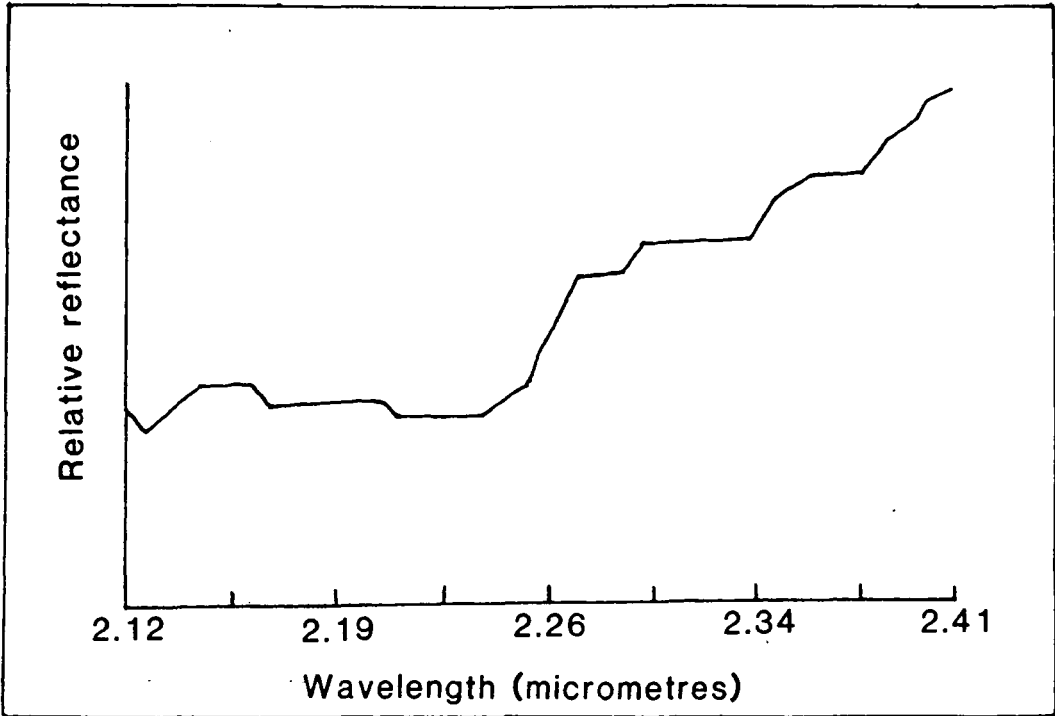
Figure 5.13   An airborne log residual spectrum of green vegetation from the Pinnacle creek site. This curve shape has been noted at other vegetated sites, such as Plateau (described later in the text).

from the area. A probable interpretation is that the calcite has been mobilised away from the weathered rock surface.

The airborne spectrum confirmed the presence of a large clay feature (figure 5.12) centred at 2.2μm which bore a strong resemblance to the soil spectrum in figure 5.11, however it is a rather broad and poorly defined spectral curve.

5.8.3 Other observations.

The airborne spectra were studied to determine if any other features of interest could be identified. Apart from the locations mentioned above, very few locations had identifiable absorption features, even though the field and laboratory studies confirmed the presence of abundant clay and carbonate in the samples taken from the area. Only one other material had an identifiable spectral response, that was green vegetation. Figure 5.13 shows the spectral response obtained over thick eucalypt cover on the edge of Pinnacle creek. This spectral curve is very similar to that observed at the Plateau prospect mentioned later in this chapter.

5.9 Site 2 - Arsenopyrite prospect.

The area lies near the centre of the southern flight line, marked 2 on figure 5.2.

5.9.1 Topography and vegetation.

The topographic range is very small, a few tens of metres, the general topography is that of rolling hills with a few seasonal watercourses. The vegetation consists primarily of scattered stands of eucalypt and a patchy, thin, short grass understorey. The species of eucalpyt is related to the underlying geology, with the broad leaved iron bark seen in the regions containing the more acid intrusions.

5.9.2 General geology.

The schematic map, figure 5.14 is based on interpretation of aerial photographs of the area. Only one unit actually outcrops in this area, the Ravenswood Granodiorite Complex. However, two distinct members of the complex can be differentiated, an early granodiorite phase, which covers most of the area of the flight line at this location and a later more acidic granitic
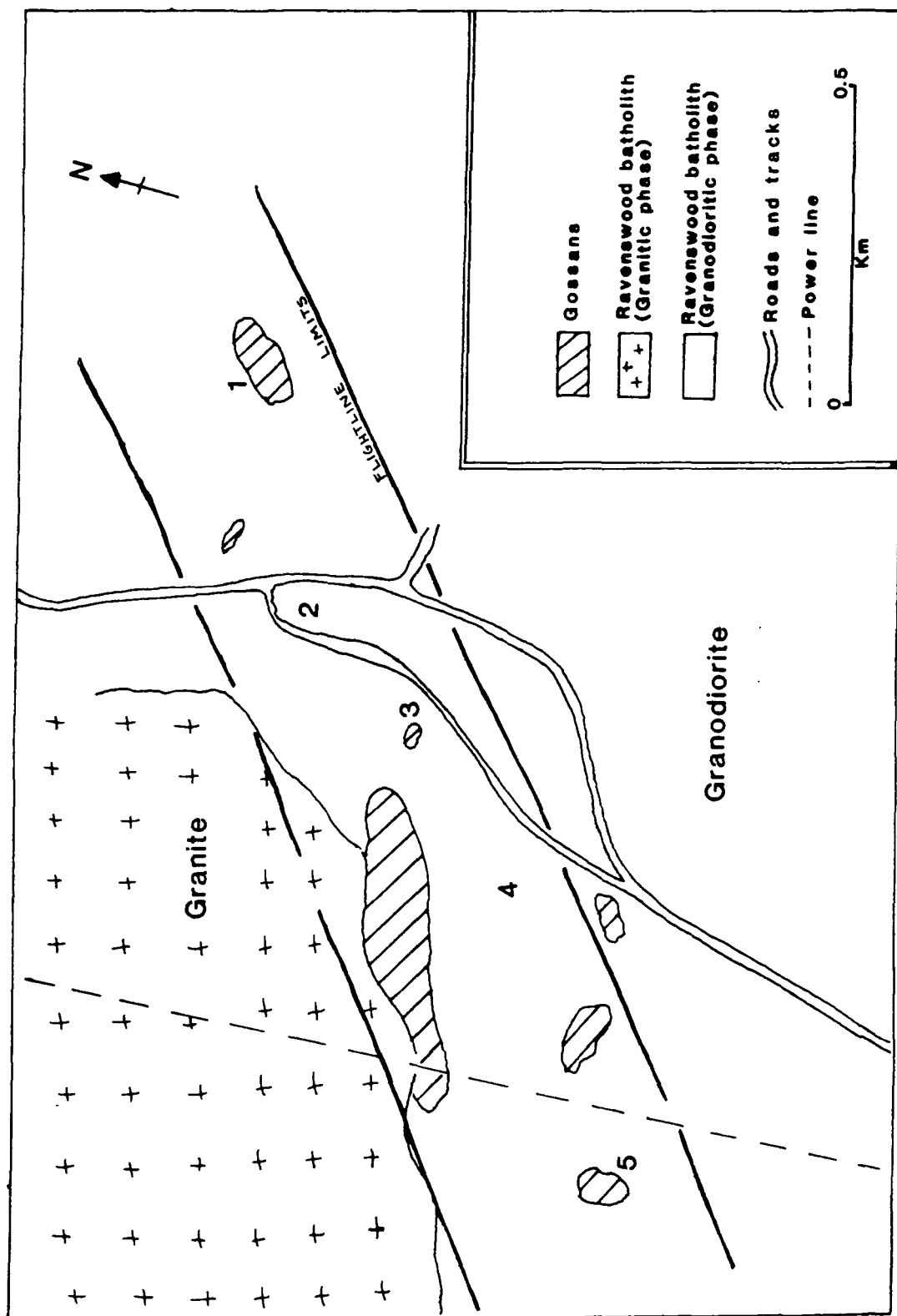
Figure 5.14 Geological and location map of the Arsenopyrite prospect
(site 2). The locations numbered are referenced in detail in the text.

phase. Although only two members of this geological unit are present in the area, there is a great variability in the surface mineralogy. This is due to hydrothermal solutions that have extensively altered and mineralised the area. The relatively fresh granodiorite in this area shows partially sericitised feldspars and the breakdown of biotite and amphiboles to give chlorite, epidote and calcite. This alteration is general and unlikely to be related to a specific mineralising event.

Figure 5.14 also shows the limits of the flight line in this area and several locations which are numbered 1 to 5. These locations are discussed below.

LOCATION 1. Is at the north-eastern end of this short strip of the southern flight line (number 1, figure 5.14). The anomalous area is clearly visible, plate 5.6, due to its redder soil. The vegetation cover is eucalypt with no understorey. The granodiorite has been pervasively altered and is cut by several sub-parallel, siliceous fractures (plate 5.7).

Thin section studies show variable alteration of the country rock. Some samples are almost entirely sericitised, with an introduction of sericite, quartz and some iron minerals along fractures. Other samples are partially sericitised with some of the original feldspar still visible and contain epidote but have no visible iron minerals. The totally altered material contains no epidote, but has extensive iron mineralisation of fractures.

XRD analyses of the soil confirms the variation noted in thin section studies. The partially altered areas show peaks due to both feldspar and sericite, while the totally altered areas show a very strong sericite peak, but no feldspar.

Laboratory spectra of rock samples, shown in figure 5.15, give a very strong sericitic response in this altered rock. Iron absorptions at 0.9μm (not shown) were also noted in the laboratory spectra.

The airborne spectrum confirms the presence of a strong clay feature centred at 2.2μm, figure 5.16. However, the problem of
. the lack of subtle changes in curve shape, make the clear identification of the clay impossible.

LOCATION 2. Is situated to the south-west of the road that runs through this area, outcrop is confined to small mounds of reasonably fresh granodiorite, with much visible epidote on exposed surfaces and in veins. (Number 2, figure

67

Plate 5.6   Location 1 at Arsenopyrite (Site 2). The anomalous area forms a large hill, which has a red-brown soil. Vegetation consists primarily of scattered eucalypt with no visible understorey.

Plate 5.7   Location 1 at Arsenopyrite (Site 2).   This is an area of alteration, with some mineralisation. The vegetation cover is primarily eucalypt, with the development of a light red-brown, granular soil.

5.14, plate 5.8).

Thin section studies show that the granodiorite in this area contains partially seriticised feldspars and anhedral quartz. A little muscovite is visible together with biotite which is altering to chlorite and epidote. Epidote veinlets are present in abundance.

XRD analyses show a quartz rich soil with feldspar, clay minerals containing a mixture of illite and kaolinite and epidote.

The laboratory spectra of rock and soil are shown in figure 5.17. There is a small clay feature centred at 2.2μm which looks like a mixture of illite and kaolinite$\big/$ with a small kaolinitic shoulder at 2.16mm. The decrease in reflectance in the laboratory spectra towards 2.35μm suggest the presence of another mineral, probably epidote.

The airborne spectrum shown in figure 5.18 is very difficult to interpret, with a very broad feature that extends from 2.2μm to 2.37μm. The feature is a real feature due to absorption by several different surface materials. A best guess, given the lack of detail in the AIS - 1 spectrum, is a mixture of clay, chlorite and epidote, with corresponding absorptions at 2.2μm, 2.32μm and 2.35μm, where epidote is the major component.

LOCATION 3. Is situated to the south-west of the previous location (Number 3, figure 5.14). The area is poorly vegetated with a few scattered eucalypts and very little dry grass, plate 5.9. The samples were taken on a short traverse from a small mound, showing extensive epidote veining, in a westerly direction for 100m. The outcrop consists of granodiorite boulders with epidote veining visible on most exposed surfaces, as shown in plate 5.10.

Thin section studies show partly sericitised feldspars, with muscovite altering to chlorite and opaques. There is abundant epidote both in veinlets and as discrete grains in the rock matrix.

XRD analyses of the soil confirm the presence of quartz, feldspar, sericite and kaolinite, with a fairly large proportion of epidote.

Laboratory spectra of rocks and soil, shown in figure 5.19, have weak clay features in the soil at 2.2μm. While epidote absorption features at 2.35μm are clearly visible in both rock and soil.

The airborne spectra taken along the traverse are shown in figure 5.20. Clearly there is a deep absorption centred near to 2.34μm - 2.35μm, although the curve shapes are not sufficiently well defined to determine the identity

Plate 5.8   Location 2 at Arsenopyrite (Site 2). Outcrop of the granodi-
orite, shows extensive epidote veining on some surfaces.
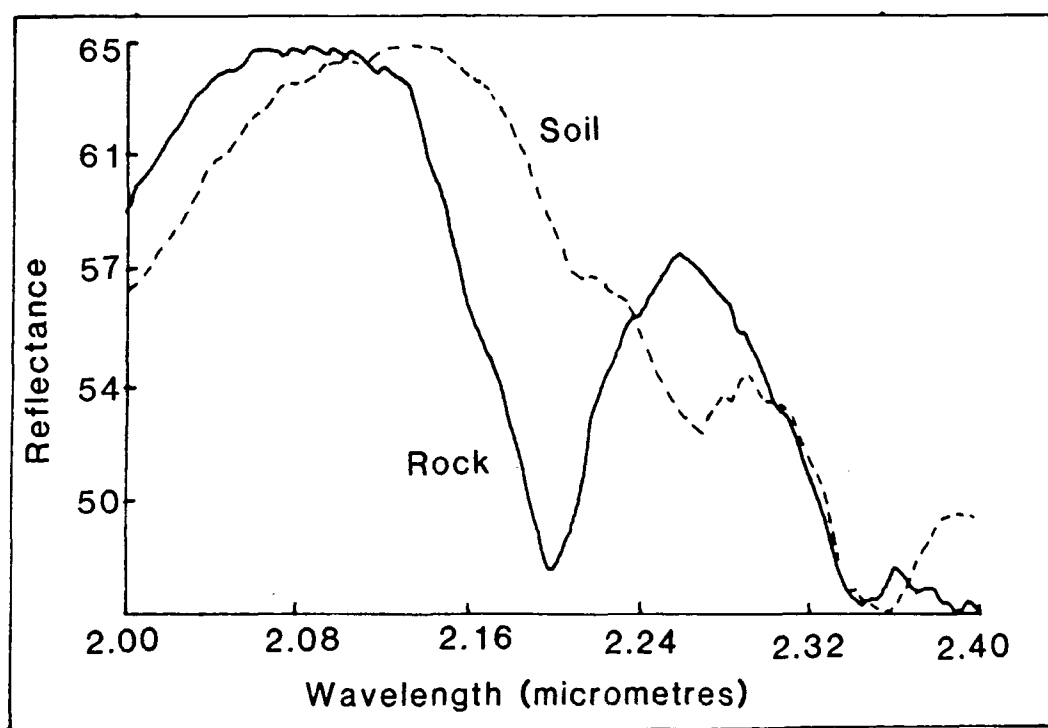
Figure 5.17 Laboratory spectra from Arsenopyrite, location 2. The rock
shows a strong clay feature that resembles a kaolinite/illite mixture.
The soil spectrum has a drop off in reflectance towards 2.35μm that
may be due to the presence of much epidote.
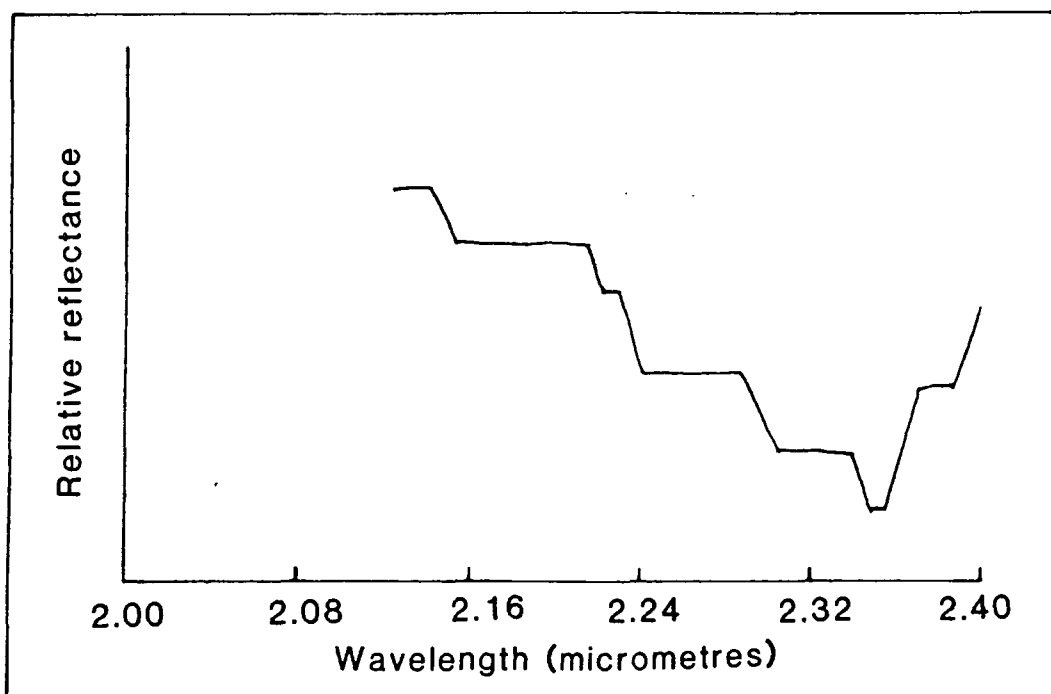
Figure 5.18 An airborne spectrum from Arsenopyrite, location 2. The
feature is very broad and ill defined and may be due to a mixture of
several different surface materials, perhaps clay and epidote.
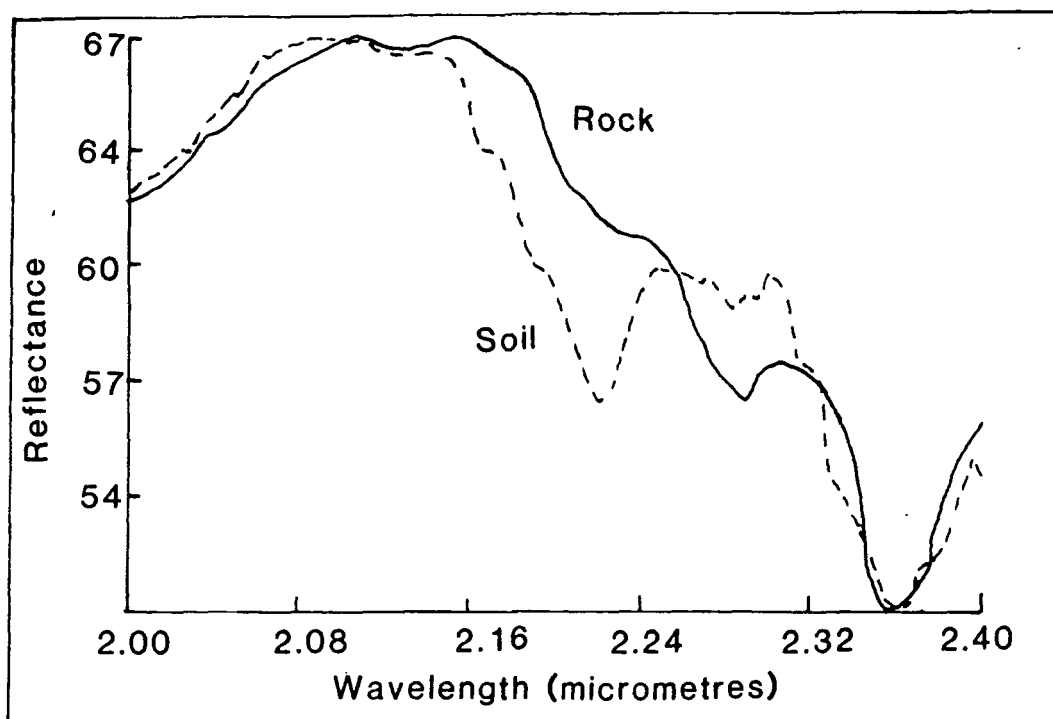
Figure 5.19   Laboratory spectra from Arsenopyrite, location 3. Weak
clay features are noticeable, however, the spectra are dominated by
the presence of epidote, with deep absorptions centred near 2.35μm,
and minor absorptions near 2.28μm.
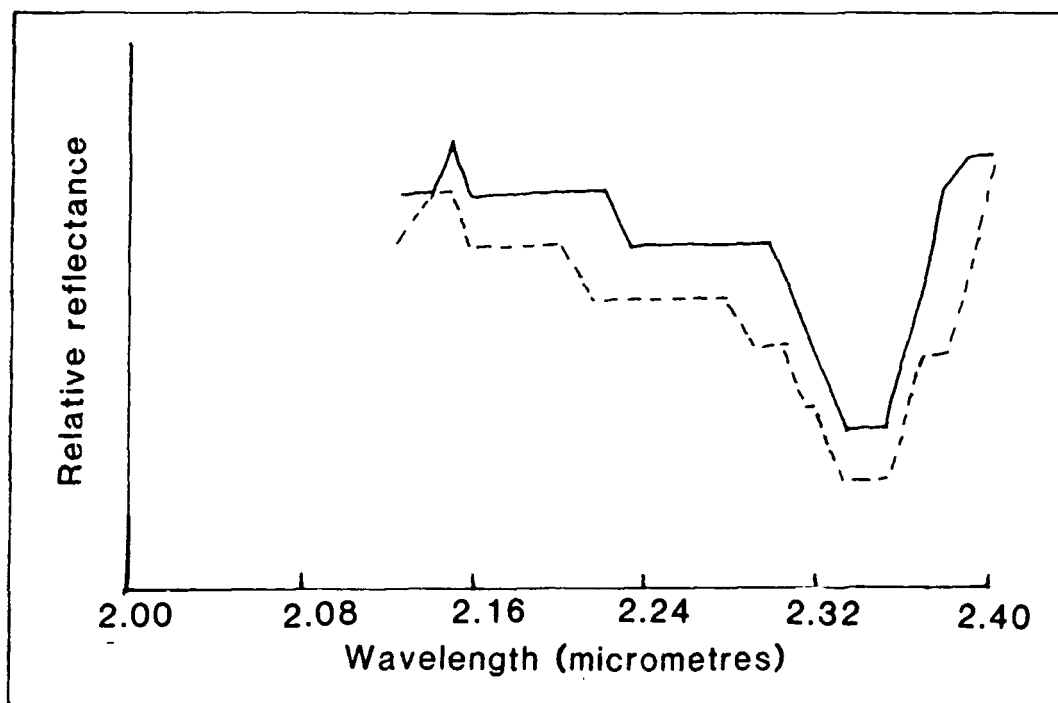
Figure 5.20   Airborne spectra from Arsenopyrite, location 3. Although
broader and poorly defined, the main absorption located at 2.33μm to
2.34μm may be due to epidote, clearly seen in the laboratory
rock and soil spectra. The two curves above are 3x3
pixel averages along the traverse.

Plate 5.9 Location 3 at Arsenopyrite (Site 2). The area is poorly vege-
tated with a few scattered eucalypt. Outcrop is rare and confined to
small mounds in the area.

Plate 5.10 Location 3 at Arsenopyrite (Site 2). The extensive epidote
veining in this anomalous area, is clearly visible on most exposed
surfaces of the granodiorite.

of the mineral causing the absorption. The absorption is probably due to epidote on the exposed rock surfaces and in the soil.

LOCATION 4. Is situated towards the centre of the flight line in this area (Number 4, figure 5.14). The ground is very flat, with little to no outcrop. Scattered eucalypts are present with a patchy covering of green and dry grass. The location is centred on a large tree, plate 5.11. This tree coincides with a small anomaly, located by visual observation of a single band of the processed AIS -1 data. The anomalous area is darker than the background in the chosen band which is centred on a wavelength of 2.35μm.

No rock outcrops are visible near the tree. However, the underlying rock is still granodiorite. There is considerable leaf litter below the tree canopy and a thin covering of dry grass as shown in plate 5.12.

XRD analyses of the soils near the tree gave a composition of quartz, feldspar, illite, kaolinite and epidote. The proportions of these minerals in the soil are very similar to the background soil values observed at some distance from known anomalies (See Table 6).

A laboratory spectrum, figure 5.21, shows a small, unidentifiable clay feature centred near 2.2μm.

The airborne spectrum for this location is shown in figure 5.22. No identifiable spectral features are evident. The spectrum only shows a decreasing response from 2.12μm to 2.41μm. The reason for the visual identification of this location as anomalous, is due to the low value of the spectrum in the 2.35μm wavelength region, which is a general feature of the spectrum and not due to a mineral absorption. This decrease in the spectrum in this wavelength region must be related to the vegetation, although at this time it is impossible to identify whether it is due to the green vegetation or the dry vegetation.

LOCATION 5. Is situated in the south-west part of the flight line covering this area (Number 5, figure 5.14). The topography is fairly flat with scattered eucalypt and a little dry grass. The anomalous area consists of red-weathering and gossanous material, plate 5.13.

Thin section studies show the presence of an almost pure quartz-sericite rock with later additions of quartz along fractures.

XRD analysis of the soil confirms the presence of large amounts of quartz, with a little feldspar and sericite.

Plate 5.11   Location 4 at Arsenopyrite (Site 2). The location is centred
on a tree. There is no visible outcrop at this location, although there
is an anomaly in the imagery.

Plate 5.12 Location 4 at Arsenopyrite (Site 2). The anomaly may be due to a combination of the soil, dead leaf litter and dry grass, found below the tree.
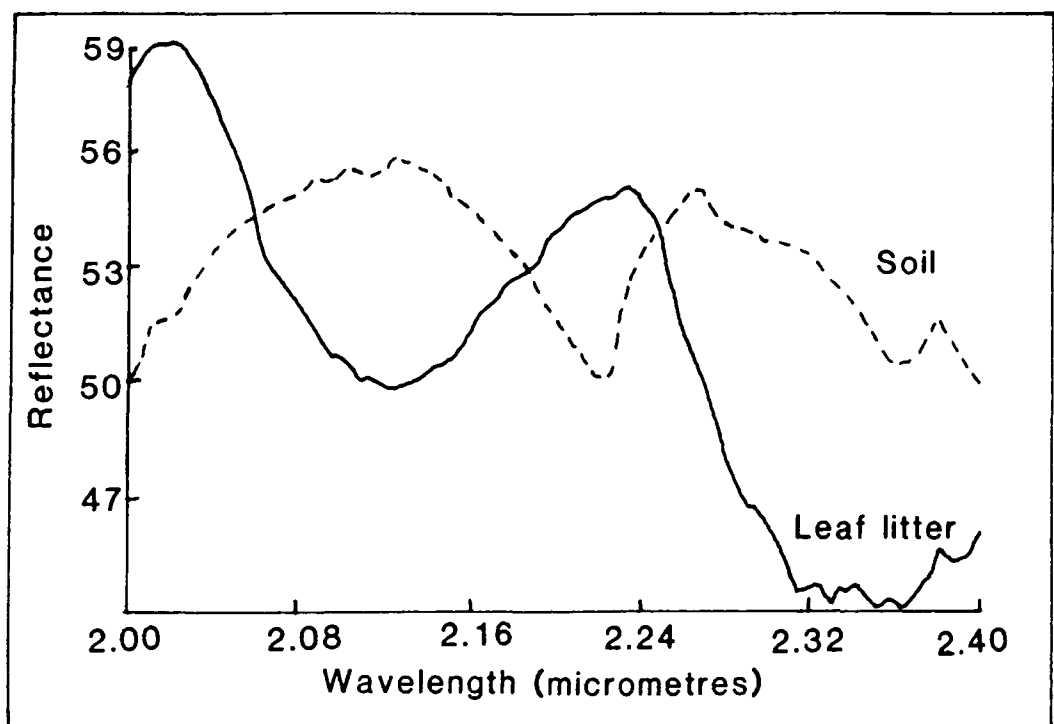
Figure 5.21   Laboratory spectra from Arsenopyrite, location 4.   The anomaly is centred on a tree with no outcrop. The soil shows a small unidentifiable clay feature. A spectrum of the dry leaf litter present at the location is also shown.
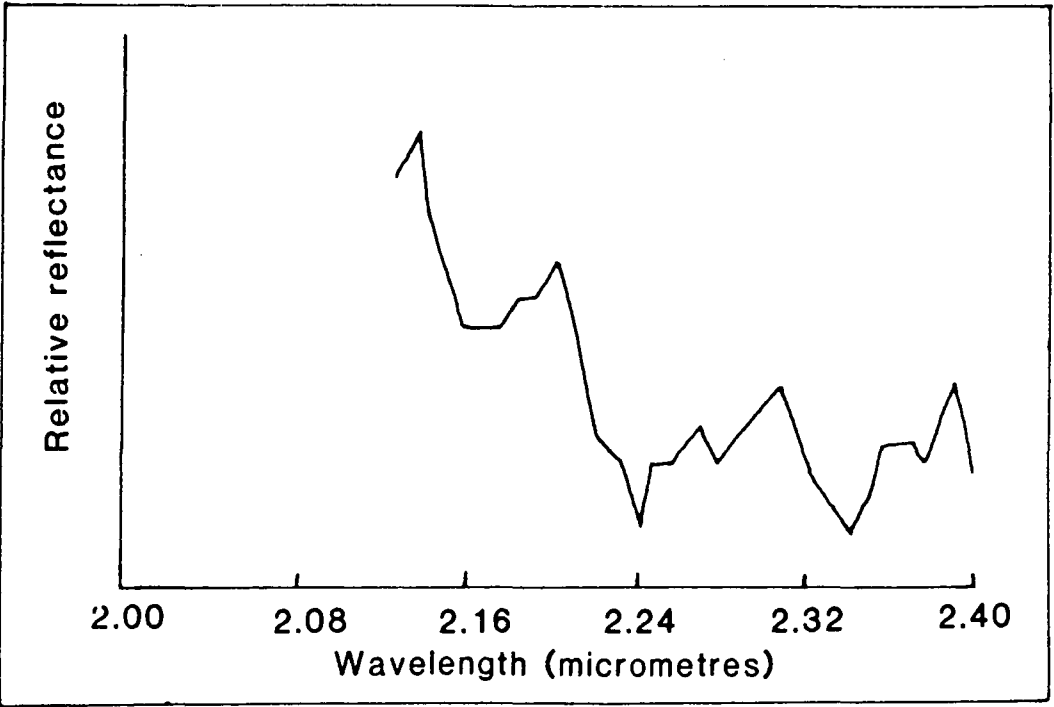
Figure 5.22   An airborne spectrum from Arsenopyrite, location 4. The anomalous area is broad and poorly defined, but may be related in part to a mixture of soil and leaf litter.
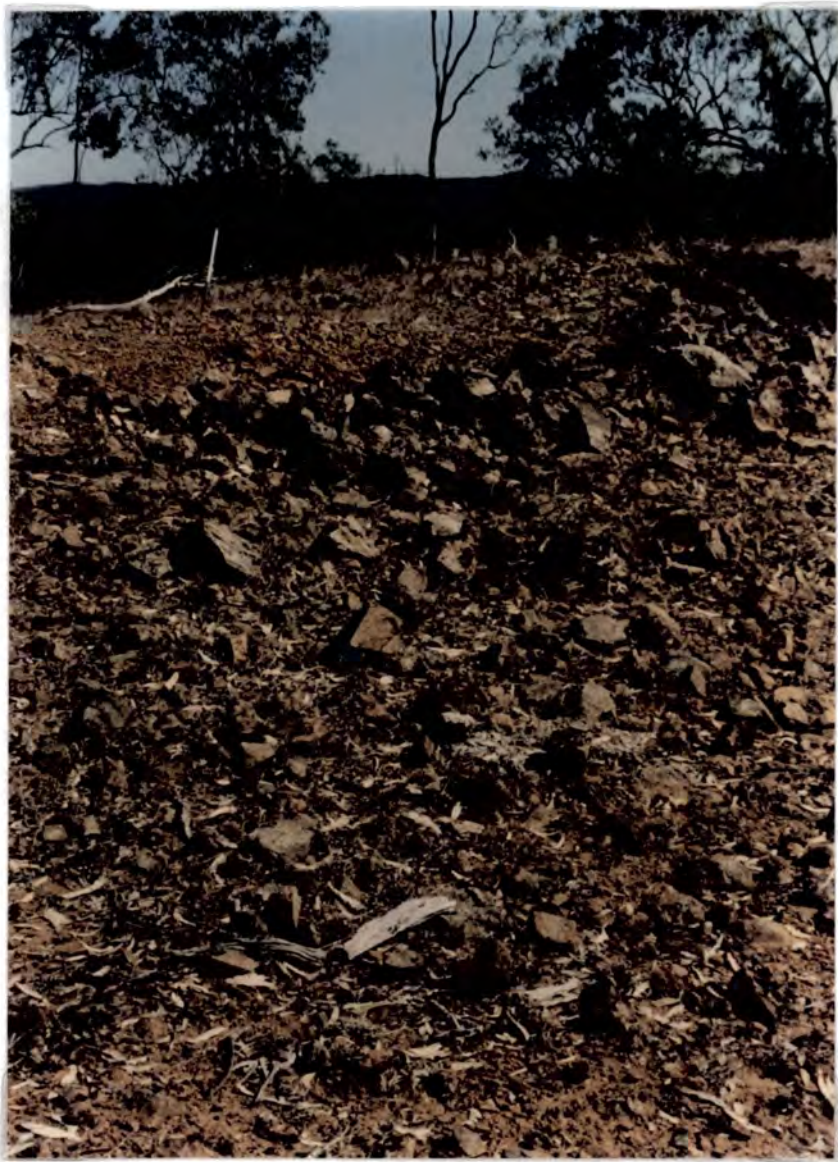
Plate 5.13   Location 5 at Arsenopyrite (Site 2). The topography is fairly flat, with scattered eucalypt. The anomaly consists of red-weathering soil and gossanous material showing extensive silicification.

XRD ANALYSES - ARSENOPYRITE PROSPECT			
STANDARD SOILS			
Quartz	47	53.7	45.5	53.7
Feldspar	35	30.1	36.2	26.9
Muscovite*	6.5	9.1	8.3	8.0
Epidote	7.7	7.1	10.0	7.5
Kaolinite	3.8	-	-	3.9

GOSSANS (ANOMALOUS IN IMAGERY)			
Quartz	73.5	77.0	59.5
Feldspar	11.7	10.0	14.8
Muscovite*	14.7	13.0	7.4
Epidote	-	-	7.4
Kaolinite	-	-	10.7

GOSSANS (NON-ANOMALOUS IN IMAGERY)			
Quartz	65.7	45.6	41.6
Feldspar	6.5	23.2	15.0
Muscovite*	14.4	14.4	7.5
Epidote	-	10.4	20.0
Kaolinite	4.6	-	-
Goethite**	8.5	6.4	15.8

* Illite present in some cases

** Haematite present in some cases.

Table 6.

A laboratory spectrum, figure 5.23 of the rocks and soil confirms the presence of sericite, which gives a strong absorption feature centred at 2.2μm with a strong narrow water absorption feature at 1.4μm related to the OH in the sericite (not shown in this diagram). The soil spectrum has a much more subdued response with a much weaker clay feature centred at 2.2μm.

To help give a direct comparison between anomalous and non-anomalous sites in this area, samples were also taken from a location 45m to the north east in a standard non-anomalous area. Here the rock is fresh granodiorite with some epidote veining visible on some surfaces, plate 5.14.

The XRD analysis of the soil from this standard area, showed a lower quartz content, more feldspar, less clay and some epidote.

The laboratory spectrum of the soil, shown in figure 5.23, has a very small clay feature centred at 2.2μm.

The airborne spectra for these two areas are the most convincing evidence for differences between the anomalous areas and the standard non-anomalous areas. The spectrum (figure 5.24) of the anomalous area has a deep absorption centred at 2.2μm. The feature is broad, but is quite clearly a clay absorption. In contrast, the spectrum of the standard area is relatively flat and featureless, as expected.

It is clear from this that the anomalous areas can be identified from the airborne data. However, the broadness of the spectral absorption features in the airborne data prevents accurate identification of the clay mineral species present, although the laboratory spectra strongly suggest sericite.

5.9.3   Other observations.

Many soil and rock samples were taken to determine the characteristic mineralogy of the area. XRD analyses of the soils showed that the standard background soil consisted of quartz, feldspar, muscovite (sericite) and epidote, with a few samples containing kaolinite. (Table 6).

The anomalous clay areas showed much higher quartz and sericite values and lower feldspar and epidote than the standard areas. Invariably these anomalous areas contained gossans and bright red soils, however, they did not have high iron values. This was confirmed by the XRD traces, which have low background values and no obvious iron peaks, by thin sections which have no visible iron staining or opaques and by laboratory spectra with no strong iron
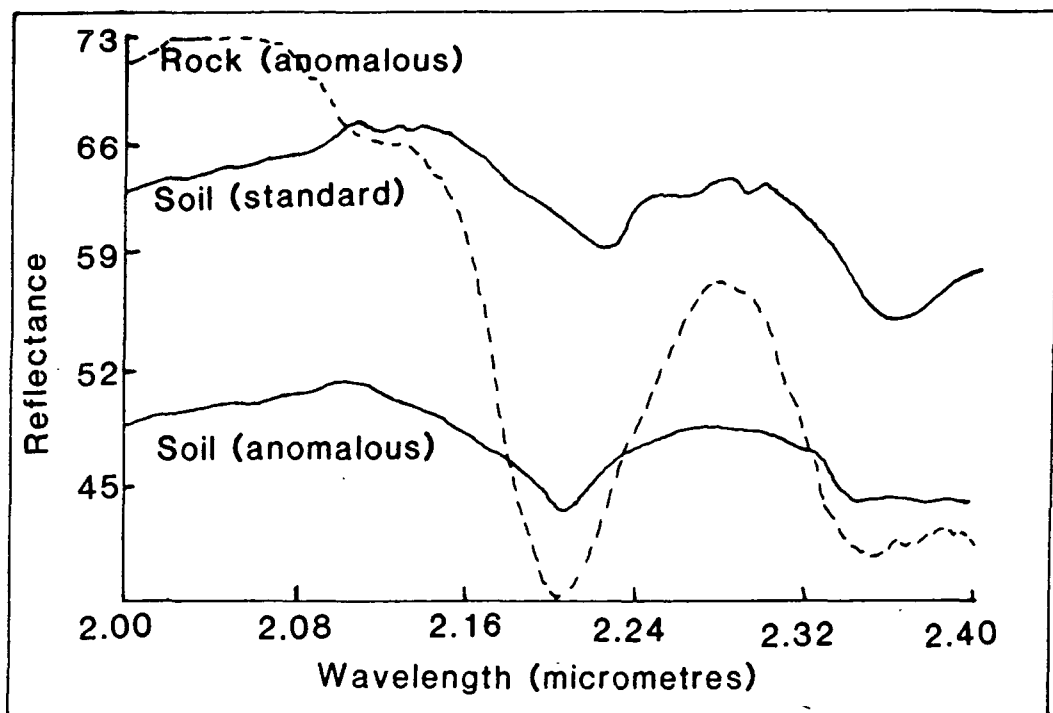
Figure 5.23   Laboratory spectra from Arsenopyrite, location 5. The rock
and soil from an anomalous area gave well defined sericitic features
in the rock.   While the standard area nearby, showed a small clay
absorption and a drop off in reflectance towards 2.35μm, probably
due to epidote.
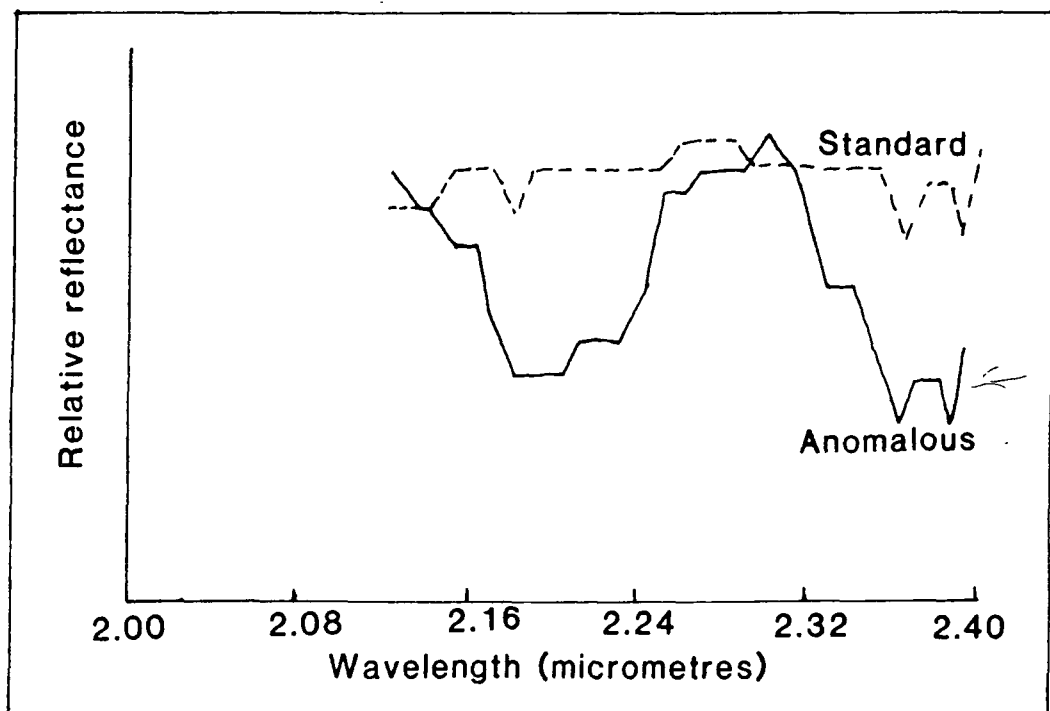
Figure 5.24   Airborne spectra from Arsenopyrite, location 5. The dif-
ferences between the anomalous and standard areas are striking. A
broad deep absorption is present in the anomalous area due to clay.
The standard area is spectrally flat.

Plate 5.14   Location 5 at Arsenopyrite (Site 2). The sample location is
over a standard area near the gossan. Here we have fresh granodiorite
with some epidote veining.

features in the 0.9μm wavelength region.

Some non-anomalous areas observed in the field contained gossans, but had a light brown soil. These areas had very low quartz values less than those of the standard soils, similar feldspar and clay values to the anomalous gossans, but with additional epidote and noticeably high iron values. These areas show a mineralogy very similar to that mentioned previously for the mineralisation of the Ravenswood II epoch, with high sulphide, low silica gossans. The difference in mineralogy between these gossans and those of the anomalous areas must be due to either a spatial or temporal variation in the mineralising solutions.

The variations in composition as determined by XRD analysis are shown in relative terms. The sizes of the quartz peaks are used as a relative scale to give semi-quantitative comparisons of composition, shown in table 6.

5.10   Site 3 - plateau prospect.

The area lies in the south-western part of the northern flight line (number 3 on figure 5.2).

5.10.1   Topography and vegetation.

The area is part of the more heavily vegetated region to the south-west. The topographic range is perhaps 100m, the general topography is that of a relatively flat tableland of lateritic material, cut by seasonal watercourses, producing buttes and mesas. The vegetation density and composition is variable and is partly dependent on the underlying geology.

The north-eastern part of this area is on relatively flat lateritic terrain, with scattered eucalypt cover and no real understorey. The vegetation density is variable and much thicker near very small drainage features that dissect the laterite.

Over the rhyolite in the area the eucalypt cover is thicker, but again with no obvious understorey.

The thickest vegetation cover is over the andesites. Here there is broken eucalypt cover with the development of a thick grass understorey. The grass has the local name of Kerosene grass, based on its peculiar smell when crushed.

5.10.2   General geology.

GEOLOGICAL KEY
PLATEAU

Campaspe beds
(late Tertiary)

Laterite
(mid Tertiary)

Shales
(early Tertiary)

Sandstone
(early Tertiary)

Andesite
(Cambro-Ordovician)

Rhyolite
(Permo-Carboniferous)

Granite
(Permo-Carboniferous)

Flight line limits

N

0   0.5   1
Km
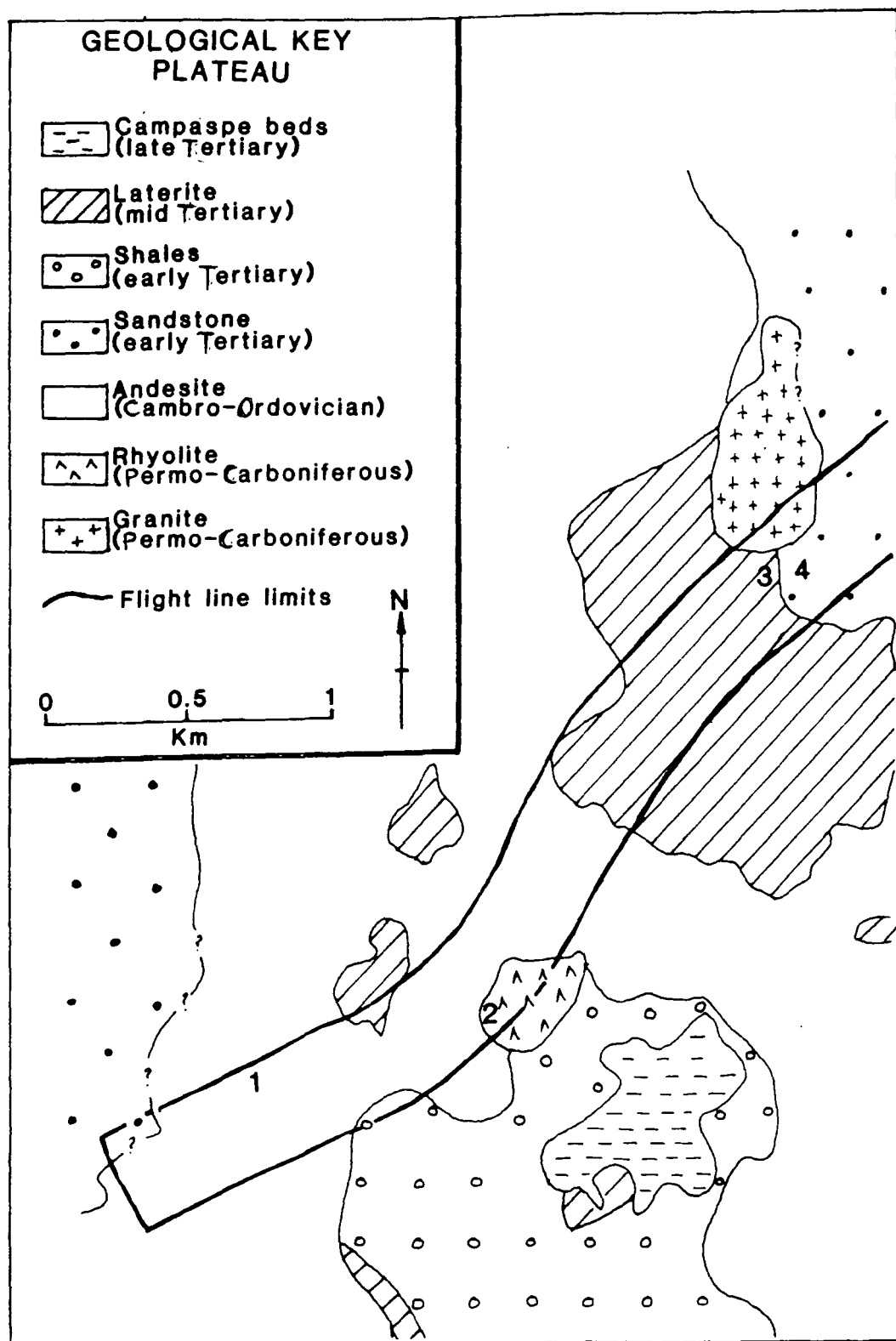
Figure 5.25   Geological and location map of site 3, the Plateau prospect. The flightline is marked. The locations are described in detail in the text.

GEOLOGICAL KEY   PLATEAU

Campaspe beds (late Tertiary)

Laterite (mid Tertiary)

Shale and sandstone (early Tertiary)

Andesite (Cambro-Ordovician)

Rhyolite (Permo-Carboniferous)

Granite (Permo-Carboniferous)
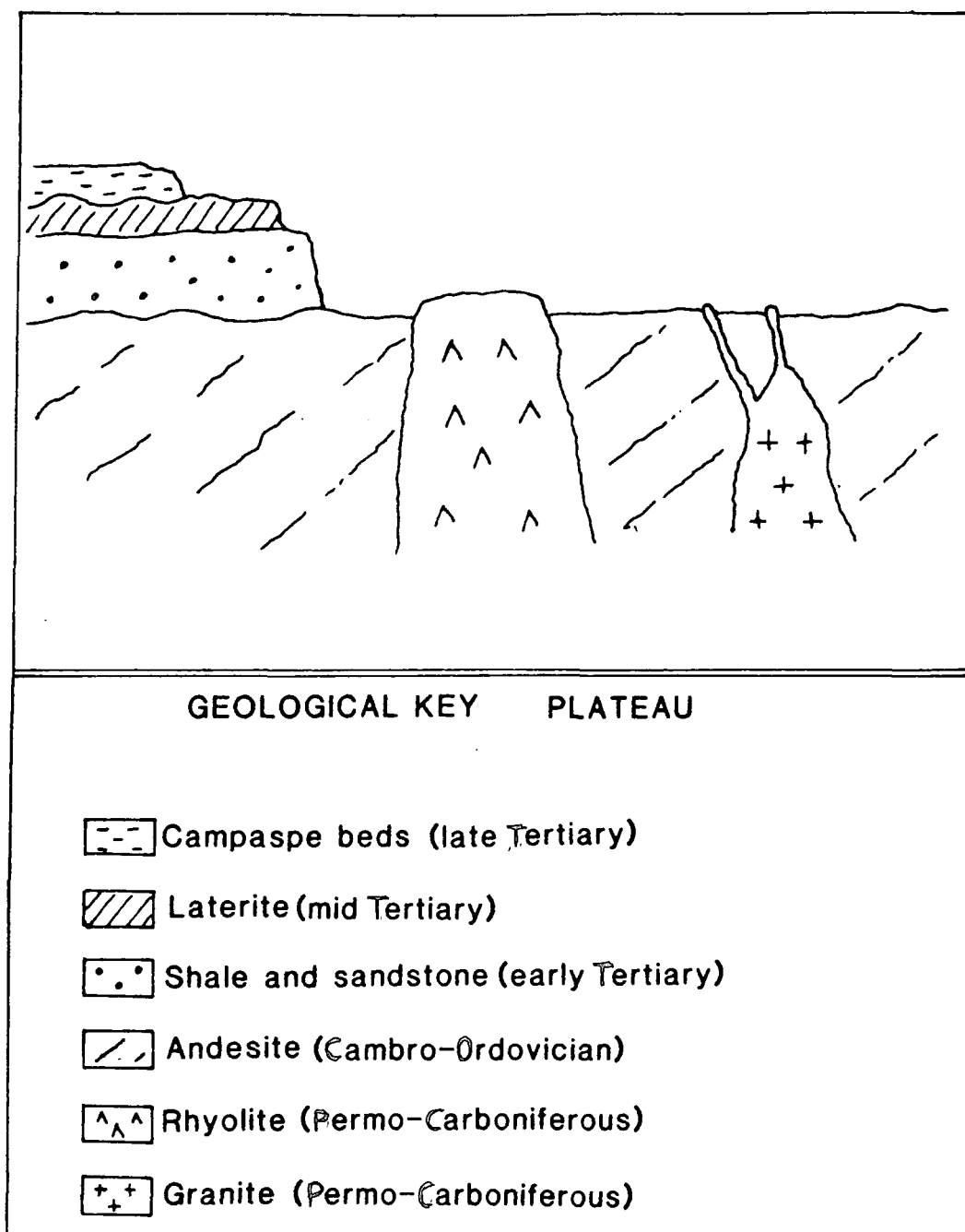
Figure 5.26   Schematic geological cross section of the Plateau prospect.

The area was mapped in great detail by Terra Search Ltd., of Queensland. The map shown in figure 5.25 is based largely on their work. There are five main units in this area,

(1) Andesitic volcanics of the Mount Windsor Group (Cambro-Ordovician)

(2) Acid intrusives and volcanics (Permo-Carboniferous)

(3) Sandstones and Shales (Early Tertiary)

(4) Laterites (Mid Tertiary)

(5) Sandstone and siltstone of the Campaspe Beds (Late Tertiary)

The relationships of the five units are shown in figure 5.26. In the area covered by the flight line, only the first four units are present. Figure 5.25 shows the extent of the flight line and the location of areas studied in detail (numbered 1 to 4).

LOCATION 1. Is to the south-west of the rhyolite plug known as the plateau prospect (number 1, figure 5.25). The area has been mapped as an area of epidote altered andesite. The vegetation consists of scattered eucalypt and a thick understorey of long, dry Kerosene grass as seen in plate 5.15. Surface samples are brown weathering, although some clearly show the presence of epidote in large quantities, plate 5.16.

Thin section studies showed the presence of much epidote and feldspar, with some amphibole, chlorite and a little quartz.

XRD analysis of the soils confirmed the high epidote and low quartz values. Also present were feldspar and amphibole. No chlorite was noted in the XRD analysis.

The laboratory spectra of rocks and soils shown in figure 5.27 have variable amounts of epidote, with the characteristic absorptions at 2.35μm and 2.25μm. The very high values were due to epidote veins on the rock surfaces, while the soils gave only an indication of the presence of epidote.

The airborne spectrum from the area showed a deep, strong absorption centred near 2.33μm, figure 5.28. When matched against the laboratory spectrum, the absorption position is approximately correct, but the curve shape is far from ideal.

Plate 5.15   Location 1 at Plateau (Site 3). The sample location is in an area of dense vegetation cover, with eucalypt and a thick dry grass understorey.

Plate 5.16   Location 1 at Plateau (Site 3). The surface samples are brown-weathering, some clearly showing the presence of epidote.
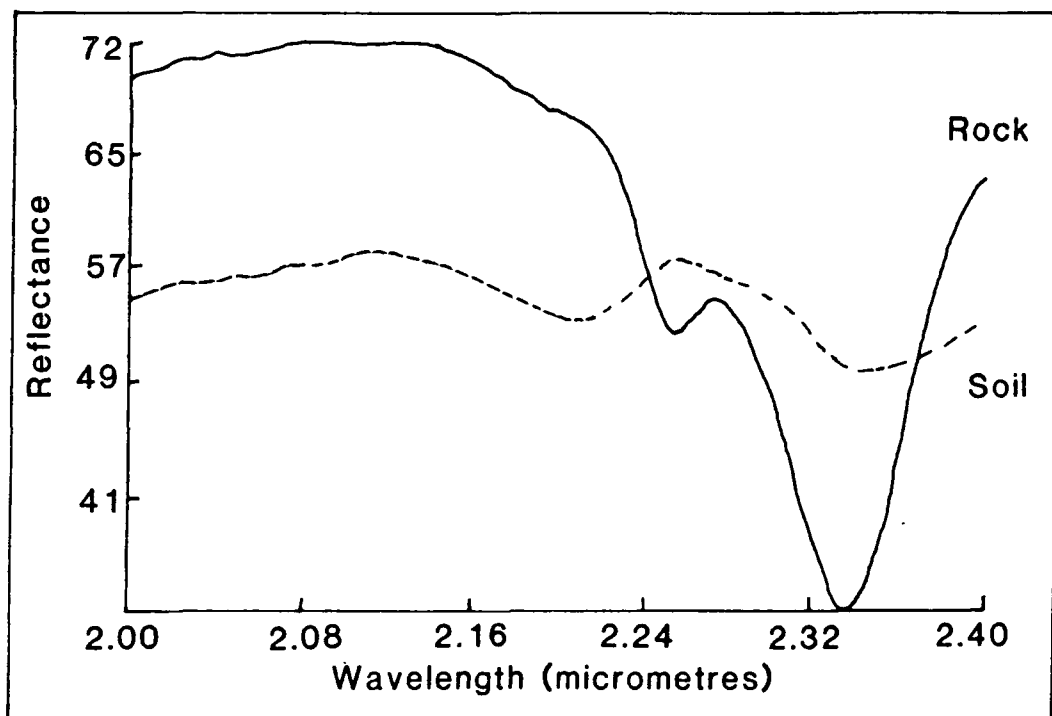
Figure 5.27   Laboratory spectra from Plateau, location 1. The rock
spectra show deep absorptions at 2.35μm due to epidote. The soil
shows only a small clay feature at 2.2μm and a drop off in reflectance
towards 2.35μm that may be due to epidote.
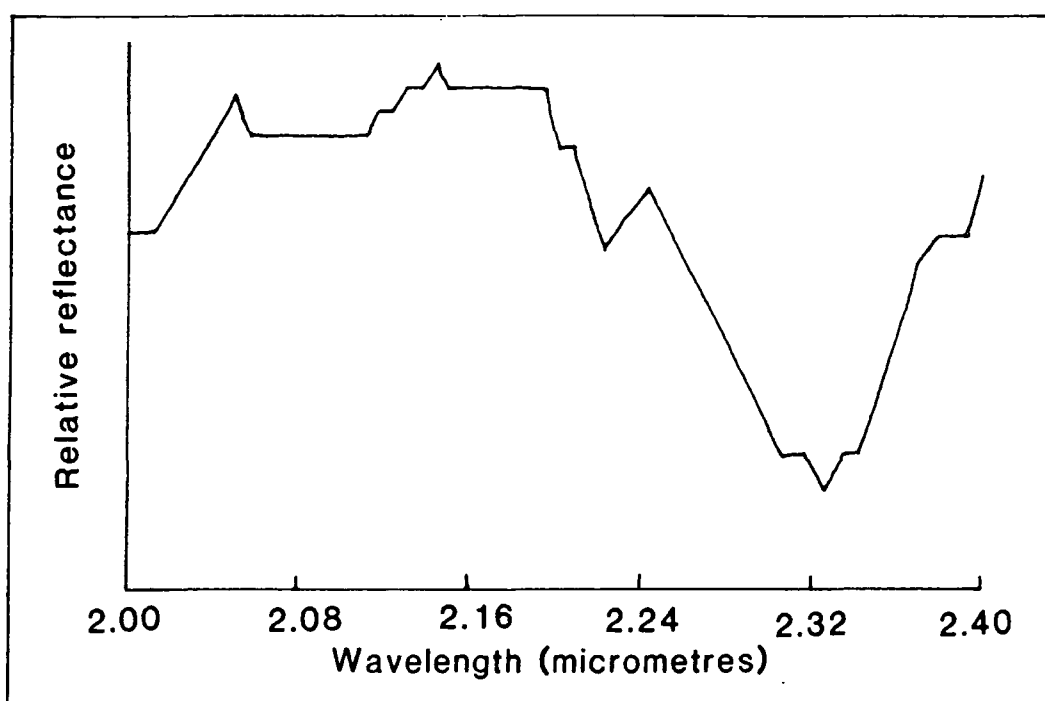
Figure 5.28   An airborne spectrum from Plateau, location 1. The spec-
trum is broad and deep, centred near 2.33μm. It strongly resembles
the epidote observed in the laboratory spectra.

LOCATION 2. Is situated on the rhyolite plug itself. (Number 2, figure 5.25). The vegetation cover is thin, with scattered eucalypt and very little dry grass. Large areas of the rhyolite plug have been bulldozed to enable drilling of the prospect to take place. The rock outcrop consists of a creamy-yellow massive to banded rock, with iron staining on most surfaces, plate 5.17.

Thin section studies reveal very fine grained rocks, but with noticeable amounts of quartz, muscovite and opaques.

XRD analysis of the soils confirm the presence of much quartz, the remainder of the soil consisting almost entirely of sericite.

Laboratory spectra shown in figure 5.29 for both rock and soil clearly reveal the presence of sericite, with a strong 2.2μm feature, although in some cases a mixture of clays containing some kaolinite, with a 2.16μm shoulder seems possible.

The airborne spectrum, figure 5.30, showed the presence of a strong clay feature, but it is impossible to determine the identity of the clay from the broad spectral feature centred near 2.2μm.

LOCATION 3. Is situated to the north-east of the plateau prospect, on the northern edge of the laterite (number 3, figure 5.25). The vegetation consists almost entirely of widely scattered eucalypt on a cream to light brown soil, plate 5.18. The area is highly anomalous in the imagery. On visiting the area, it was clear that this was an extension of the laterite that covers a large area to the south-west, but with the upper red layer of the laterite stripped away by weathering processes to reveal the kaolinitic mottled zone beneath (Butt, 1981. plate 5.19).

Thin section analysis showed the presence of much quartz in the rock with a few iron rich veinlets. The rock was of extremely fine grain size.

XRD analysis confirmed the presence of much quartz, but also the presence of large amounts of the clay kaolinite and high values for both haematite and goethite.

Laboratory spectra shown in figure 5.31, clearly have the characteristic curve shape of kaolinite, with the deep absorption centred at 2.2μm and the shoulder in the curve shape at about 2.16μm. Although not shown on this diagram, there is a deep iron absorption in the near infrared at about 0.9μm.

The airborne spectrum is shown in figure 5.32. From this we can see that
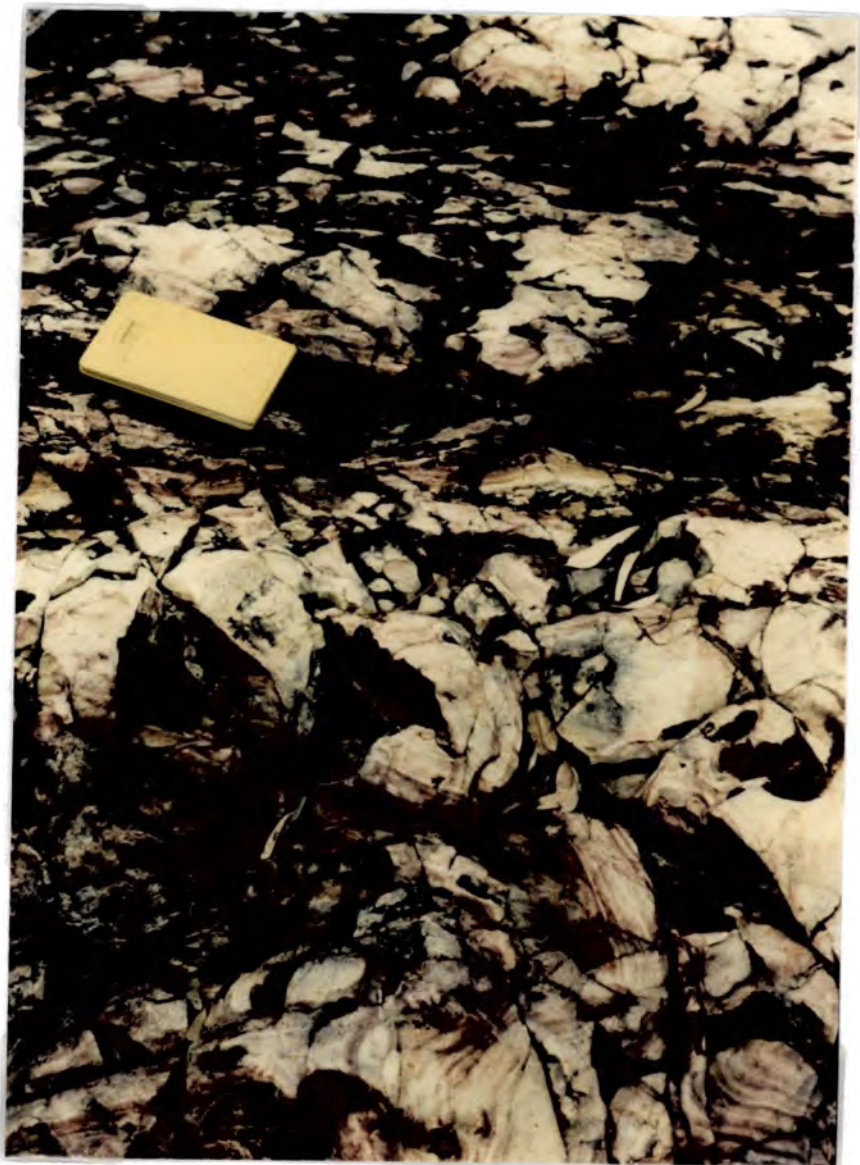
Plate 5.17   Location 2 at Plateau (Site 3). Large areas of rhyolite outcrop.
The rock is creamy-yellow in colour, banded, with some iron staining
on the upper surfaces.
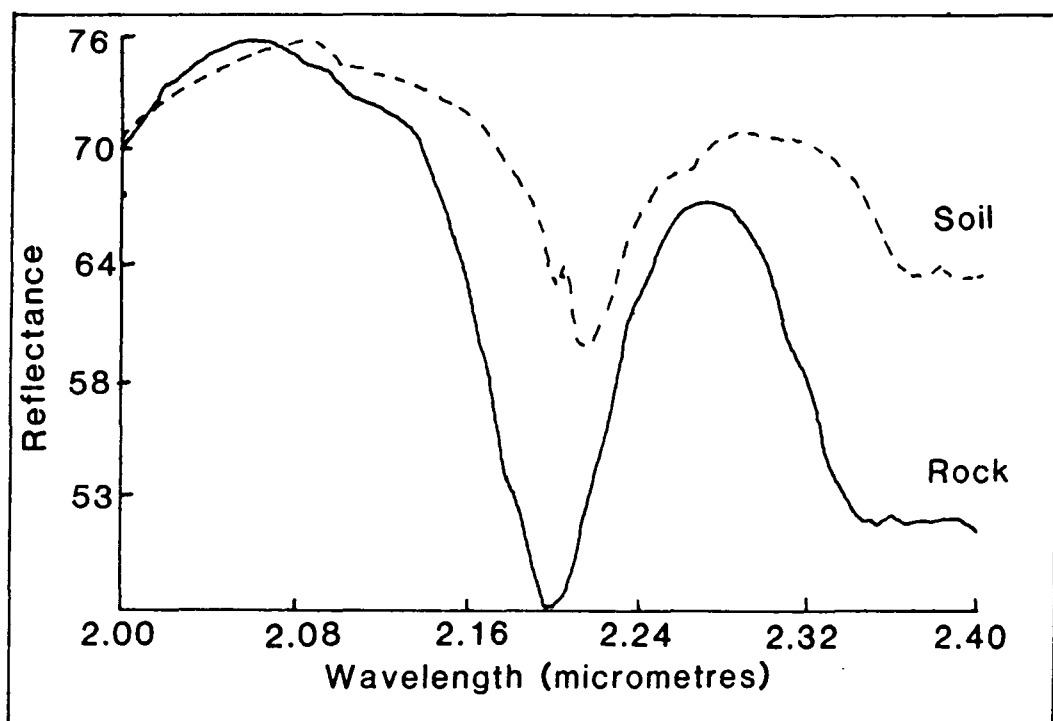
Figure 5.29 Laboratory spectra from Plateau, location 2. Both rock and soil show a strong sericitic response with a major absorption centred at 2.2μm. Note the small spectral shift of the soil spectra, that may be due to a problem with the lab instrument.
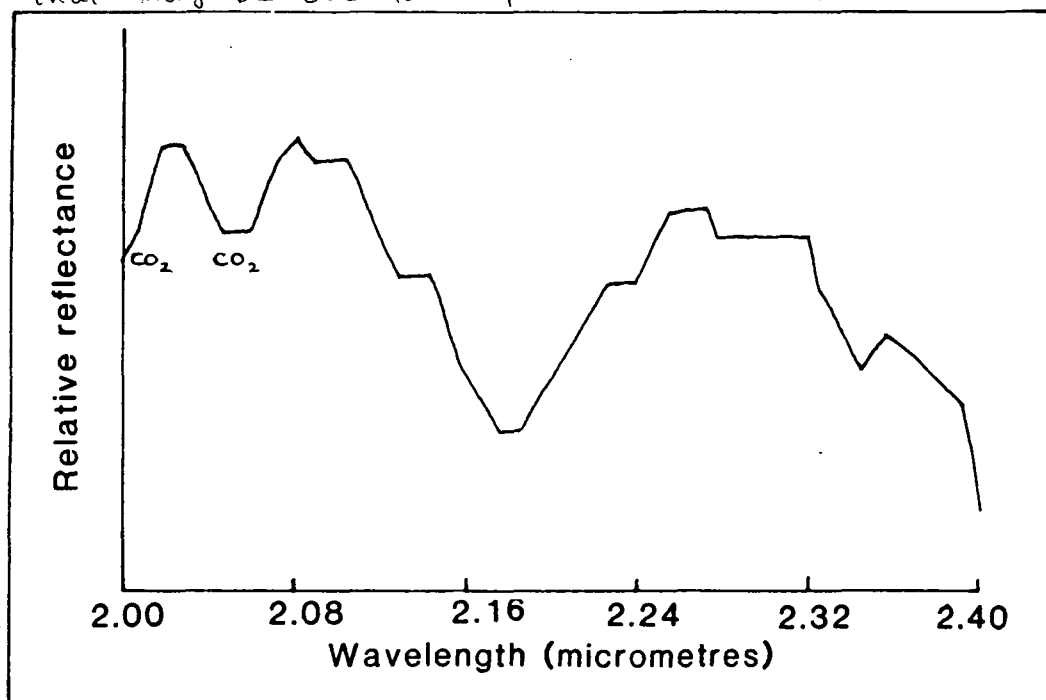
Figure 5.30 An airborne (log residual) spectrum from Plateau, location 2. A broad feature is visible at 2.18μm that is probably due to clay in the scene. Note that the atmospheric CO_2 absorptions are still present in the data near 2.00μmand have not been removed by the log residuals processing.
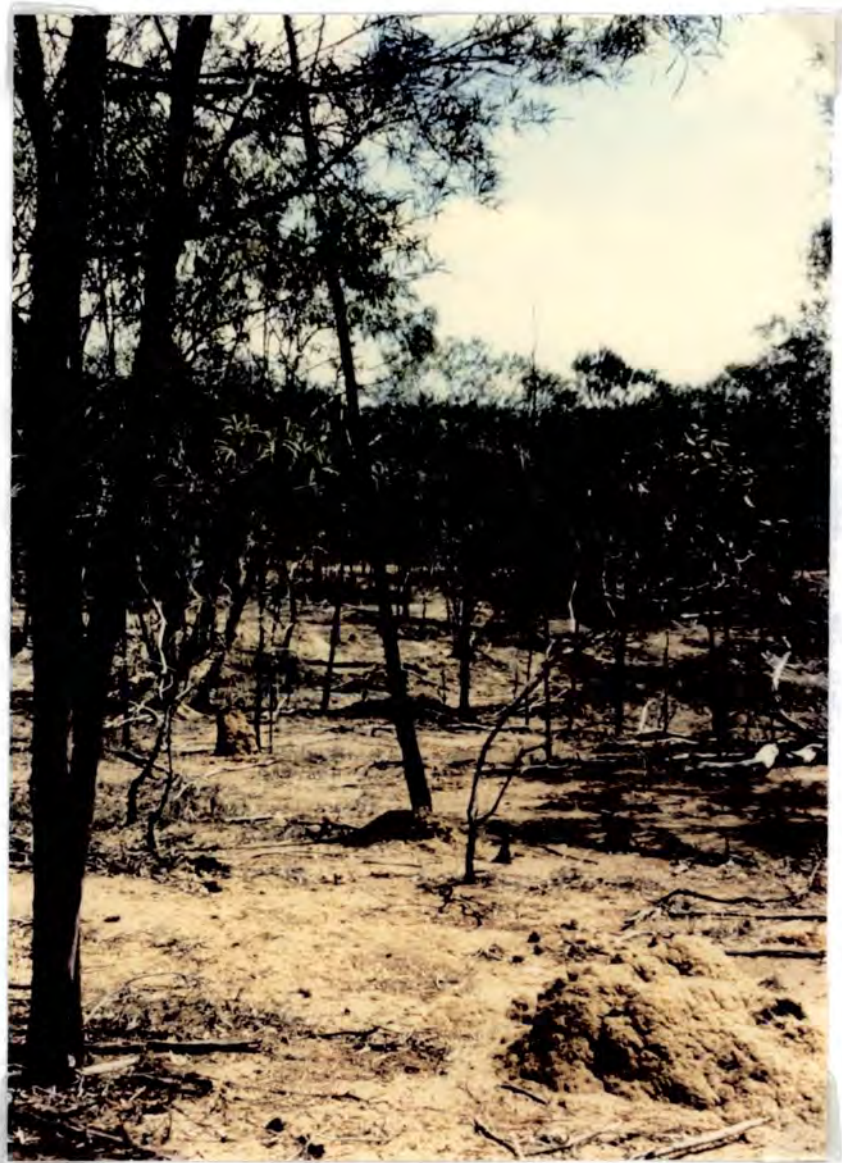
Plate 5.18   Location 3 at Plateau (Site 3). A partially dissected laterite, with a thin vegetation cover of eucalypt, over a cream to light brown soil. There is no outcrop, or visible grass understorey.
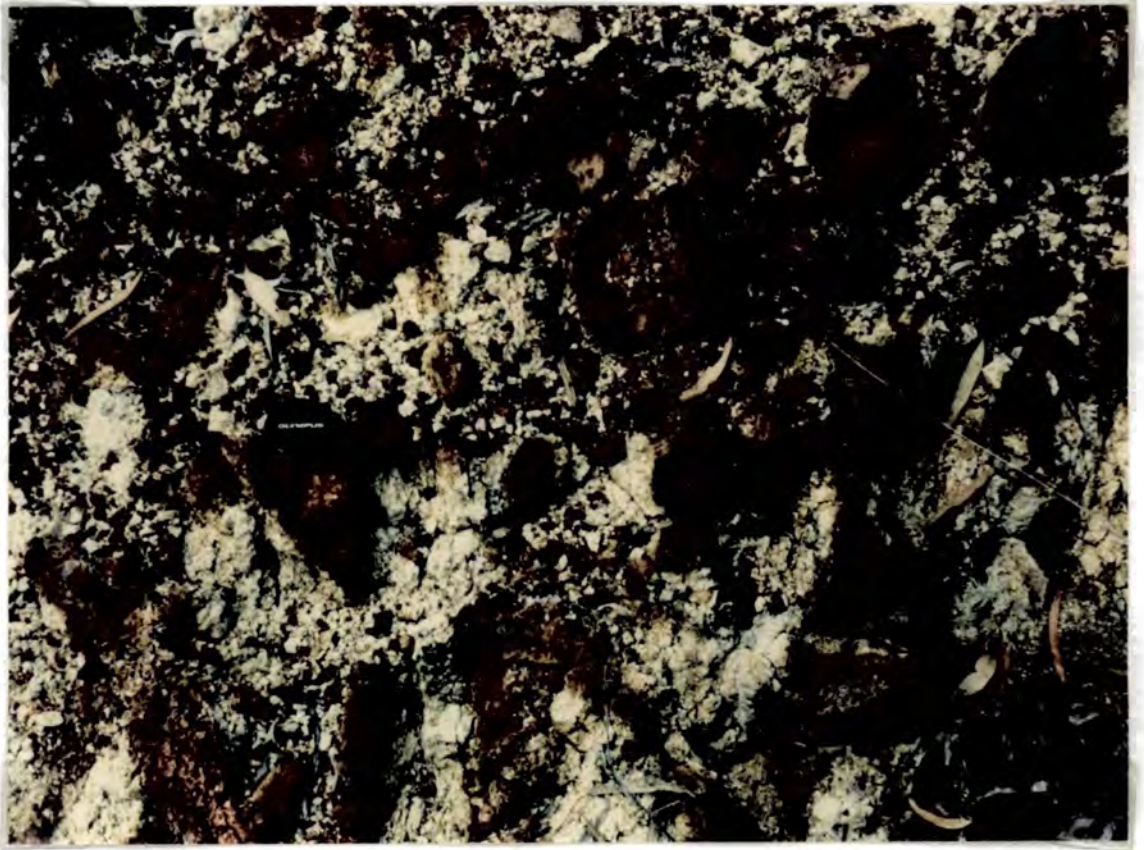
Plate 5.19   Location 3 at Plateau (Site 3). The edge of the laterite, here
we can see the exposed mottled zone, which is rich in kaolinite. (Butt,
1981).
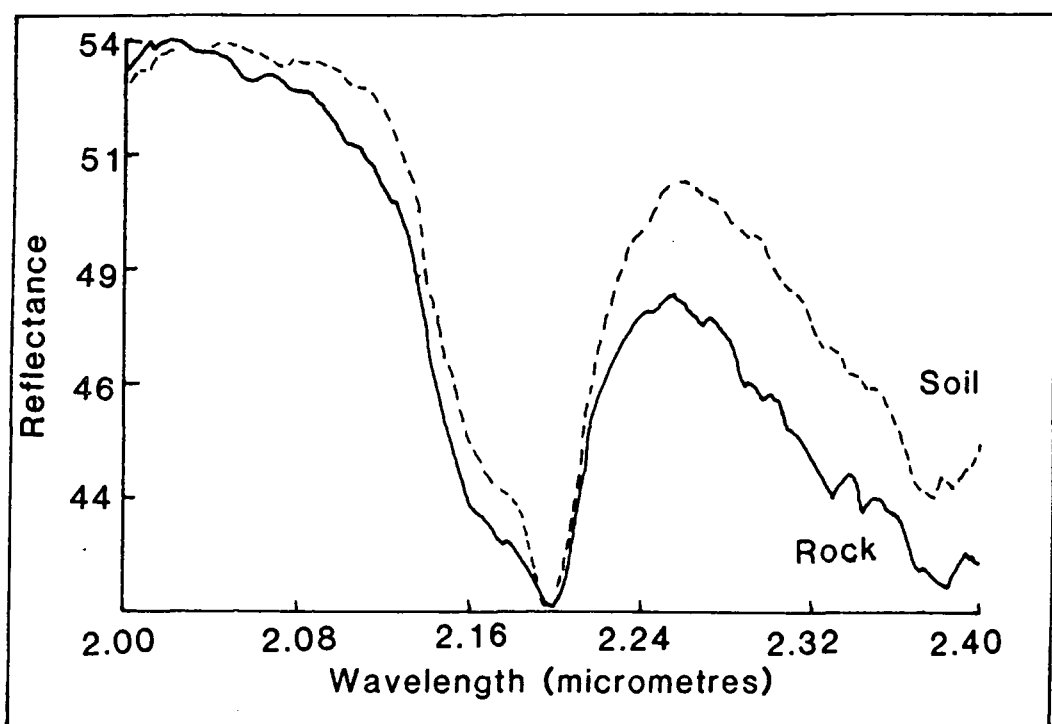
Figure 5.31   Laboratory spectra from Plateau, location 3.   Both rock
and soil show the diagnostic doublet of kaolinite (2.16μm shoulder,
2.2μm minima).
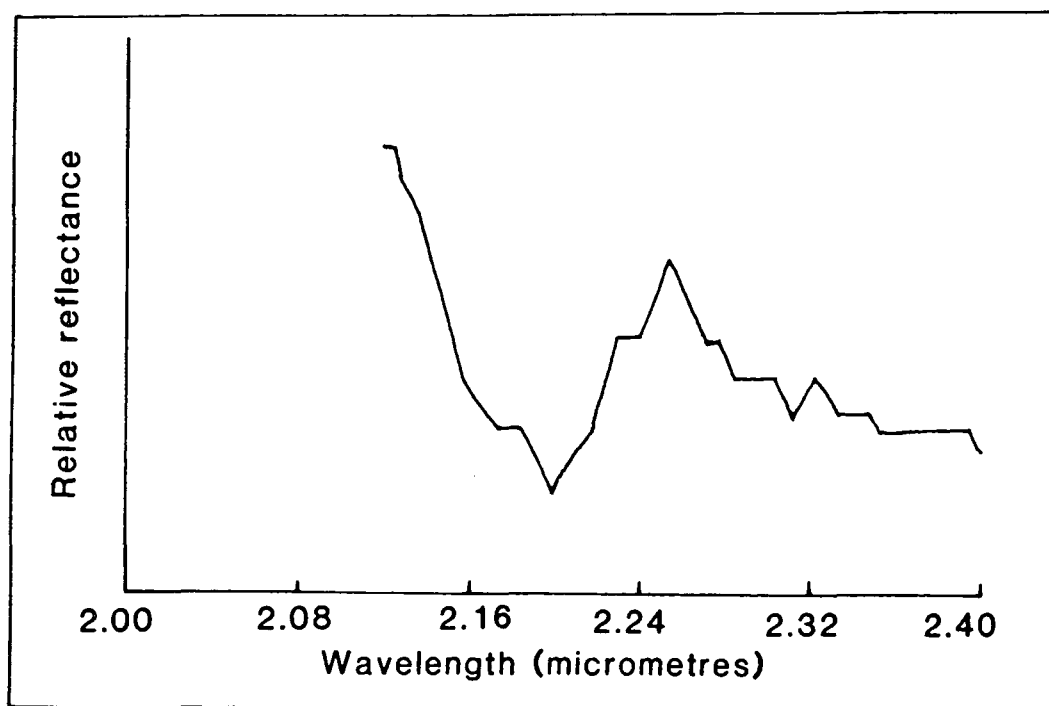
Figure 5.32   An airborne spectrum from Plateau, location 3.   A deep
absorption is present at 2.2μm that matches the laboratory spectra
quite closely, indicating the presence of kaolinite.

the clay absorption approximates to that of kaolinite.

LOCATION 4. Is to the north-east of the laterite. (Number 4, figure 5.25). The area stands out visually as an area with an absorption in a single band centred at a wavelength of 2.35μm. The area was investigated on the ground and was found to be located in a valley plain on either side of a seasonal watercourse. The area is highly vegetated with thick eucalypt cover, dry grass and an extensive litter of dead leaves from the surrounding trees, as shown in plates 5.20 and 5.21.

Airborne spectra from the area are shown which bear a clear similarity to laboratory spectra of dead plant material taken from this region, figure 5.33. Note the cellulose absorptions, producing the deep, broad 2.1μm feature and the decrease in reflectance in the 2.27μm to 2.32μm wavelength region.

5.11   Discussion.

5.11.1   Mineralisation and alteration.

At Pinnacle creek (Site 1), we could clearly identify anomalies. These are related to regional metamorphism and extensive weathering of the surface materials (the volcanic breccias for example).

At Arsenopyrite (Site 2), "CLAY" anomalies related to mineralisation were detected, although some gossans with low quartz and high iron values were not detected. The "CARBONATE" anomalies were related to the presence of epidote. The epidote is found in much of the granodiorite and is due in part to weathering and low grade metamorphism. The variability in the amount of epidote accounted for the anomalies detected by the sensor, however, the distribution of the epidote seems unrelated to the mineralisation in this area.

At Plateau (Site 3), again we can clearly see the mineralogical features related to weathering, producing lateritic kaolinite. The andesites tend to be rich in chlorite and epidote and give a spectral response in the 2.32μm to
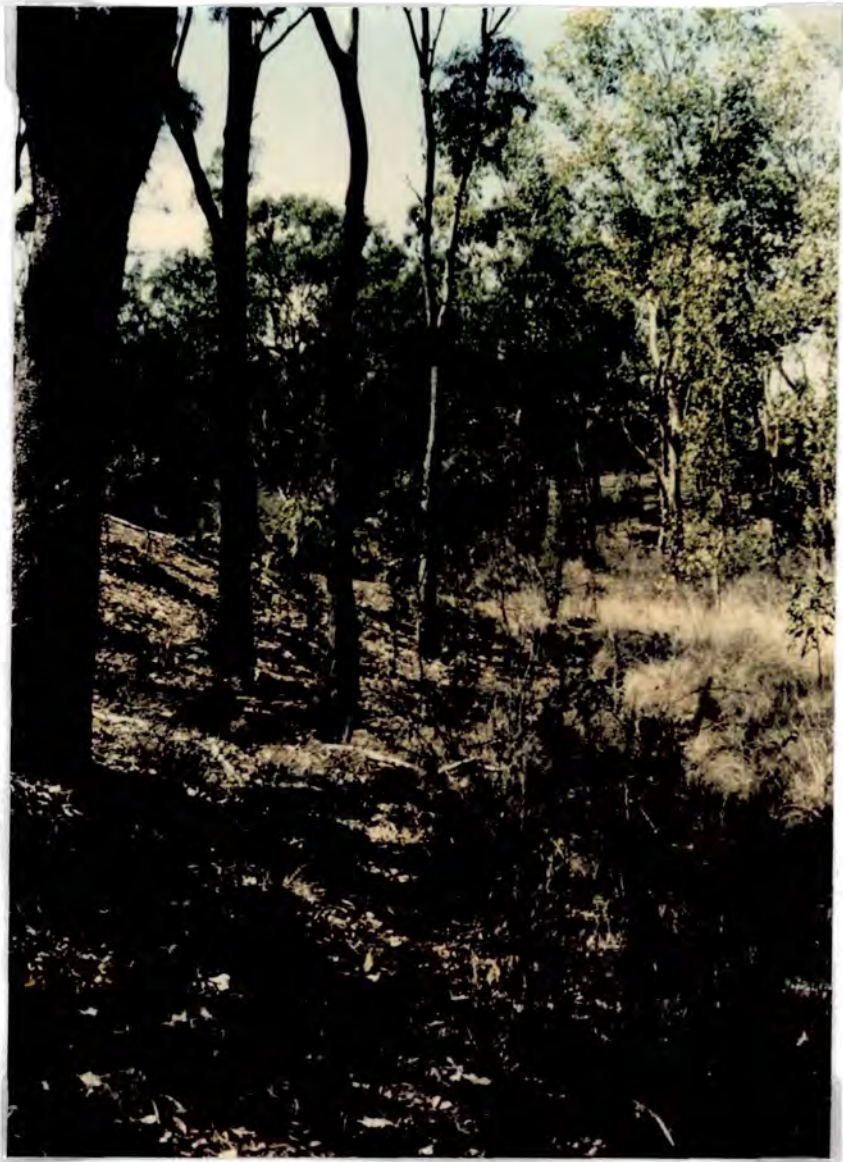
Plate 5.20   Location 4 at Plateau (Site 4). The location is in a highly
    vegetated area on either side of a seasonal watercourse. There is thick
    eucalypt cover and an extensive understorey of dry grass, with much
    leaf litter.

Plate 5.21   Location 4 at Plateau (Site 4). A close up reveals the large amounts of dry grass and leaf litter in this highly vegetated area.
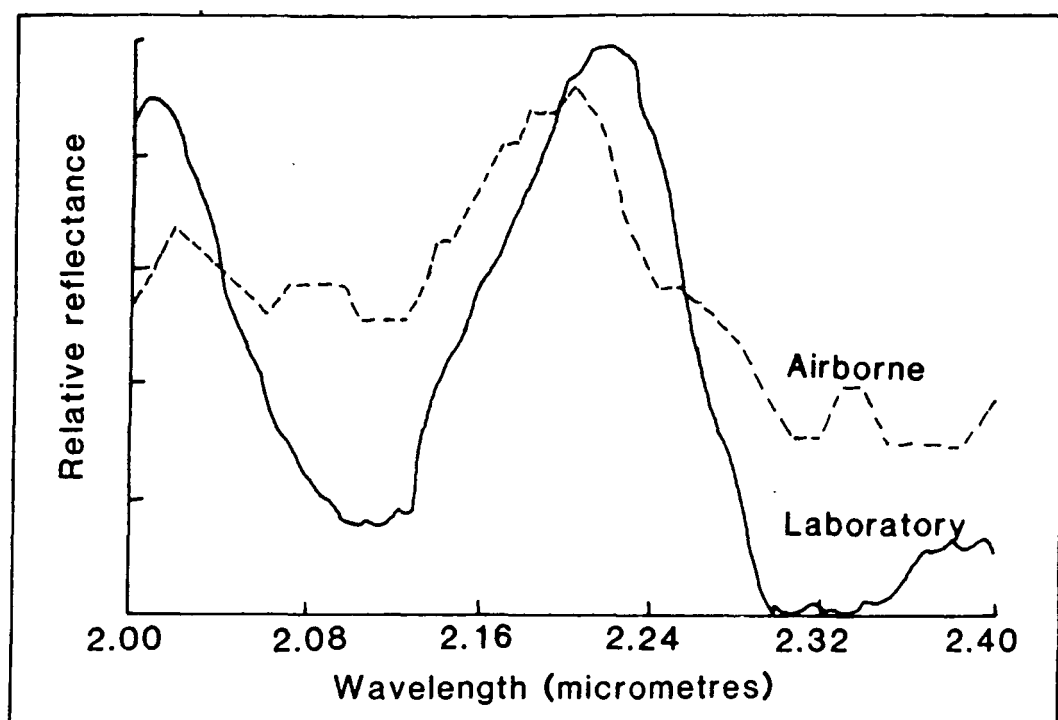
Figure 5.33   An airborne spectrum from Plateau, location 4, is compared
    to the equivalent laboratory spectrum for dry vegetation collected at
    this location.

2.35μm wavelength region that could be related to both minerals. The alteration of the andesites seems unrelated to the mineralisation observed near the rhyolite plug in the area. The rhyolite itself, shows spectral features due to weathering and mineralisation. Sericitic alteration of the rhyolite is seen, however, a kaolinitic feature due to the breakdown of the rhyolite in the soil is also evident in the laboratory spectra.

5.11.2   General

Several important conclusions can be reached regarding the AIS - 1 data. It is clear that in circumstances where there is a pure, strong, mineral absorption feature visible in both the field and laboratory data, then it will also be evident in the AIS - 1 data.

At Pinnacle creek, where the volcanic breccias gave a strong sericitic response in laboratory spectra of the rock samples and in the XRD analysis of the soils, a strong clay absorption was also evident in the AIS - 1 data. The quality of the AIS - 1 data was such that the best identity we could assign to the feature was "CLAY" (that is, the major absorptions are related to $Al - OH$ vibrational overtones and combination tones).

In all locations discussed, the field data and laboratory data gave strong, clearly identifiable mineral profiles, for example kaolinite over the laterites and epidote in the altered andesites and granodiorite. The airborne data however, could not be used in such a precise way and we could only assign vague terms such as "CLAY" or "CARBONATE" (that is, the major absorptions are related to $Mg - OH$ or CO_3 vibrational overtones and combination tones)

At the start of this chapter, the declared aims of this study were,

(1) To test the mineralogical mapping capabilities experimental AIS - 1 system.

(2) To assess its performance in an area of variable vegetation density and deep weathering profiles.

It is clear that data quality problems reduced the capabilities of the sensor, in its prime function of mineralogical identification.

After studying several locations at three different sites, it can be seen that the instrument can detect and map out anomalous areas, which have distinct spectral features related to weathering and hydrothermal alteration. It can

also be seen that although a general mapping capability exists, enabling the mapping of mineralogical groupings such as "CLAY" and "CARBONATE", the instrument is not currently capable of identifying the minerals that make up these groups.

With regard to the second aim, experience over highly vegetated andesitic terrain, indicated that anomalous features were still noticeable, although subdued, for example the epidote features at the Plateau prospect. Clearly vegetation must affect the spectral response clear evidence for this being the false anomaly generated by the tree at the Arsenopyrite prospect.[*] At the present time this effect is too poorly understood to make a clear judgement.

The effects of weathering need further study. It was seen at the Arsenopyrite prospect that areas of hydrothermal alteration, forming gossans, produced strongly anomalous features in the AIS - 1 data. These anomalous areas have suffered from the effects of weathering, but clearly still persist as features of interest. Only in areas that have suffered deep tropical weathering, producing lateritic profiles, do we lose the features of interest.

We can conclude therefore that the AIS - 1 data can be used successfully to identify anomalous areas which have experienced normal weathering conditions. However, when we are dealing with areas of deep tropical weathering, we can only identify the features of the weathering profile and not the original mineralogy.

5.12 Summary.

The AIS - 1 data was processed using the RGN technique. The output residual images were used to visually identify areas of the scene for further study through identification of absorptions in the 2.2μm band and the 2.35μm band. Three sites were chosen for follow up work. At all three sites the distinctive features shown in the AIS - 1 data were confirmed by ground analysis.

It was found that the identification of surface materials was greatly hindered by the low signal to noise ratios of the AIS - 1 instrument and that only broad classifications into "CLAY" groups with features near 2.2μm and "CARBONATE" groups with features near 2.35μm were possible, even after spatial averaging.

76

* See Briggs et al. (1988) for other examples.

Further summary.

Noise in the airborne data reduces identification accuracy. However, with access to laboratory spectra obtained from the area, it was possible in many cases to make clear unequivocal identification of the mineral present in the airborne data.

Without this ancillary data it is more difficult to make a clear identification but by no means impossible (for example in figure 5.32, kaolinite is clearly visible in the airborne spectrum).

5.13 Conclusions.

(1) Processing using the RGN technique did visually highlight areas showing absorption features of interest.

(2) Broad classification of the anomalies into two generic groups was possible, but an improvement in the data quality is necessary to make identification of mineral species a possibility, when no ancillary data is available.

(3) The variations in mineralogy were usually closely related to variations in lithology on occasion, although the original lithology could not be determined from the spectral response.

(4) The effects of second order overlap could not be clearly identified in the data set, however, this effect will have reduced the ability to detect mineral absorption features present in the data.

(5) The effects of surface weathering need more study, within the framework of high spectral resolution studies. The spectral differences between weathered rock surfaces and the fresh rock need to be measured and the reasons for the differences determined.

(6) Basic mineralogical differences could be mapped.

(7) The depths of absorptions gave some indication of the proportions of minerals present.

(8) With a little ground knowledge, clear identification of minerals is possible.

(9) Generic classification into different groups was clearly possible without ground knowledge.

CHAPTER 6

INTERPRETATION AND DISCUSSION OF THE RESULTS, OBTAINED FROM THE GER - II INSTRUMENT FLIGHT OVER AN AREA OF NORTHERN NEVADA, USA.

6.1 Introduction.

High spectral resolution data were collected by BP Minerals America Ltd., as part of an ongoing effort to evaluate such data sets for mineral exploration. The sensor used was the Geophysical Environmental Research 64 band scanning instrument (GER - II). The GER - II data was collected on the 17th August 1987, the parameters of the flight are given in Table 7.

The flight was over an area 30km south-east of Winnemucca in northern Nevada, USA, figure 6.1. The research aims for this flight were,

(1) To test the mineralogical mapping capabilities of the GER - II scanner.

(2) To compare the GER - II and AIS - 1 instruments and to determine the effects of the different spatial and spectral resolutions of the instruments.

(3) To determine which unique features in the visible and near infrared would be of use in mineral identification. Note that this wavelength region, 0.4μm to 1.0μm was not available in the AIS - 1 instrument.

6.2 Climate, topography and vegetation.

The climate of the area is arid to semi-arid (Willden, 1964), with hot, dry summers and cold, dry winters. Most precipitation takes place in the winter months usually as snowfall.

The topographic relief varies across the area. The eastern area is relatively flat and consists primarily of Quaternary alluvium deposits, heavily dissected by small gullies. The western area extends into the rounded foothills of the Sonoma range, rising 300m or more above the alluvium . The hills are separated by deep gullies formed by the major streams.

Vegetation is primarily sagebrush of several species, while some areas have

```
┌─────────────────────────────────────────────────────┐
│              GER-II   FLIGHT   PARAMETERS             │
│                AMERICAN   FIELD SITE                  │
├─────────────────────────────────────────────────────┤
│                                                       │
│   LOCATION  -   30km South-east of Winnemucca,        │
│                 Nevada.                                │
│                                                       │
│   DATE OF FLIGHT  -  August 17th 1987.                │
│                                                       │
│   ATMOSPHERIC CONDITIONS  -  Good                     │
│                                                       │
│   ALTITUDE  -   4200m  A.S.L.                         │
│                 2840m  above ground                   │
│                                                       │
├─────────────────────────────────────────────────────┤
│                                                       │
│   APERTURE      -   4.6 M RAD (0.26°)                 │
│                                                       │
│   GIFOV         -   12.9m                             │
│                                                       │
│   SWATH WIDTH   -   5.7 km                            │
│                                                       │
│   LINE LENGTH   -   14.0 km                           │
│                                                       │
└─────────────────────────────────────────────────────┘
```

Table 7.
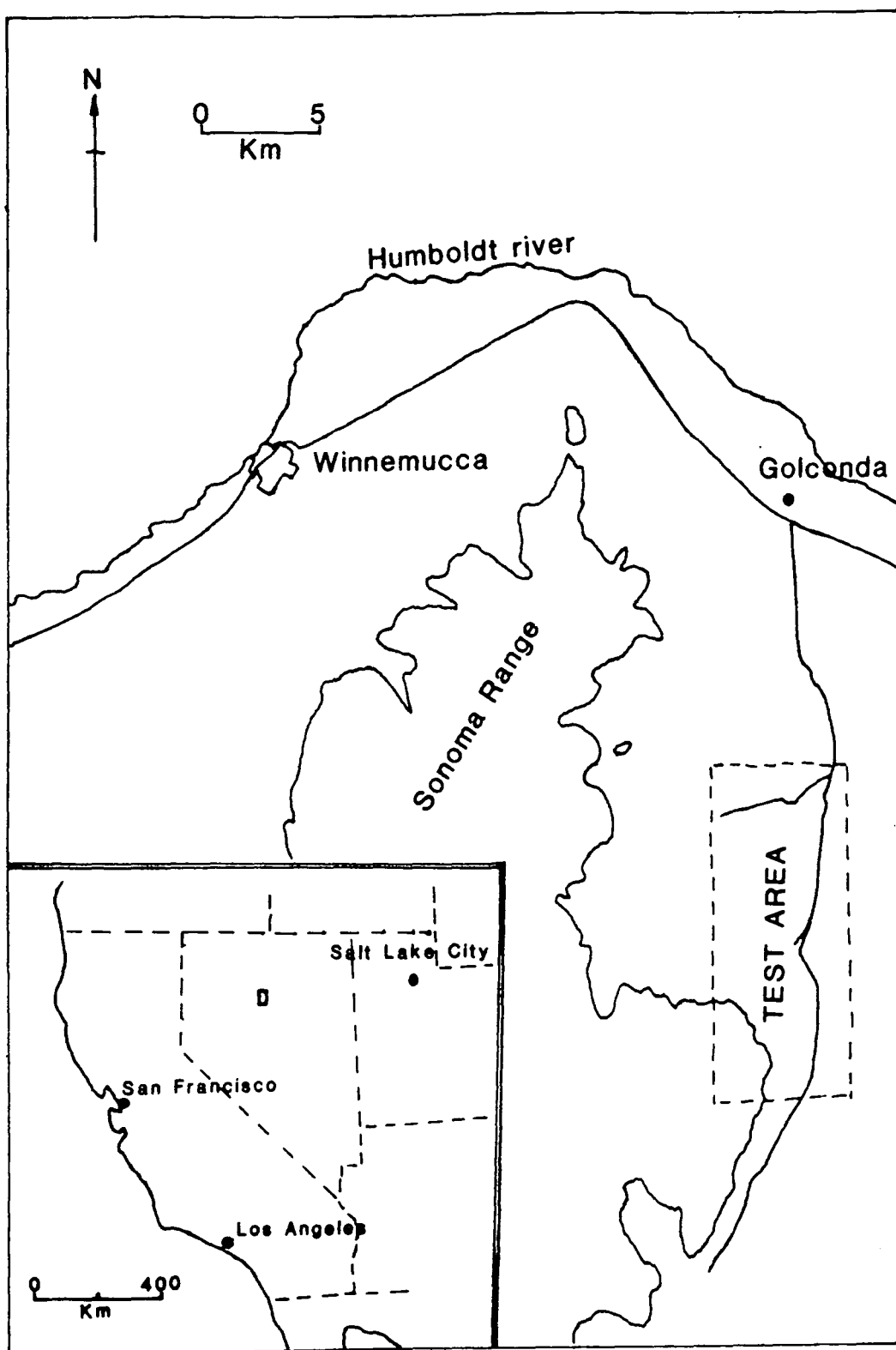
Figure 6.1 Location map of the American test area, near Winnemucca, northern Nevada, USA.

extensive dry grass cover. The vegetation density is very variable, with the greatest development in the stream beds (100%) where small bushy trees are common. The lowest densities (8%) are found on hill tops showing the effects of hydrothermal alteration and silicification (N. Drake, pers. comm.).

6.3 General geology.

The area is located in the Basin and Range province of the western United States. It has suffered four periods of intense compressive deformation between middle to late Palaeozoic and late Cretaceous to early Tertiary times and in addition, at least one period of high angle faulting of late Tertiary to Recent times (Willden, 1964).

The only major outcropping units in the area are the Cambrian Preble formation and the Ordovician Sonoma Range and Valmy formations. These early Palaeozoic rocks were thrust faulted and folded during the four periods of intense compressive deformation and finally intruded by a large granodiorite body in the late Cretaceous to early Tertiary, producing extensive thermal metamorphism close to the intrusion. The mineralisation observed in the area has been related to the intrusion of the granodiorite, although field relationships also suggest a later period of mineralisation in the late Tertiary (Willden, 1964).

A geological map of the area is shown in figure 6.2, largely based on that drawn up by BP Minerals. The limits of the flight line are approximately the edges of the map, althoug h the flight line extends further to the south. The only unit outcropping in the area of study is the Cambrian Preble formation. This unit can be divided in to two main sub-units within the bounds of the flight line, these are,

(1) Labelled Ep on the map, it is the Main Body of the Preble formation and consists of greenish to yellow-grey phyllite with interbedded quartzite. It is intensely deformed, with much folding and a secondary cleavage close to the bedding plane. Where it is close to the contact with the underlying granodiorite, the unit has been thermally metamorphosed to a quartz-mica schist.

(2) The unit labelled Epl on the map. It is a light to dark grey dolomitic

79
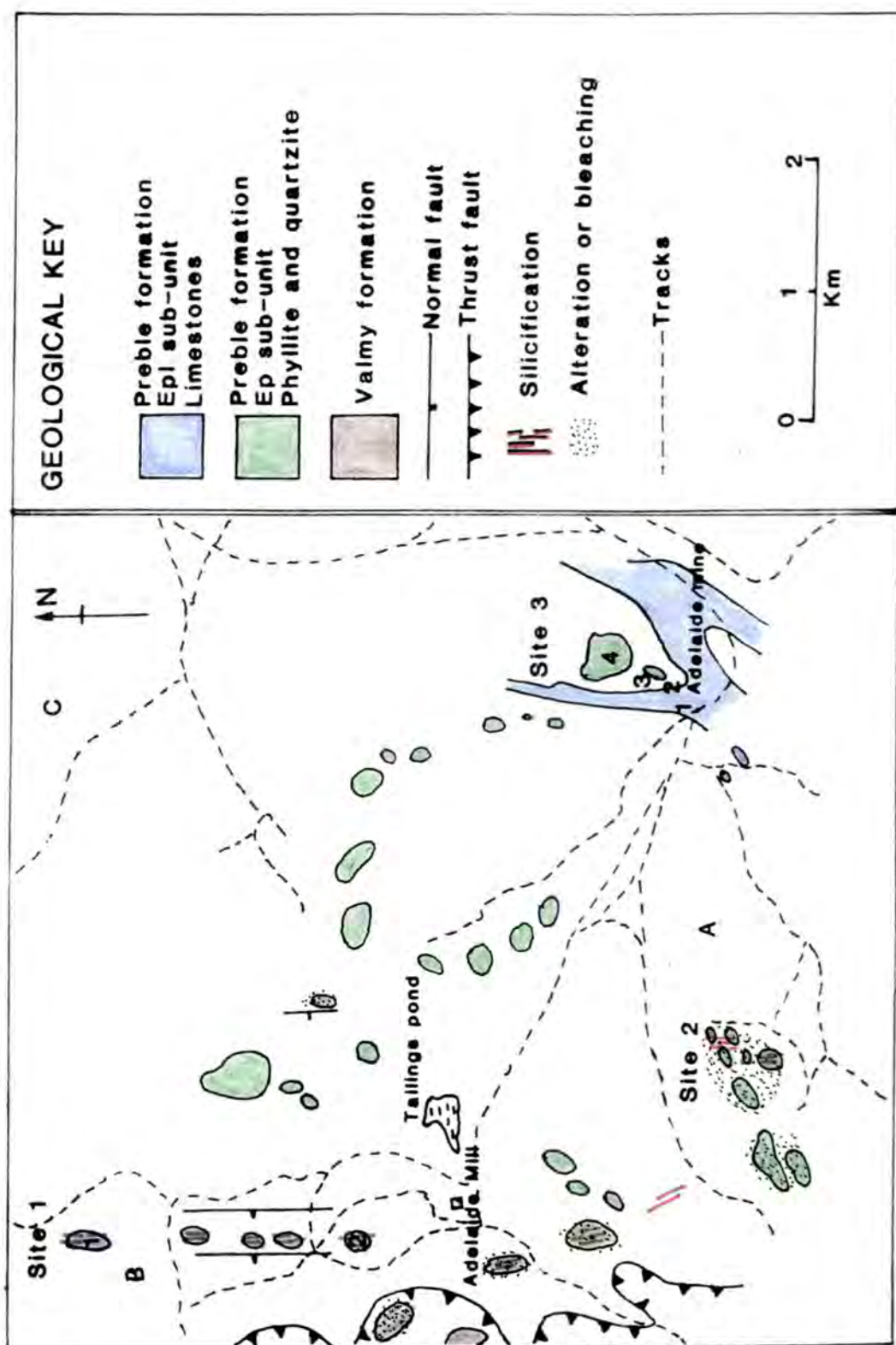
Figure 6.2 Geological and location map of the Adelaide test area. Based largely on the work carried out by BP Minerals America. The locations and sites are discussed in detail in the text.

limestone that weathers blackish grey and includes some shale beds. Most of the limestone is recrystallised to a medium to coarse grained aggregate, cut by calcite veinlets and brown chert veinlets and nodules. The chert imparts a rough surface to the weathered rock.

These sub-units identified by the geologists from BP Minerals, have both been heavily folded and faulted. In places extensive silicification and bleaching of the rocks has taken place, related to mineralising episodes in the Cretaceous and Tertiary.

6.4 Mineralisation and alteration.

Mineralisation is clearly evident in the area, with extensive copper and gold mining over the last century. The copper mineralisation is closely related to the alteration of the limestone during the intrusion of the Cretaceous granodiorite. The gold mineralisation is believed to be more recent, with the development of quartz rich NW - SE to N - S trending lodes. Current exploration is aimed at finding disseminated gold deposits, with large alteration haloes.

The alteration can cover much ground, with large areas of argillic and phyllic alteration, providing a mineralogy dominated by the clay minerals kaolinite, montmorillonite, illite and muscovite (sericite). Silicification is also clearly visible in the area, with quartz veining along north - south fault planes and very dark weathering iron rich jasperoids (siliceous rocks).

The spectral responses of the rock types and alteration zones in this area, are discussed by Krohn (1986).

6.5 GER - II Data processing and analysis.

Before visiting the field area for the first time, the GER - II data set was prepared, processed and partly analysed. Figure 6.3 is a outline of the data preparation and processing steps. The processing technique used was the log residuals / IARR technique. The RGN method was not used, as the green vegetation component is quite low, is confined primarily to the stream beds and does not obscure mineral absorptions.

The output required for field studies, consisted of three output images

```
                    ┌─────────────────────────┐
                    │   Tape to disk copy     │
                    └────────────┬────────────┘
          ┌──────────────────────┴────────────────────────┐
          │ Rescale data to byte for display device        │
          └──────────────────────┬────────────────────────┘
```

┌─ ─ ─ ─ ─ ─ ─ ─ ─ ┴─ ─ ─ ─ ─ ─ ─ ┐
│   DATA PREPARATION   │
├─ ─ ─ ─ ─ ─ ─ ─ ┬─ ─ ─ ─ ─ ─ ─ ─ ┤
│   │
│   Vertical destriping – Coleq.for │
│   │
│   Horizontal destriping – Roweq.for │
│   │
│   Spectral noise filter – Filter.for │
└─ ─ ─ ─ ─ ─ ─ ─ ─ ─ ─ ─ ─ ─ ─ ─ ─ ┘

┌─ ─ ─ ─ ─ ─ ─ ─ ─ ─ ─ ─ ─ ─ ─ ─ ─ ┐
│   DATA PROCESSING   │
├─ ─ ─ ─ ─ ─ ─ ─ ─ ─ ─ ─ ─ ─ ─ ─ ─ ┤
│ Log residuals   IARR – Step 1   RGN – Step 1 │
│   Logr.for   Norm.for   Norm.for   │
│   │
│   IARR – Step 2   RGN – Step 2 │
│   Aver.for   Model.for │
└─ ─ ─ ─ ─ ─ ─ ─ ─ ─ ─ ─ ─ ─ ─ ─ ─ ┘

┌─ ─ ─ ─ ─ ─ ─ ─ ─ ─ ─ ─ ─ ─ ─ ─ ─ ┐
│   ANALYSIS   │
├─ ─ ─ ─ ─ ─ ─ ─ ─ ─ ─ ─ ─ ─ ─ ─ ─ ┤
│   SPAM───────────── Images of bands │
│   0.9um, 2.2um   │
│   Spectral curves   and 2.35um   │
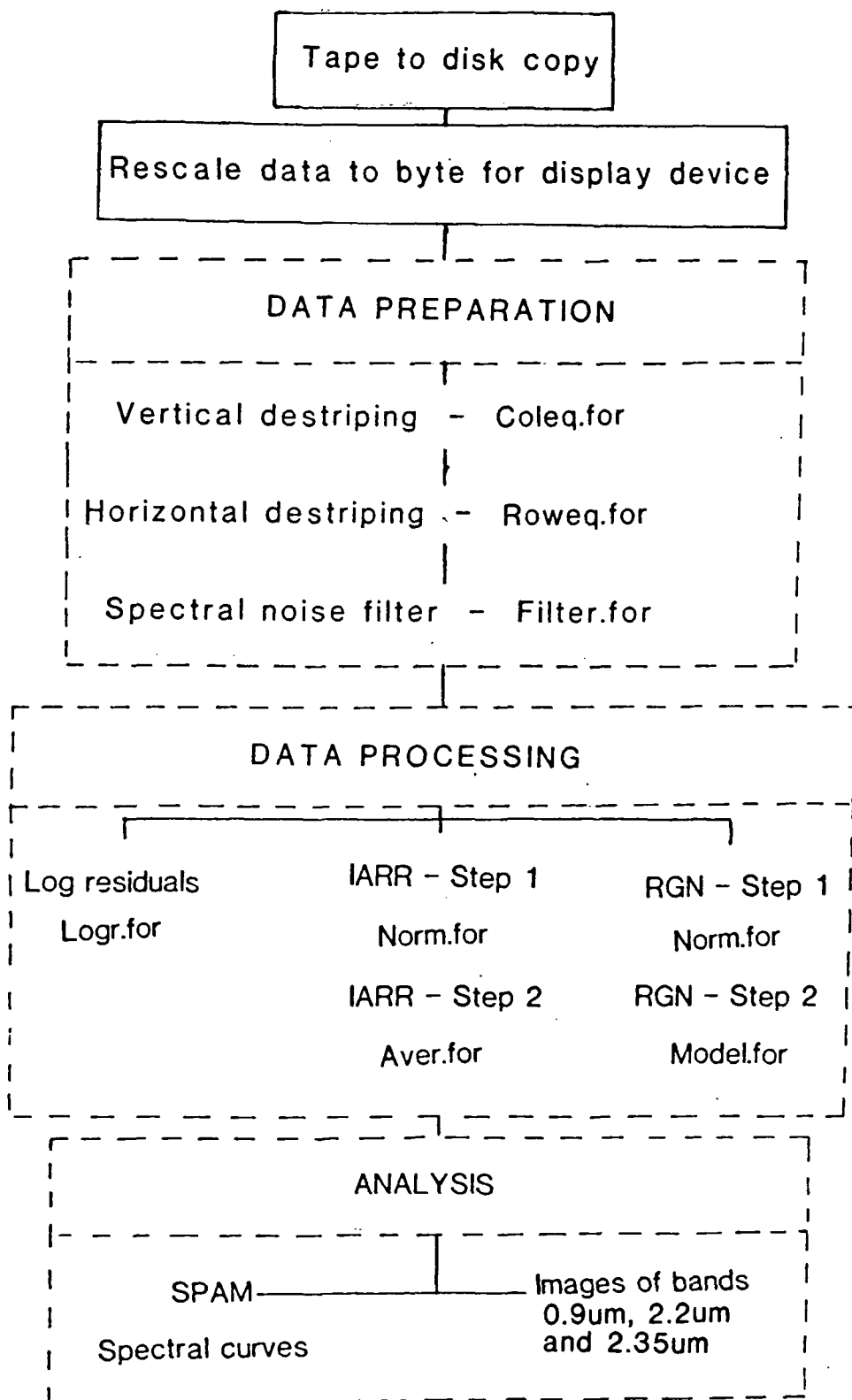└─ ─ ─ ─ ─ ─ ─ ─ ─ ─ ─ ─ ─ ─ ─ ─ ─ ┘

Figure 6.3   A flow diagram of the data preparation, processing and analysis steps used on the GER - II scanner data.

or anomaly maps. One output image covering the wavelength range around 0.9μm the iron absorptions, one at 2.2μm the clay absorptions and one covering the wavelength region around 2.35μm. From these absorption maps three sites were chosen for ground follow up work.

Analysis using the SPAM package was performed at the end of the field season, extracting spectra from chosen sites over the anomalous areas previously indicated. Due to the poor data quality of the instrument, even after spectral filtering, spectral plots were obtained for an average of several pixels, usually nine, unless otherwise stated. This technique enhances the signal, but also introduces problems from spectral mixing of the different components making up the averaged area.

6.6   Expected spectral response.

During the field season, data for the three anomalous areas were collected. Laboratory and field observations confirmed the presence of several spectrally distinct materials in the 0.4μm to 2.45μm spectral range. The materials identified are listed below,

(1) Green vegetation.

(2) Dry vegetation.

(3) Sericite (Muscovite).

(4) Illite.

(5) Kaolinite.

(6) Calcite.

(7) Dolomite.

Diagnostic features of the material spectra are listed below and shown diagramatically in figure 6.4, excluding green vegetation.

GREEN VEGETATION (1).

Apart from the water absorptions at 1.4μm and 1.9μm, which are usually masked in the airborne data by atmospheric water absorption features. The most distinct feature is the red edge in the VNIR. Here the reflectance rises steeply from the visible to the near infrared at about 0.75μm. This feature is diagnostic of healthy, green vegetation and decreases in size as the vegetation drys out (Elvidge, 1988).
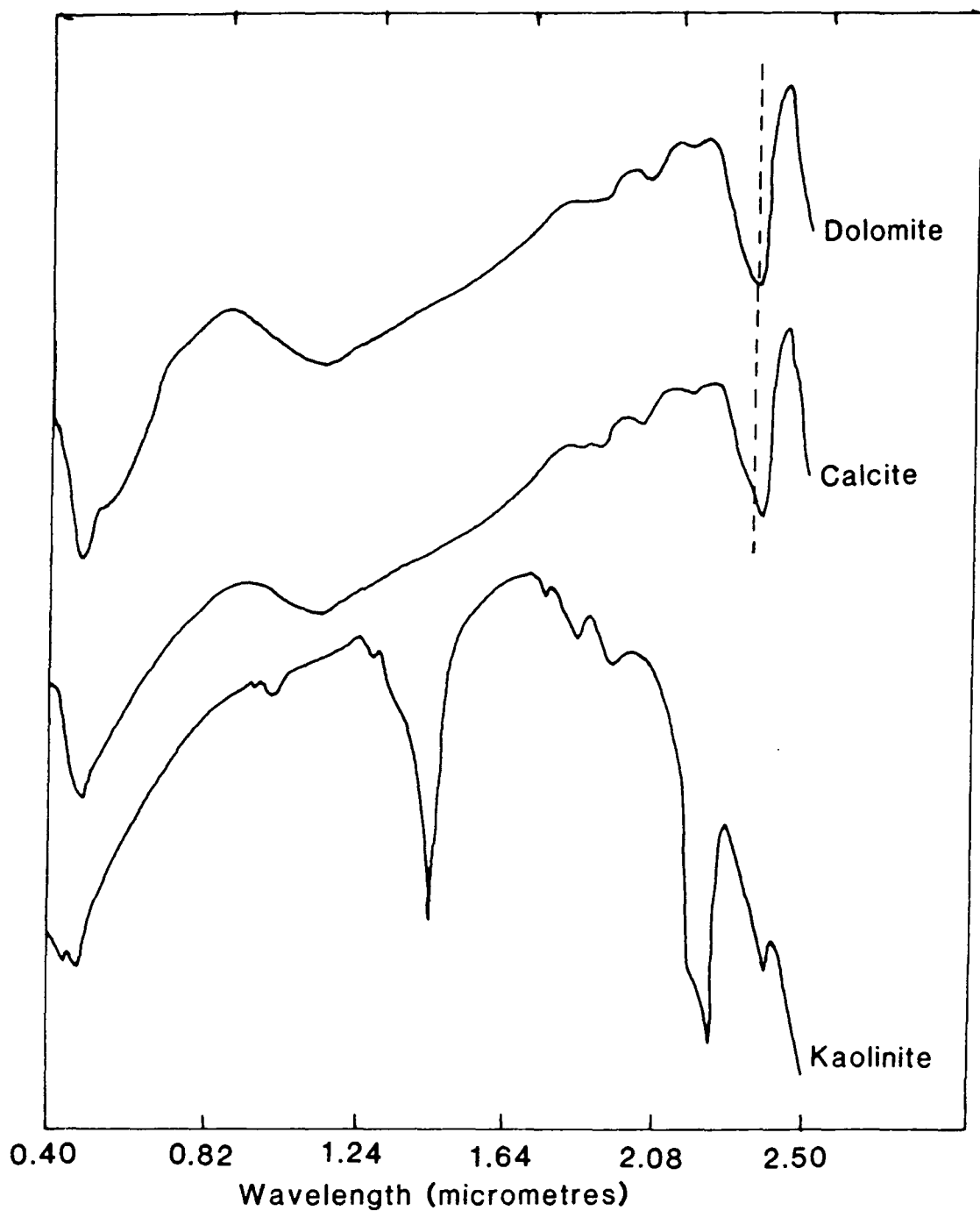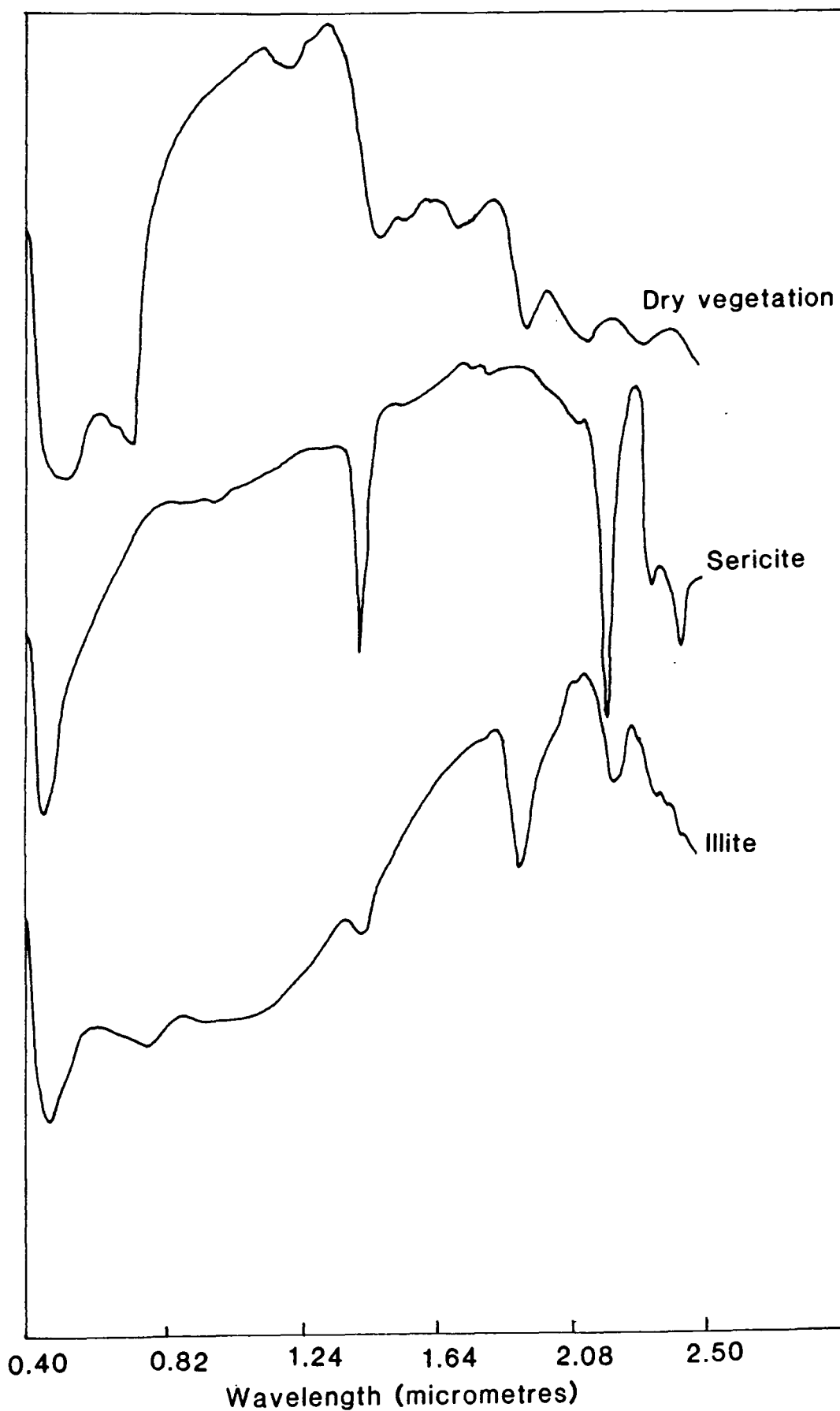
Figure 6.4 Laboratory reflectance spectra collected using an IRIS Mk IV
spectroradiometer, referenced to a barium sulphate reference panel.
The materials in these two figures are those commonly observed at
the sites of interest.

Dry vegetation

Sericite

Illite

0.40   0.82   1.24   1.64   2.08   2.50
Wavelength (micrometres)

DRY VEGETATION (2).

The diagnostic absorptions of cellulose are clearly visible, giving a strong feature at 2.1μm, with the distinct decrease in reflectance from 2.27μm to 2.32μm. A small red edge in the VNIR is often seen in partially green vegetation (Elvidge, 1988).

SERICITE (3).

The most distinct absorption is the deep, narrow feature at 2.2μm, due to the bending - stretching of the $Al-OH$ bonds. Other diagnostic features are the steep drop off to 2.32μm and the deep, narrow 1.4μm feature related to the presence of the hydroxyl ion (OH^-) in the structure (Hunt et al., 1970). The 1.4μm feature is often obscured in airborne data by the atmospheric water absorption features.

ILLITE (4).

Has a similar structure to sericite. Its main absorptions are related to the bending - stretching vibrations of the $Al-OH$ bonds. The difference in structure affects the position and depths of some of the features, giving a broader feature at the slightly longer wavelength of 2.21μm and a slightly less steep decrease in reflectance to 2.32μm.

KAOLINITE (5).

Another mineral with $Al-OH$ bending - stretching vibrational absorptions. The different structure of kaolinite produces a broad absorption with a minima at 2.2μm. A flattening of the absorption produces a distinct shoulder in the spectral curve at 2.16μm. The decrease in reflectance at longer wavelength values is more gradual (Hunt et al., 1970).

CALCITE (6).

The major diagnostic absorption features are related to the bending - stretching vibrations of the $C-O$ bonds in the carbonate ion. The major feature is a deep asymmetric absorption, with a minimum at 2.35μm (Gaffey, 1985).

DOLOMITE (7).

The major features are again related to the bending - stretching vibrations of the $C-O$ bonds of the carbonate ion. The variation in structure due to the presence of the Mg^{2+} ion shifts the deep asymmetric absorption to shorter wavelengths, from 2.35μm to 2.33μm(Gaffey, 1985).

Major iron absorptions can also be observed in the VNIR, centred near 0.9μm. These features can be diagnostic of various iron minerals, such as haematite and goethite. The spectral features of the VNIR warrant further research.

6.7 Site locations.

The flight was flown in a north-south direction. The three anomalous sites are marked as 1, 2 and 3 on the map, figure 6.2.

These sites are referred to as,

Site 1 - Dolomitic Hills.

Site 2 - Mackin's Knob.

Site 3 - Adelaide Mine.

6.8 Site 1 - Dolomitic Hills.

The area lies in the north and west part of the flight line (number 1 on figure 6.2).

6.8.1 Topography and vegetation.

The site is centred on a north-south trending line of hills, plate 6.1. The target hills are approximately 100m above the surrounding valleys at their highest points. Small saddles separate the hills, with deeper valleys to the east and west. The vegetation is primarily sage brush on the hills with some dry grass. Dry grass forms a larger proportion of the vegetation on the lower slopes. The vegetation density is highly variable, but does decrease towards the hill tops.

6.8.2 General geology.

The area consists of dolomitic limestone on the hill tops with phyllite forming the lower slopes and valleys. There is evidence for high angle north-south trending faults in the phyllite in the valleys, which seem related to the mineralisation in this area. Lines of old mine workings follow these north-south trending quartz rich fault zones. The hill crests also contain narrow north-south trending siliceous ridges, the boundaries between the ridges and the dolomitic limestone are indistinct. The introduction of the silica may have

Plate 6.1   Dolomitic hills, Site 1, Overview. This is a view from the south, looking towards the site. The site extends in a north-south direction, following a line of small red-brown weathered hills. Each hill top has material of a dolomitic composition, with siliceous north-south trending ridges on the hill crests.

been originally along fractures, but silicification of the limestone away from the fractures is also clearly visible.

6.8.3   Locations.

Two separate locations were studied in detail, but the findings apply to all the hills forming this north-south trend.

LOCATION 1. Is situated on hill 1849T, figure 6.2. The location is is described by the BP geologists as a limestone, which has been altered and silicified in places. The rocks consist of bedded calcareous rocks with chert bands and calcite veining , plate 6.2. The limestone feels gritty to the touch. There is a tendency for dun brown exterior colours and grey interiors. Silicification is evident as blocky, iron-stained north-south ridges on each hill top. The siliceous material has a red-brown exterior and a fine grained often grey interior. Vegetation cover consists of scattered sage brush with a little dry grass.

Thin section studies of the rocks confirm the field evidence. The general rock type is primarily a carbonate (calcite or dolomite), with quartz and calcite veining. The calcite veins tend to be coarser grained than the matrix. Small disseminated grains of quartz are sometimes visible.

Laboratory spectra of the dun brown weathering surfaces are shown in figure 6.5a, they gave a strong dolomitic response. The most identifiable feature is the asymmetric absorption feature centred at 2.33μm in the short wavelength infrared.

The GER - II spectrum for this area is shown in figure 6.5b. This also shows the deep asymmetric absorption centred at 2.33μm. All this evidence confirms the presence of dolomite forming the upper surface of the hill tops.

Other samples were also taken from the north-south siliceous ridges near the summit. These rocks tend to be red stained and have some associated mineralisation.

Thin section studies revealed an almost pure silica rock, with some iron staining and late veinlets of remobilised(?) carbonate. Fractures are infilled with quartz, the grain size diminishing towards the edge of the fractures.

Laboratory spectra of these very dark rocks are shown in figure 6.5c, with strong iron absorptions, centred near 0.9μm and a very weak clay feature, centred at 2.2μm.
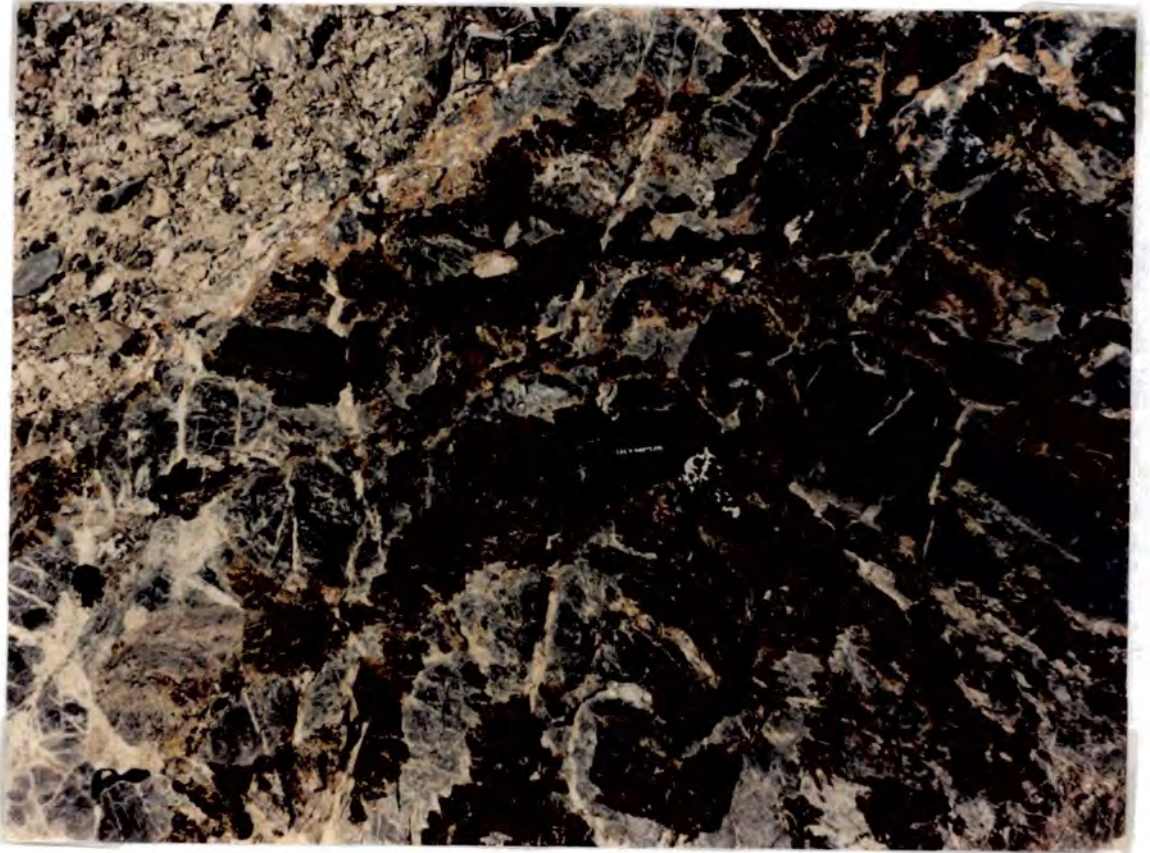
Plate 6.2   Dolomitic hills, Site 1, Location 1. The folded calcareous limestones are clearly shown, with interbedded chert and extensive calcite veining.
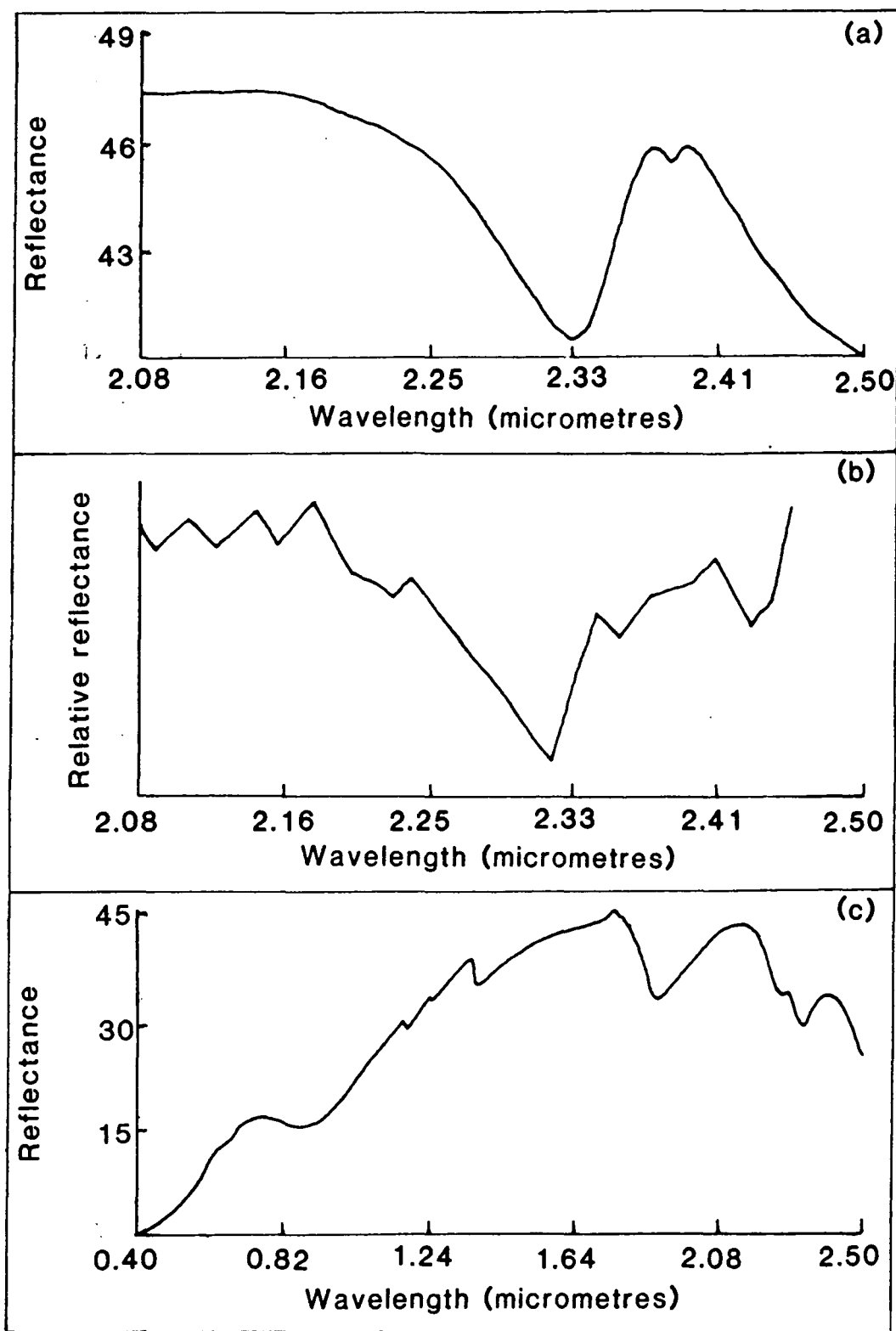
Figure 6.5 Located at site 1 (Dolomitic hills), location 1. (a) Laboratory spectrum of the dolomitic weathering crust with a deep asymmetric absorption at 2.33μm. (b) A noisier airborne spectrum also has the same deep asymmetric absorption. (c) A laboratory spectrum of the siliceous rocks shows the deep iron absorption at 0.9μm and a small clay feature at 2.2μm.

Analysis of the GER - II airborne data failed to reveal the presence of the small north-south iron-stained siliceous ridges. Images of the area showed the presence of iron at some locations, but it was impossible to define the ridges, possibly due to their narrowness.

LOCATION 2. Is situated on the hill top south of 1801T, number 2, figure 6.2. The area description is the same as that for the more northern location, with dun brown weathering, dolomitic limestone and small, siliceous, north-south trending iron-stained ridges, plate 6.3.

Thin sections reveal a calcareous rock with a larger proportion of quartz, both as grains and veins. The sectioned surface looks very fragmented and deformed. The section is very disordered, with interlocking grains of quartz and carbonate of variable grain size. The fragmentation and deformation of this rock, may be due to the fracturing of the dolomitic limestone prior to the emplacement of the siliceous north-south ridges in the area.

Laboratory spectra, figure 6.6a show the distinctive asymmetric absorption of dolomite, centred at 2.33μm.

The GER - II airborne spectrum of an averaged area of nine pixels is given in figure 6.6b. This also shows the distinctive spectral shape of dolomite.

Small areas of siliceous rocks were clearly evident at this location. The rocks consisted of red-black weathering material, which proved to be primarily quartz and opaques with a little muscovite.

Laboratory spectra, figure 6.6c show that the material has a very low reflectance with a weak iron feature at 0.9μm and a very small clay feature at 2.2μm. This small area could not be identified in the image produced from the airborne data.

6.9   Site 1 - Summary.

Clearly, the deep absorptions due to the dolomitic weathering crust of the carbonate are visible. Thin section work confirms the presence of the carbonate, while both laboratory spectra and airborne data indicate the presence of dolomite. The dark red-black coloured siliceous ridges proved impossible to to locate in the imagery, possibly due to the small size of the targets, combined with their low reflectance. This would make them difficult targets to observe

Plate 6.3   Dolomitic hills, Site 1, Location 2. The dun-brown weathering, dolomitic limestones are clearly visible on the hill top surface, forming a gravel in places.
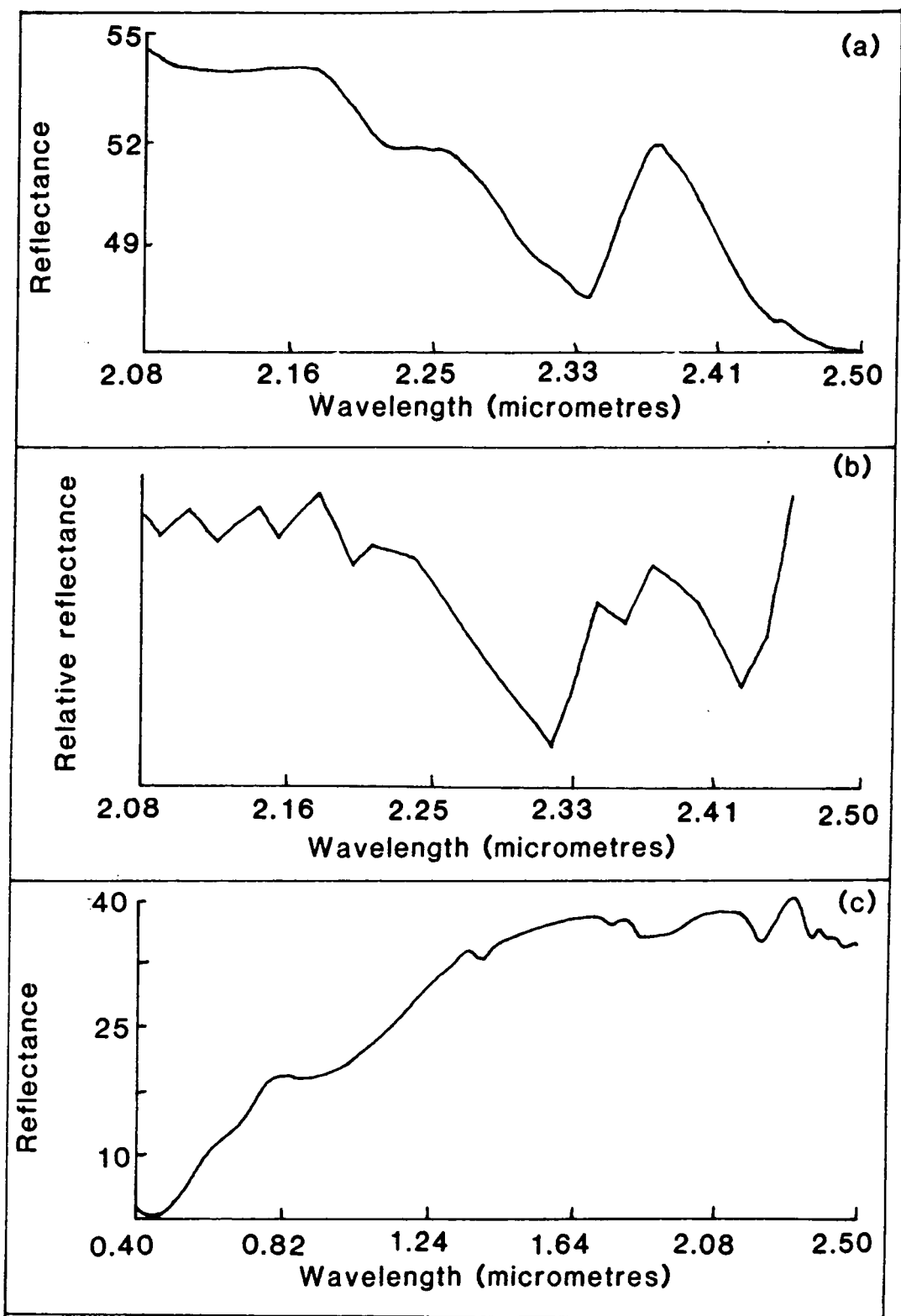
Figure 6.6 Located at site 1 (Dolomitic hills), location 2. (a) Laboratory
spectrum showing a small clay feature and the diagnostic absorption of
dolomite. (b) An airborne spectrum also shows the strong dolomitic
feature $(2.33\mu m)$. (c) A laboratory spectrum of the siliceous rocks
showed a weak iron feature $(0.9\mu m)$ and a small clay feature $(2.2\mu m)$.

due to their lower signal to noise ratios.

6.10 Site 2 - Mackin's Knob.

The site is located near the western edge of the image, forming the hill 1774T, shown in figure 6.2.

6.10.1 Topography and vegetation.

The site forms one of the eastern foothills of the Sonoma range, rising 100m above the quaternary river gravels to the east. The vegetation is predominantly sage brush, with a little grass. Vegetation density is of the order of 8% (N. Drake, pers. comm.).

6.10.2 General geology.

The area is located entirely on the Preble formation sub-unit, labelled Ep and consists of phyllites and interbedded quartzites. Much of the phyllite has been extensively altered to a bleached and friable material (plate 6.4), with highly micaceous surfaces. Silicification accompanied by extensive iron staining is evident near the summit of Mackin's knob, plate 6.5.

Thin section work showed that the phyllite is quartz rich with some iron staining. However there is obviously a major introduction of clay (sericite) into the rock, mainly along fractures. The rock is highly deformed.

The more altered, friable rocks were impossible to section, however, XRD analysis was used on the crushed rock fragments. The analysis revealed that the rock is basically a sericite-quartz assemblage, with very strong sericite peaks and noticeable quartz peaks.

Laboratory spectra of samples taken from the site shown in figure 6.7a have the very strong absorption features of sericite, with a 2.2μm maximum absorption.

The GER - II airborne data are shown in figure 6.7b. The spectrum is a nine pixel average and is compared with the SPAM library spectrum of muscovite. As we can see the spectrum can be clearly identified as muscovite (sericite).

The siliceous rocks near the summit of Mackin's Knob show much surface iron staining.

Thin section work confirmed that the rock is almost entirely quartz with

Plate 6.4   Mackins Knob, Site 2. The hill top consists of phyllite that has been highly sericitised. The platy phyllite is abundant on the upper slopes of the hill.

Plate 6.5   Mackins Knob, Site 2. Large areas of silicification are present. With red-black, iron-stained, massive rocks near the summit.
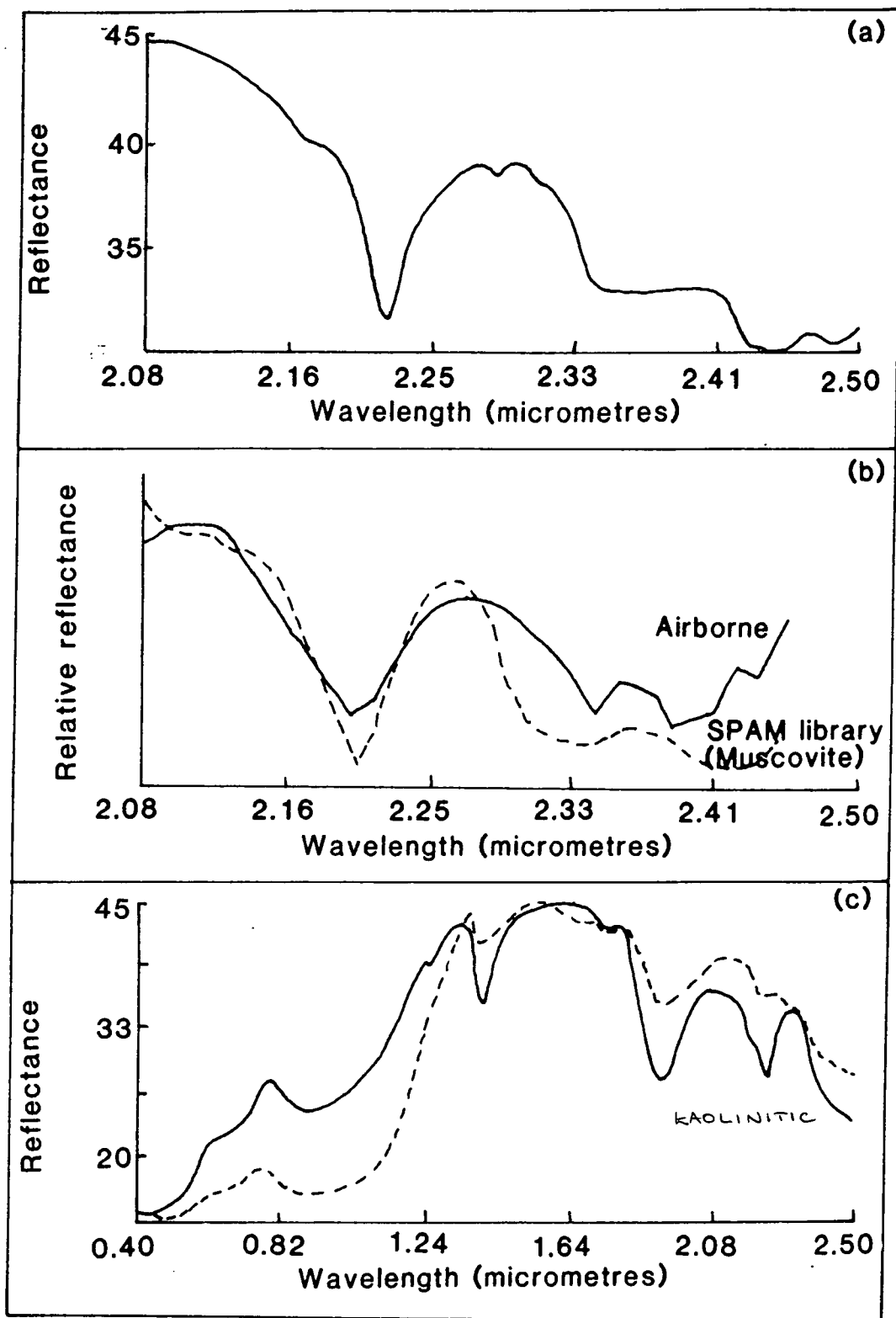
Figure 6.7   Located at site 2 (Mackins knob), (a) a laboratory spectrum
shows a strong sericitic response (2.2μm). (b) An airborne spectrum
shows the same strong response, it is compared to a library reflectance
spectra of muscovite. (c) Siliceous rocks produced strong iron absorp-
tions (0.9μm) and weak clay features (kaolinitic) in the laboratory
spectra.

a little clay and extensive iron staining.

Laboratory spectra, figure 6.7c, also show the presence of very deep iron absorptions at 0.9μm with little else in most cases. One sample, however, does show a clay absorption which bears a resemblance to kaolinite giving a 2.2μm major absorption with a shoulder in the absorption at 2.16μm.

6.11 Site 2 - Summary.

The major absorptions are clearly visible in both the laboratory and GER - II airborne spectra. The airborne spectra showing small spectral details, that help to clearly **identify** the surface material as sericite.

Note however, other small spectral features were not identified in the airborne data, such as kaolinite in the silicified outcrop. This may be due to the small amounts present relative to the sericite, or the lack of sensitivity of the sensor. The identification of the sericite probably results from its abundance, giving features of the order of three times the size of the kaolinite features in the laboratory spectra.

6.12 Site 3 - Adelaide Mine.

The site is situated in the east centre of the image, site 3, figure 6.2. The area has been mined in the past for copper and evidence of copper mineralisation can be seen in the surrounding rocks which carry the green stain of malachite. Some recent bulldozing of the upper surface of the hill has taken place.

6.12.1 Topography and vegetation.

The topographic range from the valley bottom to the top of the hill above the Adelaide mine, is of the order of 120m. The vegetation in this area is almost entirely sage brush with a little scattered dry grass.

6.12.2 General geology.

Two sub-units of the Preble formation are found in this area. The sub-unit on the lower slopes of the hill is the Epl sub-unit, which is primarily limestone with interbedded shale. The higher slopes are covered with phyllite and quartzite of the Ep sub-unit.

6.12.3 Locations.

There are four locations. The first location is at the mine entrance and the fourth on the hill top, while the other two are at intermediate heights on the hill slope.

LOCATION 1. Is situated at the entrance to the Adelaide Mine, figure 6.2, Site 3. The outcrop is primarily a grey-white limestone with a patchy staining of malachite, copper carbonate. There is also a lot of iron-stained rubble and strongly silicified banded limestone, plate 6.6.

Thin section studies revealed the presence of calcite, quartz and mica, while malachite is present as disseminated grains.

Laboratory spectra, figure 6.8, show a deep asymmetric feature situated at 2.35μm. that corresponds to calcite, not dolomite, which has a feature at 2.33μm.

LOCATION 2. To the NNE of the Adelaide Mine entrance, figure 6.2, Site 3. In a bulldozed cut on the hill slope. There is obvious silicification of the rocks which are weathering orange-brown. They are highly silicified, folded and dipping to the east, plate 6.7.

Thin section studies reveal a banded, iron-stained rock, basically consisting of quartz, clay minerals and opaques. The quartz forms an equigranular mosaic and the clay forms sub-parallel, small, elongate flakes of low birefringence with a few scattered longer flakes of muscovite. There are a few scattered opaques.

The laboratory spectra, figure 6.9, show a very strong iron absorption in the VNIR centred near 0.9μm (not shown in this diagram), and a fairly strong clay feature centred at 2.2μm, that looks like sericite.

LOCATION 3. Further to the NNE of the previous location, figure 6.2, plate 6.8. The location is on an old waste tip, the rocks are very dark in colour with extensive iron staining.

Thin section work revealed a banded rock, very deformed. It consists of a quartz mosaic, with aligned small, elongate flakes of clay (mica). There are some scattered opaques.

Laboratory spectra of the rocks, figure 6.10, reveal a strong iron feature at 0.9μm, but very little else except a hint of clay at 2.2μm. The lack of recognisable features may be related to the dark-weathering, iron rich crust on the rock surfaces. These crusts are known to subdue the spectral response

Plate 6.6   Adelaide mine, Site 3, Location 1. Situated at the entrance
to the mine. The outcrop is primarily grey-white limestone, with a
patchy staining of malachite. The rocks look banded.

Plate 6.7   Adelaide mine, Site 3, Location 2. Situated above the mine
entrance in a bulldozed cutting. The folded, silicified limestones are
clearly visible.
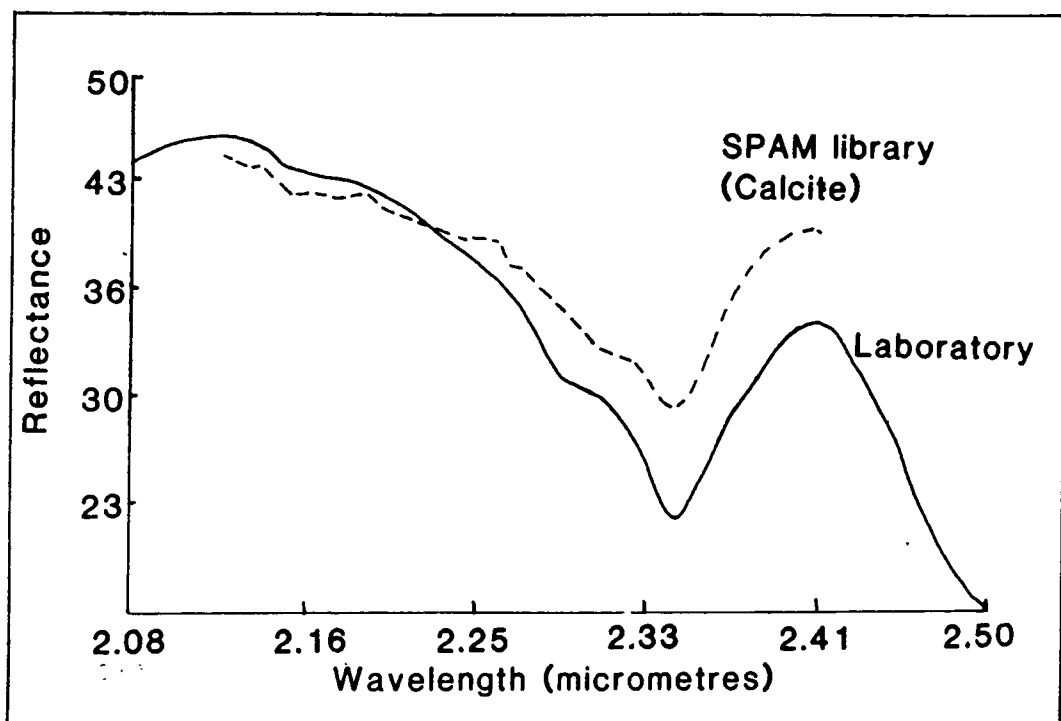
Figure 6.8   Located at site 3 (Adelaide mine), location 1. The laboratory spectrum clearly shows a calcite absorption $(2.35\mu m)$ from the limestone. The spectrum is compared with the reflectance library spectrum of calcite.
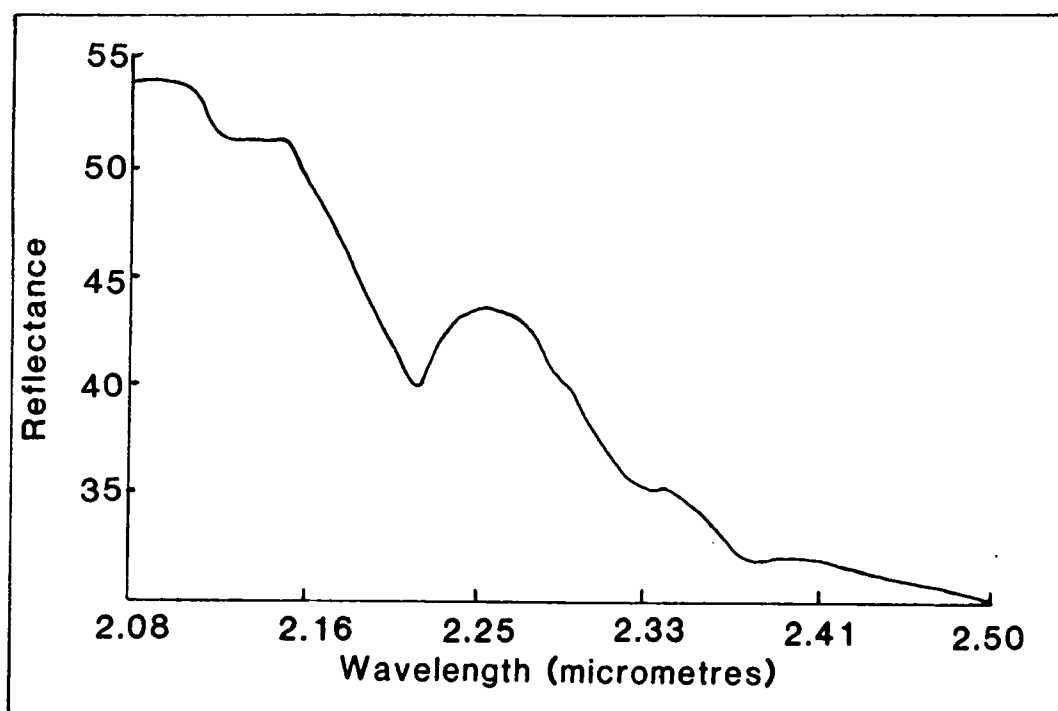
Figure 6.9   Located at site 3 (Adelaide mine), location 2. A laboratory spectrum shows a moderate sericitic feature, present in the silicified rocks of the area.

Plate 6.8   Adelaide mine, Site 3, Location 3. Situated on an old waste tip near a shaft. The rocks are very dark in exterior appearance, phyllitic, with much iron staining.

Plate 6.9   Adelaide mine, Site 3, Location 4. Situated on the hill top above Adelaide mine. The surface is littered with dark, red-black blocks of quartzite and phyllite.

Figure 6.10   Located at site 3 (Adelaide mine), location 3. A laboratory
spectrum shows the very low reflectance of the rocks in this area, due
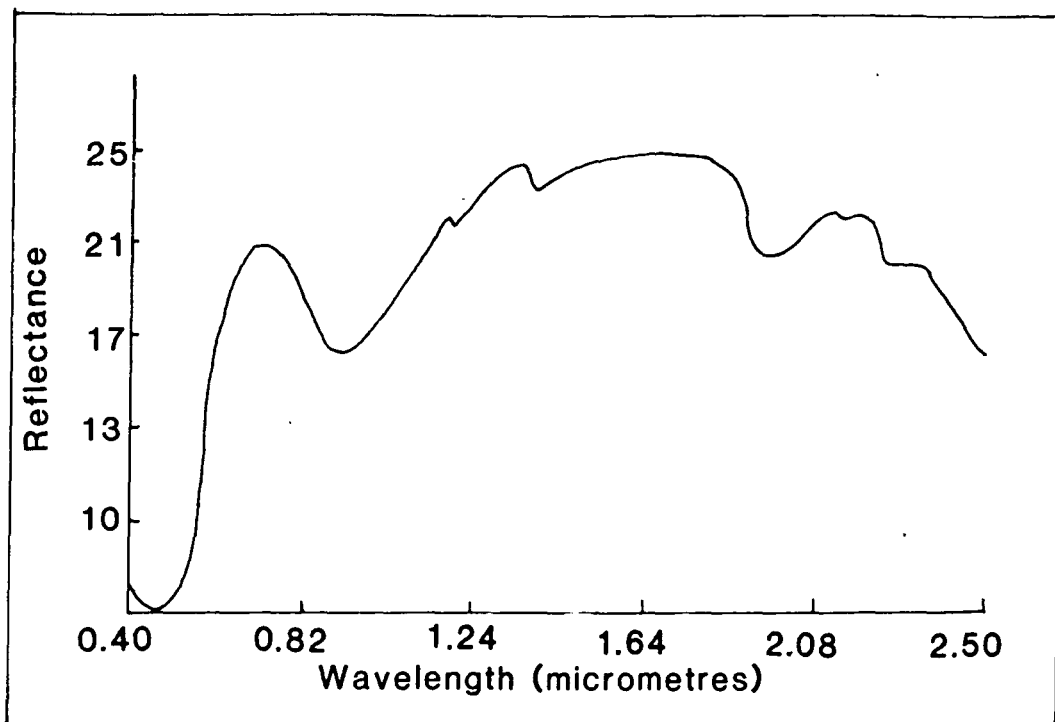to the dark weathering crusts. Only iron (0.9μm) and a weak clay
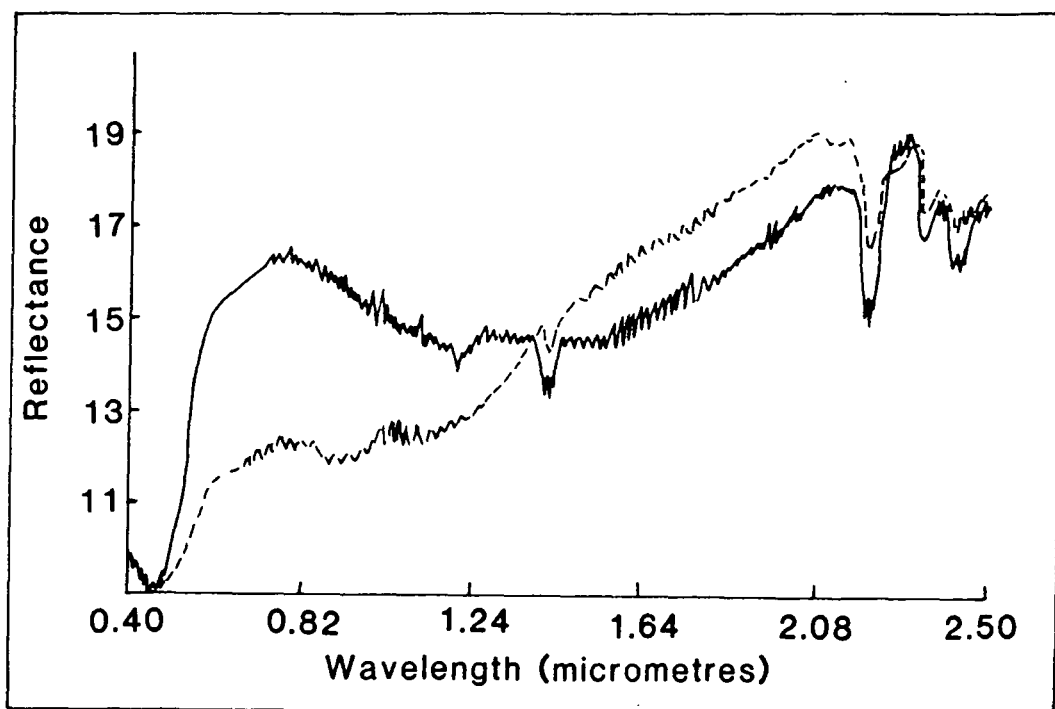feature at 2.2μm are present.

Figure 6.11   Located at site 3 (Adelaide mine), location 4. The laboratory
spectra again show the low reflectance, weak iron and clay features.

from other materials present (Krohn, 1986).

LOCATION 4. Is at the top of the hill to the NNE of the Adelaide mine, figure 6.2, Site 3. The hill slope is covered with blocky fragments seen in plate 6.9, which are weathering red-brown to black. Silicification is evident in some rocks, but some do look like recrystallised limestones and can be scratched with a penknife. Some siliceous, platy fragments are evident on the surface, with shiny, micaceous upper surfaces.

Thin section studies show a quartz-clay rock comprising a mosaic of quartz crystals, with small, elongate flakes of clay at the grain boundaries. There are a few larger quartz grains present.

Laboratory spectra of the rocks are shown in figure 6.11. They have very low reflectance values and so the noise is very distinctive. No real features of interest can be discerned.

Airborne spectra from this site proved to be too noisy, due to the low signal to noise ratios of the data. No identifiable features could be extracted from the small locations at this site. Spatial averaging of an area covering most of the upper hill slope was finally used, and successfully extracted a spectral feature. The averaged area covered 121 pixels and produced a curve that could only be classified under the group name "CLAY", figure 6.12.

6.12.4 Other observations.

Outside the range of these sites, the spectral response of other surface materials has been measured, both on the surface and from the airborne data. Figure 6.13 shows the spectral response of three different areas, one over dry grass, labelled B in figure 6.2, plate 6.10, in the north-west of the image. Showing the characteris tic absorption at $2.1\mu m$ and the steep decrease in reflectance to $2.32\mu m$. This area is compared to two large areas, 81 pixels each, composed of sage brush, situated to the east of site 2. As can be seen, a very similar curve shape is produced, labelled A.

An area of green vegetation was also studied. The area is to the northern edge of the area, labelled C in figure 6.2. The typical response of green vegetation in the $2.2\mu m$ wavelength region is shown in figure 6.14. The same area was also sampled in the VNIR wavelength region, figure 6.15. Clearly, the spectrum shows the red edge, the rise in reflectance from the visible to the near infrared, that is characteristic of green vegetation.
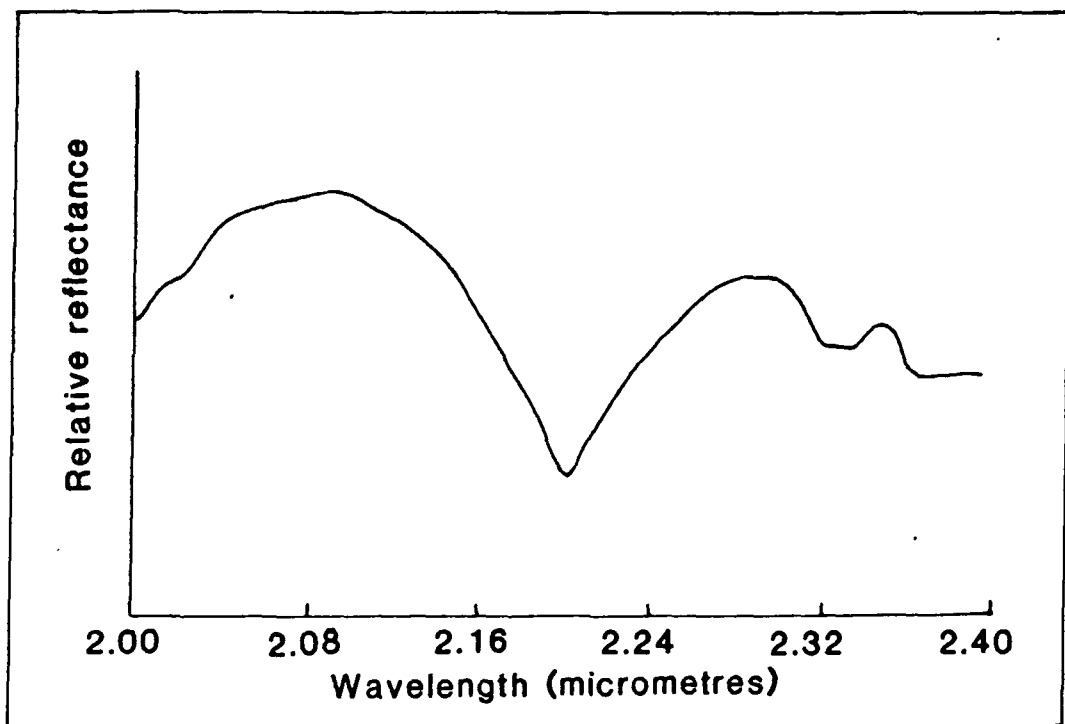
Figure 6.12   Located at site 3 (Adelaide mine). The airborne spectrum is an average of 121 pixels. It only shows the presence of an unidentifiable clay.
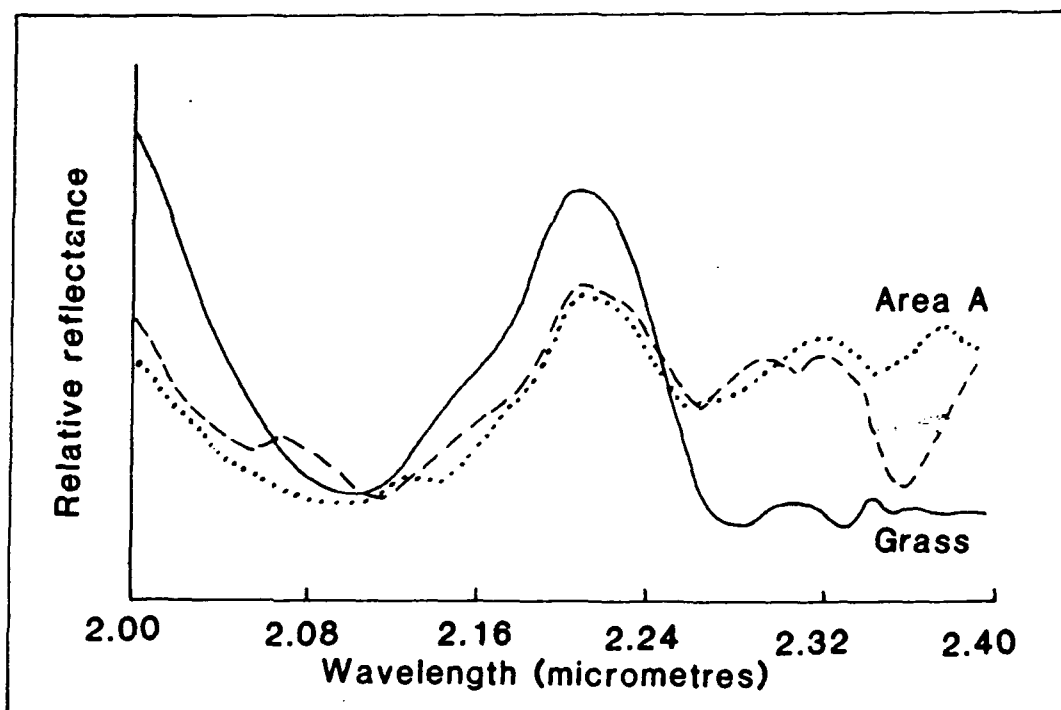
Figure 6.13   Airborne spectra of two areas of sage brush show the same typical absorption features due to cellulose, previously identified over an area of dry grass.

Plate 6.10   An area of dry grass (labelled B on the location map, figure 6.2). There is no outcrop and the grass cover is almost complete. Field spectral measurements were taken to determine the spectral response of the grass (figure 6.13).
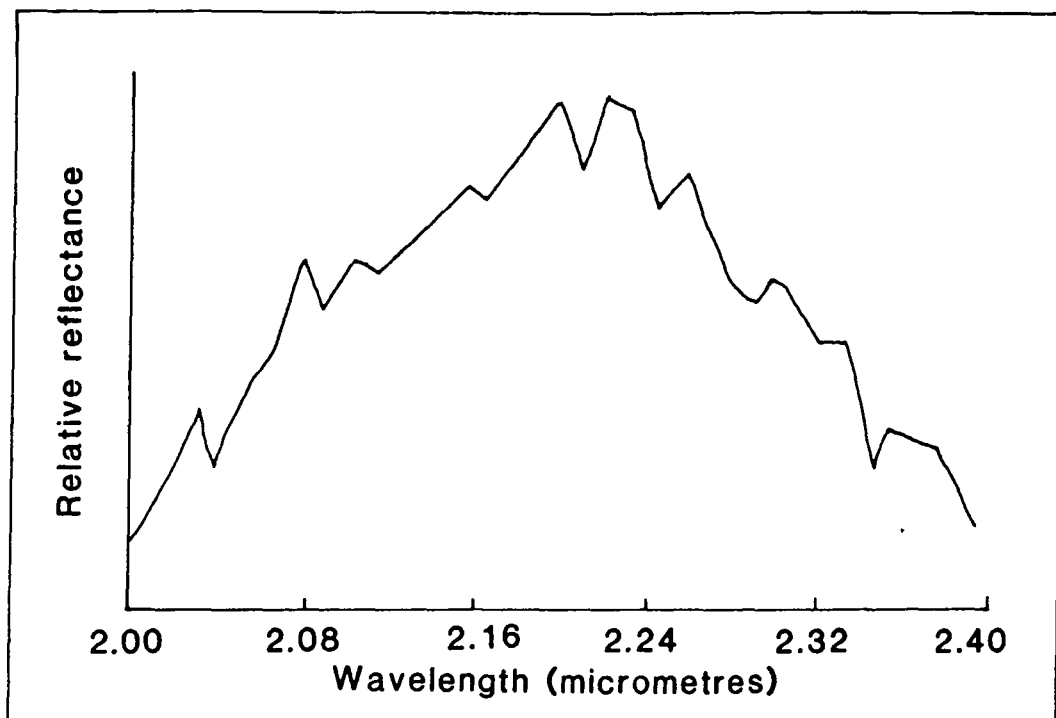
Figure 6.14 An airborne spectra over an area of green vegetation, covering the SWIR wavelength region.
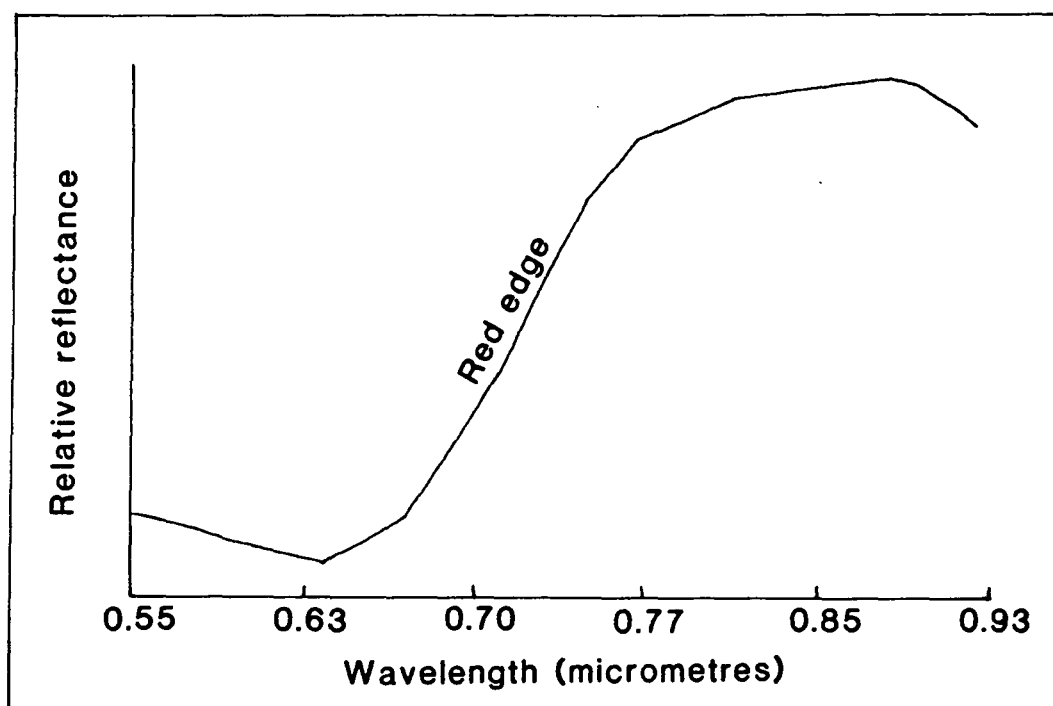
Figure 6.15 The corresponding VNIR spectra of green vegetation, from the area covered above. Note the steep rise in reflectance at the red edge.

6.13 Site 3 - Summary.

The spectral features in this area are very subdued, with no small well-defined areas of anomalous absorption visible. The presence of the limestone, giving a strong calcite feature in the laboratory spectrum, is clearly lost, possibly due to the small and mostly vertical outcrop. The only feature extracted was from the dark weathering quartzite and phyllite, that cover the upper hill slopes and this required extreme spatial averaging over 121 pixels to record that clay was present. The only possible reason for this negative result, must relate to the dark weathering crusts, that cover most of the outcrop in this area. Further work to investigate the mineralogical differences between the surface weathering crusts and the fresh rock should be undertaken.

6.14 Discussion.

6.14.1 Mineralisation and alteration

Mineralisation in the area has taken place by either contact metamorphic replacement of carbonates, or the emplacement of silica rich rocks along faults. There is also some disseminated mineralisation related to the emplacement of the silica rich rocks.

The observable spectral features in this area can be related to the mineralisation. The emplaced very dark, iron-stained jasperoids, have broad iron absorptions centred near 0.9μm and occasional small 2.2μm features (Krohn, 1986). Areas of phyllic alteration (also studied by Krohn) were noted, however, the general metamorphism of the phyllite produces a rock with similar spectral characteristics to the alteration. The only difference being the depth of the absorption at 2.2μm, the altered areas having much deeper absorptions.

6.14.2 General

The conclusions drawn from the use of the GER - II data are more positive, than those from the AIS - 1 work. Clear mineral identification was achieved at several sites, although spatial averaging over nine pixels was needed to achieve such results. This averaging helps to resolve the signal, but increases the problems of spectral mixing.

The north-south trending ,iron-rich, siliceous ridges could not be resolved

in the GER - II data, but they will contribute spectrally to any pixels containing them. The lack of resolution and thus identification in this case is a combination of the poor resolution of the instrument and the effects of mixing in the single pixels. The problems of spectral mixing have not been fully resolved and further research is needed in this area, esspecially as the sensitivity of the sensors improves.

Although the GER - II scanner gave some satisfactory results, the scene could still only be classified into the broad generic groups "CLAY", "CARBONATE", "DRY VEGETATION" or "GREEN VEGETATION". Clearly, the technique has some way to go.

Three research aims, were listed at the start of this chapter, these were,

(1) To test the mineralogical mapping capabilities of the GER - II scanning system.

(2) To compare the GER - II and AIS - 1 instruments and determine the effects of the different spatial and spectral resolutions of the instruments.

(3) To determine which unique features in the visible and near infrared would be of use in mineral identification.

With regard to the first aim, it has proved possible to identify the surface materials present in a scene, given low vegetation density, a pure, strong signal value and spatial averaging over several pixels containing the material. Generally, however, higher vegetation densities and lower signal values mean that only a general classification into a group such as "CLAY" is possible.

In respect of the second aim, the GER - II instrument proved to be far more effective than the AIS - 1 instrument, although no true comparison of the spectral or spatial resolutions of the two instruments could be made. Technical problems associated with the vibrating detector array of the AIS - 1 instrument (Vane, 1987) meant that the spectral and spatial resolutions of this instrument are only known approximately.

Finally, the only clear feature that could be extracted from the VNIR was the red edge feature related to green vegetation. No obvious mineral related feature could be extracted. More work needs to be done to confirm the useful ness of this wavelength region in mineral exploration.

Summary.

It was found that low reflectance materials in mixtures proved
difficult to identify, this combined with noise tended to
reduce identification accuracy.

However, unlike the AIS-1 data, mineral identification was
possible in several cases without the use of ground data, the
instrument performance being far superior to that of the
AIS-1, especially in the important SWIR wavelength region.

With additional ground information, it was possible to
identify clearly many more surface materials, without this
information classification into generic groups was still
possible.

6.15 Conclusions.

(1) Actual identification of mineral spectra was possible using the GER - II data. However, this required low vegetation density, pure, strong signal values and spatial averaging to extract such spectra.

(2) No identifiable features of use in mineral identification were extracted from the airborne data in the VNIR wavelength region. Further work is necessary to fully evaluate the VNIR.

(3) Generally, pixels could be classified in the same four generic groups defined in the analysis of the AIS - 1 data, "GREEN VEGETATION", "DRY VEGETATION", "CLAY" and "CARBONATE".

(4) Small areas with low reflectance values, such as the siliceous jasperoids on the dolomitic hill tops, could not be visually identified in band images of the data or on examining the output spectra covering the VNIR, where the iron rich jasperoids should have absorptions.

(5) Minor scene components such as the kaolinite found in a laboratory spectra of a sample from Mackin's knob, were not identifiable in the airborne data, possibly due to the small quantities and large spatial averages necessary to obtain identifiable spectra from this area.

(6) Spatial averaging proved necessary to obtain identifiable mineral spectra.

(7) Further work is necessary to determine the spectral variation between surface weathering crusts and the underlying fresher rock.

(8) Generally however, it is clear that the GER instrument is far superior in detecting the small spectral features that make surface material identification a possibility. *

* Mackin and Munday (1988).

CHAPTER 7

DISCUSSION, CONCLUSIONS AND RECOMMENDATIONS.

7.1 Discussion.

This summary discussion is in two parts. The first part covers the area of data preparation, processing and analysis, while the second part covers the interpretation and geological findings.

7.1.1 Part 1 - Data preparation, processing and analysis.

Experience of handling high spectral resolution data strongly suggests that a seperate **data preparation** stage is necessary, the primary aims of which should be,

(1) Data reformatting, to arrange the data in a format suitable for processing and analysis.

(2) Noise reduction, to improve identification accuracy at the analysis stage.

The AIS - 1 data set was already in a suitable form for processing and analysis, so no algorithms were necessary to convert its format. However, use of the SPAM package with the data after processing using the log residuals method, was badly affected by the presence of vertical and horizontal striping in the data. The effects of this striping "noise" were so overriding, that the matching algorithms often classified the pixels according to their column or row brightness rather than to the variation in surface composition. Purpose written algorithms were used to reduce these striping effects and greatly improve spectral matching at the analysis stage.

Further noise problems, mainly due to random noise, prevented accurate matching of single pixel plots with SPAM library reflectance spectra at the analysis stage. Spatial averaging of several adjoining pixels improved the accuracy of matching, however, the spectra were still noisy. Another purpose written smoothing algorithm was used to spectrally filter the AIS - 1 data, giving a marked improvement in the output spectral curves, although spatial averaging of several adjoining pixels was still necessary to extract consistent,

identifiable spectra.

The GER - II data set presented a different set of problems. In this case, the data had to be reformatted for analysis by the SPAM package. A purpose written data conversion program was written to perform this task. Evaluation of this data set revealed similar noise problems to the AIS - 1 data set, which required similar solutions. The algorithms used on the AIS - 1 data were modified to solve these problems.

Data preparation is required to reformat data and to reduce noise problems prior to processing and analysis. The preparation requires the development of purpose written code to address these problem areas.

Having prepared the data, the next step to consider is the **data processing**. Experience has shown that effective identification of surface materials can be made if the airborne data values can be reduced to the form of reflectance values. This has inherent advantages at the analysis stage, in that suitable methods to analyse such output spectra already exist and that comparison techniques using established libraries of reflectance spectra are already very advanced. We can therfore consider the reduction of the data to reflectance values to be a primary aim of the data processing step.

Unfortunately, to effectively reduce airborne data to reflectance data requires the use of ground collected data, whether in the form of ground spectra of recognisable targets, or atmospheric data for modelling out the atmospheric effects. This raises the question,

What information will be available to carry out the processing of the data, just the airborne data, or will ground collected data be available ?

If ground data is available, then a suitable method can be applied to achieve the desired aim of producing output reflectance spectra. However, if no ground data is available, we must consider alternative processing techniques. These alternatives will be useful for some applications, but not others. For example, if the application is to isolate and identify large areas of alteration, then fine detail both spatially (as the target is large) and spectrally (as the features are well defined) may not be required. In this case, log residual, IARR or RGN can be used to visually identify areas of alteration in the image. Output spectra can then be extracted, that will broadly approximate reflectance

spectra for identification purposes. Alternatively, if the application is to locate and identify small anomalous areas, then visual identification of these areas in an image will be difficult and the resulting output spectra may be badly distorted, depending on the scene components present. Therefore, it is important to ask the question,

What is the application for which the output data is required ?

If there are no suitable techniques to reduce the data to reflectance or pseudoreflectance (as in the use of log residuals, IARR and RGN), we have no option but to abandon the primary aim of producing output reflectance spectra and consider a third question,

What form of output is necessary for analysis ?

Presently, the only answer is reflectance or reflectance like spectra, the reason being that current analysis packages and analysis techniques are all based around the reduction of the data to such a form. However, there is an alternative, the development of analysis algorithms that do not require reflectance data, but can analyse the data in a different form.

Data analysis techniques dictated the basic requirements for all the previous steps. The data preparation techniques were developed to improve matching of spectra at the analysis stage. The data processing techniques were developed to produce an output suitable for analysis. Therefore the decisions to use particular data preparation and processing steps ultimately depends on the form of data analysis.

Primary analysis of the AIS - 1 and GER - II data has been with the SPAM package. To make effective use of the SPAM spectral library, pseudoreflectance spectra were generated using a log residuals processing approach. Analysis using the SPAM package revealed the limitations of the data preparation and processing steps, it also revealed the limitations of the package (See Chapter 4). The major limitations of the SPAM package were related to the spectral matching capabilities of the classification routines and the loss of interactive use with large data sets. These limitations could be overcome by the development of alternative analytical procedures.

These alternative procedures need to be directed, that is they "look" for key features in the spectra and identify on the basis of these limited key

features. This overcomes the limitations of the "blind" matching of points in a pixel spectra to those of a library reflectance spectra. Also the selection of only a few key features for matching will also speed up the analysis algorithms, allowing interactive use.

7.1.2 Part 2 - Geological findings.

It was clear at an early stage, that the poor data quality of the AIS - 1 imaging instrument would cause great problems in identification. However, it was also clear, that the AIS - 1 instrument could still distinguish anomalous features related to surface mineralogy.

It was noted, that when absorptions were found in laboratory spectra, that the airborne spectra had a similarly placed absorption. However, unlike the laboratory spectra, where identification was possible, the best that could be extracted from the AIS - 1 data was a mineral grouping (for example "CLAY"), except in a few cases, or where ground data was available.

It became apparent, that only four divisions of the data were possible, "CLAY", "CARBONATE", "DRY VEGETATION" and "GREEN VEGE-TATION". These four groups are distinct enough spectrally to be seperated. Only two groups have one spectral member (for our purposes), the green and dry vegetation groups. The clay group contains clay minerals and little else, while the carbonate group is the most varied, containing many different minerals (carbonates, $Mg - OH$ minerals, etc.) with absorptions in the 2.3μm to 2.4μm wavelength region.

The GER - II data was far superior to the AIS - 1 data in terms of data quality, giving much more detail than the AIS instrument. In some cases, the **identification** of the surface mineralogy was possible. The most accurate matches still required spatial averaging to highlight the smaller spectral features necessary for identification. Using spatial averaging over areas of low vegetation density, with high, relatively pure signal values, it was possible to identify sericite, illite, dolomite, dry vegetation and green vegetation (9 pixel spatial average). In areas of higher vegetation density, with less pure signal values, larger spatial averages (121 pixels) were necessary to identify features. In most cases, the small areas of different mineralogy could not be distinguished and identified, their uniqueness lost in the spatial average.

The VNIR data gave only one clear unambiguous spectrum, that of green

vegetation (the red edge). No clear identification of a mineral absorption feature was made in this wavelength region.

The current limitations on the effective use of this type of data in geological applications are set by the data quality available. Any improvement in data quality will help resolve smaller spectral features and thus increase identification accuracy. Another effect in the improvement of data quality, would be to reduce the need for spatial averaging of several adjoining pixels to get an output spectra, this would allow the minerals occupying single pixels to be resolved (such as the small area of kaolinite that could not be resolved on Mackin's knob). The effects of spectral mixing would however, become more important as data quality was improved. The separation of finer detail would highlight intimate mineral mixtures in single pixels, that would require a mixture decomposition algorithm to identify the individual components of the mineral mixture.

Finally, some consideration must be given to the VNIR wavelength region, where the problems of data quality are reduced due to the high signal to noise ratios of detectors in this wavelength region. The failing in the GER instrument seems to be related to the large spectral bandwidth of each band in the VNIR spectrometer, which seems incapable of resolving the mineralogical features that are known to exist in this wavelength region (Hunt, 1980). Further study of this wavelength region is necessary to fully evaluate its mineralogical potential.

7.2 Conclusions.

(1) It has been proven that the identification of minerals is possible, by the analysis of the position ,depth and curve shape of absorption features at visible and infrared wavelengths (Hunt, 1980).

(2) The infrared wavelength region from $2.0\mu m$ to $2.5\mu m$ has proven to be the most useful wavelength region for mineral identification.

(3) Atmospheric effects, especially in the visible, produce variable effects that can reduce identification accuracy. In some wavelength regions (the regions of major water absorptions) no useful signal can be extracted.

(4) Macroscopic ground effects (for example surface particulate variable scattering effects) and geometric distortion, reduce identification accuracy and determination of ground position.

(5) Poor detector calibration can produce a reduction in data quality and hence identification accuracy.

(6) The effects of random noise are to reduce identification accuracy when matching output spectra, with spectra from spectral libraries.

(7) The use of hull quotients or log residuals / IARR is warranted in an exploration environment, where the collection of ground data is not possible. Due either to its time consuming nature or to the lack of suitable ground targets.

(8) Current analysis packages are not effective in identifying mineral spectra, especially small targets (several pixels) of unusual mineralogy.

(9) Broad classification of anomalies highlighted in the AIS - 1 data was possible. However, actual mineral identification proved impossible ⌐in most case due to the low signal to noise ratio values of the instrument.

(10) The variations in mineralogy determined by the AIS - 1 instrument, were clearly related to variations in lithology. However, the lithology could not be determined from the spectral response, only the dominant mineralogy.

(11) Actual identification of mineralogy was possible using the GER - II data. However, this only applied when the dominant mineral had a very strong absorption feature and when the vegetation density was quite low (hill tops). In other areas spatial averaging of the data was necessary to highlight the predominant mineralogy. In these cases, only a broad spectral grouping, such as "CLAY" could be determined, unless confirmatory ground data was available to help in the identification procedure.

7.3 Recommendations.

It is clear that many areas for further research could be recommended, in this section some of these basic areas are discussed, finally concentrating on what I believe is the main issue, the need for a new, effective, versatile **data analysis** system.

The basic recommmendations are,

(1) Further research should be carried out to evaluate fully the VNIR (0.4μm to 1.0μm) wavelength region. The GER - II data may have too large a spectral sampling interval (25.4nm) to be effective in identifying mineral absorption features, also the spectral range of the instrument for the first spectrometer may need to be extended to 1.2μm from its current 1.08μm upper limit, to cover the broad Fe^{2+} feature at 1.0μm.

(2) Atmospheric modelling, should be an item for future detailed research. The application of suitable atmospheric models to the data, provides an alternative method of reducing the data to reflectance spectra. However, even if a full atmospheric model can not be applied, knowledge of the atmospheric conditions could be used to produce corrections for VNIR atmospheric scattering, prior to the use of other processing techniques.

(3) Development of suitable systems to geometrically correct scanner data is necessary. Location and identification of smaller targets is dependent on accurate ground location. These corrections become more necessary in environments with few recognisable ground features, such as the heavily weathered environment of Western Australia.

(4) Improvements in the pre-processing of the data are necessary, especially at the calibration stage, to prevent any loss of data quality.

(5) An improvement in the signal to noise ratios of the data is necessary, this can only be done by improving the instruments themselves. Trade offs in spectral sampling interval and spatial resolution should be considered in the short term, to improve the signal to noise ratios, especially in the SWIR wavelength region.

(6) Further work is necessary to fully evaluate the current processing and analysis techniques. The evaluation should involve detailed work covering a very small ground area. Several techniques should be applied, so that comparisons between various techniques can be considered.

(7) As the sensitivity of systems improves, the problems of spectral mixing of surface components will become more apparent. Some effort should be spent in evaluating the mixing problem (perhaps in the same area used to evaluate the current processing and analysis techniques). Development of suitable algorithms to analyse mixtures and determine the proportions of scene

99

components present are necessary.

(8) The effects of variable vegetation density on the spectral response of the ground surface should be investigated further.

Finally, the prime recommendation is the evaluation and thus at least partial development of a new processing and analysis system for geological applications.

The system would be based on a variant of the hull quotients technique to extract spectral features of interest. These features could then be analysed using a rules based system to extract and identify the key features and thus the mineral composition.

The advantages of the key features approach are,

(1) A reduction in the amount of data analysed during a classification, which will increase the response speeds of an interactive system.

(2) Data can be sorted and classified at different levels. Features may be classified down to the generic level, noted in the analysis of the GER - II and AIS - 1 data ("CLAY", "CARBONATE", etc.), or given more detail, down to the identity of the mineral (kaolinite, calcite).

A rules based system could be used to analyse all the data in a scene, however, in a geological application, some of this data is useless (green vegetation, dry vegetation or water). The rules base should therfore be modified to work in a hierarchical manner, a tree structure, which rejects pixels from analysis at an early stage, based on a simple test. A basic outline of such a system is given below,

Step 1 - Would carry out a simple test to exclude green vegetation from the analysis. Problems will occur in defining the boundary conditions between green vegetation and other materials, in terms of a selection cut-off. This has to be investigated.

Step 2 - Would seperate rocks and soils from dry vegetation in the scene, based on major variations in spectral response. Again the boundary conditions could be a problem area.

Step 3 - A separation of the remaining pixels into generic groups, much like those determined from the analysis of the AIS - 1 and GER - II data.

Step 4 - This could be considered to be the final level of the tree structure, the

identification of the minerals present in the generic groups. There could be several options for analysis at this stage, either a search for a chosen mineral in its generic group, or a blanket identification of every pixel in a particular generic group.

This form of analysis has many advantages, pixels can be identified down to the level of the information present in them. If the data quality is poor, only generic matching may be achieved, if the data is variable in quality, an output map may contain information on generic and specific matches of different pixels.

The basic system should be flexible and easy to use, perhaps in a work-station environment offering multi-tasking and windowing. The proposed development time is of the order of six months to develop an evaluation system.

To conclude, some time should be spent developing and evaluating a rules based identification system, using data processed by a variant of the hull quotients technique. This I believe offers the best option for using the data in geological applications.

Thus grew the tale of Wonderland:
 Thus slowly, one by one,
Its quaint events were hammered out—
 And now the tale is done,
And home we steer, a merry crew,
 Beneath the setting sun.

ALICE'S ADVENTURES IN WONDERLAND by Lewis Carroll.

REFERENCES

Abrams, M. J., and Goetz, A. F. H. (1985), Imaging Spectrometry : Past, Present, Future. *In,* Proceedings of the 3rd International Colloquium on Spectral Signatures of Objects in Remote Sensing, Les Arcs, France, 16th - 20th December 1985. ESA Publication SP-247. pp. 215-218.

Abrams, M. J. Ed. (1985), Volume 1, Final report, Appendix A, *In,* The Joint NASA/Geosat Test Case Project. American Association of Petroleum Geologists, Tulsa, OK.

Butt, C. R. M. (1981), The nature and origin of the lateritic weathering mantle, with particular reference to Western Australia. *In,* Geophysical prospecting in Deeply Weathered Terrains, Doyle, H. A., Glover, J. E., and Groves, D. I. (Eds.), Geology department and Extension Service, University of Western Australia, 6 : 11-29.

Campbell, I. D., and Dwek, R. A. (1984), Biological Spectroscopy, Benjamin/Cummings, California, 404pp.

Chahine, M. T., Mc Cleese, D. J., Rosenkranz, P. W., and Staelin, D. H. (1983), Interaction Mechanisms Within the Atmosphere. *In,* Manual of Remote Sensing, Second Edition, Colwell, R. N. (Ed.), American Society of Photogrammetry, pp. 165-230.

Clark, R. N., King, T. V. V., and Gorelick, N. S. (1987), Automatic continuum analysis of reflectance spectra, *In,* Proceedings of the Third Airborne Imaging Spectrometer Data Analysis Workshop, JPL Publication 87-30, Jet Propulsion Laboratory, Pasadena, CA, pp. 138-142.

Cocks, T. D., and Green, A. A. (1986), The application of AIS data to detecting subtle mineral absorption features, *In,* Proceedings of the Second Airborne Imaging Spectrometer Data Analysis Workshop, JPL Publication 86-35, Jet Propulsion Laboratory, Pasadena, CA, pp. 52-57.

Collins, W. E., and Chang, S. (1988), Application of Geophysical Envi-

ronmental Research (GER) Airborne Scanner data for detection of hydrothermal alteration in Nevada, *In,* Summaries, International Symposium on Remote Sensing of Environment, Sixth Thematic Conference, Remote Sensing for Exploration Geology, Houston, Texas, 16th - 19th May 1988, Environmental Research Institute of Michigan, Ann Arbor, pp. 14-15.

Conel, J. E., Adams, S., Alley, R. E., Hoover, G., and Schultz, S. (1986), Analysis of AIS radiometry with emphasis on determination of atmospheric properties and surface reflectance, *In.* Proceedings of the Second Airborne Imaging Spectrometer Data Analysis Workshop, JPL Publication 86-35, Jet Propulsion Laboratory, Pasadena, CA, pp. 31-51.

Conel, J. E., Green, R. O., Vane, G., Bruegge, C. J., and Alley, R. E. (1987), AIS - 2 Radiometry and a comparison of methods for the recovery of ground reflectance, *In,* Proceedings of the Third Airborne Imaging Spectrometer Data Analysis Workshop, JPL Publication 87-30, Jet Propulsion Laboratory, Pasadena, CA, pp. 18-47.

Crowley, J. K. (1986), Visible and Near-Infrared Spectra of Carbonate Rocks : Reflectance Variations Related to Petrographic Texture and Impurities, *J. Geophys. Res.,* 91(B5) : 5002-5012.

Davis, J. C. (1986), Statistics and Data Analysis in Geology, Second Edition, Wiley, New York, 646pp.

Elvidge, C. D. (1988), Vegetation Reflectance features in AVIRIS data, *In,* Summaries, International Symposium on Remote Sensing of Environment, Sixth Thematic Conference, Remote Sensing for Exploration Geology, Houston, Texas, 16th - 19th May 1988, Environmental Research Institute of Michigan, Ann Arbor, pp. 23-24.

Feldman, S. C. (1987), Effective use of Principal Component Analysis with high resolution remote sensing data to delineate hydrothermal alteration and carbonate rocks, *In,* Proceedings of the Third Airborne Imaging Spectrometer Data Analysis Workshop, JPL Publication 87-30, Jet Propulsion Laboratory, Pasadena, CA, pp. 48-55.

Gaffey, S. J. (1985), Reflectance spectroscopy in the visible and near-

infrared (0.35 - 2.55μm) : Applications in carbonate petrology, *Geology*, 13 : 270-273.

Green, A. A., and Craig, M. D. (1985), Analysis of aircraft spectrometer data with logarithmic residuals, *In,* Proceedings of the Airborne Imaging Spectrometer Workshop, JPL Publication 85-41, Jet Propulsion Laboratory, Pasadena, CA, pp. 111-119.

Hapke, B. (1981), Bidirectional Reflectance Spectroscopy, 1. Theory, *J. Geophys. Res.*, 86(B4) : 3039-3054.

Heute, A. R., Jackson, R. D., and Post, D. F. (1985), Spectral Response of a plant canopy with different soil backgrounds, *Remote Sens. Environ.*, 17 : 37-53.

Hunt, G. R., and Salisbury, J. W. (1970), Visible and Near - Infrared Spectra of Minerals and Rocks : I. Silicate Minerals, *Modern Geology*, 1 : 283-300.

Hunt, G. R., Salisbury, J. W., and Lenhoff, C. J. (1971), Visible and Near - Infrared Spectra of Minerals and Rocks : IV. Sulphides and Sulphates, *Modern Geology*, 3 : 1-14.

Hunt, G. R. (1980), Electromagnetic radiation : The communication link in remote sensing, *In,* Remote Sensing in Geology (B. Siegal and A. Gillespie, Eds.), Wiley, New york, 702pp.

Huntington, J. F., Green, A. A., and Craig, M. D. (1986), Preliminary Geological Investigation of AIS Data at Mary Kathleen, Queensland, Australia, *In,* Proceedings of the Second Airborne Imaging Spectrometer Data Analysis Workshop, JPL Publication 86-35, Jet Propulsion Laboratory, Pasadena, CA, pp. 109-131.

Jet Propulsion Laboratory (1985), Airborne Imaging Spectrometer, Science Investigators Guide to AIS data, Jet Propulsion Laboratory, Pasadena, CA, 14pp.

Krohn, M. D. (1986), Spectral Properties (0.4 to 25 microns) of Selected Rocks Associated with Disseminated Gold and Silver Deposits in Nevada and Idaho. *J. Geophys. Res.*, 91(B1) : 767-783.

Kruse, F. A., Raines, G. L., and Watson, K. (1985), Analytical techniques for extracting geologic information from multi-channel airborne spec-

troradiometer and airborne imaging spectrometer data, *In,* Proceedings, International Symposium on Remote Sensing of Environment, Fourth Thematic Conference, Remote Sensing for Exploration Geology, San Francisco, California, 1st - 4th April 1985. Environmental Research Institute of Michigan, Ann Arbor, pp. 309-324.

Kruse, F. A., and Clark, R. N. (1986), Atmospheric-water absorption features near 2.2 micrometers and their importance in high spectral resolution remote sensing, *In,* Proceedings of the Second Airborne Imaging Spectrometer Data Analysis Workshop, JPL Publication 86-35, Jet Propulsion Laboratory, Pasadena, CA, pp. 63-73.

Lorraway, R. (1976), The Petrology of the Camp - Oven mountain volcanic complex. Unpublished B.sc. thesis, James Cook University of North Queensland, Australia. 150pp.

Lyon, R. J. P. (1986), Comparison of the 1984 and 1985 AIS data over the Singatse Range (Yerington), Nevada, *In,* Proceedings of the Second Airborne Imaging Spectrometer Data Analysis Workshop, JPL Publication 86-35, Jet Propulsion Laboratory, Pasadena, CA, pp. 86-95.

Mazer, A. S., Martin, M., Lee, M., and Solomon, J. E. (1988), Image Processing Software for Imaging Spectrometry Data Analysis, *Remote Sens. Environ.,* 24 : 201-210.

Milton, E. J., and Wardley, N. W. (1987), Vegetation Canopy Reflectance Models : A Review, *Discussion paper No. 31,* Department of Geography, University of Southampton.

Roberts, D. A., Yamaguchi, Y., and Lyon, R. J. P. (1986), Comparison of various techniques for calibration of AIS data, *In,* Proceedings of the Second Airborne Imaging Spectrometer Data Analysis Workshop, JPL Publication 86-35, Jet Propulsion Laboratory, Pasadena, CA, pp. 21-30.

Tucker, D., and Vane, G. (1986), Radiometric Calibration of the Airborne Imaging Spectrometer, *In,* Proceedings of the Second Airborne Imaging Spectrometer Data Analysis Workshop, JPL Publication 86-35, Jet Propulsion Laboratory, Pasadena, CA, pp. 17-20.

Vane, G. (1986), Introduction to the Proceedings of the Second Air-

borne Imaging Spectrometer (AIS) Data Analysis Workshop, *In,* Proceedings of the Second Airborne Imaging Spectrometer Data Analysis Workshop, JPL Publication 86-35, Jet Propulsion Laboratory, Pasadena, CA, pp. 1-16.

Vane, G., and Goetz, A. F. (1988), Terrestial Imaging Spectroscopy, *Remote Sens. Environ.,* 24 : 1-29.

Walker, J. (1989), The colors seen in the sky offer lessons in optical scattering, *Scientific American,* January 1989 : 84-87.

Willden, R. (1964), Geology and Mineral deposits of Humboldt County, Nevada, *Bulletin 59,* Nevada Bureau of Mines and Geology, 154pp.

Wyatt, D. H., Paine, A. G. L., Clarke, D. E., Gregory, C. M., and Harding, R. R. (1971), Geology of the Charters Towers 1 : 250 000 sheet area, Queensland. *Report No. 137,* Bureau of Mineral Resources, 85pp.

Additional references.

Briggs, S. A., Mackin, S., Munday, T. J., Drake, N., Milton, E. J., and Rollin, E. M. (1988). The activities of the British National Space Centre (BNSC) in the field of imaging spectrometry. **In,** Imaging Spectrometry for Land Applications, Frascati, Italy, 19th-21st April 1988. ESA Publication SP-1101. pp 27-33.

Mackin, S., Munday, T. J., and Hook, S. J. (1987). Preliminary results from an investigation of AIS-1 data over an area of Epithermal alteration : Plateau, Northern Queensland, Australia. **In,** Proceedings of the Third Airborne Imaging Spectrometer Data Analysis Workshop, JPL Publication 87-30, Jet Propulsion Laboratory, Pasadena, CA, pp. 120-131.

Mackin, S., and Munday, T. J. (1988). Imaging Spectrometry in Environmental Science research and applications. **BNSC/RSADU report no. ADU-3.** 48pp.